



Managed by Platinum Foundation
GANDHINAGAR INSTITUTE OF TECHNOLOGY
AICTE Approved | Affiliated with Gujarat Technological University

'GIT-Journal of Engineering and Technology'

ISSN 2249–6157
(Print & Online)

Published By,

Gandhinagar Institute of Technology
Khatraj - Kalol Road, Moti Bhoyan,
Tal. Kalol, Dist. Gandhinagar-382721
Phone: 9904405900, 02764-281860/61
Fax: 02764-281862
E-mail: director@git.org.in, jet@git.org.in
Website: www.git.org.in

About Gandhinagar Institute of Technology

Gandhinagar Institute of Technology is established by Platinum Foundation in 2006. It offers under graduate programs in Mechanical Engineering, Information Technology, Computer Engineering, Electronics and Communication Engineering, Electrical Engineering and Civil Engineering and Post graduate program in MBA (Finance, Human Resource Development, and Marketing), M.E. in Mechanical Engineering with specialization in Thermal Engineering and Computer Aided Design & Computer Aided Manufacturing and M.E. in Computer Engineering with specialization in Software Engineering.

All these programs are approved by AICTE, New Delhi and affiliated to Gujarat Technological University. We have elaborate laboratory facilities and highly motivated and qualified faculty members. We are also arranging technical seminars, conferences, industry-institute interaction programs, workshops and expert lectures of eminent dignitaries from different industries and various reputed educational institutes.

Our students are innovative and have excellent acceptability to latest trends and technologies of present time. Our students have also participated in various technical activities as well as sports activities and have achieved various prizes at state level. We have two annual publications, a National level research journal 'GIT-Journal of Engineering and Technology (ISSN 2249–6157)' and 'GIT-a Song of Technocrat' (college magazine).

Trustees



Shri Hareshbhai B. Rohera



Shri Ghanshyambhai V. Thakkar



Shri Deepakbhai N. Ravani



Shri Pravinbhai A. Shah



Smt Varshaben M. Pandhi



Shri Mahendrabhai R. Pandhi

Message from the Director



It gives me immense pleasure that the eighth issue of our National journal ‘GIT-Journal of Engineering and Technology’ is being published with ISSN 2249 – 6157 for eighth successive year. The annual journal contains peer reviewed technical papers submitted by the researcher of all domains of engineering and technology. The issue is a result of imaginative and expressive skill and talent of GIT family. Research papers were invited from the researcher of all domains of engineering and technology. More than 55 research papers were received. After peer review about 26 papers are selected and are being published in this issue of the journal.

GIT was established in 2006 and during a short span of nine years; it has accomplished the mission effectively for which it was established. Institute has been constantly achieving the glory of excellence in the field of curricular, co-curricular and extra-curricular activities. For the seventh consecutive year an annual technical symposium TechXtreme-2015 was successfully organized by the institute. More than 1500 students of various technical institutions across the Gujarat participated in the Techfest. The event of Robo roller coaster was first time held in any technical institutions in India. Mr. and Mrs. Gujarat 2014 - A Talent Hunt and a pro-night with Rajdeep Chettarjee were also the main attractions. Prizes worth Rs 2 lacs and trophies were given to the winners of total 33 events. Another annual flagship event Jazba 2013 was organized on 20th September 2013. More than 1000 students of the institute participated in various cultural events of Debate, Quiz, Essay writing, Rangoli, Music, Dance, Drama etc. Famous bollywood actress Ms. Sonal Chauhan was the star attraction of the event.

The institute is two star Resource Center of IIT Bombay for conduction of Spoken Tutorials on various open source software like Linux, Latex, Scilab, Python, Java, Netbeans, C, C++, Liber Office, Php MySQL, etc. During the year institute has organized many workshops on Spoken tutorial and trained more than 1000 students and 300 faculty members. Seminars on Cisco Networking, Robotics, CAD/CAM has also been organized. The institute has also successfully organized Debate Competition, Rangoli Competition, Kite Flying competition, Ratri B4 Navaratri, and Sports activities. Institute has also arranged blood donation drives and more than 150 units were collected from the students and staff members. Students have also participated and won prizes in various sports, technical and cultural events organized by other Institutions including that of GTU. Institute has organized many industrial visits and expert lectures for the students for supplementing the class room teaching. I am extremely happy to mention that throughout the year the faculty members have worked very hard to achieve all kinds of curricular, co-curricular and extra-curricular activities.

The Institute is also emphasis on academic development of its faculty members. During the year, many International and National papers has been published and presented by the faculty members. The faculty members have also been deputed to attend large number of seminars/workshops/training programs/symposiums.

Publication of the journal of national level is not possible without whole hearted support of committed and experienced Trustees of Platinum Foundation Mr. Hareshbhai Rohera, Mr. Ghanshyambhai Thakkar, Mr. Deepakbhai Ravani, Mr. Pravinbhai Shah and Smt. Varshaben M. Pandhi. I take an opportunity to express my deep feelings of gratitude to all the trustees of Platinum Foundation and Mr. Mahendrabhai Pandhi, member of Governing body of the trust for their constant support and motivation.

It's my privileged to compliment the staff members and the students for showing high level of liveliness throughout the year. I also congratulate the team of the ‘GIT-Journal of Engineering and Technology’ for their untiring effort to bring out this eighth issue of the journal.

Dr N M Bhatt
Director & Chief Editor

Editorial Board

Dr. M N Patel	Vice-Chancellor, Gujarat University
Dr. Ketan Kotecha	Director, Institute of Technology, Nirma University
Dr. Rajul Gajjar	Principal, Vishwakarma Government Engineering College
Prof. SurendraSingh Kachhwaha	Professor & Head, Mechanical Engineering Department, School of Technology, Pandit Deendayal Petroleum University
Dr. R N Patel	Professor & Head Mechanical Engineering Department, Institute Of Technology, Nirma University
Dr. S P Parikh	Principal, VVP Engineering College
Prof. B V Buddhadev	Principal, S.S. Govt. Engineering
Dr N M Bhatt	Director & Editorial Chief, Gandhinagar Institute of Technology

Disclaimer

Views expressed in the papers are solely from respective authors. Editorial board has no responsibility of their authentication.

Index

Sr#	Name of Author and Article	Page No
1	Foundry Automation: Modernization and Mechanization of Foundries <i>Chintan Barelwala</i>	1-7
2	Automatic Copper Tube Straightening and Cutting Mechanism <i>Himanshu K Barot, Manthan Upadhyay, Hardik R Patel</i>	8-11
3	Vacuum System : Components , Performance & Applications <i>Viral Bhachech, Kuldip Dodiya, Anil Mankad</i>	12-16
4	Experimental Investigation of Double Pass Solar Air Heater with Three Obstacles on an Absorber Plate <i>Maulik Sukhadiya, Umang Patdiwala</i>	17-21
5	To study effect of recycle SAW flux on weld metal chemistry and mechanical properties <i>Prof. Dixit Patel, Arpit Patel, Shaival Parikh</i>	22-25
6	Cost Reduction in File Manufacturing by using Special Purpose Resistance Heating: A Case Study <i>Sameer S. Gajmal, Santosh Rane, Udhir Bhatwadekar</i>	26-36
7	Analytical and experimental investigations of the single stage centrifugal pump performance <i>Nilesh Tiwaria, Devranjan Kumar</i>	37-46
8	Piezoelectric Driven Miniature Thermoacoustic Refrigerator <i>Manju Lata, Nilesh Kolekar, Abhishek Swarnkara</i>	47-53
9	Separating and Feeding Sheets automatically with the help of Magnetic Force <i>Ankit V. Patel, Sunny K. Parikh, Amit R. Patel</i>	54-60
10	Finite Element Analysis of Automobile Structural Member using ANSYS <i>Tushar M Patel, N M Bhatt</i>	61-69
11	FEM based Taguchi method to Reduce the Automobile Structural Member Weight <i>Tushar M Patel, N M Bhatt</i>	70-79
12	Parametric Analysis and Working Fluid Selection of Organic Rankine Cycle for Low Grade Heat Energy <i>Jayesh vasava, V. D. Dhiman, F. S. Jariwala</i>	80-90
13	A Survey of Performance metrics for Vertical Handover between Wi-Fi and WiMAX <i>Madhuri R. Chopade</i>	91-97
14	Clustering in Data Mining: A Brief Survey <i>Sweta R. Garasia, Brinda Pandit</i>	98-101
15	Multicast Ad-hoc On-Demand Distance Vector Routing Protocol with Low Control Overhead <i>Kinjal U Adhvaryu, Pariza Kamboj</i>	102-107
16	Handwritten Character Recognition <i>Archana Singh</i>	108-115
17	Li-Fi based Optical Attocells using OFDM & SM-MIMO Techniques for 5G VLC Wireless Communication Network <i>Vineeta Nishada, Megha Bhatt, Jigisha Sureja</i>	116-127
18	Quantitative and Qualitative analysis of Single Electron Transistor <i>Shweta Khakhkhar</i>	128-133
19	Harmonics Mitigation Using Shunt Active Filter <i>Pankaj. C. Patel, D.R. Vyas</i>	134-140
20	PD Electromagnetic Pulse Analysis in Transformer by FDTD Simulation Technique <i>Hitesh Manani</i>	141-147
21	A Study on Product Related Factors Influencing Decision of Customers Purchasing Life Insurance Product in Gujarat <i>Jaideepsingh H Jetawata, Snehal Kumar Mistry</i>	148-159
22	Personality and Career Success <i>Nirupama Patel</i>	160-165
23	Study of Pressure Dependence of The Superconducting State Parameters of Ga, Cd and Sn	166-173

	Using Parameter Free Pseudopotential <i>Priyank Kumar, N. K. Bhatt, P. R. Vyas</i>	
24	Electron Scattering with 1 Pentene and Cyclopentane Molecules by SCOP Method – Total Ionization Cross sections <i>Umang R Patel, K N Joshipura</i>	174-177
25	Structural and Lattice Dynamical Properties of Al-Li Intermetallic Alloys <i>N. Y. Pandya, A. D. Mevada, P. N. Gajjar</i>	178-181
26	Delineation of Potential Groundwater after Zones using Remot Sensing and GIS-A Review <i>Madhu S Trivedi, G. P. Vadodaria</i>	182-187

Foundry Automation: Modernization and Mechanization of Foundries

Chintan Barelwala^a

^aGandinagar Institute of Technology, Gnadhinagar, India

Abstract

Foundries are a very complex environment to work in. The automation of specialised tasks such as investment casting, ingot handling or forging requires detailed process know-how and the right hardware to handle castings and cores with power and precision. Flexible manufacturing has already proven itself as a model for economic sustainability. While this strategy has been examined for general manufacturing, it has not been investigated in detail for the foundry industry. This paper proposes an approach on how flexible manufacturing automation can support the initiative for greener foundries.

Keywords: Foundry Automation; SME; Mechanization; Modernization; Robot operated Centers; EOAT, Fettingling.

Introduction

Foundry Automation has been a leading trade mark well known in the foundry field all over the world for 30 years. Automation of foundry processes is a technological innovation that improves the quality of molds and castings, reduces production costs and improves productivity and working conditions. An increasing competition in the foundry market focuses on more efficient methods of production. High quality and efficiency requirements, but also rising labor costs, will make the foundry production largely automated. [6] Foundry Automation means high quality and reliability in engineering and manufacturing of core-shooting machines suitable for all processes (Cold-Box, Hot-Box, Shell-Moulding) as well as turn-key and robot-operated core-making plants dedicated to the production of core packages for engine blocks, cylinder heads, ventilated brake discs, hydraulic valves. [5]

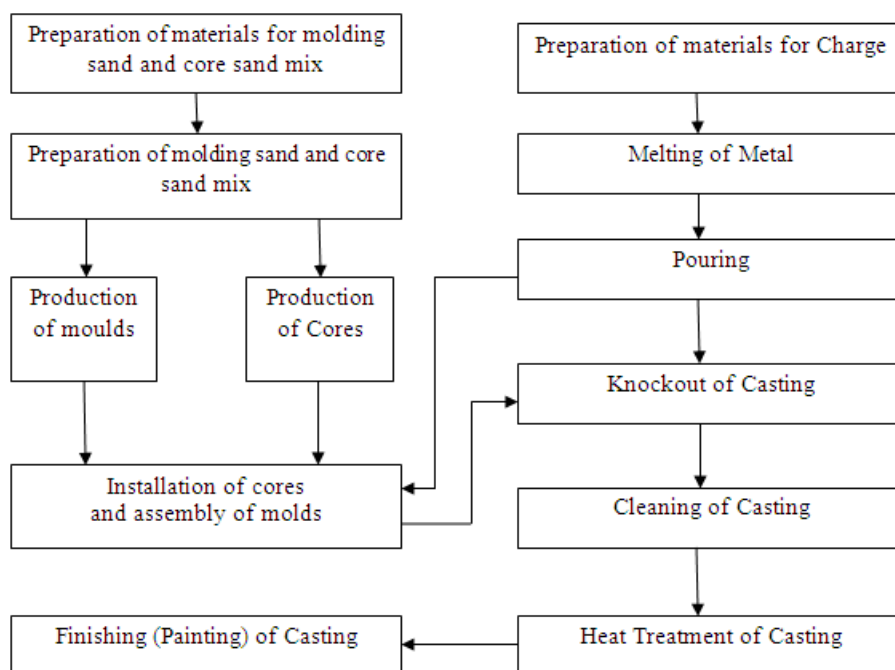


Fig. 1. General sequence of operations performed in foundry.

Persons engaged in foundry industry have to lead a very hazardous life because of the unhealthy atmosphere prevailing inside a foundry. There is thus a vital need for modernization in this particular field of industry. Measures that lead to increased production, improved quality and reduction in production costs, measures that aim to improve working conditions with an eye to ensuring a safe, healthy and happy life for the worker deserve both modernization and mechanization. Individuals engaged in foundry pouring process may tire as a grueling day wears on. For example, if a manufacturer pours 100 lb. of metal an hour spilling 10% over the course of an eight-hour shift, and operations run 24 hours/day, 365 days/year, a manufacturer can lose over 40 tons of metal per year — wasting hundreds of thousands of dollars of metal.



Fig. 2. Manual molten metal pouring process in traditional foundry.

The foundry industry is primarily made of SME (Small and Medium Enterprise) businesses with unique product and process combinations limiting their ability to develop and implement automation technologies. Foundry SMEs in particular are in need help from automation technology, and some of the reasons are as mentioned below:

1. Foundries are intensive in manual labour.
2. Sand cast parts have high variation in parts, due to multiple environmental variables such as temperature of molten metal, metal solidification defects etc. which is a huge detriment to automation.
3. The extreme environmental working condition of foundries necessitates the need for automation.
4. HSE issues in foundries are an important driver for automation in the foundry as well.



Fig. 2. New automated moulding capability has helped foundry achieve greater flexibility for its pattern changes, which has improved its customer service.

From above it is easy to notice that the first, third and fourth drivers are the main reasons supporting automation of foundries. [1] The true potential of flexible automation is now being better realized to help the foundries stay competitive in global competition.

2. Automation of Existing Foundry Equipments

Automation is a further extension of mechanization and involves adoption of automatic controls for the operations of different machines. This automatic control may be adopted for only a few operations or all the operations of a machine and accordingly the machine will be known as semi-automatic or fully automatic. Also, it may be adopted only for a single machine out of the whole lot or a series or group of such machines, depending upon the operations required for the product. Every machine carries some automation, may be to a lesser degree or higher. The extent to which it is applied is largely governed by economic considerations. It is a closed loop system in which feedback is provided by the sensors.

Automation is used to reduce the dependability over manpower. Automation of existing foundry equipments right from the muller, mixer to the automation of sand coating plants. Automation could be employed in intensive mixer, sand mixers, sand mullers, molding lines sand coating plants with batching system, automatic sand weighing and batching system, Blistering temperatures, metallic dust, and molten materials - foundries are harsh work environments. They're also one of the newest frontiers for robotic automation.

Typical foundry work includes pouring melted metal into molds, transferring the molds, breaking metal parts from their molds (degating), and sanding/deburring the final parts - all applications robots excel in. Like many other industries, foundries are constantly on the lookout for new ways to boost their productivity, cut costs and increase quality. Benefits of employing automation with robot technology are: lower production costs and scrap rates, increased up-time and consistent, superior quality.

Table 1. *Process employing automation.*

Sand Core Process	Casting	Cleaning
Core shooting	Die-casting	Deburring
Core assembling	Sand-casting	Deflashing
Core gluing	Gravity-casting	Degating
Core cleaning	Lost-foam	Pre-machining
Core handling		

3. Modernization

Modernization of foundries include: (1) changing over to better and newer foundry equipments; (2) employing newer, better and more economical moulding, melting and casting techniques; and (3) creating conditions which do not make a foundry dirty, dusty and smoke-filled, i.e., improving working condition in foundries, providing adequate illumination, air circulation, dust extraction etc.

3.1. Advantages of modernization

Modernization when properly planned carries several advantages which include the following:

1. Improving quality of the casting.
2. Boosting production.
3. Reducing production cost.
4. Increasing safety to the workers.
5. Making working conditions pleasant and less tiring.
6. Building up morale of the workers.

4. Mechanization

Mechanization implies an endeavour or trend towards minimizing the human efforts, to the extent it is possible by adopting mechanical means or methods for different processes previously performed by hand. [2] Such a trend may be in material handling, loading and unloading of components, actual operations done on the job or transportation, etc. But, no feedback is provided by the process, operation or machinery.

Machinery may be used for preparing sand, moulding and core making, pouring, material handling and many other similar conditions. The extent to which a foundry can be mechanized depends upon the quality and type of production. For small orders as well as for the production of large-sized castings, mechanization is both uneconomical and unpractical. On the other hand, a foundry making automobile parts, electric motors, and similar others where the jobs are of a repetitive nature, mechanization is economical and practical.

4.1. Area of mechanization

Mechanization has a distinct impact on areas concerned with the preparation and control of sand, moulding and core making, melting and pouring, shake-out operations, material handling, and the control of dust and fume.

1. Sand preparation unit. The sand preparation unit consists of a magnetic separator which removes iron particles from return sand, a auto-riddle which rids foreign materials, a muller which kneads the sand for re-use and aerator which helps to improve the flowability of sand, and a hopper which acts as storage for sand before it is sent for mulling.
2. Moulding and core making unit. This unit uses a large number of different types of moulding and core making machines. The extent to which these equipments can be used depends on the nature of production.
3. Melting, pouring and shake-out unit. It consists of various types of melting furnaces, mechanical charging devices for furnaces,

mechanically operated ladles, cranes, lifting tackles, conveyors and vibrating shake-out mechanisms, etc.

4. Material handling unit. This unit includes various types of material handling equipments such as belt conveyors, apron conveyors, flight conveyors, reciprocating and oscillating conveyors, roller conveyors, bucket elevators, mono-rail hoists, different types of cranes and many others for transportation of sand, moulds, cores, molten metal, castings and raw materials required for production.
5. Dust and fume controlling unit. This unit consists of a well-designed dust and fume collector which can clear the polluted air and maintain hygienic working conditions. This includes filter, cyclone, centrifugal dust collector, scrubbers, etc.

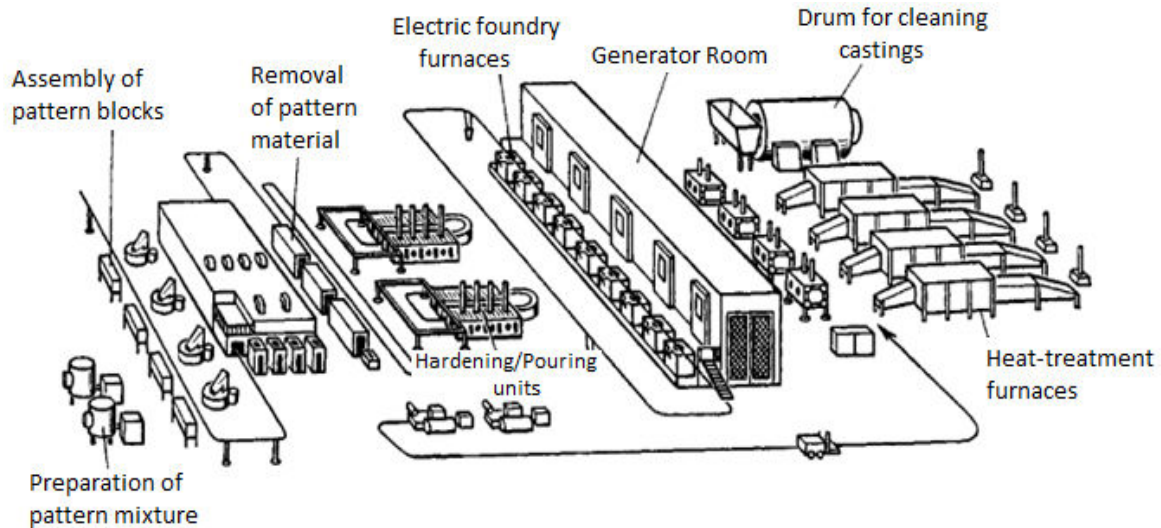


Fig. 3. Fully automated foundry for lost-wax casting.

Fig.3. shows an automated line for medium moulds with pattern circulating facility, semiautomatic pouring and secondary cooling. Manufacturing automation can enable the foundry SMEs (Small-to-Medium manufacturing Enterprises) to be economically and environmentally sustainable. [3] Foundry industry has significant challenges in the current regulatory and political environment with developing an economical and environmentally sustainable business model. Today, because of metal recycling, most foundries consider themselves as green. In reality, the foundry industry has yet to achieve the higher level of sustainability that the future will demand.

4.2. Advantages of mechanization

Mechanization when properly planned carries several advantages which include the following:

1. Increased production from a given foundry floor space and higher productivity.
2. Production of castings that possesses a higher degree of accuracy, closures tolerance and better surface finish.
3. Enormous saving of time and labour since all operations are carried out mechanically.
4. More hygienic and healthy working conditions and improved job satisfaction.
5. Minimized casting defects.
6. Reduced production cost and higher profits.
7. Increased earnings of the workers.

5. Application of Computers in Foundries

Computers are being used in every field these days and foundries cannot be an exception. In conventional practice, the failure rate of castings is high. Computer simulation minimizes the failure rate to a huge extent compared to manual production. Manual inspection of cast products is quite time consuming and there will be chances that a worker may not identify a defect. By using sensors, quality inspection may be done very easily and in less time particularly for mass production of castings. Hence, human interference can be eliminated. Application of computers in foundries helps to develop a product directly from an existing product, when no other data on the product like design sketch, material used and others are not available. It also reduces wastage and rejection rate and facilitates continuous research and development. [7] Some of the advantages of computer application are listed below:

1. Animation advantage: better imagination and presentation
2. Simulation advantage: predicting complicated outputs like flow of molten metal, possible obstacles, stress and strain, solidification sequence, chances of defects, and complex calculations like stress analysis are done in a fraction of second.

3. Database advantage: facilitates Research and Development. Computer can suggest alternative materials and design options from its inbuilt database to save cost, weight, size, availability, and to vary properties.
4. Communication and networking advantage: better history management, collecting order and feedback, easy interacting with team members, and better customer support.
5. The machine advantage: using simulation Software Packages in foundries. Simulation software's are generally known as CAD/CAM/CAE tools. Some of them are CATIA (Computer Aided Three Dimensional Analysis), It is a highly versatile package, which assists in almost all kinds of design such as drawing production, mechanical design, machine parts, sheet metal designing, free style shaper, hybrid design, structural analysis, mold and die casting design, prismatic machining, manufacturing plant layout, and so on. Unigraphics, Solid Edge, Pro E, and iDeas are already developed software packages. IDEas package can optimize design at early stages, which greatly improves product quality while reducing time and cost. Solid Works can create geometry, refine features of a part, make drawings, model trajectories of cutting tools, and develop numeric control.

5.1 Robot-Operated Centers

Metal casting industry expands globally but shrinks domestically. Like many other industries, foundries must be looking constantly for new ways to boost their productivity, cut costs and increase quality. Robotic automation is one of these. Robots can provide foundry floor production capability that allows the operators to respond effectively to global pressures and future market changes. Although difficult to measure, this capacity has a clear economic value. A robot can be reprogrammed and retooled so that it can be a valuable tool as customers' needs change. An automated foundry work cell will reduce direct labor and related cost and reduce the requirements for employee services and facilities.

Foundry units adopt automation as manpower shortage rises. Foundry industry is now moving towards automation amid rising manpower shortage. Moreover, the customer demand has prompted the foundry units to go for automation. Most of the foundry units have gone for automation depending upon their financial conditions. Some units that have capacity for high investments, converted their unit into fully automatic, while others are doing technical changes, Typically, investment worth Rs 20 lakh to Rs 5 crore is needed for automation in foundry units.

Traditional casting methods do not have the flexibility to cast wheels, engine/transmission components, structural components, and more complex parts with thinner walls. Robotics can help to improve quality, consistency, and profitability. Foundries are a complex and demanding work environment. The automation of specialized tasks requires detailed process know-how and the right hardware to handle castings and cores with power and precision, including Core shooting, Core assembling, Core cleaning, Core handling and placement, Ingot handling, Ladling, Deburring, Pre-machining, Inspection/x-ray/leak testing. [10]

Labor saving is not the only advantage in robotic ladling. Automated ladling can reduce a metal caster's material costs in two ways:

- By creating products with greater metal integrity, less metal will be needed to be re-worked, reducing wasted throughput time.
- Robotics minimize the amount of spilled metal, because they pour more consistently than individuals can.

5.2. Robotic Automation

Robotic automation is ideal for foundry use. Because it contains several benefits and eliminated limitations of traditional foundries.

Powerful Design:

Heavy payload capacities and wide work envelopes allow robots to tackle the heavy lifting and wide loads common in foundries. With robotic automation installed in a foundry, workers are saved from harmful repetitious movement and the strain of lifting heavy parts.

Safety: Foundries are known for being extremely hazardous. Human workers deal with the continuous threat of burns, heat exhaustion, repetition injuries, or breathing in metallic dust. Foundry robots are required to have an industrial protection rating. They can endure the hazards with ease and work without fatigue. Even when the heat is extremely intense, robotic EOAT (End of arm tooling) can be safeguarded.

Savings: Incorporating robotic automation in your foundry conserves money and time. With robots, there is less of a chance of dropping or damaging parts. Fewer accidents mean less financial output as well. Since foundry work is taxing and hazardous, there can be a high turnover of workers. Robotic automation eliminates this challenge because it's quick and easy to program robots. Robots work without breaks or vacations - saving companies and increasing productivity. Unlike their human counterparts, they don't need to rehydrate periodically.

Accuracy: Robotic automation offers top notch repeatability. This is extremely important when it comes to handling molten metal. Every movement is programmed every point exact. When it comes to deburring or sanding, robotic provide the precision necessary.

Flexibility: Robotic automation gives foundries flexibility. Robots can handle a wide range of applications - from material removal and grinding/sanding to pick and place and dispensing. Using automatic tool changers they can switch quickly between tasks, which leads to simplified, faster production.



Fig.4. Automation of foundry with Robot [8].

In investment casting Dipping wax trees in water based slurry to continuously build the ceramic shell with special sand, is a process in investment casting that is often robotized. Furthermore, robots are frequently used for post processing applications such as grinding and polishing. Ingot handling is an application found in casting shops where ingots are produced. When it comes to handling, robot is the perfect tool for the task: it comes equipped with a special purpose Pneumatic gripper for handling the solidified ingots and features a high payload.

7. Automatic Fettling

Hand-held tools such as grinders and chipping hammers, or fixed tools such as pedestal grinding machines, and band-saws are traditionally used to remove the unwanted metal. Automatic fettling is an initiative for a safer and cleaner foundry. Automatic fettling can be implemented very simply. [4]

Much of the fettling is now done with a fully-automated robot-based machine. The castings are mounted on special fixtures and placed onto a conveyor system. A robot arm then picks up the fixture and manipulates the casting so that the unwanted material is removed by large grinding and cut-off wheels. Machines called 'snag grinders' help automate the fettling process. Snag grinders are horizontal milling machines that have a grinding wheel in place of milling cutters. [10] These machines are constructed in a way that the grinding of two faces can take place at once. Grinders are also quieter than the conventional clippers, thus helping address the issues of noise pollution. The control sequences are pre-programmed, so all the operator has to do is mount the castings onto the fixtures.



Fig.5. Inside the fettling machine showing a casting mounted in a fixture and the grinding wheel.

The primary benefits of automated fettling include:

- Safer working conditions for operators through elimination of hand tools
- The operators are not exposed to any vibration.

- There is improved productivity, better ergonomics and more consistent quality.
- There is reduced exposure to noise, dust and fumes.

Many factors have to be considered-high on-time performance, short cycle time and low cost manufacturing. In addition, the operation and safety environment should also be well designed for AGVS.

8. Conclusion

Foundry customers such as marine, automobile etc. are placing demands on founder's responsibilities towards environment, and these demands are increasing every day. High level of automation in foundries helps substantially boost manufacturing competitiveness. Many innovative solutions aimed at sustaining the foundry industry have included use of flexible automation equipment, measuring energy consumption by automation and handling equipment etc.

References

- [1] S.K.Hajra Choudhury, A.K. Hajra Choudhury, Nirjhar Roy, "Elements of Workshop technology", Vol – I, Fourteenth Edition (2007).
- [2] B.S. Raghuvanshi, "Manufacturing Science", Dhanpat Rai & Co Publication, 1st Edition (2013).
- [3] Rhythm Suren Wadhwa, Terje Kristoffer Lien, N.T.N.U., Valgrinda, Trondheim 7491, Norway, Manufacturing Automation for Environmentally sustainable foundries, 20th CIRP International Conference in Life cycle Engineering, Singapore, 2013.
- [4] Prashant Mistry, Fettleing the most ignored operation in foundries, Mahindra & Mahindra, Automotive Division.
- [5] Rhythm Suren Wadhwa, "Flexibility in manufacturing automation: A living lab case study of Norwegian metalcasting SMEs", Journal of Manufacturing Systems, Volume 31, Issue 4, October 2012, pp. 444–454.
- [6] A. Misztal, M. Butlewski, A. Jasiak, S. Janik, "The human role in a progressive trend of foundry automation", Metalurgija 54 (2015) 2, 429-432.
- [7] Dr Thoguluva Raghavan Vijayaram* and Dr Paolo Piccardo**, "Computers in Foundries", Metallurgical Science and Technology, Vol. 30-2 - Ed. 2012, pp. 28-38.
- [8] Brian W. Rooks, (1996) "Robots at the core of foundry automation", Industrial Robot: An International Journal, Vol. 23 Iss: 6, pp.15 - 18
- [9] Rhythm-Wadhwa¹, Terje-Lien², "Electromagnet Gripping in Iron Foundry Automation Part I: Principles and Framework", International Journal of Computer Science Issues, ISSN (Online): 1694-0814, Vol. 8, Issue 6, No 3, November 2011, pp. 47-51.
- [10] [http://www. Foundryinfo-india.org](http://www.Foundryinfo-india.org)
- [11] [http://www. Foundrymag.com/feature/robotic-automation-mold-foundries](http://www.Foundrymag.com/feature/robotic-automation-mold-foundries)

Automatic Copper Tube Straightening and Cutting Mechanism

Himanshu K Barot^a, Manthan D Upadhyay^a, Hardik R Patel^a

^aGandinagar Institute of Technology, Gandhinagar, India

Abstract

The main focus of this paper is a development of manual to automatic copper tube straightening and cutting, which is able to decoil the copper tube roll, making it straight and cut at the desired length with precision accuracy and a soft end edge. The design of the machine is inspired from a small manual copper tube cutting hand tool and straightening pulleys arranged in a zigzag position, going to fully change the whole manual cutting process and straightening process into a combined single line automatic process. The design consists of a roll table, straightening pulleys arranged in a zigzag, holding pneumatic fixtures, a belt with a servo mechanism for pulling tubes from a large roll & main rotary cutter portion. The machine consists of a pneumatic mechanism for holding of the tube and a servo mechanism for pulling and measurement purpose for cutting tubes into the required length with precision accuracy. The design is fully reliable and is able to be modified simply for cutting other diameter tubes by shifting of pneumatic fixtures position which have other size holes, and is also able to be put and changed whole fixtures which is portable. So, with automation in copper tube cutting, there is a reduction in lead time & delivery time. Also, the automatic machine doesn't have the need of human effort so that a worker can be allotted to do other work, so there is cost saving and reliability of workers.

Keywords: Automatic Copper Tube, Tube Straightening machine, Copper tube cutting mechanism.

1. Introduction

Manufacturing of Air Handling Units (AHU) is being increased due to their demand in all thermal products. An air handler as shown in fig.1 (a) is a device used to condition and circulate air as part of a heating, ventilating, and air-conditioning (HVAC) system. An air handler is usually a large metal container containing a blower, heating or cooling equipment, filter racks or chambers, sound attenuators, and dampers. Air handlers usually connect to a ductwork ventilation system that circulates the conditioned air through the building and returns it to the AHU. Sometimes AHUs supply and return air directly to and from the space served without ductwork.

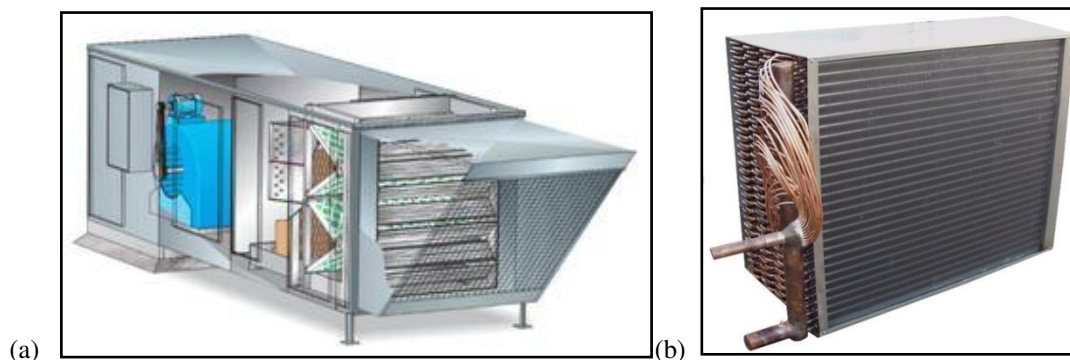


Fig. 1 (a) C/S of Air Handling unit (b) Cooling Element – Condenser Coil

A condenser coil shown in fig.1(b) is one of the many types of heat exchangers. The main purpose of a heat exchanger is to efficiently transfer heat between two mediums. Condenser coils are found in space heaters, air conditioners, and car radiators. Although there are bit differences in the function of these devices, the purpose is the same. The term condenser coil can be used to describe all heat and cooling systems. Air coils are a subset of the heat exchangers and are found in air conditioning units. The condenser coil itself has a snake-like shape.

1.1 Problem Summary

AHU assembly manufacturing, they need condenser coil as part of sub assembly in more numbers of unit quantity. Condenser coils comprise copper tubes of same dimension in parallel placed & supported with thin Steel Metal plates as fins around copper tubes and used for separate flow directive of atmospheric or forced air flowing around it.

In Cutting of Copper tubes, company presently using manual cutting using small & compact rotary cutter as shown in fig.2 which has manual effort of human workers relates to their limited work efficiency of daily cutting of copper tubes. Copper Tube Diameter used in Industry (Most preferable): 3/8", 1/2", and 5/8"

* Himanshu Barot Tel.: 8347557624

E-mail address: Himanshu.barot@git.org.in



Fig. 2 Manual rotary cutter

1.2 Interrelated/Sequential Problems with Manual Cutting of Copper Tubes

- 1) Manual Cutting of copper tubes with simple rotary cutter by human workers with limited workability of human power for daily cutting of number of tube pieces from approx. 100-120 kilogram of copper tube roll.
- 2) It leads to limited number of manufacturing condenser coils around 100 coils per month.
- 3) Further leads to limited number of manufacturing Air Handling Units(AHU).
- 4) All above factors affects Overall Production Rate of AHU. Which lead to decrease in production rate.

2.Design

To prepare design solution to convert manual to automatic, copper tube straightening & cutting machine. This will be facilitating to cut copper tubes in desired length and numbers without burring. The purpose of designing this machine will satisfy the following objectives.

- To reduce the waste of human workers
- To reduce material wastage
- To increase accuracy
- To reduce lead time of production
- To reduce cost of production
- To reduce delivery time
- To increase production rate
- To make free worker & allots to do another work
- To increase reliability of plant & workers

2.1 Functional Assembly Design

For those utilities to manage all works on single table with portability, concept had been papered for preferred and optional mechanisms for each and every single motion and operation. Possibilities have been selected prior of desired mechanism. Afterward 3D functional model with CAD utility were prepared for showing desired operations and motions with visual and graphical functional model as shown in fig.3.

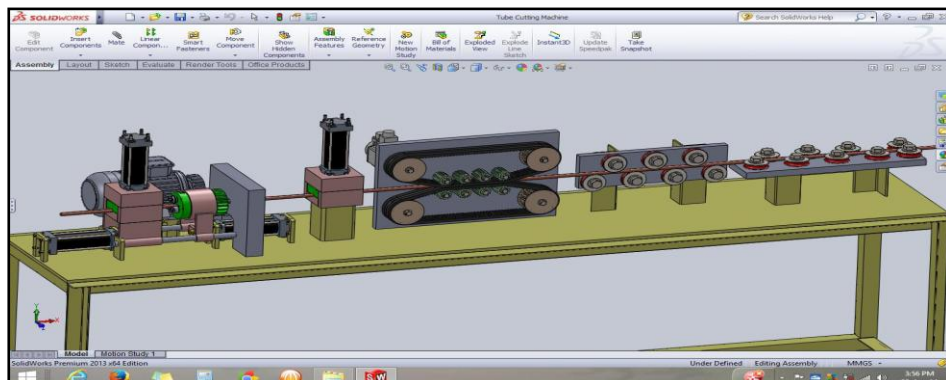


Fig .3 Overview of Assembly

2.2 Cutter Assembly

Rotary cutter assembly as shown in *fig.4 (a)* (It's transparent view as shown in *fig.4 (b)*) is main part of this design assembly because of its auto continuous functionality. Cutter comprises main part as Impression cutter, supporting roller, Allen Bolt, key with head and sliding hollow cylinder. Rotary cutter assembly is driven operated by simple electrical DC/AC motor with belt driven mechanism. Rotary cutter do only impression of approx. 1 mm in copper tube and afterward it is break at desired surface where impression done by pulling or dragging tube in tube passing direction by pneumatic fixture with pneumatic cylinder operated step motion.

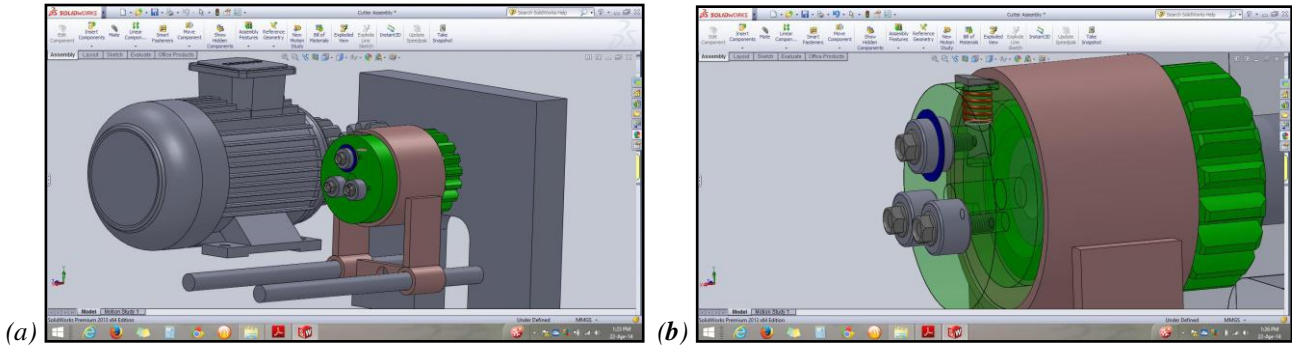


Fig. 4 (a) Rotary Cutter Assembly with Electric Motor (b) Transparent Shaded View of Cutter Plate

2.3 ImpressionCutter/roller

Impression Cutter consist of simple roller with simple small & thin plate mounted on it as shown in *fig. 5(a) & (b)*. Impression Cutter do only impression of approx. 1 mm in copper tube and afterward it is break at desired surface where impression done by pulling or dragging tube in tube passing direction by pneumatic fixture with pneumatic cylinder operated step motion. Impression Cutter/Roller rotates on its axis also with around main center axis of whole cutter assembly.

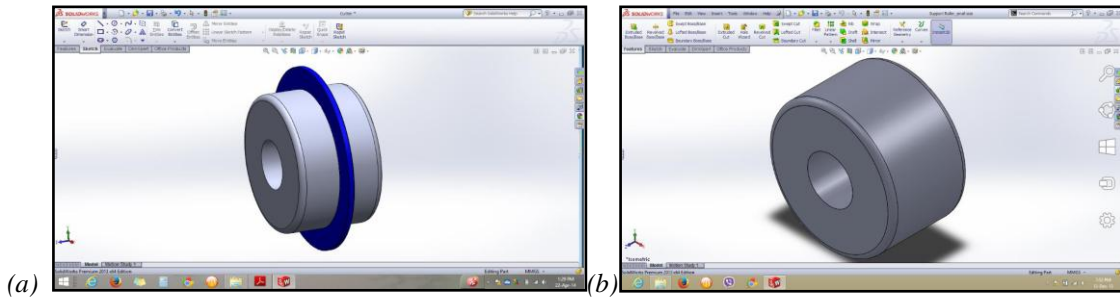


Fig.5 (a) Impression Cutter/Roller (b) Support roller

3. Automation Tools

Automation is the use of various control systems for operating equipment such as machinery, processes in factories, boilers and heat treating ovens, switching in telephone networks, steering and stabilization of ships, aircraft and other applications with reduced human intervention. The main benefit of automation is that it saves labor. It is also used to save energy and materials and to improve quality, accuracy and precision. The term automation, inspired by the earlier word automatic, was not widely used before, when General Motors established the automation department.

Automation can be achieved by various means including mechanical,hydraulic, pneumatic, electrical, electronics and computers, usually in combination. Complicated systems, such as modern factories, airplanes and ships typically use all these combined techniques.

3.1 Solution by Automation Line-Up

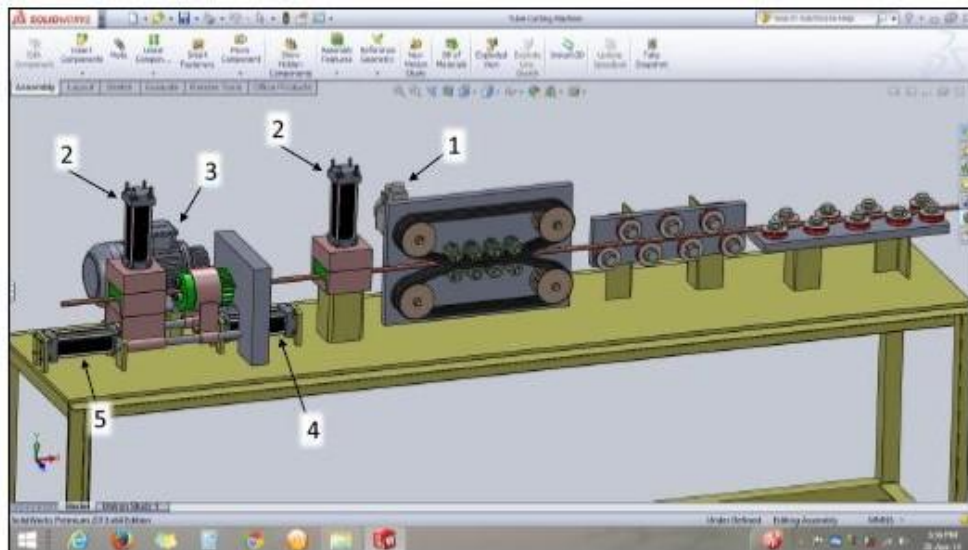


Fig.6 Setup layout

All automation run with PLC, Electronic Pneumatic flow controlled valves & asynchronous Motors. When new coil for straightening & cutting purpose was applied, first its first end exact up to sensor touch point of Large pinion attached with stepper/geared motor should be drag out so that, distance from that point to touch point of impression cutter is added in programming by default as negative length for making useful first cut. After that cut all lengths are as per user input.

So basically stepper motor rotates some round as per PLC input to drag required length of tube. After that it stops. When Stepper motor stops, PLC gives input to Electronic Pneumatic flow controlled valve for holding the tube in fixtures. With vertical Pneumatic cylinder by providing controlled flow of air pressure to move inner wall up and down which is connected with fixture blocks. When tube is been hold by pneumatic fixtures, PLC gives input to 3-phase DC Asynchronous motor to rotate rotary cutter assembly unit supported on shaft with foundation.

As shown in *fig.6* Where 3 small rollers (2 support rollers & 1 Impression roller) are also rotating with Cutter flange rotating. In this current situation, PLC gives input to Electronic Pneumatic flow controlled valve which operates horizontal pneumatic cylinder which steps forward with Hollow cylindrical cover plate. When cover plate goes forward, it presses key (Consisting slant top face) to downward which is connected with impression roller. And this impression roller is also rotating around tube with cutter flange. So, it created 1 to 2 mm circular sharp groove in tube at the point at which we want to cut but it's not cutting the tube at that situation.

In this current situation, PLC gives input to Electronic Pneumatic flow controlled valve which operates horizontal pneumatic cylinder which holding front fixture assembly and goes step forward to break the tube at grooved point by applying tensile loads. After breaking tube, both horizontal cylinder acts to step backward both cover plate and front fixture assembly for next repeat process.

Conclusion

This designed machine solution is Special purpose machine solution, but at implementation parallel mounts cutter and pulleys can be added for using same electric & pneumatic power source for more size tubes. With manual cutting of tubes, inward bended and sharp edges of tubes can be achieved. But here all edges will be soft and straight due to back process of tensile forces. Here, no cutting exists; tube is cut by breaking of it at desired edgepoint. One more important mechanism is of drawing tube using Belt with rubber overlap at outer face of belt with half circular groove. It keeps very low cost of overall assembly & no need of ball screw with fixture mechanism which is available in present retail solution.

References

- [1] Larry F. Babb, Emerson Electric Co., St. Louis, United States, 2000[us6393700b1]
- [2] David Grimbaldi, Crystal Lake, New Jersey, United States, 1950[us2622323a]
- [3] Eugene R. Capewell, Moorestown, New Jersey, United States, 1947[us2515627a]
- [4] Petersen Thorvald, Erie, Pa, Unites States, 1940[us2283572a]
- [5] Condon Ernest E., Hermanville, Md, United States, 1946[us2448578a]
- [6] Kenneth E. Thompson, Tulsa, OK, United States, 2006[us8297586b1]
- [7] Yoshiyuki Kuroiwa, Kouichi Kuroda, Tomio Yoshiyuki Kuroiwa, Kouichi Kuroda, Tomio Yamakawa, Sumitomo Metal Industries, Japan, 2012[us20120304724a1]
- [9] Wilhelm Prof. Dr.-Ing. Guericke, Wilhelm Dr. Ing. Heller, London, 2000[ep1201329b1]
- [10] Kenneth W. Stalker, Western Spring III, Goodman Manufacturing Company, a corporation of Illinois, Chicago, 1963[us3217554a]
- [11] Pneumatic cylinder control assembly, Hoge. NerJW.900 S

Review paper

Vacuum System : Components , Performance & Applications.

Mr .Viral Bhachech^a, Prof. Kuldip Dodiya^a , Mr. Anil Mankad^b

^aGandhinagar Institute of Technology, Gandhinagar, India
^bDirector – Joyem Engineers & Consultants Pvt. Ltd.

Abstract

The review introduces the Vacuum Systems; it shows the detailed understanding of vacuum pump, shell & tube heat exchanger as well as plate heat exchanger as individual components. Vacuum pump principle and working is explained along with its advantage in the industries. The effect of components of vacuum system like vacuum pump, and piping volume effecting the selection of heat exchanger for correct and trouble free running of the vacuum system is briefly discussed. This paper is attributed to the use of such vacuum system in industries and how it is useful in making the processes more time effective and efficient. The review of vacuum system and applications of vacuum has been made to emphasis the use of this process efficient system in industries.

Nomenclature

mm Hg. =millimeter of mercury

Torr =unit for vacuum measurement

Bar = Pressure unit

Vacuum refers to the zone of pressure below atmospheric pressure. It has no perfect definition it just represents the emptiness of air. There is a pressure which is exerted on us by atmosphere, its value is standard measured as **1.01325 bar OR 760 mm Hg.** lowering the pressure below this value means creating vacuum, It is very useful in industries, varied applications of vacuum are as follows;

- In food processing & beverage industries for drying, deodorizing purposes.
- In dairy industries for making milk powder, making cheese, under vacuum sterilization.
- In chemical industries for evaporation, distillation, deodorization etc.
- In Pharma industries for evaporation, API Plants, bulk drugs, formulation etc.
- In paper industries for drying of paper, cardboards.
- In textile industries for decadizing, drying of cloth etc.
- In confectionary industries for manufacturing of candies, chocolates etc.
- In breweries for alcohol manufacturing.
- In thermal power stations for condenser exhaust, waste oil refining.

Vacuum pump^[1]

Vacuum pump is device which creates vacuum

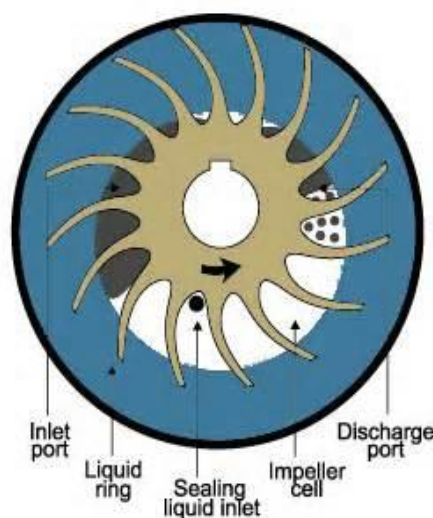
Vacuum is generated by the evacuated portion created by centrifugal action of eccentrically mounted rotor or impeller in the vacuum pump. This principle is for water ring vacuum pump.

The water ring is formed by the rotating impeller in the casing which creates the region devoid of air in the central portion which entrains the surrounding air to fill and thus suction force s developed obtained with the help of the ports provided in the control plates.

Vacuum pump is mounted such that vapors or the air from the process enters the vacuum pump and the same is discharged on the other end, normally at the discharge end, a separator tank is provided which separates water from the air or gas.

The vacuum pump construction consists of following parts

Impeller, Casing, Control plates, Bearing cover, Shaft ,Side Cover .Vacuum pump can be coupled with various devices to boost up & maintain the continuous vacuum. This advantage makes it possible for using vacuum pump in many critical processes.



Vacuum system

The vacuum pump when coupled with Twin Lobe Roots Booster the vacuum level of vacuum pump increases. Vacuum system is a combination of following components;

- Twin lobe Roots Booster
- Vacuum pump
- Intercondenser or Heat Exchanger (This is generally a shell & tube condenser)
- Suitable piping between various components.
- Suitable valves & gauges.
- Recirculation system (Optional)
- A common base frame over which the entire system is mounted.

Twin Lobe Roots Booster^[2]

Booster is a construction made up with the assembly of lobular rotor mounted with the help of gears on either end enclosed in the suitable shaped casing; The rotors are duly balanced and mounted on the shaft with the alignment on the gear wheels. The bearings and the gears are normally oil cooled on the drive end and non drive end.

A lobular construction can be available in twin lobe eight shaped structure, in mechanical booster system this serves to carry the load at the same time reducing the excess load on backing vacuum pump, and increasing its vacuum and efficiency with same power.

The booster can be operated in directly coupled drive with motor or else to make the beltdriven arrangement in the same. Very good load handling can be done with homogenous vacuum generation.

Intercondenser(Heat Exchanger)

It is provided between the mechanical booster discharge and vacuum pump suction, it can be a shell & tube heat exchanger or a plate heat exchanger with the capability of cooling down the suction vapour to the acceptable limit of 40 degree Celsius near the suction of the vacuum pump.

The intercondenser serves the purpose of maintaining the acceptable temperature of the vapours that are coming in the vacuum pump; it in turn regulates the vacuum in the system as the amount of vacuum generated depends on the temperature maintained.

Intercondenser area is decided/selected based on the vacuum pump sealing water temperature required, availability of cooling water as well as the process in which the vacuum system is employed. It is an inevitable component in the vacuum system.

Shell & Tube Heat Exchanger:

Currently the fixed tube sheet type shell & tube condensers are widely used in the mechanical booster system due to their lower initial cost, ease of maintenance, also the performance of the same is satisfactory as intercondenser as well as pre condenser.

The standard material of construction used are carbon steel for shell and stainless steel for the tubes and tube sheet design, A sturdy construction helps such condensers maintain in few adverse process conditions in the acidic conditions also.

Plate Heat Exchanger:

Plate Heat exchanger is generally employed in Cleaner applications but the same can also be used in Vacuum System also for Effective Heat Transfer due to many advantages offered like that its Compactness, Competitive Cost compared to Shell & Tube Heat Exchanger.

In Vacuum System It can be used as Intercondenser as well as Pre Condenser. The preventive maintenance is easier in PHE compared to shell & tube heat exchanger due to modular designs.

Mechanical Vacuum Booster System

Apart from all of the above there are various other parameters like that of the altitude of the place, its location, ambient conditions etc. on which designing is based.

The principle of using the mechanical booster backed with positive displacement vacuum pump is used in various industries for achieving many products, the possible outcome are discussed in the literature survey about the same,

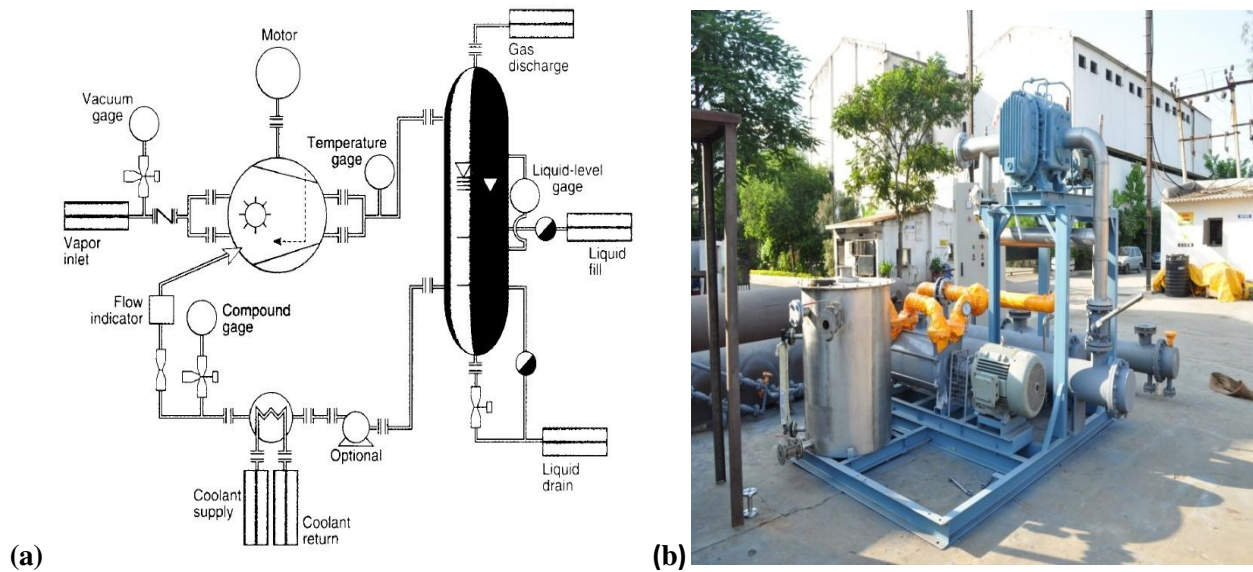


Fig.1. Illustration of Pressure Particles for (a) **Vacuum Pumping Process** and (b) **Mechanical Vacuum Booster System**^[3]

5. Review for Vacuum System

➤ **HM Akram** Online ISSN: 2249-4596 & Print ISSN: 0975-5861^[4]

This research paper discusses the proper guidelines highlighting key criteria for selecting an appropriate vacuum pump; supportive for proper vacuum production has briefly been discussed that can make the task of pump selection simpler and exact.

There are three main types of Vacuum Pump, They are;

1. **Positive Displace Pump.**
2. **Momentum Transfer Pump.**
3. **Local Entrapment Pump.**

There are various criteria's on which the Vacuum Pump is selected; the same can be discussed as follows;

1. Required vacuum in the process.
2. Time required for doing the vacuum
3. Volume to be evacuated
4. Temperature range in which it is working
5. Capital & maintenance Cost of the vacuum pump
6. Suction pressure to be handled

It is also depicted in the paper about the use of lobe pump or mechanical booster along with a backing pump for the faster evacuation of a larger volume in the medium vacuum range.

➤ **Vishal Chaudhary & Avinash Desai** ISSN 2229-5518^[5]

In this paper theoretical procedure for calculating pump-down time is explained for the given pressure and configuration of the system. These theoretical calculations are compared with the actual observations taken from the system.

The paper discusses the experimental and actual variation in the performance of vacuum system with respect to time.

Here the vacuum pump down time (i.e. Evacuation time) is measured taking the following variables into account,

- Conductance for air & gas.
- Mean effective pressure required
- Effective pumping speed
- Volume of the space
- Actual atmospheric pressure of the location
- **Ass Prof. Mr. RL Patel et. AISSN: 2321-9653 / IJRASET^[6]**

This research paper is to study & improve the performance of vacuum pump through CFD analysis.

Water Ring Vacuum Pump was numerically simulated and compared with experimentally measured data .To Improve the Efficiency of Water Ring Vacuum Pump.

The mesh of twelve bladed water ring vacuum pump impeller domain is generated using **ANSYS Workbench** detailed CFD analysis is used to predict the flow pattern inside the impeller which is an active pump component.

Paper is dedicated to the CFD approach for the working and analysis of vacuum pump.

- Experimentally result of vacuum level of the pump is **450 mm of Hg** which is after **CFD** analysis **460 mm of Hg**, so deviation is **2.25%**.
- This paper refers to the use of **CFD** analysis in the pump industry to develop and to improve performance of various pumps.
- A difference of **2.25 %** from the experimented results compared to analytical CFD results of vacuum. This validates the **CFD** analysis to be useful in the vacuum pump.

Outcomes of the Literature Review

- The vacuum pump selection is important criteria for the process, its various parameters as well as the procedure, that same are applicable to select the system for a specified vacuum range.
- Vacuum system evaluation & selection for the process based on the time to achieve vacuum, this helps further to study mechanical vacuum booster system.
- CFD analysis based on the actual noted parameters and its credibility , which has validated for its use in further analysis of booster system'

The mechanical booster system is used in large number of application which can be depicted with the industries used.

<i>Application Type</i>	<i>Industry served</i>
<i>Vacuum Distillation</i>	<i>Chemical ,Pharma, batch processes</i>
<i>Vacuum Degassing</i>	<i>Chemical , lab operations, carbon industries, oil industries</i>
<i>Vacuum Dehydration</i>	<i>Food & beverage industry , dairy industry , confectionary industry</i>
<i>Vacuum Drying</i>	<i>Food industry , cold storages, freeze drying, oil cake industry, dry fruits storage</i>
<i>Vacuum Deodorization</i>	<i>Edible oils, Food industry for preserving the natural fruits & vegetables, bio diesel plants,</i>
<i>Vacuum Casting</i>	<i>In investment casting industry</i>
<i>Vacuum Crystallization</i>	<i>Oil cake industry, Dairy Industry</i>
<i>Vacuum Freeze drying</i>	<i>In various cold storage plants , trucks etc.</i>
<i>Vacuum Brake</i>	<i>Railways , sophisticated truck designs</i>
<i>Vacuum Cooling</i>	<i>Low Temperature Cryogenics</i>

Conclusion

Concluding from the literature review various terms are being understood like that of vacuum, capacity, vacuum system etc. The detailed study shows the working principle of Vacuum pump, vacuum system with the individual components.

A brief account of heat exchangers separately have been involved which shows the more use of shell & tube heat exchangers in present vacuum systems.

The Booster Capacity ranges are also known through its detailed understanding. The application of the mechanical vacuum booster system depicts its wide range and the possible power saving through the use of this integrated technology.

Acknowledgements

I would like to sincerely thank all my mentors and guide who helped for the collection of very minor details of all the components. My guide Prof. Dodiya without whom the hierarchical structure would not have been possible. I thank to the company **JOYAM ENGINEERS & CONSULTANTS PVT LTD.** For allowing the research work and use the company records for incorporating the same in the review paper. Last but not the least thank you for the due support of the industry director Mr. Anil Mankad for giving the guidance for the write up.

References

- [1] **Design Principle and Structure from Company** – Special Permissions.
- [2] **Article on Energy saving by mechanical booster system-** By Mr. Anil Mankad –Industrial Products Finder, May 2006 Edition
- [3] **Instruction manual for vacuum system –courtesy M/s. Joyam Engineers & Consultants Pvt. Ltd.**
- [4] **Selection of Precise Vacuum Pumps for the Systems with Diverse Vacuum Ranges-** By HM Akram Volume 14 Issue 2 Version 1.0 Year 2014
Online ISSN: 2249-4596 & Print ISSN: 0975-5861
- [5] **Performance Evaluation of Vacuum System:** By Vishal Chaudhary & Avinash Desai - International Journal of Scientific & Engineering Research, Volume 2, Issue 11, November-2011 ISSN 2229-5518
- [6] **Performance Improvement of Vacuum Pump through CFD Analysis-** By Ass Prof. Mr. RL Patel et. Al-Vol. 2 Issue III, March 2014 ISSN: 2321-9653 / *IJRASET*.

Experimental Investigation of Double Pass Solar Air Heater with Three Obstacles on an Absorber Plate

Prof. Maulik Sukhadiya^a, Prof. Umang Patdiwala^a

^aGandhinagar Institute of Technology Gandhinagar, India.

Abstract

Solar air heaters are used for applications at low and moderate temperatures such as; crop drying, timber seasoning, and space heating. This method substantially improves the collector efficiency by increasing the fluid velocity and enhancing the heat-transfer coefficient between the absorber plate and air. These types of collectors had been designed as a proposal to use an absorbing plate made of aluminum cans into the double-pass channel in a flat-plate to build absorber plates of SAHs at a suitable cost. In the first type (Type I), cans had been staggered as in order on absorber plate, while in Type II they were arranged in zigzag. Type III is a flat plate arrangement with baffles. For the same flow rate, the efficiency of the double pass is found to be higher than the single pass. An efficiency test was used to find the best fin arrangement of the receiver. Air enters the upper channel and lower channel of the air heater flows to outside in the parallel direction. If 2-10 m/s speed limit of air in piping system is assumed, proposed some arrangement of technology enables an efficiency improvement in relation to the mouth pipe arrangement of the solar collector with black paint.

Keywords: Introduction, Experimental setup, Result and Discuss, Conclusion

Nomenclature

m	mass of air [kg/s],
C_p	Specific heat of air [kJ/kg K],
$T_{a, out}$	Temperature at outlet of air [°C],
$T_{a, in}$	Temperature at inlet of air [°C],
I	Solar isolation intensity [W/m ²],
A_c	Collector area [m ²]

1. Introduction

The main applications for SAHs are space heating, drying and paint spraying operations. Numerous SAH devices have been developed and used experimentally [1]. A glass or transparent cover is fixed above the absorber plate and the system is insulated thermally from the back and from the sides. SAHs are simple in design and maintenance. Corrosion and leakage problems are less severe compared with liquid heater solar systems. The main drawback of an SAH is that the heat-transfer coefficient between the absorber plate and the air stream is low, which results in a lower thermal efficiency of the heater. However, different modifications are suggested and applied to improve the heat-transfer coefficient between the absorber plate and air [2]. There are different factors affecting the SAH efficiency, e.g. collector length, collector depth, type of absorber plate, glass cover, wind speed, etc. Increasing the absorber plate shape area will increase the heat transfer to the flowing air, but on the other hand, will increase the pressure drop in the collector; this increases the required power consumption to pump the air flow crossing the collector [3]. The double-flow type SAHs have been introduced for increasing the heat-transfer area, leading to improved thermal performance. Sahu and Bhagoria [4] planned to investigate the effect for different pitch of 90 degree broken wire rib roughness on the enhancement of thermal performance of SAH. Ghoneim [5] investigated the effect of gap thickness on the performance of compound honeycomb using the solar collector. Sadasuke et al. [6] examined the performance of a collector with a flow in the upper channel on the absorber plate as well as in the lower channel. Njomo [6] examined the unsteady state heat exchanges governing the functioning of an unglazed one-pass SAH utilizing a non-porous selective absorber.

Corresponding author Tel.: +91-9428411317, 8347557029
E-mail address: maulik.sukhadiya@git.org.in

2. Experimental setup

A model of the constructed double-flow SAH system of collector is shown in Fig. 2, and photographs of the three different absorber plates of the SAH collector and the view of the absorber plate in the collector box are shown in Fig. 3, Fig. 4, and Fig. 5 respectively. In this study, three types of absorber plates were used. The absorbers were made of aluminium sheet with black selective coating. Dimension and plate thickness for all three collectors were 1m, 1m and 2mm, respectively. Normal wind ow glass of 4mm thickness was used as glazing. Single cover glass was used in all three collectors. Thermal losses through the collector backs are mainly due to the conduction across the insulation (thickness 3cm) and those caused by the wind and the thermal radiation of the insulation are assumed negligible.

The absorbers surface which is the most important part of the SAH consisted of 3 circular cross section airflow channels made of 32 (16_2, upper and bottom surfaces) aluminium cans painted in black in type I and the SAH consisted of five circular cross-section airflow channels made of 50 (25_2, upper and bottom surfaces) aluminium cans painted in black in type II. Each aluminium can was opened on the top and bottom, their surface was cleaned using water. Thermocouples were positioned evenly, on the top surface of the absorber plates, at identical positions along the direction of flow, inlet and outlet air temperatures were measured by two well insulated thermocouples. The output from the thermocouples was measured in degrees Celsius by temperature indicator. The total solar radiation incident on the surface of the collector was measured with a solar power meter. This meter was placed adjacent to the glazing cover, at the same plane, facing due south. The experimental setup was situated at Latitude 23°09'52" N and Longitude 72°26'27" E. The measured variables were recorded at time intervals of 30 min and include inlet and outlet temperatures of the working fluid circulating through the collectors, ambient temperature, absorber plate temperatures at several selected locations and airflow rates (HTCA VM-07 digital anemometer). The air was provided by a blower with a maximum capacity of rpm 16,000 and that can regulate by AC variometer. The blower placed at the outlet of the collector sucked in the air. All tests began at 10:00 AM and ended at 4:00 PM [10].

2.1 Experimental Procedures for Type – I, Type – II, and Type – III

Here in these experiments I was work with the following different conditions: Double pass solar air heater with the aluminium can place in series form [Type-I] Fig.1 (a), Double pass solar air heater with the aluminium can place in zigzag form [Type-II] Fig.1 (b), Double pass solar air heater with the aluminium baffles place in offset as parallel form [Type-III] Fig.1 (c), taking the readings for air suction from the outlet of this arrangement by thermocouple.

Here all the conditions are further work with the varying the wind velocity of the air flowing through the air heater. In case of all above four condition the wind velocity is changed with the values 2, 4, 6, 8 and 10 meters/seconds.

Table: -1 Experimental specifications

Double pass solar air heater with aluminium cans					
Arrangements	Velocity (m/s)				
Type - I	V = 2 m/s	V = 4 m/s	V = 6 m/s	V = 8 m/s	V = 10 m/s
Type - II	V = 2 m/s	V = 4 m/s	V = 6 m/s	V = 8 m/s	V = 10 m/s
Type - III	V = 2 m/s	V = 4 m/s	V = 6 m/s	V = 8 m/s	V = 10 m/s



Fig. 1 Experimental Setup of SAH (a) Type - I (b) Type - II (c) Type - III.

3. Results

An experimental investigation on DPSAH (double pass solar air heater) with aluminium cans the results as discuss below with graph of efficiency with

hrespecttotime.Foreachoperatingconditiontherearefivecomparativereadings weretakenforchangingthe velocityoftheair flowing fromthe air heater.The changeinthewind velocitychanges themassflowrate oftheair heated bytheairheater.Thewindvelocityis changedin orderof 2,4,6,8, 10m/sforeachoperateconditions.Fromtheequation3.4.1 wecangetthevalueoftheairheaterefficiency.

3.1 Calculate Thermal Efficiency

The thermalefficiencyofthesolarcollectors(η) isdefinedas the ratio between theenergygain andthe solar radiationincidentonthe collectorplane.

$$\eta = mC_p (T_{a, out} - T_{a, in}) / (IA_c) \text{ _____(1)}$$

Table 2 below which show the efficiency versus time of DPSAH of Type I as respectively different velocity to 2, 4, 6, 8, and 10 m/s.

Table: - 2 Efficiency of DPSAH Type -I arrangement

Type-I					
Time	Date:12-6-2014to 16-6-2014		Velocity:-2/4/6/8/10m/s		
	2m/s	4m/s	6m/s	8m/s	10m/s
10:00	6.24	12.4	18.55	16.19	16.24
10:30	6.7	13.48	19.09	16.92	16.51
11:00	6.76	13.73	20.28	18.41	16.86
11:30	6.86	14.29	21.41	19.21	18.54
12:00	6.91	14.83	21.57	20.01	18.51
12:30	7.18	14.93	22.37	20.71	19.78
13:00	7.45	15.05	22.95	21.24	19.45
13:30	7.63	16.49	24.61	22.35	20.23
14:00	7.36	15.51	23.94	21.31	19.03
14:30	6.96	15.01	23.19	20.01	18.75
15:00	6.81	14.74	22.88	19.28	18.43
15:30	6.6	14.41	22.28	18.01	16.51
16:00	6.46	14.08	21.42	17.11	16.14

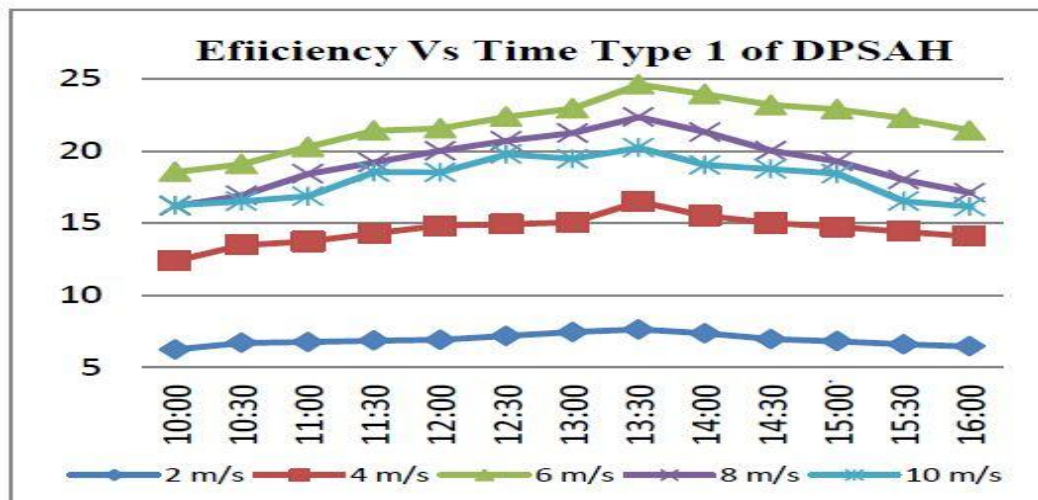


Table 3 as below which show the efficiency versus time of DPSAH of Type II as respectively different velocity to 2, 4, 6, 8, and 10 m/s

Table: - 3 Efficiency of DPSAH Type -II arrangement

Type-II

Time	Date:19-6-2014to 23-6-2014		Velocity:-2/4/6/8/10m/s		
	2m/s	4m/s	6m/s	8m/s	10m/s
10:00	6.59	13.81	18.67	17.35	17.99
10:30	6.72	14.16	20.97	18.75	18.13
11:00	7.39	14.42	21.23	19.21	18.24
11:30	7.16	14.82	21.35	19.07	18.36
12:00	7.42	15.41	21.69	20.01	18.55
12:30	7.43	15.44	22.42	20.71	19.84
13:00	7.48	15.58	23.84	21.78	20.82
13:30	8.09	16.51	26.45	22.46	21.49
14:00	7.64	16.62	25.36	21.22	20.36
14:30	7.52	16.51	24.76	20.01	18.77
15:00	7.13	16.49	24.55	19.21	18.45
15:30	6.92	16.27	24.31	19.01	17.94
16:00	6.87	15.45	23.79	18.51	16.27

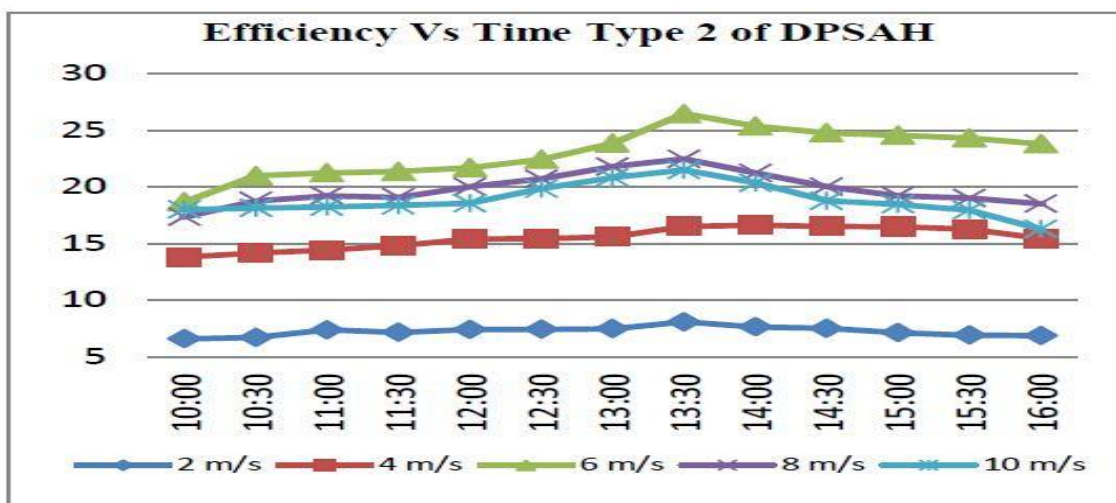
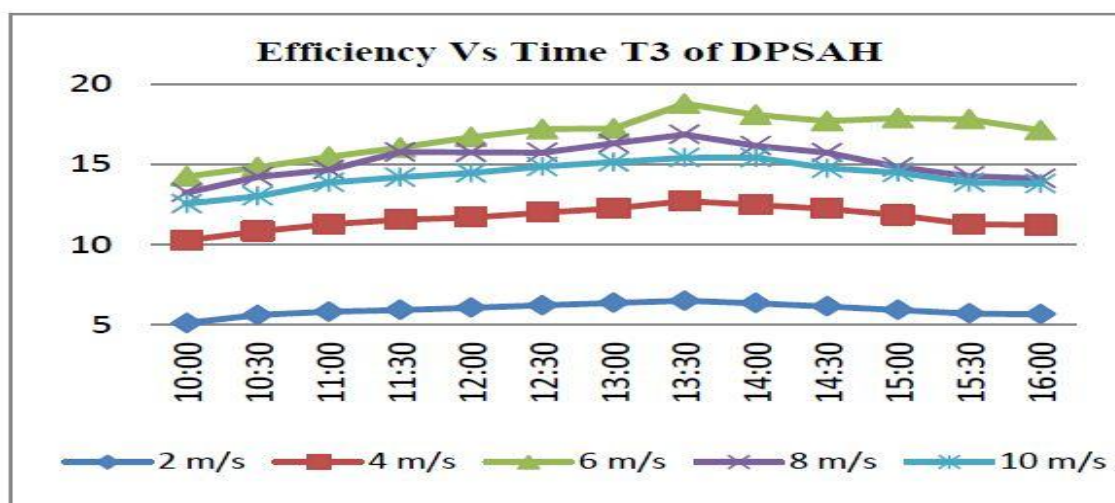


Table 4 as below which show the efficiency versus time of DPSAH of Type III as respectively different velocity to 2, 4, 6, 8, and 10 m/s.

Table: -4 Efficiency of DPSAH Type-III arrangement

Type-III					
Time	Date:23-6-2014to 30-6-2014		Velocity:-2/4/6/8/10m/s		
	2m/s	4m/s	6m/s	8m/s	10m/s
10:00	5.12	10.28	14.26	13.26	12.56
10:30	5.63	10.84	14.85	14.24	13.04
11:00	5.83	11.29	15.49	14.69	13.88
11:30	5.94	11.56	16.06	15.78	14.21
12:00	6.08	11.71	16.72	15.76	14.48
12:30	6.23	12.01	17.21	15.75	14.88
13:00	6.38	12.27	17.25	16.33	15.16
13:30	6.51	12.74	18.8	16.88	15.43
14:00	6.36	12.49	18.11	16.17	15.4
14:30	6.16	12.25	17.71	15.74	14.78
15:00	5.94	11.85	17.89	14.85	14.51
15:30	5.72	11.29	17.82	14.28	13.88
16:00	5.68	11.24	17.14	14.13	13.81



4. Conclusion

- The performance of double pass solar air heater is investigated, heat losses from the top cover is reduced in case of double pass solar air heater for the entire different range of mass flow rate.
- The efficiency of double pass solar air heater is further increase by adding aluminum cans on both the channels upper and lower.
- Comparison of these absorber plate arrangements Type – I, Type – II and Type – III of double pass solar air heater having maximum efficiency of in arrangement is Type – II.
- If there is no limitation of the air speed, an efficiency improvement in relation to the smooth flow of air arrangement of the solar collector.
- The path of the air travel is increase in case of double pass solar air heater get higher outlet temperature of the same mass flow rate. This collector minimizes the heat losses to the ambient and maximizes the heat transfer to the air stream.

References

- [1] HoCD, YehHM, WangRC. Heat-transfer enhancement in double-pass flat plate solar air heaters with recycles. *Energy* 2005; 30(15): 2796–817.
- [2] Mohamad AA. High efficiency solar air heater. *Solar Energy* 1997; 60(2): 71–6.
- [3] Essen H. Experimental energy and energy analysis of a double-flow solar air heater having different obstacles on absorber plates. *Build Environ* 2008; 43(6): 1046–54.
- [4] Sahu MM, Bhagoria J. L. Augmentation of heat transfer coefficient by using 90° broken transverseribs on absorber plate of solar air heater. *Renew Energy* 2005; 30(13): 2057–73.
- [5] Ghoneim AA. Performance optimization of solar collector equipped with different arrangement of square-celled honeycomb. *Int J Ther Sci* 2005; 44(1): 95–105.
- [6] Njomo D. Unglazed “Selective absorbers solar air collector: heat exchange analysis” *Heat Mass Transfer* 2000; 36(4): 313–7.
- [7] A. P. Omojaro, L. B. Y. Aldabbagh et al. “Experimental performance of single and double pass solar air heater with fins and steel wire mesh absorber”, 2010.
- [8] Ebru Kavak Akpınar, Fatih Kocyiğit. Energy and exergy analysis of a new flat-plate solar air heater having different obstacles on absorber plates
- [9] K. Sopian, M. A. Alghoul, Ebrahim, M. Alfegi, M. Y. Sulaiman et al. “Evaluation of thermal efficiency of double-pass solar collector with porous–nonporous media”, 2009.
- [10] Filiz Ozgen, Mehmet Esen, Hikmet Esen. “Experimental Investigation of Thermal Performance of a Double-Flow Solar Air Heater Having an Aluminium Cans”, 2009.

To study effect of recycle SAW flux on weld metal chemistry and mechanical properties

Prof. Dixit Patel^a, Mr. Arpit Patel^b, Prof. Shaival Parikh^a

^aGandhinagar Institute of Technology, Gandhinagar, India

^bHindustan Doooliver, Ahmedabad 382445, India

Abstract

The flux used for shielding in submerged arc welding is converted into slag during welding which is a waste and has to be disposed of. Slag generated during submerged arc welding has been recycled. Slag was crushed and meshed to the granular size typical of fresh flux. This recycled slag in combination with EL8 and EM12k filler wire was used in these investigations. It was further investigated that the weld metal chemical composition and mechanical properties of weld metal prepared using recycled slag is within the acceptable range of AWS (American Welding Society) specifications or not.

Keywords: Submerged arc welding, Slag, Weld metal composition, Basicity Index

Nomenclature

SAW	Submerged Arc Welding
YS	yield strength
UTS	ultimate tensile strength
C	Carbon
Mn	Manganese
Si	Silicon

Introduction

In general, submerged arc welding (SAW) produces a coalescence of metal by heating them with an arc between an electrode and base metal. The arc and molten metal are submerged in blanket of fusible flux. Flux and welding parameters are the two main variables in SAW process [1]. Chemistry of weld metal is depends on combination of electrode and flux. The flux used for shielding in submerged arc welding is converted into slag. In general, one kg of flux is consumed for every kg of weld metal deposited. Flux consumption increases with increase in arc voltage. Presently slag generated during submerged arc welding is thrown away as a waste and needs land fill space for dumping. It is not possible to stop the generation slag as it is a bio-product of the process but could be reused. So an attempt has been made to recycle the slag. Recycled flux is a flux that is reconstituted form a fused slat that is taken from the surface of the SAW welds & which is recrushed and screened to the desired particle size. It requires greater consideration because in addition to crushing & screening required, the weld fused slag ordinarily will require corrective additions. Most of the oxide content in the slag will be close to those of original slag. Admixture of recrushed slag to reconstitute a usable flux requires knowledge of the composition of slag & clear objective for the final composition & nature of flux required for further SAW operations. In this investigation slag has been processed in such a manner that allows it to be used as a flux and its effect on chemistry of weld metal and mechanical properties has been investigated.

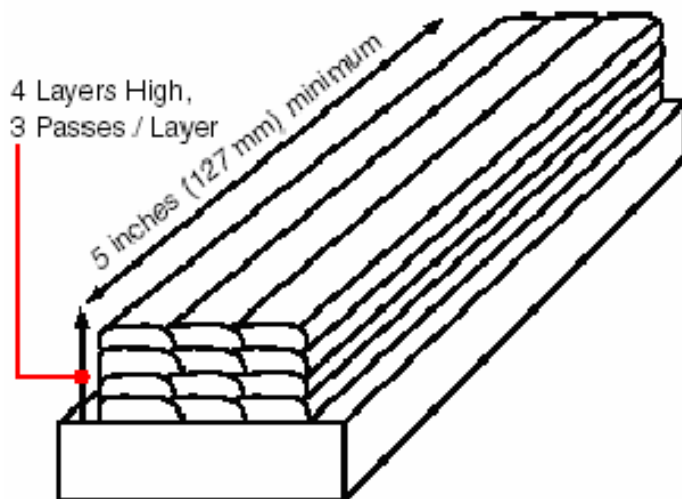
Experimental Work

- In this experimental work SAW wires EL-8 and EM-12k of 3.15 mm diameter with agglomerated flux of basicity index 1.6 used. The chemical composition of electrodes and base metal used in this work are given in Table 1. Weld metal pad for chemical analysis with combination of EL-8 and EM12k electrode with fresh and crushed slag made as per ASME SFA-5.17[2] shown in Fig 1. Chemical analysis of weld pad given in Table 2.

Table 1. Chemical composition of Base metal and Electrode

Elements (%)	Base Metal	EL-8	EM-12K
C	0.165	0.08	0.1
Mn	0.4	0.5	1

Si	0.17	0.05	0.2
S	0.05	0.018	0.018
P	0.046	0.018	0.018
Cu	-	0.25	0.25

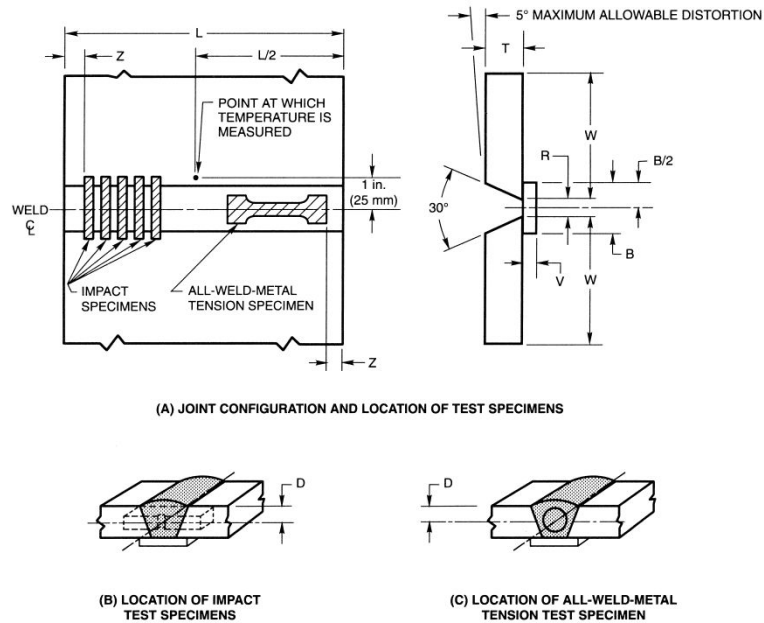


• Fig. 1. Weld metal pad for chemical analysis (ASME SFA-5.17)[2]

Four groove weld joints were made with constant voltage D.C submerged arc welding power source using 3.15 mm diameter wires with fresh and crushed slag as shown in Fig 2. To expel any moisture absorbed during storage of flux was heated in a draying oven at 300°C for 2 hours prior to use. DCEP polarity was used throughout the experimentation. The inter pass temperature was kept minimum 150°C. The welding parameters and other conditions were in accordance with ASME SFA 5.17 .Mechanical properties of groove weld test assembly given in Table 3.

Table 2. Weld Pad Chemical composition (wt %)

Electrode	Flux	C	Mn	Si
EL-8	Fresh Flux	0.052	0.700	0.250
EL-8	Crushed slag	0.030	0.547	0.170
EM-12K	Fresh Flux	0.080	1.300	0.450
EM-12K	Crushed slag	0.050	0.800	0.323



Letter	Dimensions	in.	mm
L	Length (min)	12	305
T	Thickness	1 ± 1/16	25 ± 1.5
W	Width (min)	5	127
V	Backup Thickness	1/2 ± 1/16	13 ± 1.5
D	Specimen Center	3/8 ± 1/32	9.5 ± 1.0
B	Backup Width (min)	2	50
R	Root Opening	1/2 ± 1/16	13 ± 1.5
Z	Discard (min)	1	25

Fig. 2: Groove Weld Test Assembly for Mechanical testing (ASME SFA-5.17)[2]

Result and Discussion

Chemical composition

As is well known, the reactions between liquid weld metal and fused flux in the SAW process are similar to those between molten metal and slag in the steel making process.[3]

- As shown in Table II carbon, manganese, silicon, phosphorus, sulphur of the weld metal decrease when weld metal produced with electrode and crushed slag combination.

- Transfer of Carbon*

It is very difficult to predict the extent of carbon transfer during welding, but usually the weld metal has a lower carbon content than expected from nominal composition of electrode due to effect of dilution and Oxidation of carbon.

- In the present study, percentage of Carbon in weld metal deposited with EL8 and crushed slag is 0.03% which is less than the EL-8 and fresh flux shown in Table 2. It is due to oxidation of carbon as deoxidizers have already been exhausted from the slag.

- Transfer of Manganese*

Manganese content of weld metal depends on the initial manganese content of filler wire, basicity index, amount of manganese and manganese oxide of the flux. Slag metal reaction involving an exchange of manganese.

In the present study, percentage of Manganese in weld metal deposited with EL8 and crushed slag is 0.547% which is less than the EL-8 and fresh flux shown in Table 2.

- Transfer of Silicon*

The loss of silicon from the weld metal deposited with pure slag is expected due to oxidation. However it is observed that silicon content of weld metal deposited with pure slag is 0.17% which is more than the filler wire used. It indicates that silicon has been

transferred from slag to weld metal. which may be attributed to the dissociation of SiO₂ present in the slag.[3]

Weld metal mechanical Properties

The mechanical properties of weld metal are primarily the result of: (i) the weld metal chemical composition, (ii) microstructure and (iii) the cooling rate. The cooling rate experienced by weld metal deposit is controlled by a combination of heat input and heat extraction . Under identical condition of welding, viz. joint design and plate thickness, heat extraction maybe assumed to be remain same. Therefore, weld metal chemical composition and heat input controlling microstructure are the governing factors responsible for the mechanical properties of weld metal.

YS and UTS value decrease when weld metal produced with crushed slag because of decrease in carbon and manganese percentage in weld metal as shown in Table 3.

Table 3. Mechanical properties of groove weld assembly

Wire	Flux	YS (Mpa)	UTS(Mpa)	Impact Value (J at -40 °C)
EL-8	Fresh Flux	360	430	20
EL-8	Crushed slag	290	350	13
EM-12K	Fresh Flux	420	520	50
EM-12K	Crushed slag	355	420	22

Conclusion

Form above experiment we can say that Submerged arc welding slag can be recycled. Recycled slag with EM12k can produce weld metal having chemical composition and mechanical properties within the acceptable range of AWS of EL8 and fresh flux.

References

- [1] P. Kanjilal , T.K. Pal , S.K. Majumdar, Combined effect of flux and welding parameters on chemical composition and mechanical properties of submerged arc weld metal, Journal of Materials Processing Technology,2006,pp .223–231
- [2] ASME Boiler and Pressure vessel Code, Section II Part C, SFA 5.17,New York Edition 2013.
- [3] KULWANT SINGH, V. SAHNI, S. PANDEY, Slag Recycling in Submerged Arc Welding and its Influence on Chemistry of Weld Metal Asian Journal of Chemistry,vol21

Cost Reduction in File Manufacturing by using Special Purpose Resistance Heating: A Case Study

Sameer S. Gajmal^a, Prof. Santosh Rane^b, Prof. Sudhir.G Bhatwadekar^c

^a Gharda Institute of Technology, Lavel
SPCE, Mumbai

^c K.I. T.'s college of Engineering, Kolhapur.

Abstract

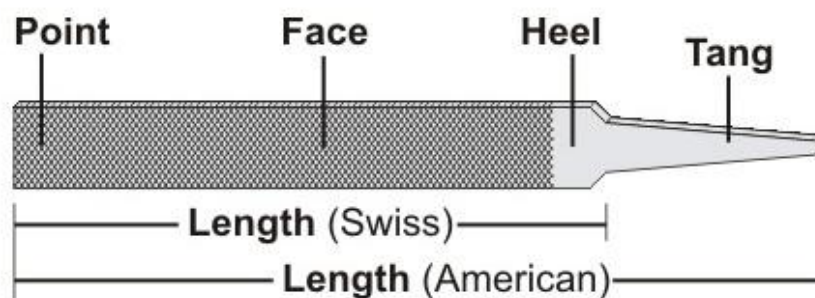
File manufacturing industry is having a tremendous scope in the market. There is a large variety of files which are manufactured in mass production. Out of 11 nos. of operations, one of the operation is tang forging operation. The raw material is heated and is made undergo through open die forging process. In the present paper a case study of an small scale industry is discussed. For the tang forging operation the source used for heating the raw material was Gas heating. Special Purpose Resistance Heating Furnace was replaced instead of Gas heating. It was found that the cost of tang forging operation was reduced to almost 80%. Also it was found that the operator was put into a comfortable and safe work environment due to replacement of Gas Fired Furnace by Resistance heating Furnace.

Keywords: File, Gas Heating ,Resistance Heating.

Introduction:

A file is a metalworking, woodworking and plastic working tool used to cut fine amounts of material from a work piece. It most commonly refers to the hand tool style, which takes the form of a steel bar with a case hardened surface and a series of sharp, parallel teeth. The file is one of the most basic and essential tools found in the any type of industry. The proper file can rough out a shape rapidly or refine and smooth the finest of details. Having a good selection of files will enhance your creative potential. While files seem so common, they are actually quite amazing tools. The first files were made completely by hand with each tooth formed by striking a chisel at the proper angle and interval. The first successful file cutting machines came into use in the mid eighteenth century. This, along with improvements in the refining of iron ore into steel and better heat treating processes, led to the development of the modern files.

Figure 1. Basic Parts of a File



* Sameer S. Gajmal
Email Address: sameergajmal@git-india.edu.in

Types of Files:

A. Depending on the Type of Cut:

1. Extra Rough Cut and Rough Cut Files

Both these types of files are used for the initial filing where the amount of material removed is quite a lot while precision is not a concern since it is normally carried out at the beginning of a filing operation.

2. Middle Cut, Bastard Cut and Second Cut Files

These types of files are used for intermediate operations after the heavy material removal is complete and before finishing the final smoothening out operation.

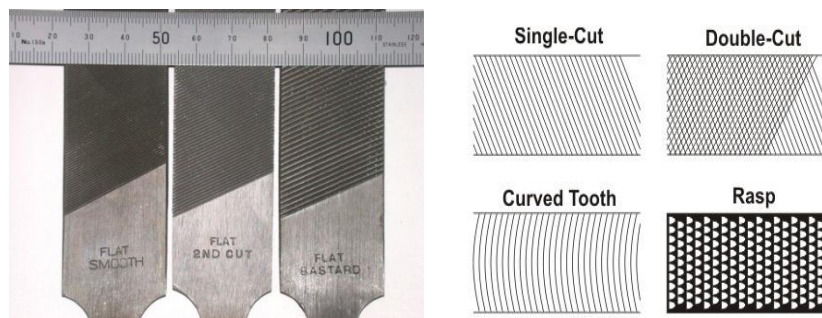
3. Smooth Cut and Dead Smooth Cut Files

These files are used for finishing the filing operation by smoothening out the irregularities which are left by the previous two operations.

In the above file classification is must be noted that the various types of cuts are made possible with the variation of teeth density of the file. A rough cut file and other coarse files have relatively less number of teeth per inch while the smoother files have the maximum number of teeth. The cut of the file refers to how fine its teeth are. They are defined as (from roughest to smoothest): rough, middle, bastard, second cut, smooth, and dead smooth. A single-cut file has one set of parallel teeth while a cross-cut or double-cut file has a second set of cuts forming diamond teeth.

Some of the important files types are listed as follows

Figure 2: Types of Files Depending upon cut



B. TYPES OF FILES DEPENDING ON THE SHAPE OF THE SHANK:

1. Flat Files:

As the name itself suggests, these files have flat shank shape which have teeth on both sides and are mostly used for level filing work involving straight surfaces.

Figure No-03: Flat File



2. **Round Files:** The blade or the shank of this type of files is round in shape and the teeth are formed on that round surface. The diameter of the whole shaft is uniform towards one end, while it slightly tapers at the outward end. These files are very useful in filing round shapes such as round holes or enlarging them.

Figure N0-04: Round File



Table No.-01 Various Sizes of Round File

Code No.		04RD	05R D	06R D	08R D	10R D	12R D	14R D	16R D	18R D
Size	Inches	4	5	6	8	10	12	14	16	18
	mm	100	125	150	200	250	300	350	400	450
Thickness	mm	3.8	5	6.3	7.15	9.25	12	16	19	22

3. Square Files:

These files are very similar in construction to the above mentioned round files with the only difference that the cross-section of the shaft is of square shape which is uniform towards the handle end but gets slightly tapered towards the outside end while maintaining its square shape.

Figure N0-05: Square File



C. COMMERCIAL TYPES OF FILES:

I. Saw Files:

1. Mill Regular
2. Mill Blunt – One Round
3. Mill Blunt – Two Round
4. Mill Blunt - Two Square
5. Band Saw
6. Band Saw Blunt
7. Heavy Taper
8. Regular Taper
9. Slim Taper
10. Extra Slim Taper
11. Double Extra Taper
12. Double-Ender
13. Pit Saw
14. Cross Cut
15. Cant Saw
16. Rotary Mower
17. Round Chain Saw
18. Farmers Own
19. Double Edge Saw
20. Feather Edge Saw

II. Machinists' Files

1. Flat
2. Hand
3. Half
4. Square
5. Round
6. Three Square
7. Pillar
8. Warding
9. Knife

III. Rasp Files

1. Flat Rasp
2. Half Round Rasp
3. Round Rasp
4. Cabinet Rasp
5. Horse Rasp - Plain
6. Horse Rasp - Tanged

7. Shoe Rasp
8. File and Rasp Combination

IV. Needle Files:

1. Hand
2. Flat
3. Three Square
4. Square
5. Half Round
6. Round
7. Knife
8. Barrette
9. Crossing
10. Slitting
11. Crochet
12. Hand With Round Edge

V. Diamond Coated Needle Files

- | | |
|-----------------|---------------|
| 1. Hand | 5. Half Round |
| 2. Flat | 6. Round |
| 3. Three Square | 7. Knife |
| 4. Square | |

Application of Files:

Files are often used to put the finishing touches on a machined work piece, either to remove burrs or sharp edges or as a final fitting operation. Intricate parts or shapes are often produced entirely by skilled workers using files.

Case Study:

In this paper a case study from a small scale industry named Sharda Maa Engineering Located at MIDC Gane-Khadpoli, Taluka- Chiplun District- Ratnagiri is discussed. The component under consideration is Round File 06 inch Size. The Raw material for files is File Steel.

List of Manufacturing Operation in File Manufacturing:

1. Raw Material Cropping
2. Tang Forging
3. Tang Cutting
4. Annealing
5. Grinding

6. Teeth Cutting
7. Inspection
8. Stamping
9. Hardening
10. Scoring
11. Proving & Packing

Tang Forging Operation:

Out these operations the Tang Forging Operation of Round File (06 Inch) was taken was study. The details of the operations before study and modification are as follows:

Figure No-06: Tang Forged Round File



Before Study:

- Machine Used for Forging:
Auto Forging Hammer (Hammer of 15 Kg, 25 Kg.)
- Gas Furnace:
Fuel: LPG
Temperature required: 550°C
- Job Holding Tools:
(Pair of tongs, Hand Gloves, etc)

Figure No-07: Tang Forging Set Up with Gas Fired Furnace



After Study:

Machine Used for Forging:

Auto Forging Hammer (Hammer of 15 Kg, 25 Kg.)

- Resistance Heating Furnace:

Specification: 03 Phase, AC Voltage 440 V,

Temperature required: 550°C

- Job Holding Tools:

Not required.

Figure No-08:Tang Forging Set Up with Special Purpose Resistance Heating Furnace



About Special Purpose Resistance Heating Furnace:

The Furnace used is fully automatic, Water-cooled heavy duty ESR Transformer suitable for different sizes of furnishing rods, with suitable clamping and water cooled heavy duty thyristorised, Latest heat sequence electronic control panel, Electronic control system consists of water-cooled thyristor assembly, necessary sensors for automation and protection & for achieving maximum productivity.

FIRST TIME IN INDIA – special purpose Resistance Heating Machine which is very useful for Engineers' File manufacturers has been used. This machine is used in place of existing Gas Burners for

heating the file ends before forging. The special design used in this machine helps to heat the job faster with considerable less current. Since the Time and Current is less, the electrical energy consumption, which is proportional to the time and square of current, is considerably reduced and hence the operation cost of this machine is negligible compared to gas heating. Apart from the financial benefits, this machine is absolutely Eco friendly compared to gas heating.

Salient Features:

- Low Power Consumption
- Fully Automatic
- Thyristorised Electronic Precision control ensures accuracy
- Absolutely eco-friendly compared to conventional gas heating
- Precise localized heating pattern ensures superior product quality

Table N0.-02: Machine Description:

TECHNICAL SPECIFICATIONS		MACHINE SPECIFICATIONS	
TRANSFORMER		OVERALL DIMENSIONS (mm)	400W X 650DX800H
KVA	15 KVA to 30 KVA	WEIGHT (kg)	150
COOLING	WATER		
INSULATION	CLASS-F		
POWER SUPPLY	415 V – 1 Ph		

During the study it was found that the tang forging operation with Gas Fired Furnace was not efficient, also the operator was not comfortable with the hot environment because of the Gas Fired Furnace nearby the workplace.

For one shift about 06-07 Kg of LPG was consumed for forging 600- 650 Nos. of files.

Table N0.-03: Cost of Gas Heating

Sr. No.	Particulars	LPG Consumed	Production of Files
1	For One Shift	06-07 Kgs.	600-650 Nos. of Files
2	For Three Shift	18-19 Kgs	1800 Nos. of Files
Cost of LPG required per day			Rs. 1600/- + Transport Charges

After carrying out a deep study, it was suggested to carry out the Tang Forging operation with Special Purpose Resistance Heating Furnace instead of Gas Fired Furnace.

Salient features of resistance Heating Furnace;

- Compact
- Water Cooled Electrode
- Pneumatic Clamping
- Timer for adjusting the heating time period.

Table N0.-04: Cost of Resistance Heating

Sr. No.	Particulars	Electricity Consumed	Cost of Electricity Consumed
---------	-------------	----------------------	------------------------------

1	For One Shift	10 Units	10 X 8 =Rs.80
2	For Three Shift	30 Units	30 X 8 =Rs.320/-
Cost of Resistance Heating per shift			Rs. 320/- Only

Results and Findings:

- By replacing Gas Fired Furnace by Special Purpose Resistance Heating Furnace , the net saving in Tang Forging Operation Cost was Rs.1280/- Per shift.
- Machine Operator got relief from the hot environment which improved his overall efficiency. The file can be handled without using any of the work holding devices, which was required in the previous case of Gas Heating.

Figure No-09: Manual Handling of heated File



- Workplace became safe since Gas Fired Furnace was eliminated.
- Now with Special Purpose Resistance Heating Furnace the component is heated only for the required tang length of 15 mm, excessive heating (along the length) of component is avoided.
- Since the net cost saving in the Tang Forging operation was Rs.33,280/- per month, the capital investment of Rs.1,50,000/- done in procuring the Special Purpose Resistance Heating Furnace was going to be recovered in 4.5 months which was acceptable by the industry.

Conclusion:

The cost of Tang Forging operation was reduced down to almost 80 % (Initial Cost Rs.1600/- Per shift, Cost After Modification Rs.320/- per shift for the Monthly Production of 1800 Nos. of Round File of 06 Inch Length) which was appreciated by the industry where the study was carried out.

References:

[1]Professor em. Dr.-Ing. Klaus Ehrlenspiel,Dr.-Ing. Alfons Kiewert,Professor Dr.-Ing. Udo Lindemann, “Cost-Efficient Design”,Springer Berlin Heidelberg, 2007 ,pp 143-384.

- [2] Philip K. Freakley, “Rubber Processing and Production Organization” , Springer US, 1985, pp 353-395
- [3] P. Selvaraj, P. Radhakrishnan , M. Adithan, “An integrated approach to design for manufacturing and assembly based on reduction of product development time and cost”, International Journal of Advance Manufacturing technology, June 2008, pp 13-29
- [4] Sanjay Sharma, “ Effects of an increase in manufacturing rate in the context of cyclic production”, The International Journal of Advanced Manufacturing Technology, November 2008, Volume 39, Issue 7-8, pp 821-827.

Analytical and experimental investigations of the single stage centrifugal pump performance

Nilesh Tiwari^a, Devranjan Kumar^a

^aDept. of Mechanical Engineering, S.V.M.I.T., Bharuch, 392001

Abstract

The pump is one of the most common machines in all industries, whether its small scale or heavy industries. In the present scenario of energy crisis, it would be advisable to conserve, even the minute proportion of energy. In the centrifugal pump, the inefficiency is mainly due to the hydraulic losses in its various components. In this phase, mathematical analysis is done to predict the performance characteristics curve of the single stage centrifugal pump. This methodology is based on the estimation of the geometrical parameters of the various components of a pump and respective loss in each of these components. This procedure would be beneficial to understand the effect of various parameters on the performance of the centrifugal pump. This would help to create alterations in the actual pump in the initial stages of pump design to improve its performance. This method is comparatively easy, as compared to experimental or software based analysis. In the subsequent stages of the project, experimental validation would be done to verify the theoretical analysis. In the further stages of the project, an attempt would be made to implement this methodology on industrial multistage pump, to study the effect of various real condition parameters on its performance.

Keywords: Centrifugal pump; performance characteristics; hydraulic loss method.

Nomenclature

A	cross section area
A_{1q}	impeller inlet throat area ($A_{1q} = a_1 \times b_1$)
A_{2q}	area between vanes at impeller outlet ($A_{2q} = a_2 \times b_2$)
A_{3q}	diffuser/volute inlet throat area ($A_{3q} = a_3 \times b_3$)
a	distance between vanes
b	width of channel in the meridional section
c_f	friction coefficient of a flat plate
c_p	pressure recovery
D, d	diameter
d_{3q}	equivalent diameter of volute throat
d_b	arithmetic average of diameters at impeller or diffuser
d_m	geometric average of diameters at impeller or diffuser
d_n	hub diameter
d_s	inner diameter of suction nozzle
e	vane thickness
i	incidence ($i = \text{blade angle} - \text{flow angle}$)
L	length
n	rotational speed (revolutions per minute)
Q_{La}	flow rate through impeller
r	radius
r_{3q}	equivalent radius of volute throat area
s	gap width
w	relative velocity
w_{1q}	average velocity in impeller throat area $w_{1q} = Q_{La} / (Z_{La} \times A_{1q})$
Z_h	hydraulic losses (impeller: Z_{La} diffuser: Z_{Le})
Z_{La}	number of impeller blades
Z_{Le}	number of diffuser vanes
<i>Greek symbols</i>	
α	angle between direction of circumferential and absolute velocity
β	angle between relative velocity vector and the negative direction of circumferential velocity
γ	impeller discharge coefficient (slip factor) equivalent roughness
ϵ	equivalent roughness

ζ	loss coefficient
ν	kinematic viscosity
ϕ	flow coefficient
<i>Subscripts</i>	
1	impeller blade leading edge (low pressure)
2	impeller blade trailing edge (high pressure)
3	diffuser vane leading edge
4	diffuser vane trailing edge
a,m,i	outer, mean, inner streamline
B	blade angle (impeller, diffuser, volute cutwater)
d	discharge nozzle
h	hydraulic
La	impeller
Le	diffuser
LE	leading edge
m	meridional component
r	radial
s	inlet or suction nozzle
sch	blade or vane
Sp	volute
SS	suction surface (suction side)
TE	trailing edge
th	theoretical flow conditions (flow without losses)
u	circumferential component
<i>superscripts</i>	
'	with blade blockage
*	dimensionless quantity
'	with blade blockage
*	dimensionless quantity
	$b_2^* = b_2/d_2, w_1^* = w_1/u_2$

Introduction

1.1. Performance of centrifugal pump

Performance of the centrifugal pump is primarily estimated base on its head. Head is also of two types, theoretical and actual heads. There is a deviation of actual head from the theoretical head. This deviation is due to the losses that occur in the centrifugal pump. So, in order to estimate the actual performance, firstly theoretical head is to be calculated and then from that that all the losses are to subtracted to obtain the actual head.

1.2. Losses in centrifugal pump

A study of losses in centrifugal pump may be undertaken one of the following reasons:

- To know the actual characteristics from theoretical characteristics it is required to deduct the loss head from theoretical head.
- Information about the nature and magnitude of losses may indicate the way to reduce these losses.
- If the losses are known, it is possible to predetermine the head-capacity curve of a new pump by first assuming or establishing in some other manner the head-capacity curve of an idealized pump.
- Pump performance curves can be predicted by means of theoretical or empirical calculation models for each single type of loss.

1.2. Different types of losses

In centrifugal pump there are basically two types of losses hydraulic or primary losses and another is secondary losses, hydraulic losses is mainly due to vortex dissipation, difference in flow angle and blade angle, flow deceleration and skin friction, whereas secondary losses is due to leakage, friction in bearing and shaft seals. These losses depend on the design of the pump, i.e. on the selection of anti-friction versus journal bearings or stuffing boxes versus mechanical seals.

2. Literature review

Author	Journal/Book Title	Year	Conclusion
--------	--------------------	------	------------

Andrzej WILK	Hydraulic efficiencies of impeller and pump obtained by means of theoretical calculations and laboratory measurements for high speed impeller pump with open-flow impeller with radial blades	2010	Stated parameters that affect performance of centrifugal performance and their relation with the performance.
Fraser, Warren H.	Recirculation in centrifugal pumps	1981	Elaborates indications of the recirculation and their individual diagnosis.
Gölcü, Mustafa, and Yaşar Pancar	Investigation of performance characteristics in a pump impeller with low blade discharge angle	2005	Comparative study of performance of the pump with and without splitter blades.
Gulich, Johann F.	Centrifugal pumps	2008	Detailed study and analysis of all the aspects of centrifugal pump, considering each parameter.
Khalid Rababa	The Effect of Blades number and Shape on the Operating characteristics of Groundwater Centrifugal Pumps	2011	Effect of number of blades on the performance of centrifugal pump depends on viscosity of the working fluid.
W. G. Li et. al.	Influence of the number of impeller blades on the performance of centrifugal oil pumps	2012	Estimate the effect of number of impeller blades on the performance of industrial centrifugal pumps
M.G. Patel and A.V. Doshi	Effect of Impeller Blade Exit Angle on the Performance of Centrifugal Pump	2013	Increase in blade exit angle increase the performance of the centrifugal pump.
Memardezfouli, Mohamad, and Ahmad Nourbakhsh	Experimental investigation of slip factors in centrifugal pumps	2009	Slip factor in the centrifugal pump depends on Reynolds number, the geometrical shape of the impeller and the conditions of operation, and impeller-outlet velocity profile.
Mohamed F., Ali Khalil, Sadek Z. Kassab, Ahmed A. Abdel Naby Azouz	Prediction of a Centrifugal Pump Performance Characteristics Under Variable Speed Conditions	2013	Experimental and theoretical estimation of the centrifugal pump performance has been made based on model given by J. F. Gulich
Nemdili, Ali and Dieter-Heinz Hellmann	Development of an empirical equation to predict the disc friction losses of a centrifugal pump	2004	Loss due to disk friction depends on Reynolds number, axial gap, width of volute and surface roughness
Shi, Weidong, Ling Zhou, Weigang Lu, Bing Pei, and Tao Lang	Numerical prediction and performance experiment in a deep-well centrifugal pump with different impeller outlet width	2013	Estimate the effects of oversize and undersize impeller on the performance of the centrifugal pump.
Thanapandi P., and Rama Prasad	Centrifugal pump transient characteristics and analysis using the method of characteristics	1995	The dynamic characteristics of the test pump have been checked by a numerical model utilizing the method of characteristics. The model predicts well the pattern of the dynamic head characteristics amid transients.
Thin, Khin Cho, Mya Mya Khaing, and Khin Maung Aye	Design and Performance Analysis of Centrifugal Pump	2008	Considering losses in the centrifugal pump, estimation of the best performance point on the performance curve has been estimated.
Thummar A., Pipalia V., Javiya T	Experimental investigation of open well centrifugal Pump performance	2012	Experimental analysis of pump with impellers with different impeller width.
Walker, Craig I. Greg C. Bodkin	Empirical wear relationships for centrifugal slurry pumps: Part 1: side-liners	2000	Estimated the empirical relation between the parameters, that causes wear in pumps.
Sahoo T	Strategies to Increase Energy Efficiency of Centrifugal Pumps.	2012	Stated strategies to increase performance of centrifugal pump to conserve energy.

3. Objectives

The objective of work concentrated towards the performance analysis of a centrifugal pump by empirical method and comparison of result with experimental methods. Centrifugal pump has chosen because the availability of experimental testing in our fluid machinery laboratory.

The following objective has covered in present work:

- To carry detailed study about centrifugal pump.
- To study the empirical models for analysing the performances of centrifugal pump given by J.F Gulich.
- To estimate the hydraulic losses by empirical model by J.F Gulich.

4. Proposed methodology

Various models have been proposed to predict performance characteristics curve of centrifugal pump. From these, model suggested by J.F. Gulich has been selected, according to conclusion inferred from the literature review.

$$H_{th,without\ slip} = \frac{u_2^2}{g} \left(1 - \frac{Q_{La}}{A_2 u_2 \tan \beta_{2B}} \right) \dots eqn(01)$$

Now, theoretical head with slip,

$$H_{th,with\ slip} = \frac{u_2^2}{g} \left[\gamma - \frac{Q_{La}}{A_2 u_2 \tan \beta_{2B}} \left\{ \tau_2 + \frac{A_2 d_{1m}^* \tan \beta_{2B}}{A_1 \tan \alpha_1} \right\} \right] \dots eqn(02)$$

4.1. Hydraulic losses in impeller

Various hydraulic losses in impeller are to be calculated in this sub-section. Some parameters are required for its estimation. Average relative velocity in impeller channel:

$$w_{av} = \frac{2Q_{La}}{z_{La}(a_2 b_2 + A_{1q})} \dots eqn(03)$$

Here, impeller inlet throat area, A_{1q} is calculated by $A_{1q} = a_1 b_1$
Friction coefficient,

$$c_f = \frac{0.136}{\left\{ -\log \left(0.2 \frac{\epsilon}{L_{sch}} + \frac{12.5}{Re} \right) \right\}^{2.15}} \dots eqn(04)$$

here, Reynolds number, Re is calculated by,

$$Re = \frac{w_{av} L_{sch}}{\nu} \dots eqn(05)$$

Hydraulic diameter,

$$D_h = \frac{2(a_2 b_2 + A_{1q})}{a_1 + b_1 + a_2 + b_2} \dots eqn(06)$$

Dissipation coefficient,

$$c_d = (c_f + 0.0015)(1.1 + 4b_2^*) \dots eqn(07)$$

hereb b_2^* can be calculated by

$$b_2^* = \frac{b_2}{d_2} \dots eqn(08)$$

Now, friction and mixing losses can be calculated by:

$$\zeta_{La,R} = 2g \frac{Z_{La,R}}{u_2^2} = 4c_d \frac{L_{sch}}{D_h} \left(\frac{w_{av}}{u_2} \right)^2 \dots eqn(09)$$

Now, relative velocity at meridian is calculated by:

$$w_{1m} = \sqrt{c_{1m}^2 + (u_1 - c_{1u})^2} \dots eqn(10)$$

Velocity in impeller throat,

$$w_{1q} = \frac{Q_{La}}{Z_{La} A_{1q}} \dots eqn(11)$$

Shock loss at impeller inlet,

$$\zeta_{La,C} = 2g \frac{Z_{La,C}}{u_2^2} = 0.3 \left(\frac{w_{1m} - w_{1q}}{u_2} \right)^2 \dots eqn(12)$$

The value of shock loss at impeller inlet is only to be considered, when $\frac{w_{1q}}{w_{1m}} > 0.65$, otherwise it can be neglected

Total impeller loss,

$$\zeta_{La} = \zeta_{La,R} + \zeta_{La,C} \dots eqn(13)$$

Head loss in impeller,

$$H_{\text{loss in impeller}} = \zeta_{La} \times \frac{u_2^2}{2g} \dots eqn(14)$$

4.2. Hydraulic losses in volute

Parameters that contribute to the losses in the diffuser are given here.

Flow velocity in throat,

$$c_{3q} = \frac{Q_{La}}{Z_{Le} a_3 b_3} \dots eqn(15)$$

Friction losses in inlet region,

$$\zeta_{2-3} = 2g \frac{Z_{2-3}}{u_2^2} = (c_f + 0.0015) (a_3^* + b_3^*) \frac{\pi^3 (\varphi_2 b_2^*)^2}{8 (Z_{Le} a_3^* b_3^*)^3} \left(1 + \frac{c_2}{c_{3q}} \right)^3 \dots eqn(16)$$

Diffuser loss including overflow channel,

$$\zeta_{Le} = 2g \frac{Z_{Le}}{u_2^2} = \zeta_{2-3} + \left(\frac{c_{3q}}{u_2} \right)^2 \left\{ 0.3 \left(\frac{c_2}{c_{3q}} - 1 \right)^2 + 1 - c_p - \frac{1 - \zeta_{ov}}{A_R^2} \right\} \dots eqn(17)$$

Diffuser nozzle,

$$\zeta_{Sp,D} = \left(\frac{c_x}{u_2} \right)^2 \left(1 - c_p - \frac{1}{A_R^2} \right) \dots eqn(18)$$

Shock loss in case of vaneless diffuser,

$$\zeta_{LS} = \varphi_{2,La}^2 \left(\tau_2 - \frac{b_2}{b_3} \right)^2 \dots eqn(19)$$

Friction losses in vaneless diffuser with constant width,

$$\zeta_{LR} = \frac{2c_f r_2}{b_3 \sin \alpha_3 \cos^2 \alpha_3} \left(\frac{c_{2u}}{u_2} \right) \left(1 - \frac{r_2}{r_4} \right) \dots eqn(20)$$

Total coefficient of losses in volute,

$$\zeta_V = \zeta_{Le} + \zeta_{Sp,D} + \zeta_{LS} + \zeta_{LR} \dots eqn(21)$$

Thus, total head loss in volute,

$$H_{\text{loss in volute}} = \zeta_V \times \frac{u_2^2}{2g} \dots eqn(22)$$

Inlet casing head loss,

$$H_{\text{loss in Inlet casing}} = \frac{c_{1m}^2}{2g} \zeta_E \dots eqn(23)$$

where inlet casing loss coefficient

$$\zeta_E = 0.75 \left(\frac{d_1^2 - d_n^2}{d_s^2} \right) \dots eqn(24)$$

Total head loss,

$$H_{\text{Total loss}} = H_{\text{loss in Inlet casing}} + H_{\text{loss in volute}} + H_{\text{loss in impeller}} \dots eqn(25)$$

Therefore actual head loss,

$$H_{\text{actual}} = H_{\text{th,with slip}} - H_{\text{Total loss}} \dots eqn(26)$$

To obtain the performance characteristics curve for centrifugal pump, graph of H_{actual} versus discharge (Q) is plotted. [4]

5. Analysis and results

Here, centrifugal pump of the model type KDS1030++, has been selected, to measure the geometric dimensions of all the parts of the pump.

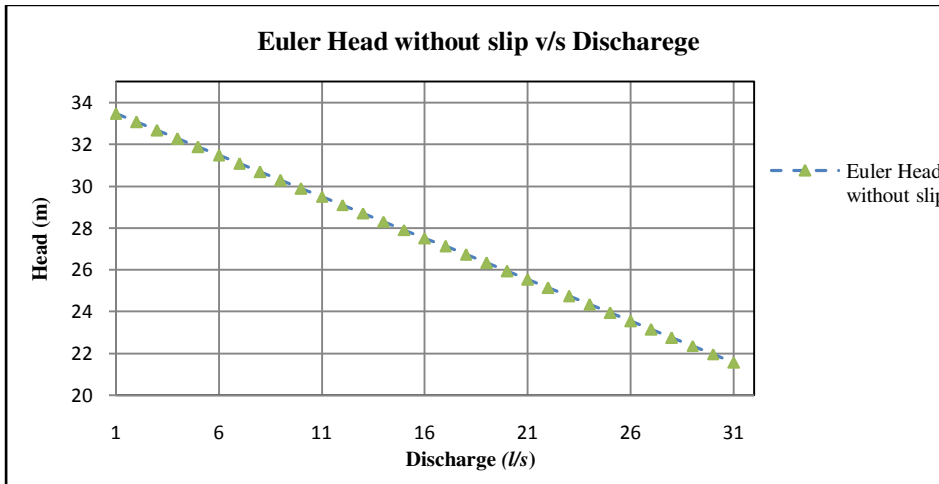


Fig. 1. Euler without slip Head

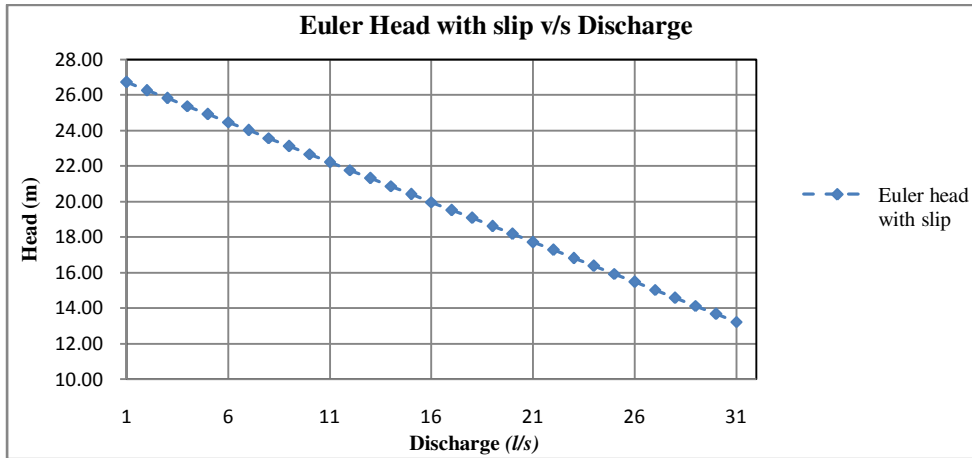


Fig. 2. Euler Head with slip

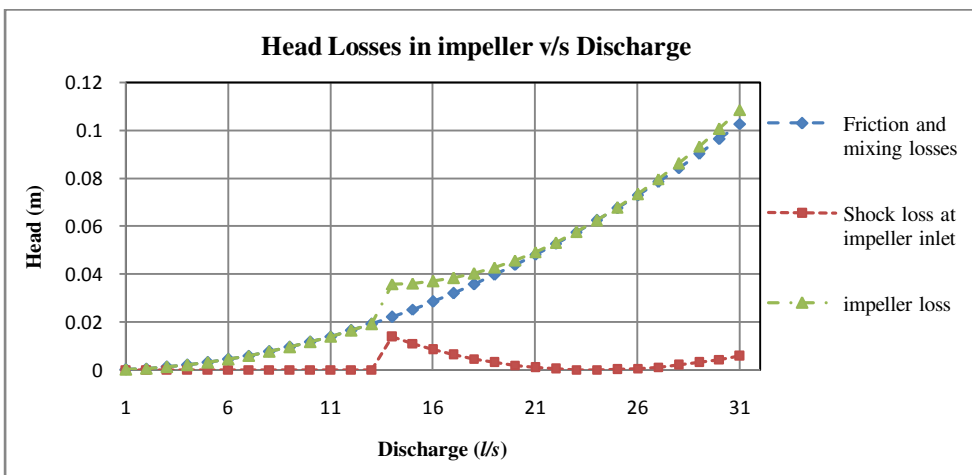


Fig. 3. Losses in impeller

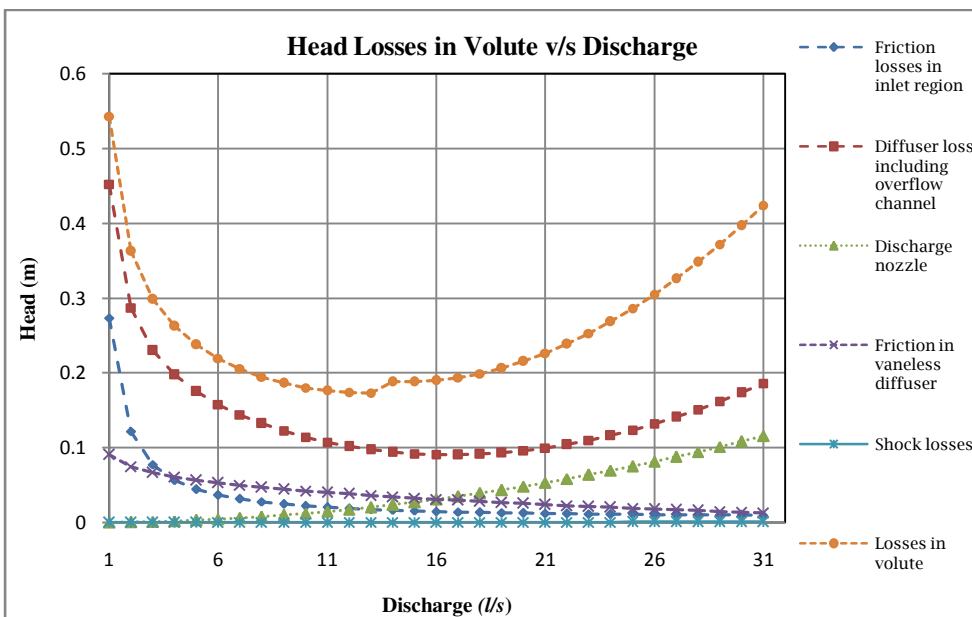


Fig.4. Losses in Volute

Actual head is calculated by subtracting all the head losses in the centrifugal pump from the theoretical head with slip. These head losses include head loss in impeller, head loss in volute and inlet casing head loss.

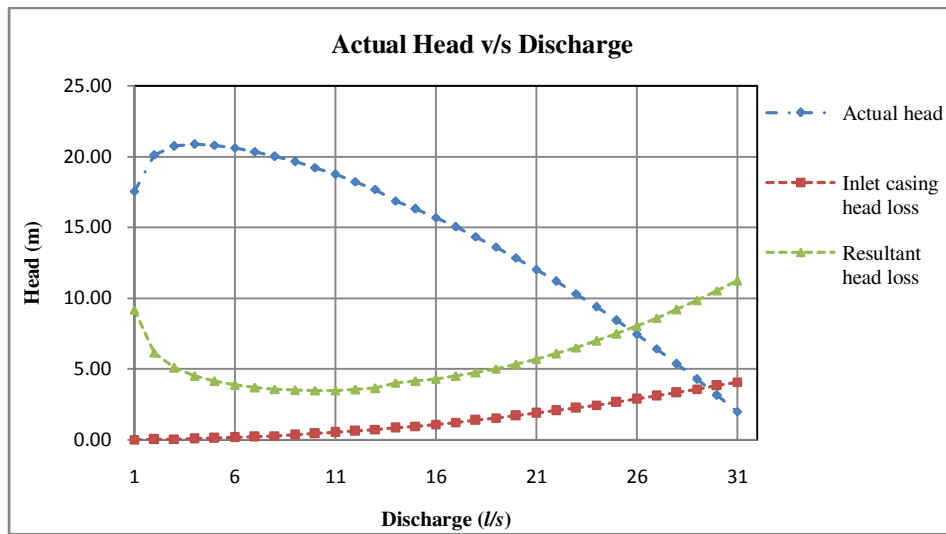


Fig.5. Total losses.

6. Conclusions

- The trajectory of the curves without the considerations of the losses in various components of the centrifugal pump, is a straight line.
- The values of head with consideration of slip factor are lower than that of head without consideration of slip factor for all values of discharge.
- The trajectory of the curves with the considerations of the losses in various components of the centrifugal pump, is parabolic curve. Here, the maximum head of 20.86 m is obtained at 4l/s discharge.

References

- [1] Andrzej, W. I. L. K. "Hydraulic efficiencies of impeller and pump obtained by means of theoretical calculations and laboratory measurements for high speed impeller pump with open-flow impeller with radial blades.", *International journal of mechanics*, Vol. 4, (2010):39-41.
- [2] Fraser, Warren H. "Recirculation in centrifugal pumps." *Materials of Construction of Fluid Machinery and Their Relationship to Design and Performance* (1981): 65-86.
- [3] Gölcü, Mustafa, and Yaşar Pancar. "Investigation of performance characteristics in a pump impeller with low blade discharge angle." *World Pumps* 2005.468 (2005): 32-40.
- [4] Gülich, Johann F. *Centrifugal pumps*. Berlin: Springer, (2008).
- [5] Khalid.S.Rababa , "The Effect of Blades number and Shape on the Operating characteristics of Groundwater Centrifugal Pumps", *European Journal of scientific research*, Vol 2, No.6, (2011) : 243-251.
- [6] Li, W. G. "Blade exit angle effects on performance of a standard industrial centrifugal oil pump." *Journal of applied fluid mechanics* 4.2 (2011): 105-119.
- [7] Li, W-G. "Influence of the number of impeller blades on the performance of centrifugal oil pumps." *World Pumps* 427 (2002): 32-35.
- [8] M.G.Patel and A.V.Doshi, "Effect of Impeller Blade Exit Angle on the Performance of Centrifugal Pump" , *International Journal of Emerging Technology and Advanced Engineering* Volume 3, Issue 1.(2013):702-706
- [9] Memardefouli, Mohamad, and Ahmad Nourbakhsh. "Experimental investigation of slip factors in centrifugal pumps." *Experimental thermal and fluid science* 33.5 (2009): 938-945.
- [10] Mohamed F., Ali Khalil, Sadek Z. Kassab, Ahmed A. Abdel Naby Azouz, "Prediction of a Centrifugal Pump Performance Characteristics Under Variable Speed Conditions", *Eleventh International Conference of Fluid Dynamics*, Alexandria, Egypt, (2013):01-10
- [11] Nemdili, Ali, and Dieter-Heinz Hellmann. "Development of an empirical equation to predict the disc friction losses of a centrifugal pump." *The Sixth International Conference on Hydraulic Machinery and Hydrodynamics, BP*. Vol. 1505. (2004):235-240.
- [12] Sahoo T., "Strategies to Increase Energy Efficiency of Centrifugal Pumps", *International Rotating Equipment Conference, Pumps Users Forum 2008*, Dusseldorf, (2008): 28-29
- [13] Shi, Weidong, Ling Zhou, Weigang Lu, Bing Pei, and Tao Lang. "Numerical prediction and performance experiment in a deep-well centrifugal pump with different impeller outlet width." *Chinese Journal of Mechanical Engineering* 26, no. 1 (2013): 46-52.
- [14] Thanapandi, P., and Rama Prasad. "Centrifugal pump transient characteristics and analysis using the method of characteristics." *International Journal of Mechanical Sciences* 37.1 (1995): 77-89.
- [15] Thin, Khin Cho, Mya Mya Khaing, and Khin Maung Aye. "Design and Performance Analysis of Centrifugal Pump." *world academy of science*,

engineering and technology 46 (2008): 422-429.

[16] Thummar A., Pipalia V., Javiya T. , "Experimental investigation of open well centrifugal Pump performance." *International Journal of Advanced Research in Science, Engineering and Technology*, Vol.01, Issue 03, (2012) : 01-08

[17] Walker, Craig I., and Greg C. Bodkin. "Empirical wear relationships for centrifugal slurry pumps: Part 1: side-liners." *Wear* 242.1 (2000): 140-146.

[18] Foslie, S. "Design of Centrifugal Pump for Produced Water" (Master of Science in Mechanical Engineering). Norwegian University of Science and Technology. (2013)

Appendix : Table-1: Geometrical dimensions of the parts of centrifugal pump

Symbols	Dimensions and Descriptions
d_n	0.068 m - hub or eye diameter
d_s	0.06 m - inner diameter of suction nozzle
b_1	0.03 m - width of impeller at inlet
b_2	0.0212 m - width of impeller at outlet
a_1	0.01012 m - distance between blades at inlet
a_2	0.0248 m - distance between blades at outlet
Z_{La}	6 - number of blades
α_1	90° - angle between of circumferential and absolute velocity
α_3	8° - absolute angle at the diffuser vane leading edge
e_1	0.004 m - vane thickness
β_{1B}	19° - blade angle at impeller inlet
β_{2B}	24° - blade angle at impeller outlet
L_{sch}	0.14 m - length of blade
d_3	0.23 m - diameter of the diffuser vane leading edge
b_3	0.0211 m - width of the diffuser vane leading edge
a_3	0.0248 m - distance between blades of the diffuser vane leading edge

Table-2: Calculations of different head with respect to discharge

Q_{la} (Discharge)	H_{th} (Head with slip)	ζ inlet casing (Inlet casing loss coefficient)	ζ resultant loss (Resultant loss coefficient)	$H_{resultant\ loss}$ (Total head loss)	$H_{inlet\ casing\ loss}$ (Inlet casing loss head)	H_{Actual} (Actual theoretical Head)
1	26.72	0.846	0.542422	9.181084	0.004238	17.53
2	26.27	0.846	0.362456	6.134954	0.016950	20.12
3	25.82	0.846	0.298441	5.051441	0.038138	20.73
4	25.37	0.846	0.262223	4.438412	0.067801	20.86
5	24.92	0.846	0.237582	4.021330	0.105939	20.79
8	23.57	0.846	0.194413	3.290659	0.271203	20.01
9	23.12	0.846	0.186093	3.149832	0.343241	19.63
11	22.22	0.846	0.175863	2.976665	0.512743	18.73
13	21.32	0.846	0.173029	2.928704	0.716145	17.67
14	20.87	0.846	0.187966	3.181526	0.830559	16.86
17	19.52	0.846	0.193272	3.271347	1.224651	15.02
18	19.07	0.846	0.198767	3.364353	1.372965	14.33
22	17.27	0.846	0.238373	4.034725	2.050972	11.19
24	16.37	0.846	0.268350	4.542122	2.440826	9.39
28	14.57	0.846	0.347708	5.885338	3.322236	5.36
31	13.22	0.846	0.423551	7.169069	4.072282	1.98

Piezoelectric Driven Miniature Thermoacoustic Refrigerator

Manju Lata^{a*}, Nilesh Kolekar^b, Abhishek Swarnkar^a

^aMechanical Engineering Department, Gandhinagar Institute of Technology, Gandhinagar, India

^bMechanical Engineering Department, A.G. Patil Institute of Technology, Solapur, India

Abstract

Thermoacoustic Refrigerator is an attractive refrigeration technology which does not require any moving parts and harmful refrigerants in its operation. This technology use acoustic waves to pump heat from cold end to hot end. Majority of Refrigerators have used electromagnetic loudspeaker to generate the acoustic waves as input but in this research work piezoelectric driver is used to generate the acoustic input. Refrigerator is driven at high frequency by piezoelectric driver. The working fluids used are N₂, CO₂, Ar and He pressurised at 10 bar. The operating frequency is high, therefore the refrigerator is compact. This mini refrigerator can be used for space applications where electronic component need to be cooled. Experimental investigation is done on piezoelectric driven miniature thermoacoustic refrigerator and results are shown.

Keywords: Thermoacoustic refrigerator, acoustic power, stack

Nomenclature

δ_k Thermal penetration depth	x_n Normalized stack position
K Thermal conductivity of gas (W/mK)	D Drive ratio
ω Angular frequency (radian)	σ Prandtl number
ρ Density of the gas (Kg/m ³)	δ_{kn} Normalized thermal penetration depth
C_p Specific heat of gas (J/kgK)	ΔT_{mn} Normalized temperature difference
δ_{kn} Normalized thermal penetration depth	B Blockage ratio
Q_{cn} Normalized cooling power	u Volume velocity
W_n Normalized acoustic power	k Wave number
γ Ratio of isobaric to isochoric specific heat	p_0 Pressure amplitude
L_{sn} Normalized stack length	p_m Mean pressure
A Sound velocity in gas	x Cold heat exchanger position from driver

1. Introduction

Thermoacoustic is a science which is concerned with the interaction between heat (thermo) and pressure oscillations in gas (acoustic). Thermoacoustic devices use the ideal gas law and second law of thermodynamics to transfer heat into sound waves known as thermoacoustic engine or to use oscillations of sound to transport heat which is known as thermoacoustic refrigerator.

Most of the new refrigerants which are available now are ozone friendly but many of them contribute to greenhouse gas emission therefore there is urgent need to develop refrigeration system utilizing green refrigerants so thermoacoustic refrigerator is one of the effective technology to come over it. It is a green and a new technology. The working medium of thermoacoustic refrigerator is inert gases and the gases which are not hazardous to the atmosphere. When a sound wave travels through the air or any other compressive fluid it creates pressure and motion oscillations in the gas, temperature of the gas also oscillates. When sound waves travel through the gas in small channel heat also flows to and from the channel walls. The combination of all such oscillations produces thermoacoustic effect.

*Corresponding Author Tel: +91 8347010868

E-mail address: manjulata.pal@git.org.in

2. Thermoacoustic Refrigerator

Thermoacoustic refrigerator is based on the principle that sound waves are pressure waves. These sound waves propagate through the air via molecular collisions. The molecular collision causes a disturbance in the air, which in turn creates constructive and destructive interference. The constructive interference makes the molecules compress and destructive interference makes the molecules expand. This principle is basic behind the thermoacoustic refrigerator.

Thermoacoustic refrigerator mainly consists of resonator, acoustic driver attached to an acoustic resonator filled with a gas, stack, hot heat exchanger and cold heat exchanger, function generator, amplifier. In the resonator a stack and two heat exchangers are placed.

2.1 Acoustic Driver

Bimorph driver is a standard commercial item used in most piezoelectric tweeters because it can be very efficient. This driver consists of a pair of piezoelectric plates in parallel working against each other, this causes a powerful bending action. When the power is supplied to the piezoelectric tweeter it oscillates back and forth due to this pressure wave is generated in the resonator. It is driven by a function generator and a power amplifier to provide the required power to excite the working fluid inside the resonator.

2.2 Resonator

It is one of the components of the TAR in which sound wave propagates. It is a hollow tube in which stack and heat exchangers are placed. Resonator used in this research is called quarter wave length resonator which means one end of the resonator is open and another end is closed. End of the resonator attached with the compliance is a pressure node and velocity antinode. The end near the tweeter has boundary conditions pressure antinode and velocity node. End attached with compliance acts as an open end and another end attached with tweeter acts as a closed end. The approximate resonator length is calculated as

$$\bullet L = \frac{v}{4f}$$

2.3 Stack

Stack plays an important role in thermoacoustic devices. It is the heart of the thermoacoustic refrigerator and it is used to maintain imperfect thermal contact between the working gases and stack material which causes to phase shift between temperature and pressure oscillation of the gas molecules, this converts temperature oscillations into temperature gradient. The amount of heat that is pumped through the stack depends upon various parameters of the stack such as material of the stack, spacing between the stack plates, position of stack in the resonator. Spacing between the stack plates depends upon the thermal penetration depth (δ_k). Thermal penetration depth is defined as the distance through which heat diffuses into the gas. Generally spacing between the stack is $2\delta_k$ to $4\delta_k$. In this research work mylar is used as a stack material because of its low thermal conductivity.

The expression for the thermal penetration depth (δ_k) is given by:-

$$\delta_k = \sqrt{\frac{2k}{\rho C p \omega}}$$

The equation for heat and work flow that is flowing in thermoacoustic parts is given by:-

$$Q_{cn} = -\frac{\delta_{kn} D^2 \sin 2x_n}{8\gamma(1+\sigma)\Lambda} [\Delta T_{mn} \tan x_n (1 + \sqrt{\sigma} + \sigma) / (\gamma - 1) B L_{sn} (1 + \sqrt{\sigma} - (1 + \sqrt{\sigma} - \sqrt{\sigma} \delta_{kn}))],$$

$$W_n = \frac{\delta_{kn} D^2 L_{sn}}{4\gamma} (\gamma - 1) B \cos x_n^2 \left[\frac{\Delta T_{mn} \tan x_n}{(\gamma - 1) B L_{sn} (1 + \sqrt{\sigma}) \Lambda} - 1 \right] - \frac{\delta_{kn} L_{sn} D^2 \sqrt{\sigma} (x_{ns})}{4\gamma B \Lambda}$$

Where,

$$\Lambda = 1 - \sqrt{\sigma} \delta_{kn} + 0.5 \sigma \delta_{kn}^2$$

$$\Gamma = \frac{\Delta T_{mn}}{(\gamma - 1) B L_{sn}} \tan x_n$$

2.4 Heat Exchangers

Heat exchangers are generally made up of copper and often have similar cross sectional profiles as the stack. The porosity of the heat exchanger should match that of the stack in order to maintain the velocity of the flow through the stack. Two heat exchangers hot and cold heat exchanger are placed both of the stack. One heat exchanger is used to pump the heat from the refrigerator to the atmosphere; it is called as hot heat exchanger and another is used to pump from cooling place to the working gas is called as cold heat exchanger. The length of heat exchanger is decided by displacement amplitude of the gas molecules that is taking place because of driver. The displacement amplitude of the gas molecules is given by

$$L_1 = \frac{u}{\omega} = \frac{p_0}{\omega \rho_m a} \sin kx$$

2.5 Working Gas

The working gas used must have high sound velocity and thermal conductivity for better performance. Because of high thermal conductivity and sound velocity the thermal penetration depth of the gas decreases. Thermal penetration depth should be optimum because large thermal penetration depth means large plate spacing and therefore less gas molecules will get chance to interact with stack plates hence less thermoacoustic phenomena occur. When the thermal penetration depth is small then manufacturing of the stack becomes difficult. In this work He, N₂ CO₂ and Ar are used.

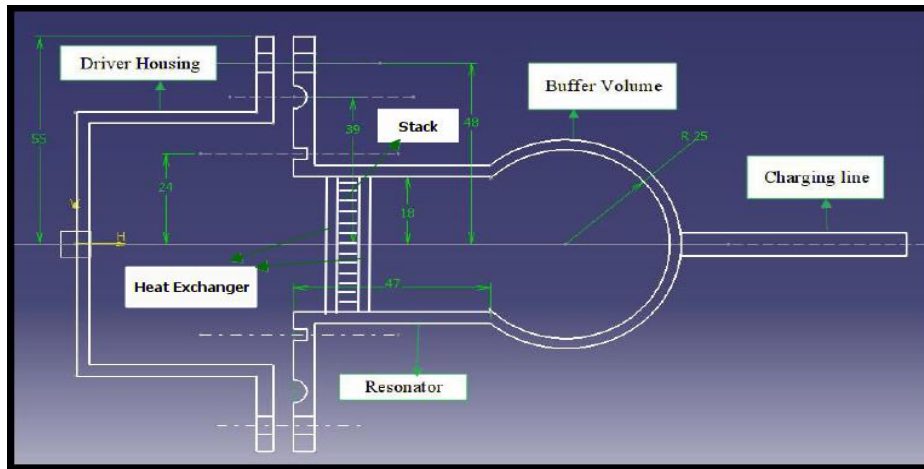


Figure 1: Schematic diagram of Miniature thermoacoustic refrigerator

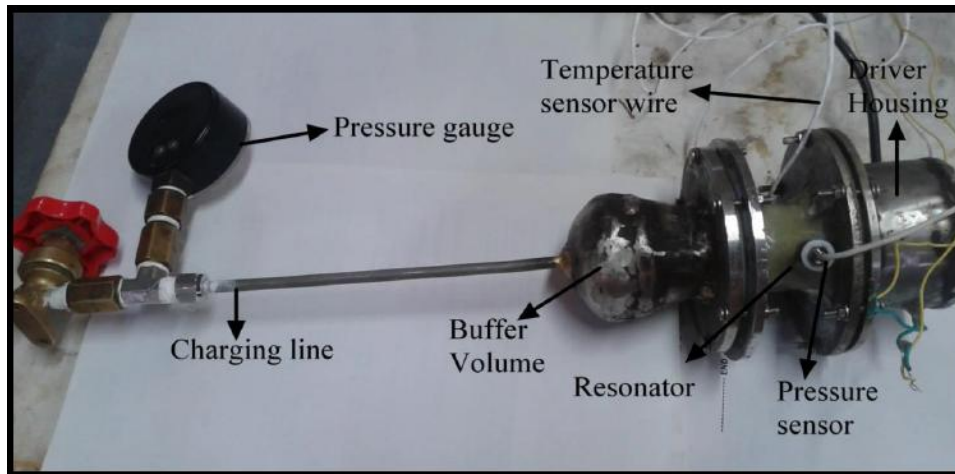


Figure 2: Assembly of actual Miniature Thermoacoustic Refrigerator

3. Instrumentation

Appropriate measurements and instrumentation is another vital role in this research. For measuring different parameters such as pressure, temperature sophisticated instruments with high accuracy are used. The sensors and instruments are well calibrated. The necessary arrangement is made to measure different parameters like pressure amplitude, hot end and cold end temperature during experiments.

3.1 Pressure Transducer

In order to measure the pressure amplitude and pressure, piezo- resistive type pressure transducers are used. Pressure sensor is mounted on resonator. This pressure sensor is attached to the resonator with the help of adopter made up of Teflon material in order to make whole setup leak proof. The signals from pressure transducer are need to be conditioned, also external excitation voltage is required for transducer and therefore for supply external excitation voltage and signal conditioning, a DC amplifier is used. Output from transducer is logged through Labview software by using USB 6341 DAQ card.

3.2 DC Amplifier

The output from pressure transducer is given to the DC amplifier. A 3-channel DC differential voltage amplifier with manually or programmable control is used for given pressure transducer. The signal from pressure transducer requires excitation voltage, which can be given with the help of DC amplifier. It also conditioned and amplifies the signal for further processing to USB DAQ card. Low pass filter is used to reduce the high frequency signal.

3.3 Temperature Measurement

Hot end and cold end temperature measurement is done by using resistance temperature detector PT 100. The lead wires from temperature sensors are connected to NI 9219, 4-channel universal C series module. Temperature is logged through Labview software and measurement can be done on personal computer. For temperature measurement appropriate circuit is programmed in the front panel of Labview software.

3.4 Function Generator and Amplifier

The function generator is used to generate frequency sinusoidal input signal to drive the piezoelectric tweeter . Since power delivered by the function generator is not enough to get desired pressure amplitude so amplifier is used to bring the signal upto the desired amplitude. This amplified signal drove the piezoelectric tweeter which is the input to the thermoacoustic refrigerator.

4. Results and discussions

The performance of miniature thermoacoustic refrigerator is assesed by using four gases at different pressure. The effect of frequency on pressure amplitude and the effect of charging presssure on pressure amplitude are shown below. Experiments on each gases are performed at 2bar, 4bar, 6bar, 10 bar. Effect on pressure amplitude by varying frequency is noted. The frequency at which the pressure amplitude is maximum that frequency is known as Resonant Frequency, at this frequency impedance of loudspeaker and impedance of refrigerator system matches with each other. Temperature drop at the cold heat exchanger is obserbed at frequency near about the resonant frequency. Performance of each working fluid also shown.

4.1 Effect on pressure amplitude

Effect on pressure amplitude by varying frequency and charging pressure are show by using N₂, Ae, He and CO₂ gases.

4.1.1 Frequency

(a) Argon

Experimental setup is charged by using Argon as the working fluid at 10 bar. Through function generator and amplifier input is given to the piezoelectric tweeter. Frequency is varied from 2 KHz to 7 KHz by function generator and pressure amplitude for different frequency is noted which is plotted in figure. This figure 3(a) shows effect on pressure amplitude by varying frequency. It is observed that maximum pressure amplitude of 250mbar is obtained at 5.8 KHz. This frequency is known as Resonant Frequency.

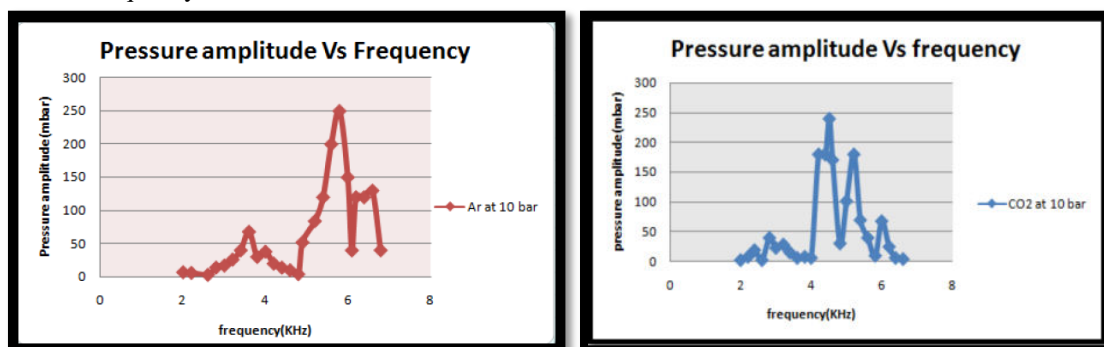


Figure 3: Effect of frequency on pressure amplitude a) Ar b) CO₂

(b) Carbon Dioxide(CO₂)

Figure 3(b), shows effect on pressure amplitude by varying frequency from 2 KHz to 7 KHz by giving same power input to the piezoelectric tweeter .Maximum pressure amplitude of 240 mbar is obtained at frequency 4.5 KHz. So,obtained resonant frequency for carbon dioxide gas is 4.5 KHz.

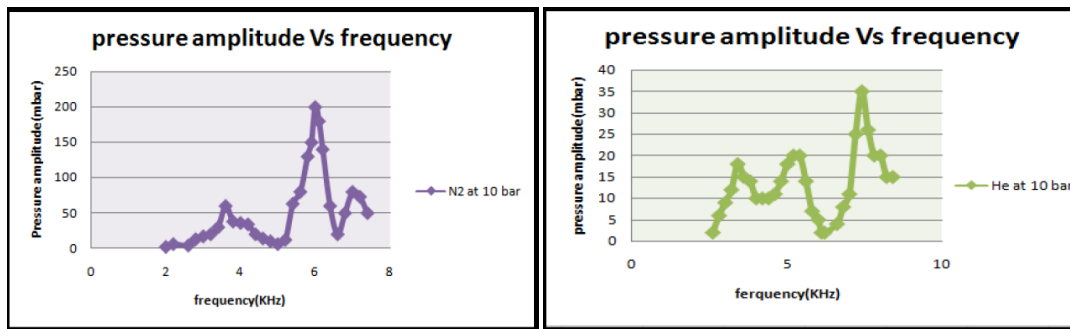


Figure 4: Effect of frequency on pressure amplitude a) N₂ b)He

Figure 4(a), shows change in pressure amplitude by varying frequency through function generator. Here also frequency is varied from 2KHz to 7 KHz and maximum pressure amplitude obtained is 200mbar at frequency 6 KHz.

(c) Helium(He)

Maximum charging pressure of Helium is 10 bar and frequency is varied from 2 KHz to 8 KHz. In this figure 4(b), it is shown that at 7.4 KHz frequency ,maximum pressure amplitude i.e. 35 mbar is obtained from same power input.

4.1.2 Charging Pressure

(a) Argon

Figure 5(a), shows effect on pressure amplitude by varying charging pressure at 5.8 KHz resonant frequency. It is obsered that pressure amplitude increases by increasing charging pressure. At 2 bar, pressure amplitude obtained is 14 mbar and at 10 bar, pressure amplitude is 250 mbar.

(b) Carbon Dioxide (CO₂)

Effect on pressure amplitude by varying charging pressure at resonant frequency 4.5 KHz is shown in figure 5(b). From this figure it is observe that as charging pressure increases the pressure amplitude also increases. At 2 bar, pressure amplitude obtained is 61 mbar and at 10 bar pressure amplitude obtained is 240 mbar.

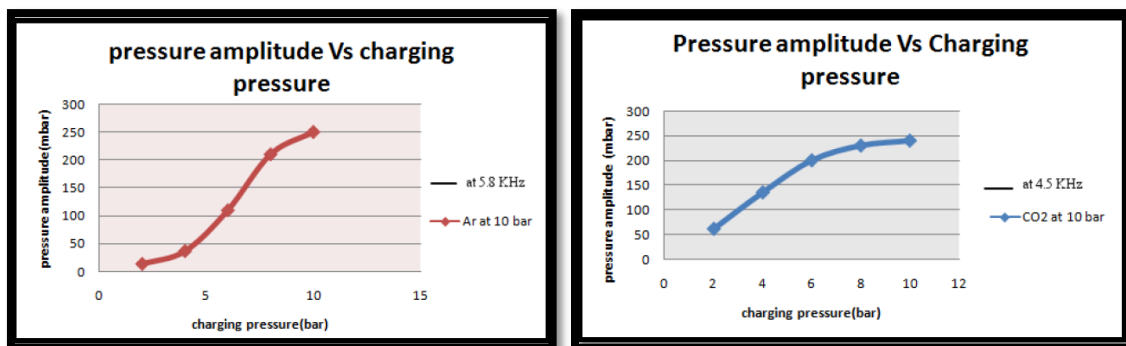


Figure 5: Effect of charging pressure on pressure amplitude a) Ar b) CO₂

(c) Nitrogen

Figure 6(a) shows effect on pressure amplitude by varying charging pressure at 6 KHz resonant frequency. At 2 bar, pressure amplitude obtained is 14.2 mbar and at 10 bar, pressure obtained is 200 mbar. This indicates that as charging pressure increases pressure amplitude also increases.

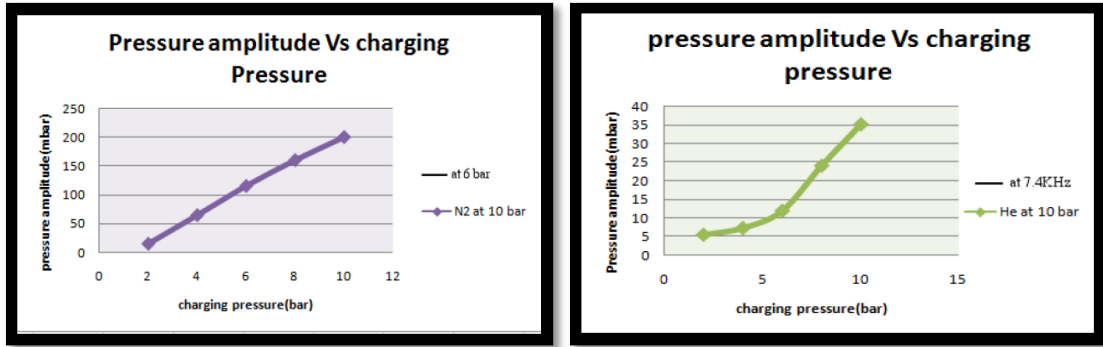


Figure 6: Effect of charging pressure on pressure amplitude a) N₂ b) He

(d) Helium (He)

Variation of pressure amplitude with charging pressure is shown in figure 6(b), same trend is also seen for helium. At 2 bar pressure amplitude obtained is 5.6 mbar and at 10 bar pressure amplitude is 35 mbar at resonator frequency of 7.4 KHz.

4.1.3 Effect on Cold End Temperature with Time

(a) Argon(Ar)

Figure 7(a), shows temperature drop at the cold end. As time increases temperature drop goes on increasing upto certain point and after that it remains constant. Temperature drop takes place from 36.47°C to 34.72°C at frequency 5.6 KHz in 158 minutes.

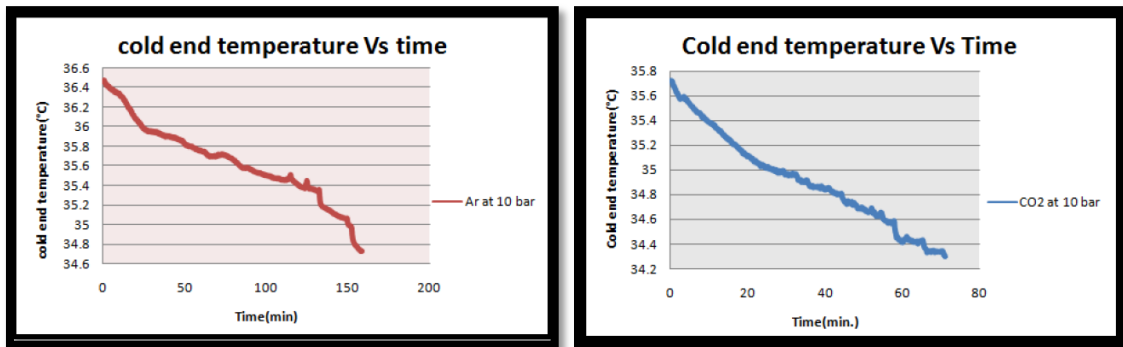


Figure 7: Effect on cold temperature with time a) Ar b) CO₂

(b) Carbon Dioxide(CO₂)

Drop in cold end temperature with respect to time at frequency 5.6 KHz is shown in figure 7(b). As the time increases it is observed that at 4.4KHz temperature drop starts from 5.6 KHz . As the time increases it is observed that at 4.4 KHz temperature drop starts from 35.71°C to 34.30°C in 72 minutes.

(c) Nitrogen(N₂)

It is observed from figure 8(a) that at frequency 5.8 KHz in 27 minutes temperature of cold end decreases from 32.90°C to 32.36°C and after that it remain constant.

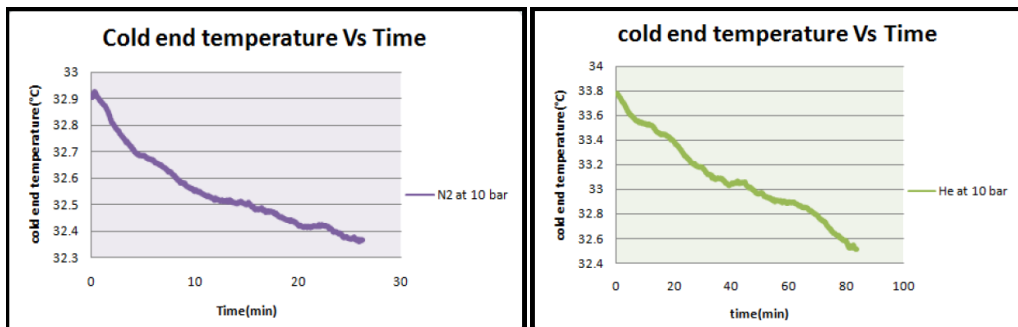


Figure 8: Effect on cold temperature with time a) N₂ b) He**(d) Helium (He)**

Figure 8(b), shows effect on cold temperature with time. Temperature drop from 33.778°C to 32.51°C is obtained at frequency 7.45 KHz.

Conclusions

Conclusions obtained from the above experiment are as follow:-

- Resonant Frequency for different gases are not same but changes with working fluid .
- Pressure amplitude of the gases changes linearly with respect to charging pressure.
- Maximum temperature drop of 1.75°C is obtained while working with Argon.
- Resonant frequency plays a vital role in the operation of miniature thermoacoustic refrigerator. It is found that pressure amplitude reached a maximum value when the operating frequency is close to the resonance frequency. Away from the resonance the pressure amplitude is negligible even at high input power.
- In order to get temperature drop, high pressure amplitude is required. At low pressure amplitude, the rate of temperature drop in thermoacoustic refrigerator is very slow which is negligible because of external heat leaks.

References

- [1] Tijani MEH., 2001, “Loudspeaker Driven Thermoacoustic refrigerator”, PhD Dissertation, Technical University of Eindhoven, Netherland.
- [2] Hofler TJ,1986, “Thermoacoustic refrigeration design and performance”, PhD Dissertation, Physics department, University of california, San Diego.
- [3] Daniel George,2010, “Piezoelectrically driven thermoacoustic refrigerator”, Master of Science,University of Maryland, college park.
- [4] Swift G.W.,2002, “Thermoacoustics: a unifying perspective for some engines and refrigerators”, Acoustic society of America.
- [5] <http://www.lanl.gov/thermoacoustic/ehistory.pdf>

Separating and Feeding Sheets automatically with the help of Magnetic Force

Ankit V. Patel^a, Sunny K. Parikh^a, Amit R. Patel^a

^aGandhinagar Institute of Technology, Gandhinagar, India

Abstract

The Purpose of the Paper is to provide a Solution against the manual feeding of the sheets into the Sheet Rolling Machine. In Industry people are using manually fed sheet rolling machine. Magnetic Sheet Separator and Feeder will feed the sheets automatically with the use of magnetic force. That will Increase the production, reduce the labour cost and works continuously. Manual sheet feed operation is mainly intermittent which will increase the total lead time in production. So, The Automatic sheet feeder is the best solution against it.

Keywords: Scissor table with Rack & Pinion Mechanism; Permanent Magnet; Electric Motor; Pusher Mechanism

Nomenclature

W	Load on the table (N)
L	Half of the length of arm (mm)
L_t	Length of the Scissor table (mm)
B_t	Breadth of the Scissor table (mm)
T_t	Thickness of the Scissor table (mm)
M	Moment (N.mm)
I	Polar Moment of Inertia (mm^4)
b	Width of the Arm
d	Depth of the Arm

Greek symbols

ϕ	Angle between the arm with Horizontal line at maximum position of Scissor Table (degree)
σ_b	Bending Stress
σ	Normal Stress
τ_{xy}	Shear Stress

Subscripts

R_{EX}	Reaction at point 'E' in X- Direction (N)
R_{EY}	Reaction at point 'E' in Y- Direction (N)
F_{CX}	Force at point 'C' in X- Direction (N)
F_{CY}	Force at point 'C' in Y-Direction (N)

Introduction

- Today in all Industries like Paper, Printing, Food, Automobile, Can making industries sheets are used. In past all industries were using the manually feed sheet rolling machine. But now a days the requirement is increasing. So for satisfying it production must be increase which can be possible by automation. Automatic Sheet feeder is now a days using in mostly industries like printing, paper and automatic. In can making small industries still they are using manually fed sheet rolling machine. So, Mechanism suggested in this paper can be used for automatic feeding. Design suggested in this paper is for can making industries.

Brief about Mechanism

- Magnetic Sheet Separator and Feeder will Separate the sheet from the Stack of sheet and feed it in to the Sheet Rolling Machine by creating Magnetic Repulsion force between the sheets. Repulsion force is created by permanent Magnet (NdFeB) which creates its own persistent magnetic field. Sheet is fed in the Rolling machine by Pusher

Mechanism. Scissor table will move upward after feeding one sheet in the machine for feeding the next Sheet. The upward motion of the table is stopped by the Light Sensor. Rack and pinion is used in the Scissor table which will provide better locking capability against the hydraulic or pneumatic table, also provide accurate Lift and capability of handling load at specific elevation for specific period of time.

Scissor Table

- A lift table is a device that employs a scissors mechanism to raise or lower goods and/or persons. Typically lift tables are used to raise large, heavy loads through relatively small distances. Extension is achieved by applying pressure to the outside of a set of supports located at one end of the mechanism, elongating the crossing pattern.
- There are mainly three types of scissor table available in the market. (i) Hydraulic (ii) Pneumatic (iii) Mechanical with Lead screw driven.
- Scissor table mentioned in this paper is Rack & pinion type which provides very accurate lift. Electric motor will drive the Pinion and the rotary motion of it is transferred to the rack in reciprocating motion. One end of the rack is fixed with the one of the arm of the table. Both the arms of the table is joined by hinge joint so that motion of one will be transferred to the other. So that when pinion rotates rack will reciprocate that motion is copied by one of the arm, but as the constraints are provided on the table’s arm the table will move upward or downward as per the rotation of the motor.

Permanent Magnet

- A neodymium magnet (also known as NdFeB, NIB or Neo magnet), the most widely used type of rare-earth magnet, is a permanent magnet made from an alloy of neodymium, iron and boron to form the Nd₂Fe₁₄B tetragonal crystalline structure. Developed in 1982 by General Motors and Sumitomo Special Metals, neodymium magnets are the strongest type of permanent magnet commercially available.

Light Sensor

- Light Sensor is used to stop the upward motion of table So that another sheet can be pushed to the Rolling Machine. The Light Sensor is a passive devices that convert this “light energy” whether visible or in the infra-red parts of the spectrum into an electrical signal output. Light sensors are more commonly known as “Photoelectric Devices” or “Photo Sensors” because they convert light energy (photons) into electricity (electrons).

2.4 Pusher Mechanism

Pusher Mechanism is basically a Slider-Crank Mechanism Works by the motor will push the sheets by the reciprocating link. Pusher Mechanism can also work on a different motor or also work on a motor which drives the rack in scissor table by belt or chain arrangement.

Design of Scissor Table

Collected Data

Table 1. Collected Data Table

1. Input Parameters of Rolling Machine	2. Values (mm)	3. Input Parameters of Raw Material	4. Values
5. Bigger Roller Diameter	6. 66	7. Dimension of Sheet	8. 870*940*1 (mm ³)
9. Length of The Roller	10. 39	11. Material	12. Tin

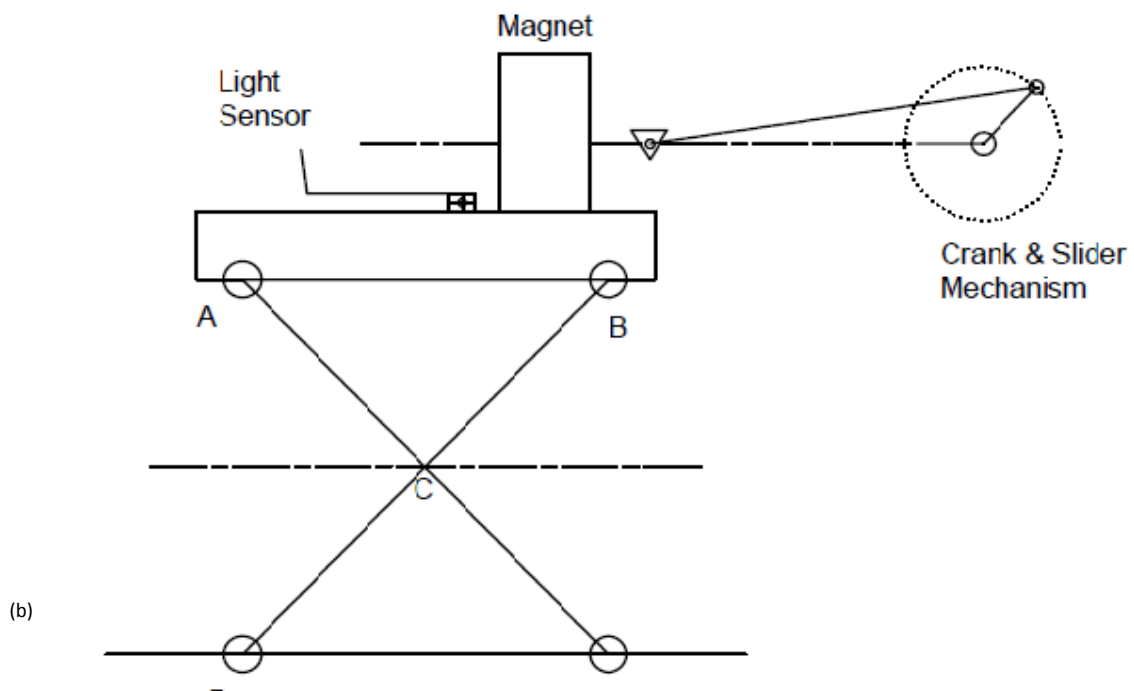
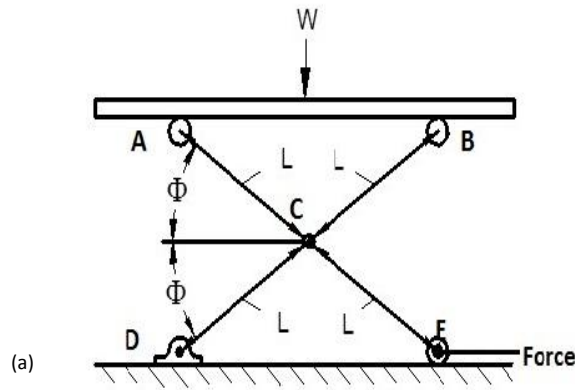
13. Height of the Machine from Ground

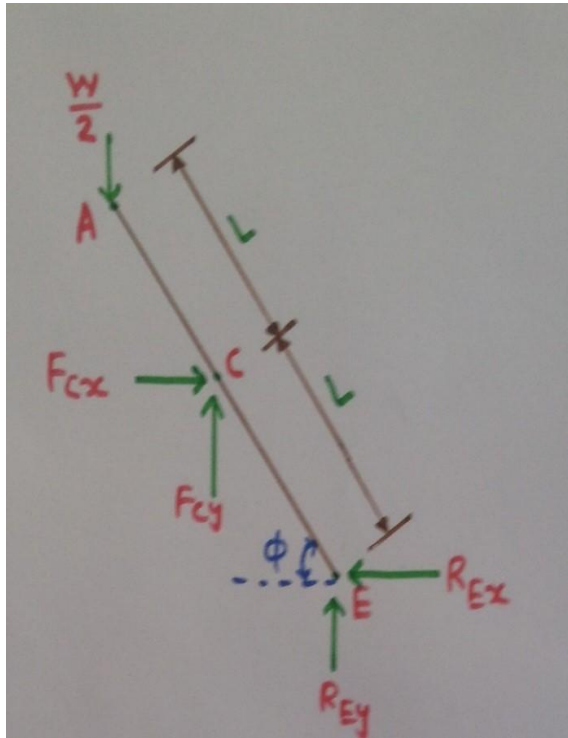
14. 840

15. Density

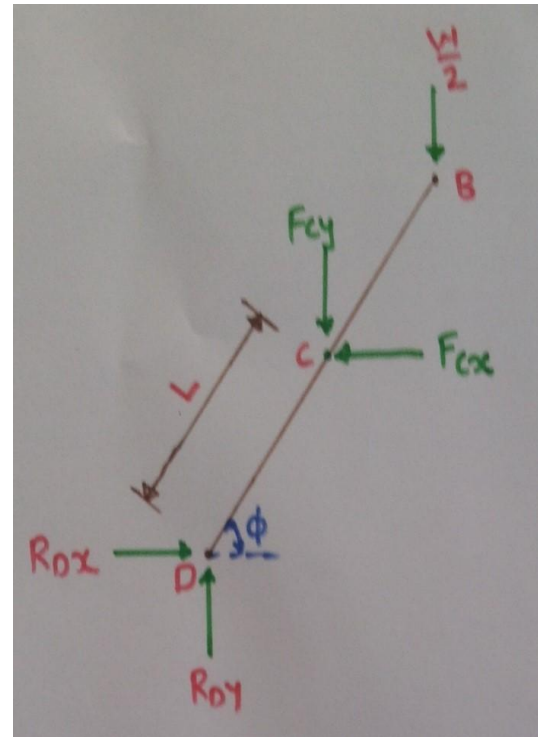
16. 7280 kg/m³

Author Artwork





(c)



(d)

Fig. 1. (a) Free Body Diagram of Table, (b) Basic Diagram of Magnetic Separator & Sheet Feeder, (c) Free body diagram of link AE, and (d) Free body diagram of link BD

Basic Design of Table

Load on the table is due to stack of sheets and that will produce bending stress on the table. Material of the table is ASTM Grade 30 [ISO Grade 200, EN-JL 1030 Grey Cast Iron]. By applying Bending equation the thickness of the table can be find out.

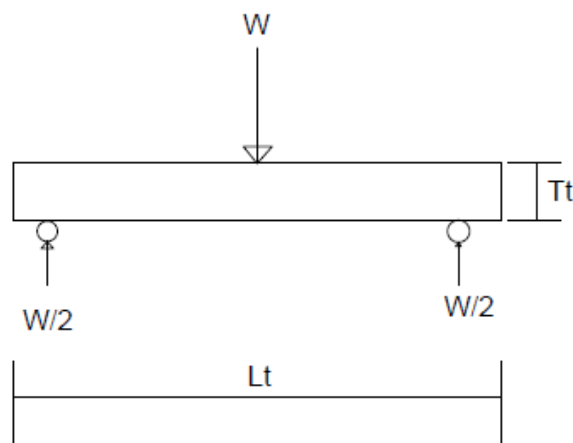


Fig 2. Load on the Upper Part of the Table.

Length of the table $L_t = 1000$ mm
 Breadth of the table $B_t = 400$ mm

$$\sigma_b = \frac{M}{Z} \quad [1]$$

Height of the table from the ground = 840 mm.
 Distance between two arm = 800 mm
 So, Length of the Arm = 1151 mm
 $\phi = 46^\circ$

Now, Writing down the elementary equations of Statistic Equilibrium

$$\begin{aligned} \sum M_{\text{Fixed point}} &= 0 \\ \sum F_H &= 0 \\ \sum F_V &= 0 \end{aligned}$$

Reactions at different points are,

$$\begin{aligned} R_{EX} &= 1000 \text{ N} \\ R_{DX} &= 1000 \text{ N} \\ R_{YE} &= 500 \text{ N} \\ R_{DY} &= 500 \text{ N} \end{aligned}$$

Basic Design of Arm

Material Selected for Arm is AISI 1045 Medium carbon Steel. Cross section of the arm is rectangular.

$$\frac{b}{d} = 2 \quad \bullet \text{ Assumption-}$$

Compressive normal load on Arm = Resultant of R_{DX} and $R_{DY} = 1118$ N

$$\sigma = \frac{P}{A} \quad [2]$$

$$\sigma = \frac{5559.016 \text{ N}}{d^2 \text{ mm}^2}$$

Now,

Bending stress will produced in the arm because of the load of the sheets and the reaction R_{DY}

$$\sigma_b = \frac{M}{Z}, \text{ where } M = \frac{W}{2} * 800, Z = \frac{bd^3}{12}$$

$$\sigma_b = \frac{24 * 10^5 \text{ N}}{d^3 \text{ mm}^2}$$

Applying principal stress theory,

$$\sigma_{1,2} = \frac{\sigma_x + \sigma_y}{2} \pm \sqrt{\left(\frac{\sigma_x - \sigma_y}{2}\right)^2 + \tau_{xy}^2} \quad [3]$$

Here, $\sigma_x = \sigma$, $\sigma_y = \sigma_b$, $\tau_{xy} = 0$

$$\sigma_1 = \frac{559.0165}{d^2} \frac{N}{mm^2},$$

$$\sigma_2 = \frac{24 * 10^5}{d^3} \frac{N}{mm^2}$$

Equating it with the Strength of the material and taking Factor of Safety= 2.0

Width of the arm (b) = 50 mm

Depth of the Arm (d) = 25 mm

3.5 Construction of References

- Books: -

[1] Strength of Material by S. Timoshenko, Page No.-92

[2] Strength of Material by S. Timoshenko, Page No.-4

[3] Statics and Mechanics of Material by Beer & Johnston, Page No.-577

- Websites: -

[1] www.pmlindia.com/products/magnetic-plate

[2] www.rajmanicastings.com/cast-iron-flat-bar--1558072.html

[3] www.gudel.com/products/mechanical-components

Acknowledgements

I would like to express my deepest appreciation to our final year project guide Ass. Prof. Amit R. Patel, whose contribution in stimulating suggestions and encouragement, helped me to coordinate my project especially in writing this report. My Sense of Obligation also goes to Industry's owner Mr. Kureshi, for giving me such attention and time.

A special gratitude to GIT-JET, for giving me chance to write this paper.

References

[1] Strength of Material by S. Timoshenko, Page No.-92

[2] Strength of Material by S. Timoshenko, Page No.-4

[3] Statics and Mechanics of Material by Beer & Johnston, Page No.-577

[4] http://www.electronics-tutorials.ws/io/io_4.html

[5] http://en.wikipedia.org/wiki/Neodymium_magnet

[6] PSG Design Data Book

[7] Sheet Feeder for a sheet processing Machine, US Patent US-4635924

Properties of the Material

Properties Of ASTM Grade 30 [ISO Grade 200, EN-JL 1030 Grey Cast Iron]

Ultimate tensile strength $s_{ut} = 250$ MPa

Shear Strength $s_{sy} = 276$ MPa

Modulus of Elasticity $E = 113$ GPa

Yield tensile Strength $S_{yt} = 130$ MPa

Properties Of AISI 1045 Medium Carbon Steel

Ultimate tensile strength $s_{ut} = 565$ MPa

Yield tensile Strength $S_{yt} = 310$ MPa

Modulus of Elasticity $E = 200$ GPa

Finite Element Analysis of Automobile Structural Member using ANSYS.

Tushar M Patel^{a,*}, Dr N M Bhatt^b

^aResearch Scholar, Mewar University, Gangrar, Rajasthan, India.
^bGandhinagar Institute of Technology, Gandhinagar, India

Abstract

Truck chassis is the structural backbone of any vehicle which supports the components and payload placed upon it. Reduction of fuel consumption and CO₂ emissions is one of the most important challenges facing the automotive industry. One way to reduce consumption is by optimizing the weight of the vehicle. Determination of the stresses of a truck chassis before manufacturing is important due to the design optimization. This paper presents the static load analysis of the automobile structural member using ANSYS workbench. The stress and deformation has been calculated for the chassis frame and the FE analysis has been done for the validation on the chassis frame model. In this present work chassis is modeled in Creo Parametric 3.0 and static load characteristics are analyzed using ANSYS workbench.

Keywords: FEA; Automobile Structural Member; Chassis Design; Ansys; Ladder Frame.

Nomenclature

FEA	Finite element analysis
CAD	Computer aided design
CAE	Computer aided engineering
E	Modulus of elasticity
SF	Safety factor

1. Introduction

Automobile chassis usually refers to the lower body of the vehicle including the tires, engine, frame, driveline and suspension. Out of these, the frame provides necessary support to the vehicle components placed on it. Also the frame should be strong enough to withstand shock, twist, vibrations and other stresses. The main functions of the chassis are to support the chassis components and the body to withstand static and dynamic loads without undue deflection or distortion. The frame must be rigid enough to support or carry all the loads and forces that the vehicle is subjected to in operation. A frame must also be flexible enough to handle shock loads and the twists, bends, sway and sag that it encounters under different road or load conditions. The frame should be able to flex under different situations, while being able to return to its original shape when loads or forces are removed.

Along with the strength, an important consideration in the chassis design is to increase the stiffness (bending and torsion) characteristics. Adequate torsional stiffness is required to have good handling characteristics. Normally the chassis are designed on the basis of strength and stiffness. The design of the chassis with adequate stiffness and strength is necessary.

Trucks are generally classified into following broader categories.

- Light Duty Truck
- Medium Duty Truck
- Heavy Duty Truck

Comparison of medium weight truck chassis frame is given in Table 1

* Tushar M PatelTel.: +91-9879799575.

E-mail address: tushar.modasa@gmail.com

Table 1: Comparison of medium duty truck

Make	Model	Frame Size (mm x mm x mm)	Load Body Length (mm)
TATA	1518	219x65x6	6582
LPT	1618	219x 65x6	7090
Eicher	11.14	210x76x6	5808
	11.12	210x76x6	4937
	11.10XP	210x76x6	6355
	11.10	210x76x6	6355
	10.95	210x76x6	4300
	10.90	210x76x6	4300
Ashok	1012 Strong	225x60x6	4267
Leyland	1012 Smart	225x60x6	4267
Ecomet	1212 Strong	225x60x6	5242
	1212 Smart	225x60x6	5242
	1616il	220x65x7	5486
Ashok	1616il/1	220x65x7	6096
Leyland	1616il/2	220x65x7	7315
	1616il/3	220x65x7	9753
AMW	1618	256x75x7	5315

From the comparison, it has been found that Eicher has lowest height of frame section and Eicher 11.10 has a maximum load body length (length of Frame). So this frame is having the greatest possibility of bending among all. So this frame has been considered for the case study.

Thus, the main objective of the project is to analyze Eicher 11.10 chassis frame. The chassis frame is made of two side members joined with a series of cross members.

2. Literature Review

Structural optimization using Finite Element Analysis (FEA) and other computational tools has become a major part in research and development process in recent years. The method has wide application and enjoys extensive utilization in the structural, thermal and fluid analysis areas.

Shroff et al. (2002) performed the optimization of the automotive chassis with the constraints of stiffness, strength and natural frequency. Structural systems like the chassis can be easily analyzed using the finite element techniques. A proper finite element model of the chassis was developed. The chassis was modeled with beam elements and pipe elements in ANSYS. Weight optimization was done on the modeled chassis using the first order optimization methods [6]. Karita et al. (2003) observed that aluminium was successfully used as the material for the chassis frame which was a main structural member of heavy-duty trucks, to significantly reduce the truck weight and so allow the payload to be increased. The shape and configuration of the aluminium frame design were optimized while maintaining strength and rigidity equivalent to those of a standard steel frame by using computer-aided-engineering analysis. Using the aluminium frame thus developed [7]. Butdee et al. (2008) applied the TRIZ principle and parameters to assist a light weight bus body design which was compared to the existing design. The bus body model was created by CAD and transfer data to CAE using FE analysis. The weight reduction process was then followed up from the analysis. The new light weight bus body design was tested by the same method of FE analysis. The same result of body strength was accepted and used for design and manufacturing. The tested TRIZ method can save material used, production cost and time [8]. Husaini et al. (2009) presented an analysis of the static stress that acts on the upper surface of the truck chassis. Finite element analysis helped in accelerating the design and development process by minimizing the number of physical tests, thereby reducing the cost and time for analysis. The commercial finite element package Algor was used for this simulation. 3-D model of the truck chassis was drawn by using Solid Works. Results showed the critical part of the chassis and some modifications were also suggested to reduce the stress and to improve the strength of the truck chassis [9]. Nor et al. (2012) performed Finite element modeling (FEM), simulations and analysis using a modeling software i.e. CATIA V5R18. Firstly, a 3-D model of low loader based on a design from SESB was created by using CATIA. The results of analysis revealed that the location of maximum deflection and maximum stress agree well with the theoretical maximum location of simple beam under uniform load distribution [10].

3. Finite Element Analysis

3.1 Basic Concept of FEA

The finite element analysis (FEA) is a computational technique used to obtain approximate solutions of boundary value problems in engineering. Simply stated, a boundary value problem is a mathematical problem in which one or more dependent variables must satisfy a differential equation everywhere within a known domain of independent variables and satisfy specific conditions on the boundary of the domain.

An unsophisticated description of the FE method is that it involves cutting a structure into several elements (pieces of structure), describing the behavior of each element in a simple way, then reconnecting elements at nodes as if nodes were pins or drops of glue that hold elements together (Figure 1). This process results in a set of simultaneous algebraic equations. In stress analysis these equations are equilibrium equations of the nodes. There may be several hundred or several thousand such equations, which mean that computer implementation is mandatory.

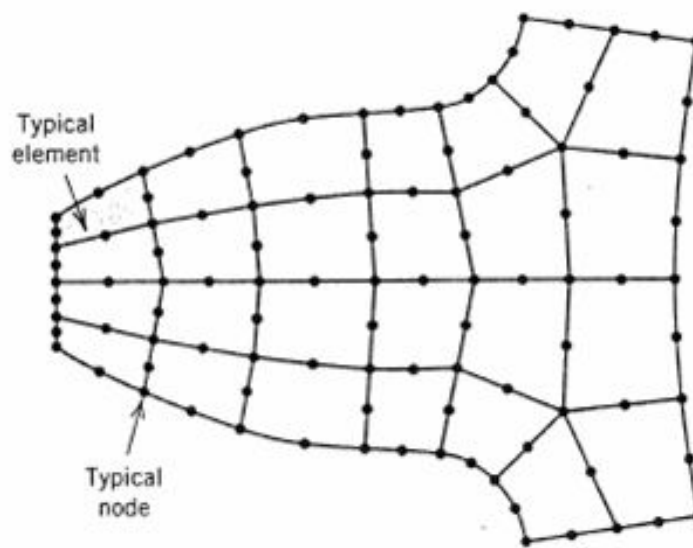


Figure 1: Discretization of model [4]

3.2 General Procedure for FEA

There are three main steps, namely: pre-processing, solution and post processing. In pre-processing (model definition) includes: define the geometric domain of the problem, the element type(s) to be used, the material properties of the elements, the geometric properties of the elements (length, area, and the like), the element connectivity (mesh the model), the physical constraints (boundary conditions) and the loadings.

In solution includes: the governing algebraic equations in matrix form and computes the unknown values of the primary field variable(s) are assembled. The computed results are then used by back substitution to determine additional, derived variables, such as reaction forces, element stresses and heat flow. Actually the features in this step such as matrix manipulation, numerical integration and equation solving are carried out automatically by commercial software.

In post processing, the analysis and evaluation of the result is conducted in this step. Examples of operations that can be accomplished include sort element stresses in order of magnitude, check equilibrium, calculate factors of safety, plot deformed structural shape, animate dynamic model behavior and produce color-coded temperature plots. The large software has a pre-processor and postprocessor to accompany the analysis portion and the both processor can communicate with the other large programs. Specific procedures of pre and post are different dependent upon the program.

4. Modeling and Analysis of Existing Chassis Frame

The model of existing chassis as per the dimension is created in Parametric Creo 3.0 as shown on Figure 2. The model is

then saved in *.x_t (Parasolid) format which can be directly imported into ANSYS workbench. Figure 3 shows the imported model in ANSYS workbench.



Fig. 2: CAD model of chassis in PTC Creo 3.0

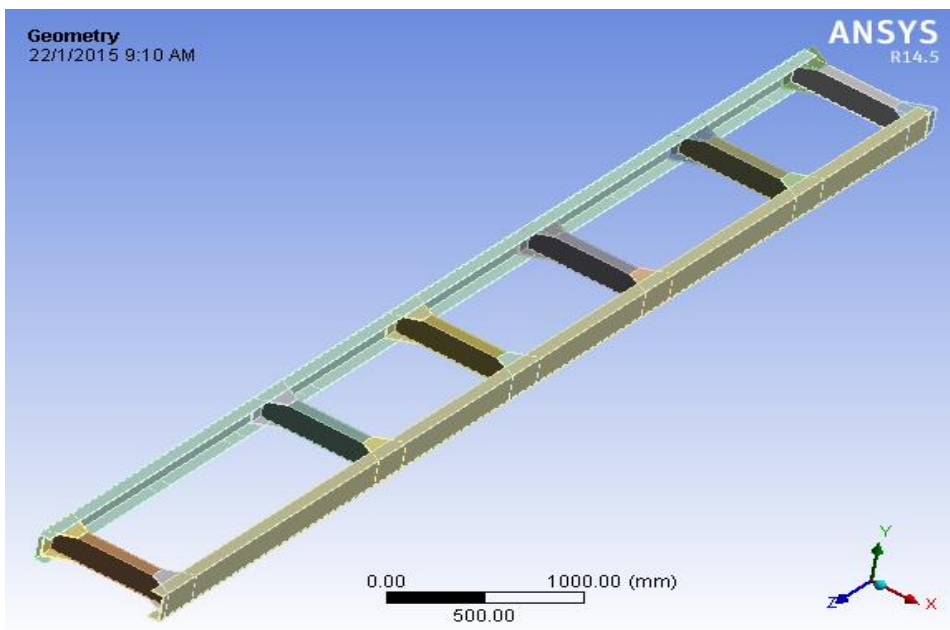


Fig. 3: Geometry of chassis frame in Ansys

4.1. Material of Model

For the frame geometry of chassis generally steel and its alloys are used. For the frame models, variety of materials, composite materials and different kind of alloys can be used. In the present study, ST 52 is used and its properties are as given below.

Table 1: Material properties of chassis [1]

Material	ST 52
Modulus of Elasticity E	2 x 10 ⁵ N/mm ²
Possion Ratio	0.3

Tensile Strength	520 N/mm ²
Yield Strength	360 N/mm ²

4.2. Connection Type

The connection type between the side bars, bracket and cross bar can be welded, riveted or it can be bolted. Normally riveted joint is used so here the riveted connection is defined in modeling as shown in Figure 4.

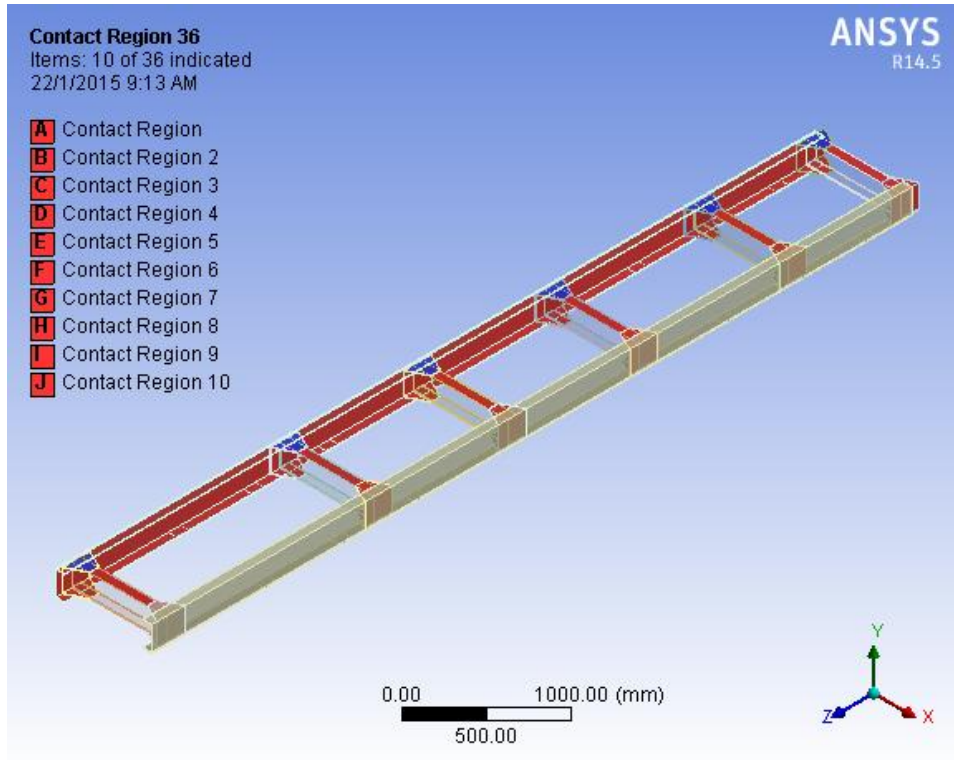


Fig. 4: Connection type of chassis frame

4.3 Meshing of Chassis Frame

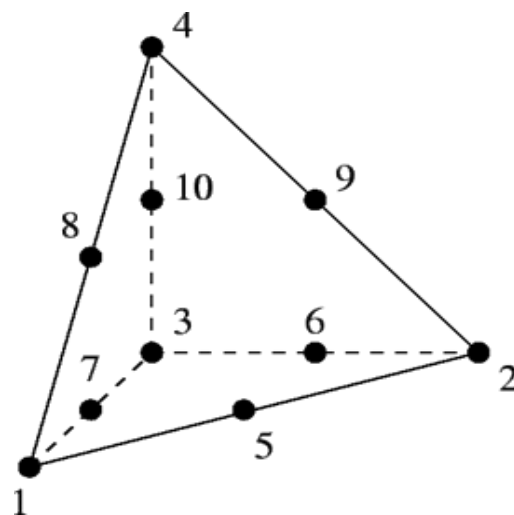


Fig. 5: Ten node tetrahedral element

For the meshing, 10 node-tetrahedral elements were chosen to model the solid chassis. Study by previous researcher

found that 10 node-tetrahedral elements gave a closer dynamic behavior to the experimental results [5]. Figures 5 and 6 show tetrahedral element and meshing of model respectively.

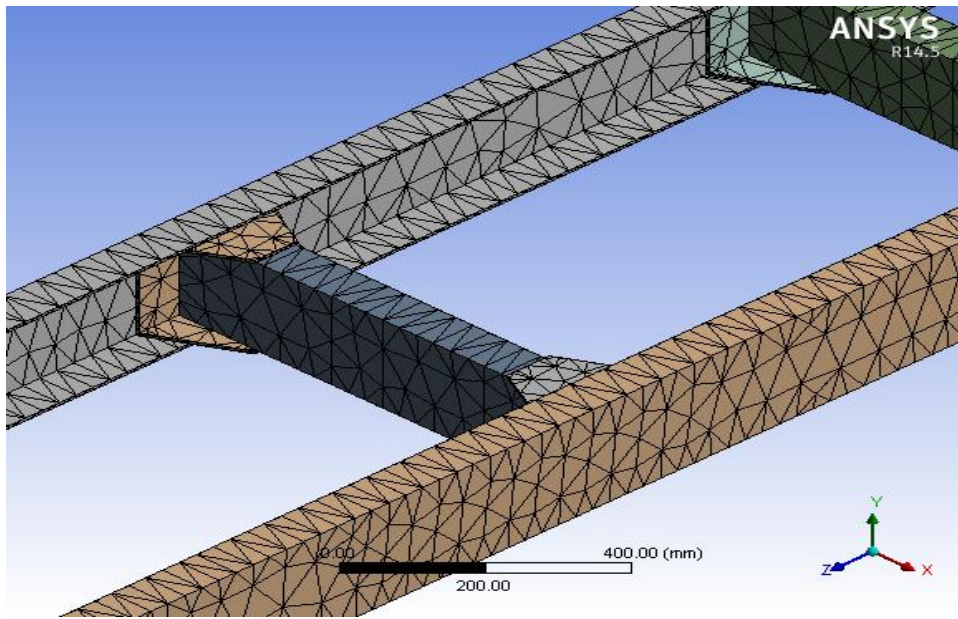


Fig. 6: Meshing of chassis frame

4.4. Loading Condition of Chassis Frame

The truck chassis model is loaded by static forces from the truck body and load. For this model, the maximum loaded weight of the truck plus the body is 12,000 kg. The load is assumed as a uniform distributed obtained from the maximum loaded weight divided by the total length of chassis frame [4]. Detail loading on the chassis frame model is shown in Figure 7. The magnitude of force on the upper side of the chassis is 117720 N which is carried by two side bars so load on one sidebar is 58860 N.

The chassis is fixed at four supports (wheels) two in front and two at the rear side as shown in Figure 8 [4].

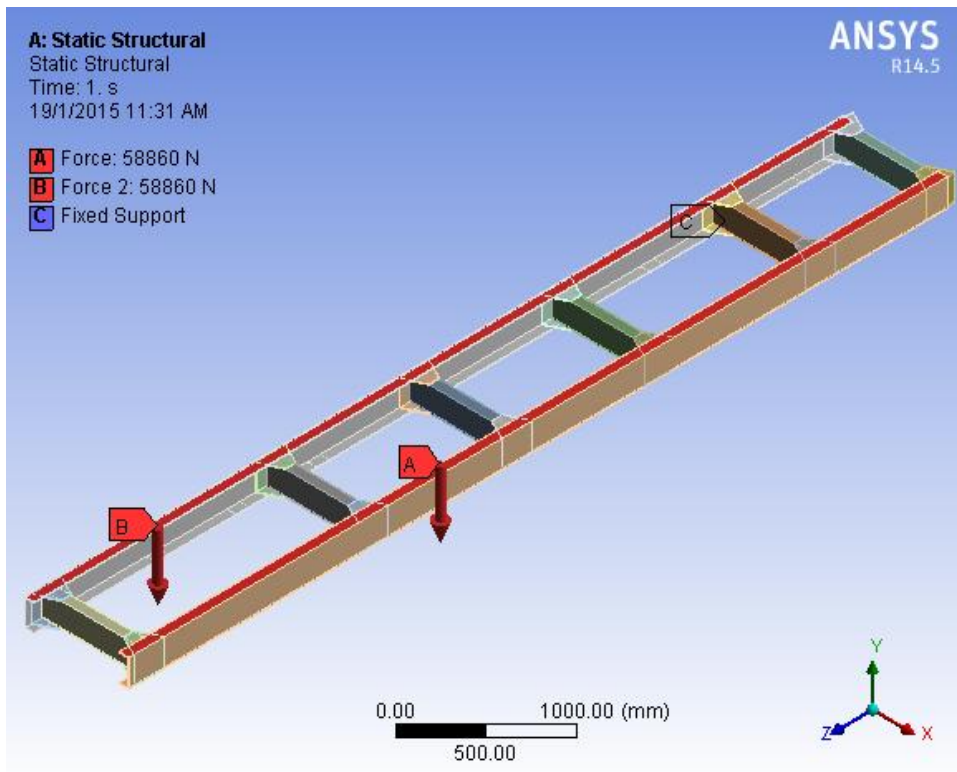


Figure 7: Loads on sidebar of chassis frame

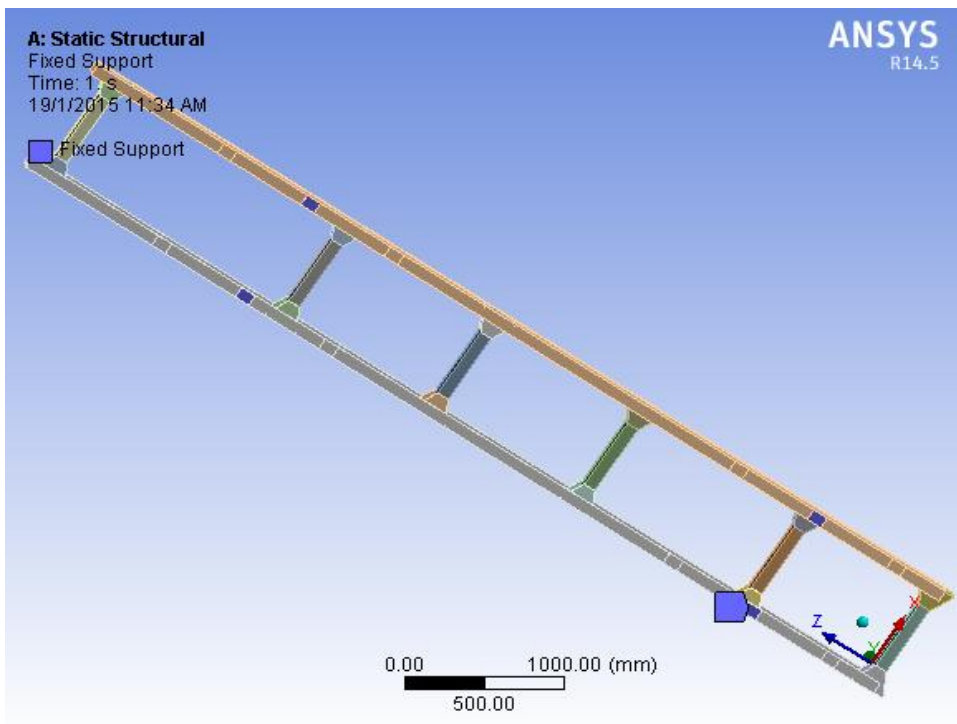


Fig. 8: Fix supports of sidebar

5. Results of Analysis

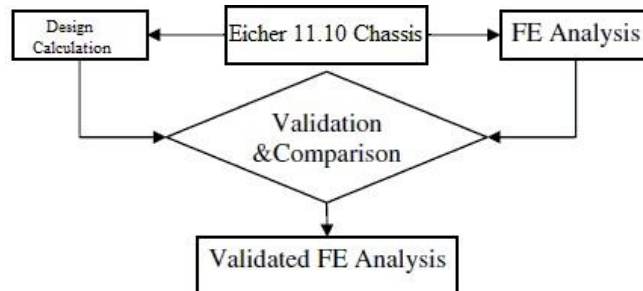


Fig. 9: Flow chart for validation

The analysis done on the chassis model gives the maximum generated equivalent stress value 88.171 KN (figure 11). The formula of design stress is defined as follow [1].

$$\text{Design Stress} = \frac{\text{Yield Stress}}{\text{Factor of Safety}}$$

Based on static safety factor theory, the magnitude of safety factor for this structure is 1.43 [5]. Vidosic (1957) recommends some value of safety factor for various condition of loading and material of structures. The value of 1.5 to 2 for well known materials under reasonably environmental condition, subjected to loads and stresses that can be determined readily [2]. Based on this result, it is necessary to reduce the stress magnitude of critical point in order to get the satisfy SF value of truck chassis. The truck chassis can be modified to increase the value of SF especially at critical point area. The value of the factor of safety recommended by “National Code of Practice, Heavy Vehicle Modifications Section H Chassis Frame” is 3 [3]. So, the permissible value of stress for material ST 52 is (360/3) 120 Mpa.

The generated equivalent stresses are less than the permissible value so the design is safe. The equivalent stress and deformation are as shown in Figure 10, 11 and 12.

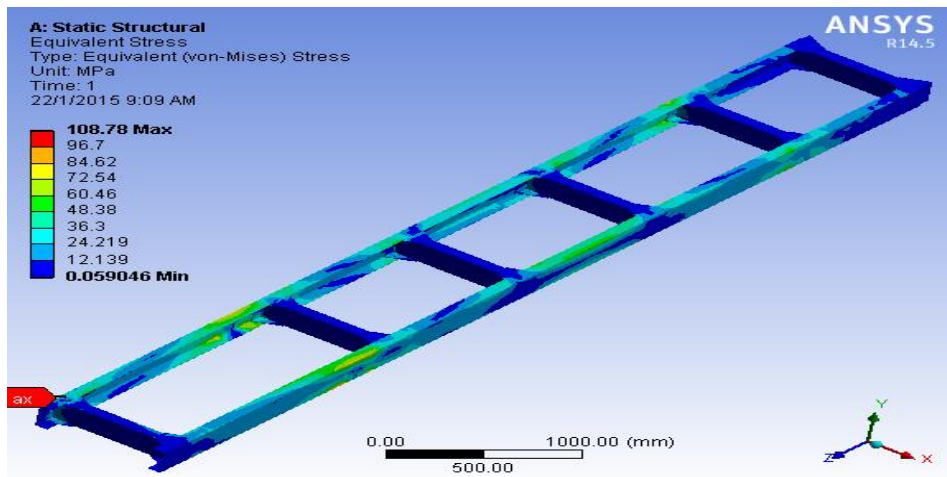


Fig. 10: Von misses stress on chassis frame (maximum at bracket)

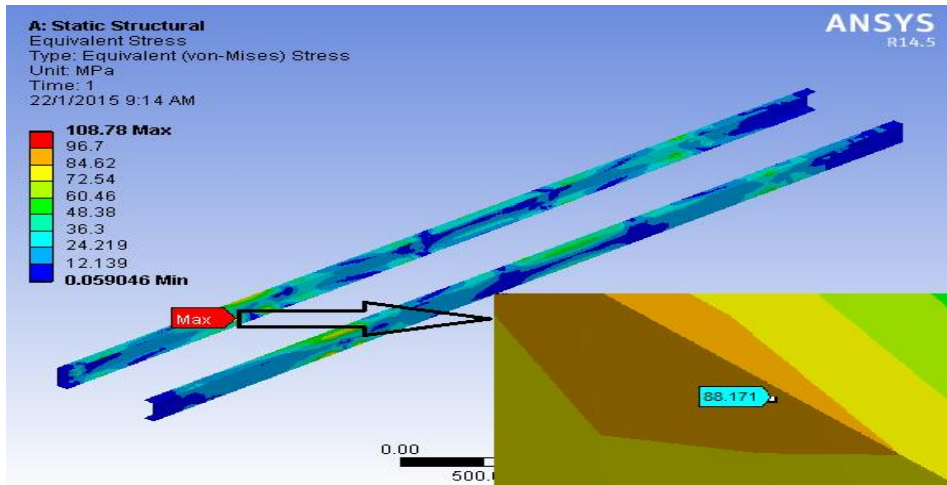


Fig. 11: Von misses stress on sidebar (maximum at sidebar)

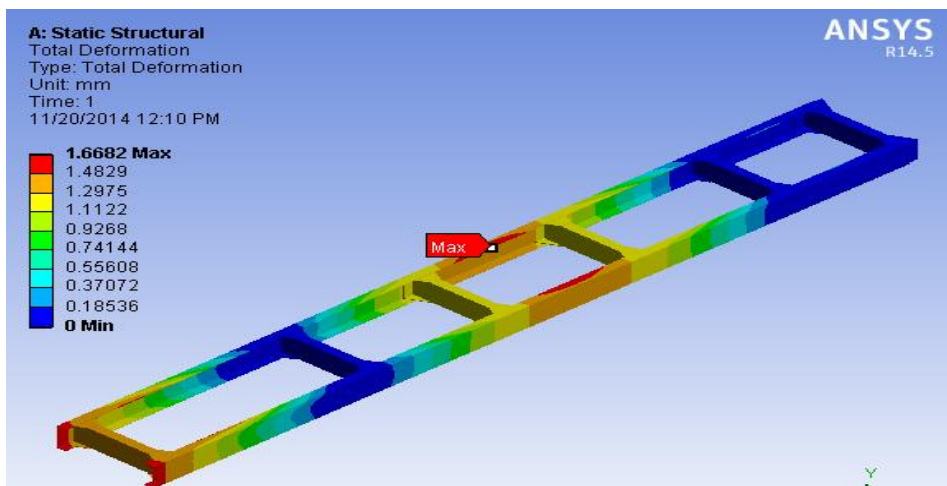


Fig. 12: Deformation of chassis frame

6. Conclusions

The generated equivalent stresses are less than the permissible value so the design is safe. The analysis gives maximum equivalent stress and total deformation which are in desired limit as shown in table 2.

Table 2: Comparison of analysis and calculated results

	FEA result	Calculated result
Equivalent stress Mpa	88.171	95.43
Deformation mm	1.67	2.85

This percentage variation is caused by simplification of model and uncertainties of numerical calculation.

References

- [1] Data, D. (2004). Data book of Engineers. PSG Tech, Coimbatore.
- [2] Vidosic, J.P. (1957). Machine Design Project, Ronald Press, New York.
- [3] National Code of Practice, Heavy Vehicle Modifications Section H Chassis Frame.
- [4] Dubey, A., & Dwivedi, V. (2012). Vehicle Chassis Analysis: Load Cases and Boundary Conditions for Stress Analysis. In Proceedings 11th National Conference on Machines and Mechanics (p. 395).
- [5] Abdul Rahman, R., Yusof, M., & Tamin, M. (2009). Development of a truck chassis (Doctoral dissertation, Universiti Teknologi Malaysia).

- [6] Shroff, R. (2002). Structural Optimization of Automotive Chassis (Master's dissertation, Indian Institute of Technology, Bombay).
- [7] KARITA, K. KOHIYAMA, Y., KOBIKI, T., Ooshima, K., & Hashimoto, M. (2003). Development of Aluminum Frame for Heavy-Duty Trucks. *Technical Review in Japan*, 15, 81-84.
- [8] Butdee, S., & Vignat, F. (2008). TRIZ method for light weight bus body structure design. *Journal of Achievements in Materials and Manufacturing Engineering*, 31(2), 456-462.
- [9] Husaini, M., & Wahab, A. (2009). Stress analysis on truck chassis (Doctoral dissertation, UNIVERSITI MALAYSIA PAHANG).
- [10] Nor, M. A. M., Rashid, H., Mahyuddin, W. M. F. W., Azlan, M. A. M., & Mahmud, J. (2012). Stress Analysis of a Low Loader Chassis. *Procedia Engineering*, 41, 995-1001.

FEM based Taguchi method to Reduce the Automobile Structural Member Weight

Tushar M Patel^{a,*}, Dr N M Bhatt^b

*Mewar University, Gangrar, Rajasthan, India.
Gandhinagar Institute of Technology, Gandhinagar, India.*

Abstract

Nowadays, fuel consumption reduction is an important challenge. One way to reduce fuel consumption is by weight reduction of the vehicle. The chassis frame serves as a backbone for supporting the body and different parts of the automobile. It should be rigid enough to withstand the shock, twist, vibration and other stresses. Along with strength, an important consideration in chassis design is to have adequate bending stiffness. The main objective of the research is to obtain the minimum weight of Eicher 11.10 chassis frame. The chassis frame is made of two side members joined with a series of cross members. The number of cross members, their locations, cross-section and the sizes of the side and the cross members becomes the design variables. The chassis frame model is to be developed in Parametric Creo 3.0 and analyzed using Ansys. Since the no. of parameters and levels are more, the probable models are too many. So, to select optimum parameters among them large no of modeling and analysis work is involved which consumes more time. To overcome this problem Taguchi method is used along with FEA. The weight reduction of the sidebar is achieved by changing the Parameters using the orthogonal array. Then FEA is performed on those models to get the best solution. This method can save material used, production cost and time.

Keywords: Parametric optimization; Chassis frame; FEA; Taguchi method; Weight reduction

Nomenclature

FEA	Finite element analysis
DOE	Design of experiment
E	Modulus of elasticity
S/N	Signal to noise ratio
n	Number of repetitions of experiment
Y _i	Measured value of quality characteristic
SF	Safety factor

Introduction

In automotive type vehicles, the frame is considered to be the foundation or "Backbone". The frame in conjunction with the vehicles suspensions, axles, wheels and tires makeup the principal load-carrying components of a vehicle. The frame and other components not only carry the weight of the vehicle, but its payload as well. In addition to the load carrying function, the frame and suspension also transfer the forces from the axles to the vehicle structure. This includes the forces of brake torque reaction as well as the drive forces that propel or move the vehicle. The frame acts as a foundation or base for the body structure of vehicles, the axles with their suspensions and the engine/transmission package. The frame must be rigid enough to support or carry all the loads and forces that the vehicle is subjected to in operation. A frame must also be flexible enough to handle shock loads and the twists, bends, sway and sag that it encounters under different road or load conditions. A frame that is too rigid is most likely to fail even under normal operations. Ideally the frame should be able to flex under different situations, while being able to return to its original shape when loads or forces are removed.

The reduction of fuel consumption and CO₂ emissions is one of the most important challenges facing the automotive industry. One way to reduce consumption is by reducing a weight of vehicle [1].

* Corresponding author. Tel.: +91-9879799575.

E-mail address: tushar.modasa@gmail.com

Thus, the goal of the present work is to provide the basis to save millions tone of fuel and carbon dioxide due to significantly reduced vehicle weight. About one-third of a passenger car's total fuel consumption directly depends on its weight. A weight reduction of 100 kg represents a fuel savings of between 0.3 - 0.5 litres for every 100 km driven according to industry estimates [2].

The main objective of the present work is to reduce the weight of Eicher 11.10 chassis frame. This optimum design is being constrained by the maximum strength and stiffness requirements. The chassis frame is made of two side members joined with a series of cross members. The number of cross members, their locations, cross-section and the sizes of the side and the cross members are the design variables. As the chassis frame is analysed using the finite element techniques, appropriate model of the frame is to be developed. The weight reduction is achieved by changing the Parameters (Size Optimization) of the side bar and cross bar. Then FEA is performed on those models to get the best solution. Since the numbers and levels of parameters are more, the probable models are too many. So, to select optimum parameters among them large numbers of modelling and analysis work is involved which consumes more time. To overcome this problem, Design of Experiment technique can be use along with FEA.

Literature Review

Structural optimization using computational tools has become a major research field in recent years. Methods commonly used in structural analysis and optimization may demand considerable computational cost, depending on the problem complexity. Among these various techniques of DOE may be combined with classic analysis, to reduce the computational effort without affecting the final solution quality. Menon et al. (2007) proposed an automation process in MATLAB that incorporates a response surface approximating tool called MQR. The results obtained from the proposed method were compared with ANSYS Design Xplorer goal driven optimization which was based on DOE and ANSYS First order optimization technique [6]. Chauhan et al. (2006) Optimized weight of the HMT (Hydraulic Modular Trailer) to have higher pay load capacity. Frame was optimized using design optimization module available in ANSYS using first order optimization method. They have concluded that frame was optimized and feasible design was obtained with 52 % reduction in mass. This reduction in mass of the frame increases the payload capacity by 4.900 tones approximately. During optimization of frame, it was found that web thicknesses value should be kept more than the flange thicknesses value for side long member [7]. Hsu et al. (2009) has been used a FEM-based Taguchi method to investigate the effects of various factors to find the robust design of the body cage. The FEM-based Taguchi methods have effectively decreased the time and efforts required for evaluating the design variables of implants and had fairly assessed the contribution of each design variable [8]. Acherjee et al. (2012) carried out a systematic investigation on laser transmission contour welding process using finite element analysis (FEA) and design of experiments (DOE) techniques. A three dimensional thermal model was developed to simulate the laser transmission contour welding process with a moving heat source. Design of experiments was employed to plan the experiments and to develop mathematical models based on simulation results [9].

Methodology

As an important subject in the statistical design of experiments, the Taguchi method is a collection of mathematical and statistical techniques useful for the parametric optimization and analysis of problems in which a response of interest is influenced by several variables and the objective is to optimize this response. Taguchi method is used to examine the relationship between a response and a set of quantitative experimental variables or factors [10].

Steps for the Experiment:

- Formulation of the problem – the success of any experiment is dependent on a full understanding of the nature of the problem.
 - Selection of the output performance characteristics most relevant to the problem.
 - Selection of parameters.
 - Selection of factor levels.
 - Design of an appropriate Orthogonal Array (OA).
 - To Perform FEA with appropriate set of parameters.
 - Statistical analysis and interpretation of experimental results.
 - Modeling and FEA with optimum parameter set for validation
- Flow chart of experiment is given in Figure 1.

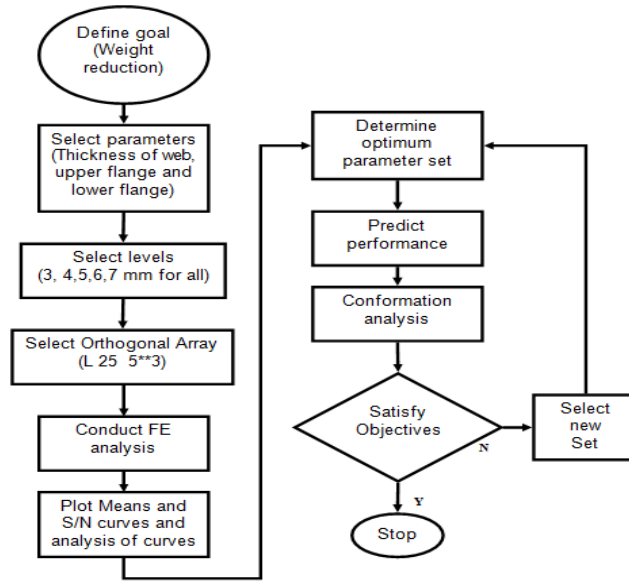


Fig. 1: Flow chart of Experiment [10]

Factors and Levels

Experiments are planned according to Taguchi’s L25 orthogonal array for web, upper flange and lower flange as shown in fig.2. It has 25 rows corresponding to the number of testes with 5 columns at five levels and 3 parameters as shown in Table 1. This orthogonal array is chosen due to its capability to check the interactions among factors.

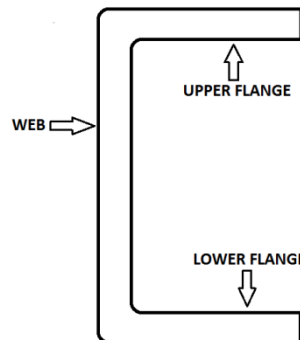


Fig. 2: C channel

The experimental results are then transferred in to a Signal to Noise (S/N) ratio. There are three categories of quality characteristic in the analysis of the S/N ratio, (i) the-lower-the-better, (ii) the-higher-the-better and (iii) the-nominal-the-better. Regardless of the category of the quality characteristic, process parameter settings with the highest S/N ratio always yield the optimum quality with minimum variance. The category the-lower-the-better was used to calculate the S/N ratio for both quality characteristics stress and deformation, according to the equation (1):

$$S/N = -10 \log_{10} \left[\frac{1}{n} \sum_{i=1}^n Y_i^2 \right] \tag{1}$$

Table 1: Factors and their levels

Factor	Level 1	Level 2	Level 3	Level 4	Level 5
Thickness of Web (mm)	3	4	5	6	7
Thickness of Upper flange (mm)	3	4	5	6	7
Thickness of Lower flange (mm)	3	4	5	6	7

For finding out optimum thickness of web, upper flange and lower flange the value of equivalent stress, deformation and weight is measured using ANSYS. Series of analysis is conducted to obtain the optimum weight for allowable stress and deformation condition. Taguchi method is being applied to select the control factors levels (thickness of web, upper flange and lower flange) to come up with optimal response value (weight, equivalent stress and deformation).

Result And Discussion

The equivalent stress and deformation are measured for each set of parameter using FEA in Ansys, and the Results of FEA are analysed using Minitab 16. Minitab offers four types of designed experiments: factorial, response surface, mixture, and Taguchi (robust). The steps follows in Minitab to create, analyse, and graph an experimental design are similar for all design types. After conducting the analysis and entering the results, Minitab provides several analytical and graphing tools to help understand the results. Minitab version 16 is used for the analysis of result obtained by Finite element analysis. The S/N ratio for minimum equivalent stress and deformation are coming under “Smaller-is-better” characteristic, which can be calculated as logarithmic transformation of the loss function.

Taguchi designs experiments using especially constructed tables known as “orthogonal arrays” (OA). The use of these tables makes the design of experiments very easy and consistent.

From the Table 2 it is identified that minimum equivalent stress value 82.59 N/mm^2 and minimum deformation value 1.56 mm are obtained at the experiment no 25 having values of thickness of web, thickness of upper flange and thickness of lower flange 7 mm , 7 mm and 6 mm respectively.

Table 2: Experimental Results Table

Sr. No.	Thickness of web (mm)	Thickness of upper flange (mm)	Thickness of lower flange (mm)	Weight (kg)	Equivalent stress (N/mm^2)	Deformation (mm)
1	3	3	3	258.79	155.010	2.7456
2	3	4	4	268.65	128.200	2.4531
3	3	5	5	278.50	118.160	2.3040
4	3	6	6	288.35	115.500	2.0070
5	3	7	7	298.20	103.390	1.9712
6	4	3	4	279.75	118.570	2.3789
7	4	4	5	289.43	112.420	2.2216
8	4	5	6	299.11	102.610	2.0315
9	4	6	7	308.79	96.970	1.9020
10	4	7	3	294.27	131.150	2.0324
11	5	3	5	300.53	108.040	2.1390
12	5	4	6	310.04	97.007	1.9759
13	5	5	7	319.54	93.031	1.8437
14	5	6	3	305.28	121.770	1.8836
15	5	7	4	314.79	108.200	1.8382
16	6	3	6	321.14	97.780	1.9437
17	6	4	7	330.47	88.380	1.8470
18	6	5	3	316.47	110.080	1.8411
19	6	6	4	325.80	97.607	1.7505
20	6	7	5	335.14	88.780	1.6814
21	7	3	7	341.57	87.279	1.7835
22	7	4	3	327.83	100.250	1.7895
23	7	5	4	336.99	93.288	1.6615
24	7	6	5	346.15	86.179	1.6027
25	7	7	6	355.31	82.599	1.5638

Main Effects Plot for Mean data and S/N ratio data are shown in Fig. 3, 4, 5, 6, 7 and 8 that shows effect of thickness of web, thickness of upper flange and thickness of lower flange on weight, equivalent stress and deformation.

The effects of thickness of web, thickness of upper flange and thickness of lower flange on weight of chassis frame are shown in Fig. 3 and Fig. 4.

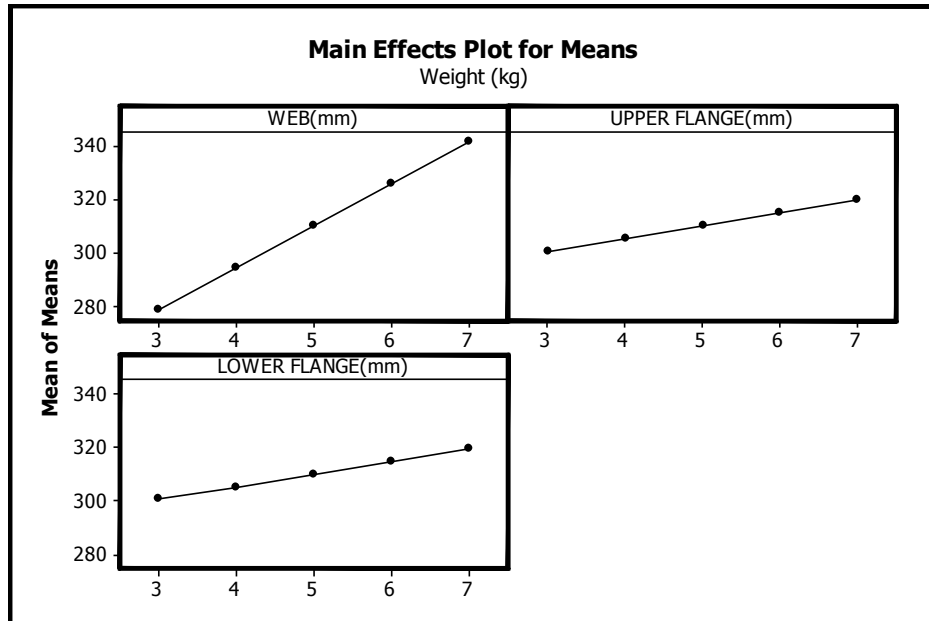


Fig. 3: Main Effects Plot for Means: Weight

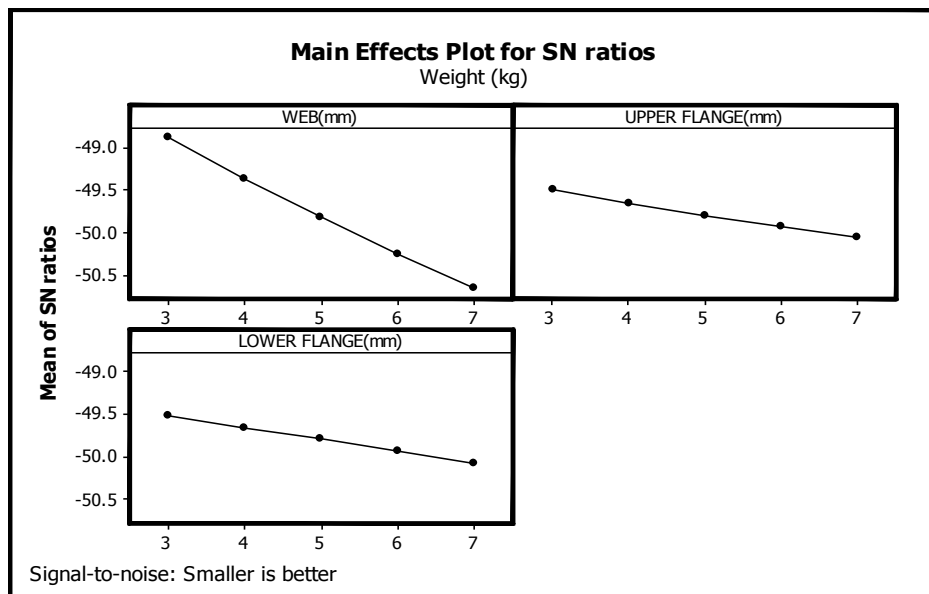


Fig. 4: Main Effects Plot for S/N ratio data: Weight

In the investigation, it has been found that as the values of web thickness, upper flange thickness and lower flange thickness are increased, the weight is increased and when these values are decreased the weight is also decreased as shown in Fig. 3 and Fig. 4.

The effects of thickness of web, thickness of upper flange and thickness of lower flange on equivalent stress of chassis frame are shown in Fig. 5 and Fig. 6.

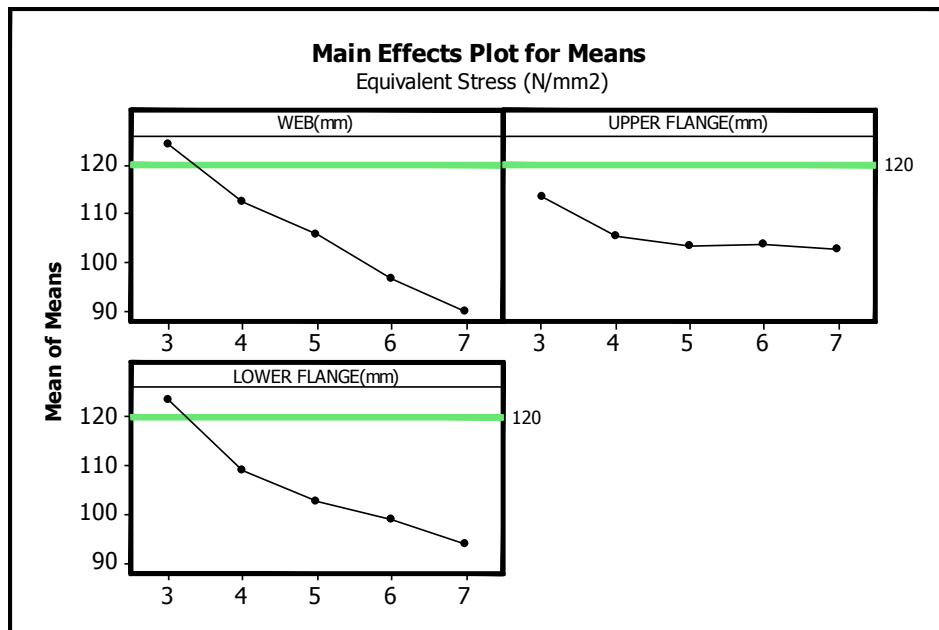


Fig. 5: Main Effects Plot for Mean data: Equivalent stress

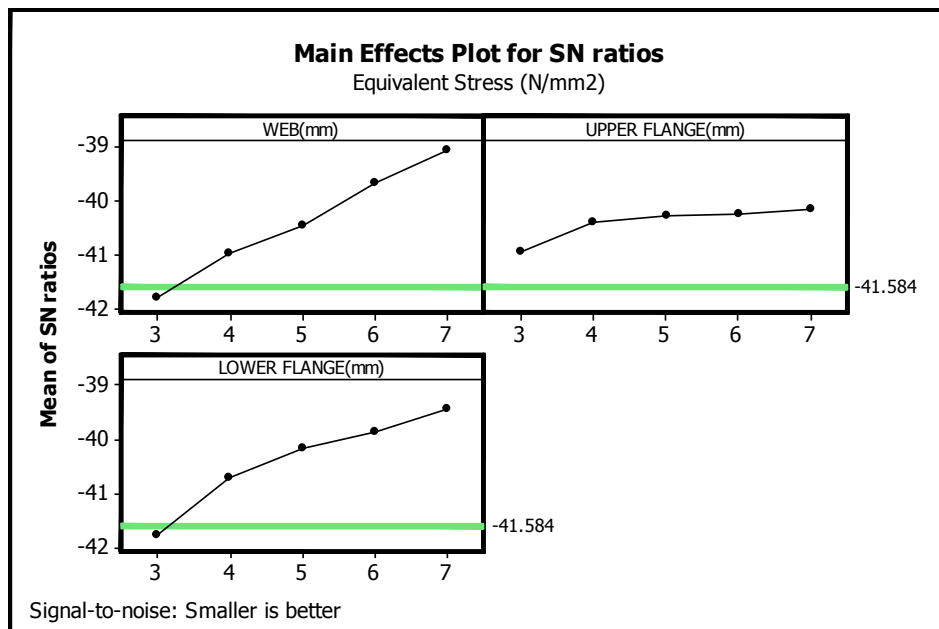


Fig. 6: Main Effects Plot for S/N ratio data: Equivalent stress

Vidosic (1957) recommends some value of safety factor for various condition of loading and material of structures. The value of 1.5 to 3 for well known materials under reasonably environmental condition, subjected to loads and stresses that can be determined readily [4]. It is necessary to reduce the stress magnitude of critical point in order to get the satisfy SF value of truck chassis. The truck chassis can be modified to increase the value of SF especially at critical point area. The permissible value of equivalent stress for material ST 52 is $360/3 = 120$ Mpa (considering factor of safety is 3 for design) [5]. The formula of Safety Factor (SF) is defined by [3]

$$\begin{aligned} \text{Design stress} &= \text{yield strength} / \text{safety factor} \\ &= 360 / 3 \\ &= 120 \text{ MPa} \end{aligned}$$

The corresponding value of S/N ratio is -41.584 for smaller is better characteristics.

Results of Main Effects Plot for Mean data for weight (Fig. 7) and Main Effects Plot for S/N ratio data for weight (Fig.

8) analysis are given in Table 3. As per the results chassis with 4mm web thickness, 3 mm upper flange thickness and 4 mm lower flange thickness is having optimum weight.

Table 3: Analysis for Equivalent stress

Criteria	Web Thickness (mm)	Upper Flange Thickness (mm)	Lower Flange Thickness (mm)
Generated Stress >120 For Size	3	-	3
	4	3	4
	5	4	5
	6	5	6
	7	6	7
Generated Stress < 120 For Size	4	3	4
	5	4	5
	6	5	6
	7	6	7
	7	7	7
Optimum Size	4	3	4

The effects of thickness of web, thickness of upper flange and thickness of lower flange on deformation of chassis frame are shown in Fig. 7 and Fig. 8.

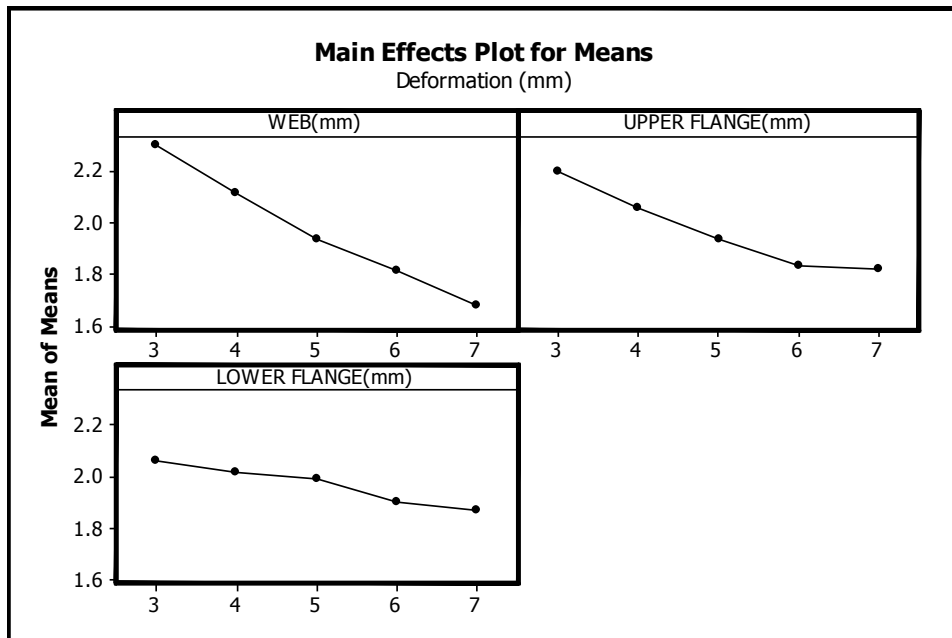


Fig. 7: Main Effects Plot for Mean data: Deformation

According to deformation span ratio allowable deformation for overhanging beam is $l / 300$. So for 6355mm length allowable deformation for simply supported beam is 21.18 mm. Fig. 7 and Fig. 8 shows following effects:

As the web thickness of chassis frame is varied from 3 mm to 7 mm, the deformation developed in chassis decreased from 2.3 mm to 1.68 mm.

As the Upper flange thickness of chassis frame is varied from 3 mm to 7 mm, the deformation developed in chassis decreased from 2.2 mm to 1.8 mm.

As the lower flange thickness of chassis frame is varied from 3 mm to 7 mm, the deformation developed in chassis decreased from 2.06 mm to 1.87 mm.

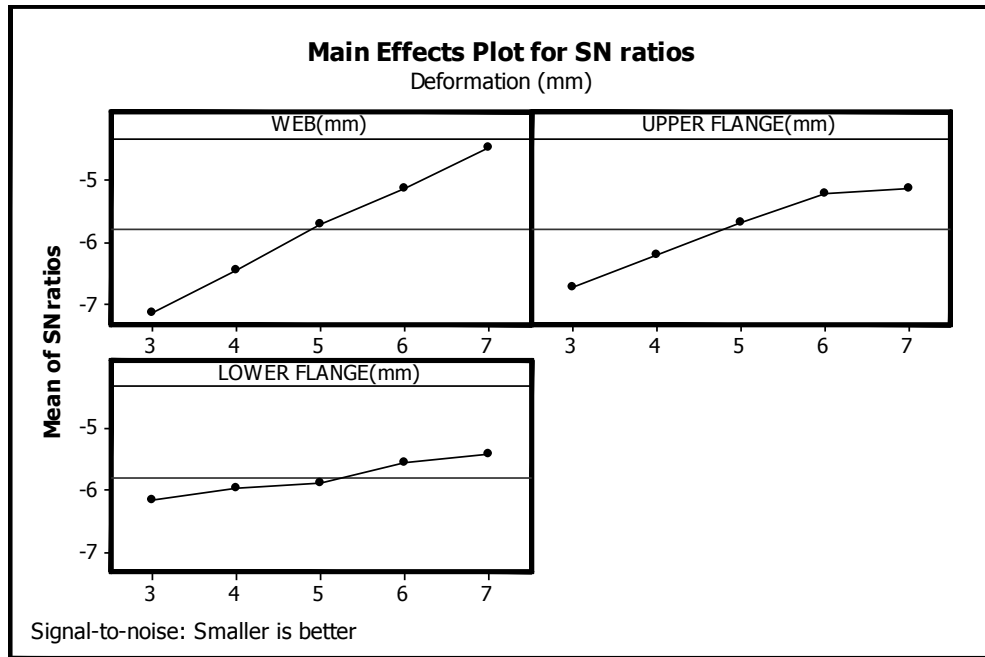


Fig. 8: Main Effects Plot for S/N ratio data: Deformation

The deformations for all the value of web, upper flange and lower flange thickness are within the safe limit. From the above analysis the Optimum set of parameters which is having the minimum weight is given in Table 4.

Table 4: Optimum set of parameter and Predicted Value of stress

Web Thickness (mm)	Upper Flange Thickness (mm)	Lower Flange Thickness (mm)	Predicted Value of stress MPa
4	3	4	119.46

Validation Of Taguchi Result

The model of modified chassis as per the dimension given in Table 5 is created in Parametric Creo 3.0 as shown on Fig. 9. The model is then saved in *.x_t (parasolid) format which can be directly imported into ANSYS workbench.

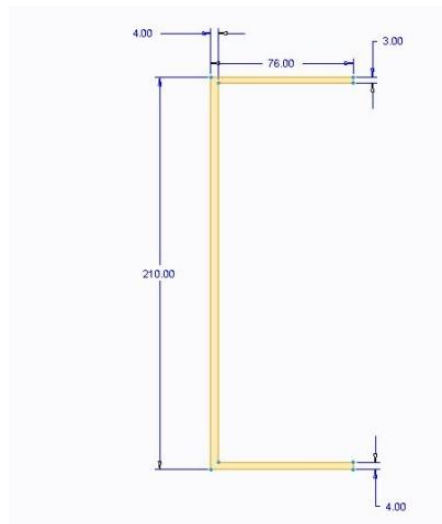


Fig. 9: Modified section

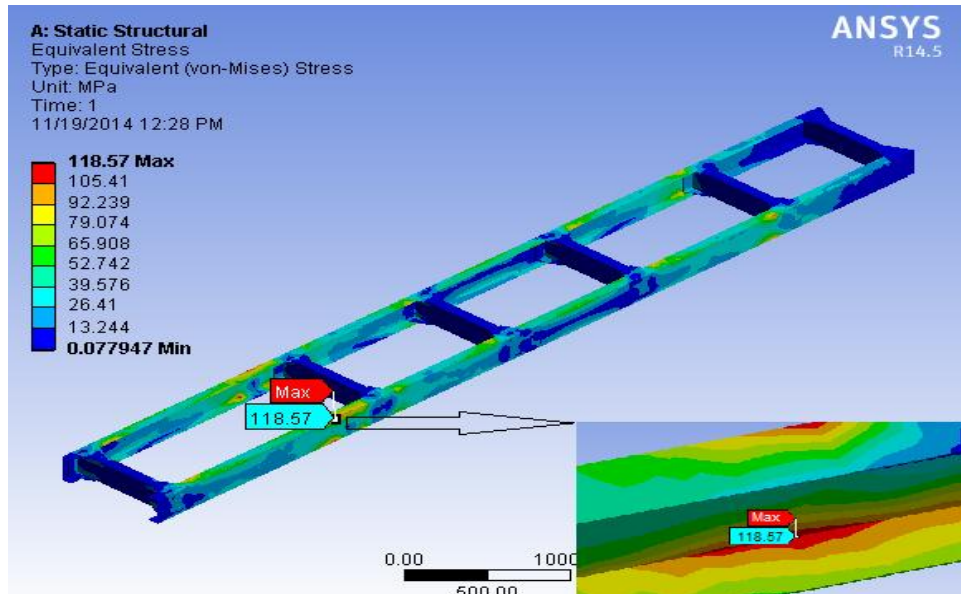


Fig. 10: Equivalent stress in modified chassis

The generated equivalent stresses (118.57 Mpa) are less than the permissible value (120 Mpa) so the design is safe. The equivalent stress is as shown in Fig. 10.

Table 5: Variation in results of Taguchi and FEA

Predicted Value of stress Mpa	FEA Result of stress Mpa	% Variation
119.46	118.57	0.75

Table 6: Reduction in Weight of chassis

Weight of Actual Chassis Kg	Weight of Modified Chassis Kg	Weight Reduction %
335.14	279.75	16.5

The generated equivalent stresses are less than the permissible value so the design is safe. The analysis gives maximum equivalent stress which is within desired limit and it is also nearer to Taguchi’s prediction as shown in Table 5. This percentage variation is caused by uncertainties of Taguchi Prediction and accuracy of FEA.

Weight reduction achieved by FEA-DOE hybride model is 16.5% as shown in Table 6.

Conclusion

The FEM-based Taguchi methods have effectively decreased the time and efforts required for evaluating the design variables of implants.

The optimal parameter combination for the minimum weight with permissible value of stress is obtained by using the analysis of S/N ratio. According to the results 4 mm Web thickness, 3 mm Upper Flange thickness and 4 mm Lower Flange thickness are the optimal parameters for permissible stress.

FEA results obtained from the confirmation analysis using optimum combination are shown excellent agreement with the predicated result. Weight reduction achieved by FEA-DOE hybrid modeling is 16.5%.

References

[1] Mellios, G., Hausberger, S., Keller, M., Samaras, C. & Ntziachristos, L. (2009). Parameterization of fuel consumption and CO₂ emissions of passenger cars and light commercial vehicles for modelling purposes. European Commission of Research & Innovation in transport. Publications Office of the European Union, Luxembourg.
 [2] Pratelli, Antonio. & Brebbia, C. A. (2011) Urban Transport Seventeen, Part XVII. WIT Press, Southampton, UK.
 [3] Data, D. (2004). Data book of Engineers. PSG Tech, Coimbatore.

- [4] Vidotic, J.P. (1957). Machine Design Project, Ronald Press, New York.
- [5] National Code of Practice, Heavy Vehicle Modifications Section H Chassis Frame.
- [6] Menon, A. (2007). Structural Optimization Using Ansys And Regulated Multiquadric Response Surface Model, (Ph.D. thesis, The University of Texas, Arlington).
- [7] Chauhan, D. M., Soni, S. B., & Gohil. (2006), A. M. Parametric Optimization of Hydraulic Modular Trailer Frame using ANSYS (APDL). Nirma University International Conference on Engineering.
- [8] Hsu, W. H., Chao, C. K., Hsu, H. C., Lin, J., & Hsu, C. C. (2009). Parametric study on the interface pullout strength of the vertebral body replacement cage using FEM-based Taguchi methods. *Medical engineering & physics*, 31(3), 287-294.
- [9] Acherjee, B., Kuar, A. S., Mitra, S., & Misra, D. (2012). Modeling of laser transmission contour welding process using FEA and DoE. *Optics Laser Technology*, 44, 1281-1289.
- [10] Auer, B. J. (2005). Size and Shape Optimization of Frame and Truss Structures Through Evolutionary Methods (Doctoral dissertation, University of Idaho).

Parametric Analysis and Working Fluid Selection of Organic Rankine Cycle for Low Grade Heat Energy

Jayesh vasava^{a*}, Dr. V. D. Dhiman^b, Prof. F. S. Jariwala^c

^{a,c}SVMIT Bharuch 392001, India

^bGEC Surat 395001, India

Abstract

This paper deals with study of the thermodynamic, safety and environmental properties of some unconventional fluids for use in organic Rankine cycles supplied by low grade heat energy sources. Theoretical performances as well as thermodynamic, safety and environmental properties of few fluids have been comparatively assessed for use in organic Rankine cycle systems. Study of the Organic Rankine Cycle for the conversion of low-grade heat into electrical power, as well as selection criteria of potential working fluids, screening of working fluids for the cycles and analysis of the influence of fluid properties on cycle performance are investigated. This paper presents a simple Organic Rankine Cycle (ORC) with HFCs (Hydro-Flouro-Carbons) and HCFC ((Hydro-Chloro-Flouro-Carbons) refrigerants as working fluid. R134a, R245fa and R123 are selected from 15 working fluids for parametric analysis and analyzed by using EES (Engineering Equation Solver) to simulate the system under steady-state conditions and parametric analysis is conducted to examine the effects of some thermodynamic parameters on the system performance using the selected working fluids. Thermal efficiency, Net work and Mass flow rate of working fluid of the cycle vary with the variation in turbine inlet temperature, condensation temperature and turbine inlet pressure. The results indicate the optimal working fluid among them.

Keywords: Organic Rankine Cycle, HFC, HCFC, Parametric Analysis, Working fluid selection

Nomenclature

mR	Mass flow rate	<i>Acronyms</i>	
h	Enthalpy	GWP	Global Warming Potential
Q	Heat	ODP	Ozone Depletion Potential
T	Temperature	ORC	Organic Rankine Cycle
S	Entropy	Atm	Atmospheric
W	Work or Power	ASHRAE	American Society of Heating, Refrigerating and Air conditioning Engineering
<i>Greek symbols</i>		<i>Fluids</i>	
η	Efficiency	i	Isentropic
d	Dry	w	Wet
<i>Subscripts</i>			
1–6	States in the cycle		
p	Pump		
t	Turbine		
th	Thermal		
s	Isentropic		

6. Introduction

Energy conservation in the world is becoming very important in recent years, especially the use of low grade temperature and small-scale heat sources. Energy extraction from industrial waste heat, biomass energy, solar energy, and turbine exhaust heat is becoming more popular. Organic Rankine Cycle is an effective way to convert these heat sources into

* Corresponding author. Tel.: +918460329266.

E-mail address: vasavajayesh58@gmail.com

electrical power. Organic Rankine Cycle offers the ability to deal with low temperature heat to generate power [1-3]. In order to recover energy from low-grade heat sources many cycles have been developed. The developed cycles like Organic Rankine cycle, Kalina cycle, Goswami cycle, and trilateral flash cycle offer lower equipment costs and higher profitability using other working fluids than pure water [3]. Among these cycles, Organic Rankine Cycles are less complex and require less maintenance [1-3].

The Organic Rankine Cycle has the same working principles and main components (Heat Exchanger, condenser, expander and pump) as the Steam Rankine Cycle. At the same time, there are some major differences between the two cycles. The differences are mainly related to the used working fluid in the cycle, the working fluid's thermo-physical properties, the heat source temperature and the cycle architecture. Organic Rankine Cycle can extract energy and generate power from much lower heat source temperature than traditional Rankine cycle.

This paper aims to determine the optimal working fluid for Organic Rankine Cycles by theoretical analysis of recently used HFCs and HCFCs refrigerants that can be employed in low temperature, which can result in to better thermodynamic performance and least environment impact. At present the environment friendliness of the refrigerant is a major factor in deciding the usefulness of a particular refrigerant [7]. In this study safety and environmental data are selected from ASHRAE database [19], for comparative assessment. The EES tool [18] is used for thermodynamic analysis of ORC and to evaluate comparative performance of selected working fluids.

In this paper, we have selected best working fluids for Organic Rankine Cycle which are environmentally superior and assured for consumer safety and satisfaction by comparing some recently used working fluids. Parametric analyses of selected refrigerants have been studied in terms of Turbine inlet Temperature, Condensation Temperature and Turbine inlet Pressure in order to find out optimal working fluid based on system performance comparison.

7. Preliminary selection

Organic working fluid can be characterized depending on the slope of the saturation curve on temperature - entropy diagram which may be infinite, positive, or negative. Based on the slope fluids can be classified as isentropic, dry, or wet respectively. Dry or isentropic working fluids are more appropriate for ORC systems. This is because dry or isentropic fluids are superheated after isentropic expansion. Therefore there is no concern for existing liquid droplets at turbine outlet [9]. The safety and environmental properties of working fluids are presented in Table 1. Near critical pressure, small changes in temperature are equivalent to large changes in pressure that make the system unstable. Therefore a reasonable distance between the higher limit of the cycle and the critical point of the fluid should be considered.

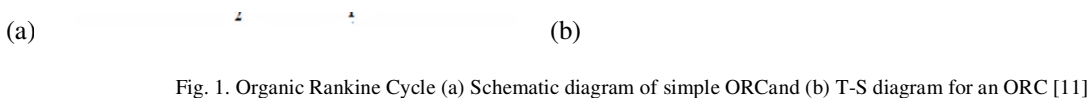
Table 1. Safety and Environmental data of refrigerants [9,11,19]

Refrigerants		Type	Safety data		Environmental data		
			Toxicity	Flammability	ODP	GWP	Atm. Life
R601	(HC)	d	Low	Low	0	~20	0.01
R500	(HCFC)	w	Low	Low	0.738	8100	n.a.
R123	(HCFC)	i	High	Low	0.020	77	1.3
R134a	(HFC)	i	Low	Low	0	1430	14.0
R245fa	(HFC)	i	High	Non	0	1030	7.6
R113	(CFC)	d	Low	Low	1	6130	85
R600a	(HC)	d	Low	High	0	~20	0.019
R114	(CFC)	d	Low	Low	1	10040	300
R290	(HC)	w	Low	High	0	~20	0.041
R141b	(HCFC)	i	Low	Low	0.12	725	9.3
R407c	(HFC)	i	Low	Non	0	1744	15.65
R12	(CFC)	i	Low	No	1	10900	100
R22	(HCFC)	w	Low	Non	0.05	1810	12
R23	(HFC)	w	Low	Non	0	14800	270
R600	(HC)	d	Low	High	0	4	~12

By evaluating and comparing 15 refrigerants properties from the above Table.1, R123, R134a and R245fa are suitable refrigerants for parametric analysis. Here R134a and R245fa are from HFC, which is best type suited as per physical, safety and mainly for environmental requirements, so they have selected for parametric analysis and R123 is from HCFC, which is also mostly used refrigerant [9, 11].

8. System analysis

The Organic Rankine Cycle has the same working principles and main components (Heat Exchanger, condenser, expander and pump) as the Steam Rankine Cycle. At the same time, working fluid is the major difference between the two cycles.



- | | |
|---|------------------------------|
| 1-2s Isentropic compression in feed pump | 4-5s Isentropic expansion |
| 1-2 Non-Isentropic compression in feed pump | 4-5 Non-Isentropic expansion |
| 2-3 Isobaric heat supplied | 5-6 De-superheating |
| 3-4' Evaporation | 6-1 Condensation |
| 4'-4 Superheating | |

A schematic diagram of the simple organic Rankine cycle is shown in Fig.1 (a) and consists of four major components: expander, condenser, pump and heat exchanger. The system structure of a simple ORC is shown in Fig.1. The condensate working fluid is pumped from the condenser where the pressure is low to the heat exchanger where the pressure is high. The process takes place at constant entropy. The high pressure liquid enters the heat exchanger and absorbs the thermal energy from low grade heat source at constant pressure. In this process the refrigerant changes the phase from saturated liquid to saturated or superheated vapour. The high pressure saturated or superheated vapour leaves the heat exchanger and expands through an expander at constant entropy to produce mechanical work. Under the expansion process, the pressure decreases to condenser pressure. After expansion process the working fluid leaves the expander and enters the condenser as unsaturated, saturated or superheated vapour depending on working conditions and the type of used working fluid. In the condenser, the working fluid condensates and changes phase to saturated or undercooled liquid with the help of a heat sink, and then the cycle is repeated. Temperature entropy diagram of the simple organic Rankine cycle with R245fa as the working fluid is shown in Fig. 1(b).

The organic Rankine cycle system is modelled based on the laws of mass and energy conservations. To simplify the theoretical analysis, some assumptions are made as follows:

- The system reaches a steady state.
- The pressure drops in vapour evaporator, regenerator, condenser, and the connection tubes are neglected.
- The working fluid at the condenser outlet is saturated liquid, and there exists a temperature difference of condenser, namely, the temperature difference of condensed temperature and cooling water temperature.
- For the turbine, the isentropic efficiency can be expressed as;

$$\eta_t = \frac{h_4 - h_5}{h_4 - h_{5s}}$$

The power output can be given by,

$$W_t = m_R(h_4 - h_5)$$

For the pump, the isentropic efficiency can be expressed as,

$$\eta_p = \frac{h_{2s} - h_1}{h_2 - h_1}$$

The pump power consumption is given by,

$$W_p = m_R(h_2 - h_1)$$

In the vapor evaporator, the heat addition into the power cycle is extracted from the external low grade heat or waste heat (engine exhaust here) source, which implies,

$$Q_{in} = m_R(h_4 - h_2)$$

The thermal efficiency is defined as,

$$\eta_{th} = \frac{W_{net}}{Q_{in}}$$

- Input data for cycle analysis [9]

Evaporating temperature	T_4	348 K
Condensing temperature	T_1	308 K
Isentropic efficiency of the turbine	η_t	0.70
Isentropic efficiency of the pump	η_p	0.80

9. Results and discussion

By considering 1 kW capacity ORC with 0.1Mpa to 4Mpa turbine inlet pressure range and fixed input parameters, cycle has been parametrically analyzed with variable mass flow rate and constant mass flow rate using EES. For each parameter from Turbine inlet Pressure, Condensation Temperature and Turbine inlet Temperature optimum Thermal efficiency, Net work and Mass flow rate have been calculated for R123, R134a and R245fa and from the optimum parameters of R123, R134a and R245fa, optimal working fluid has been selected in the light of safety and environmental data of refrigerants.

- **Variable mass flow rate**

Variation of Thermal Efficiency, Net work and Mass Flow Rate with different parameters such as Turbine inlet Pressure, Condensation Temperature and Turbine inlet Temperature are analyzed here,

During the graphical analysis of Thermal efficiency, Net work and Mass flow rate versus Turbine inlet pressure, Condensation Temperature and Turbine inlet Temperature remains constant.

During the graphical analysis of Thermal efficiency, Net work and Mass flow rate versus Condensation temperature, Turbine inlet Temperature and Turbine inlet Pressure remains constant.

During the graphical analysis of Thermal efficiency, Net work and Mass flow rate versus Turbine inlet Temperature, Turbine inlet Pressure and Condensation Temperature remains constant.

From the graphical representation, it can be understood how the variable parameters affect the system in different manner,

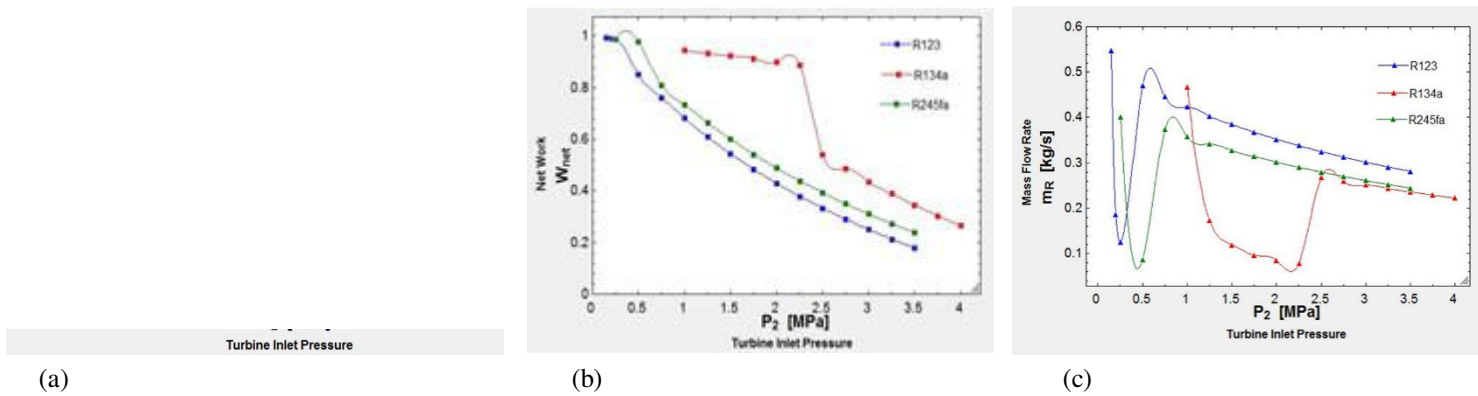


Fig. 2 Turbine inlet Pressure versus Thermal Efficiency(a), Net work(b), and Mass Flow Rate(c)

Turbine Inlet Pressure	P_2	R123	R134a	R245fa
		0.42	2.25	0.5
		Mpa	Mpa	Mpa

Table 2. Optimum Turbine inlet Pressure

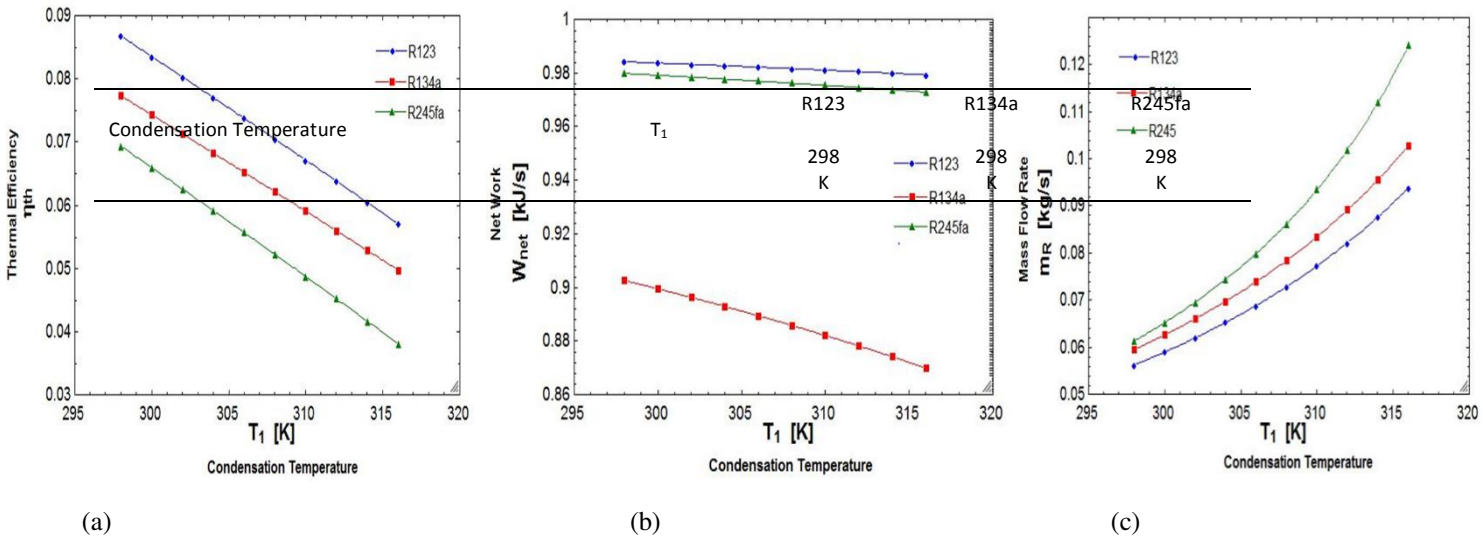


Fig. 3 Condensation Temperature versus Thermal Efficiency (a), Net work(b), and Mass Flow Rate(c)

Table 3. Optimum Condensation Temperature

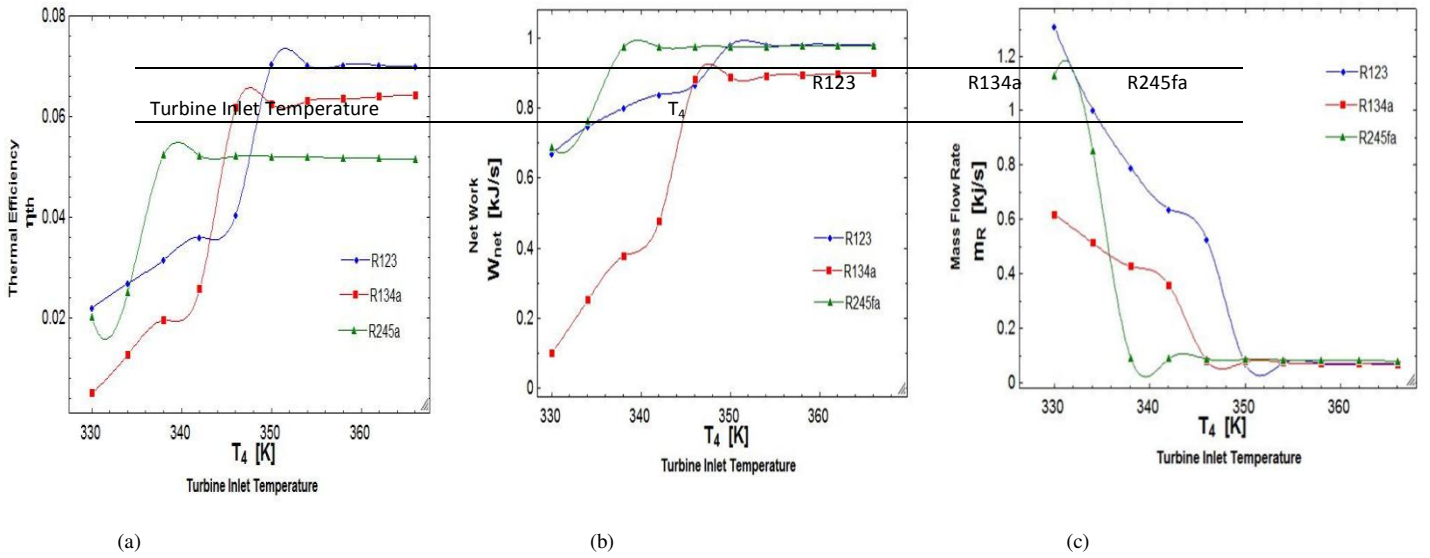


Fig. 4 Turbine inlet Temperature versus Thermal Efficiency(a), Net work(b), and Mass Flow Rate(c)

Table 4. Optimum Turbine inlet Temperature

350 K	366 K	366 K
----------	----------	----------

• **Constant mass flow rate**

During Thermal efficiency and Net work versus turbine inlet Pressure, Condensation temperature and Turbine Inlet Temperature remains constant.

During Thermal efficiency and Net work versus Condensation Temperature, Turbine inlet Temperature and Turbine Inlet Pressure remains constant.

During Thermal efficiency and Net work versus Turbine inlet Temperature, Turbine Inlet Pressure and Condensation Temperature remains constant.

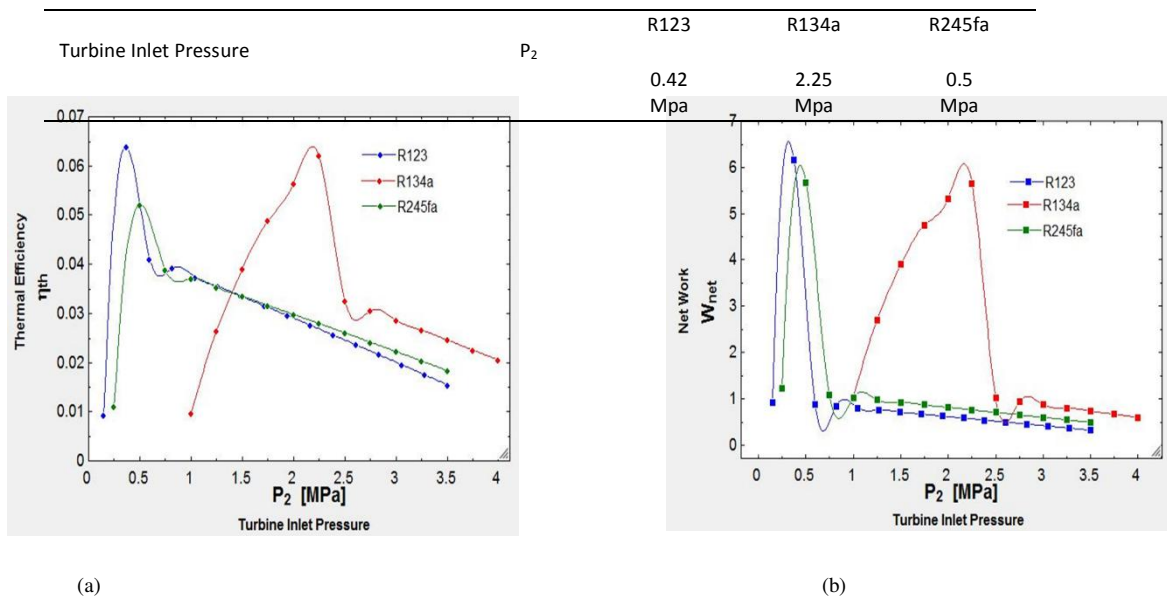
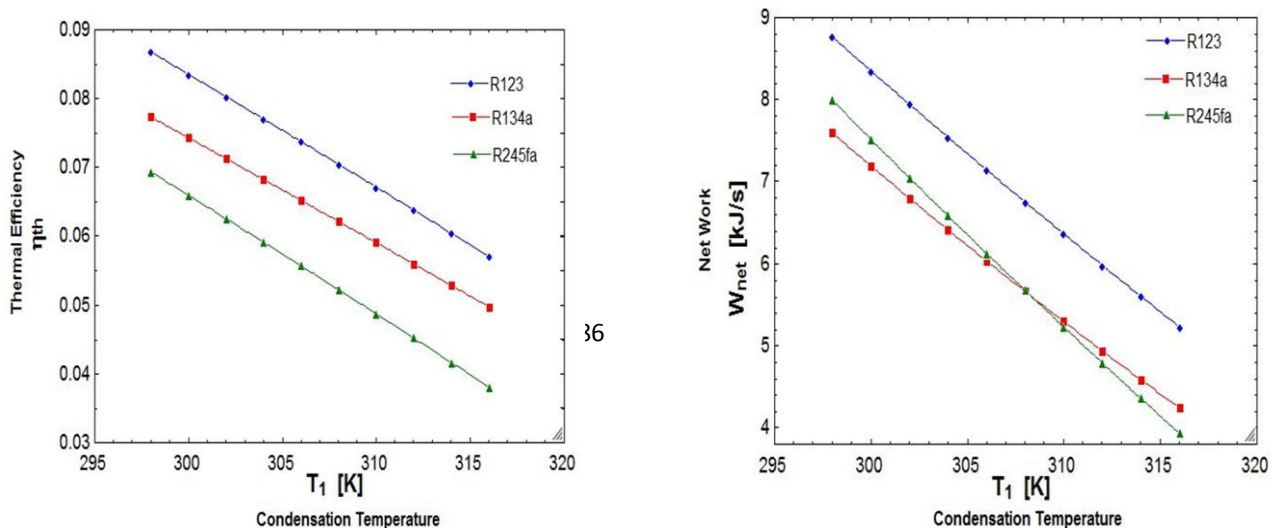


Fig. 5 Turbine inlet Pressure versus Thermal Efficiency (a) and Net work (b)

Table 5. Optimum Turbine inlet Pressure



(a) (b)

Fig. 6 Condensation Temperature versus Thermal Efficiency(a) and Net work(b)

Table 6. Optimum Condensation Temperature

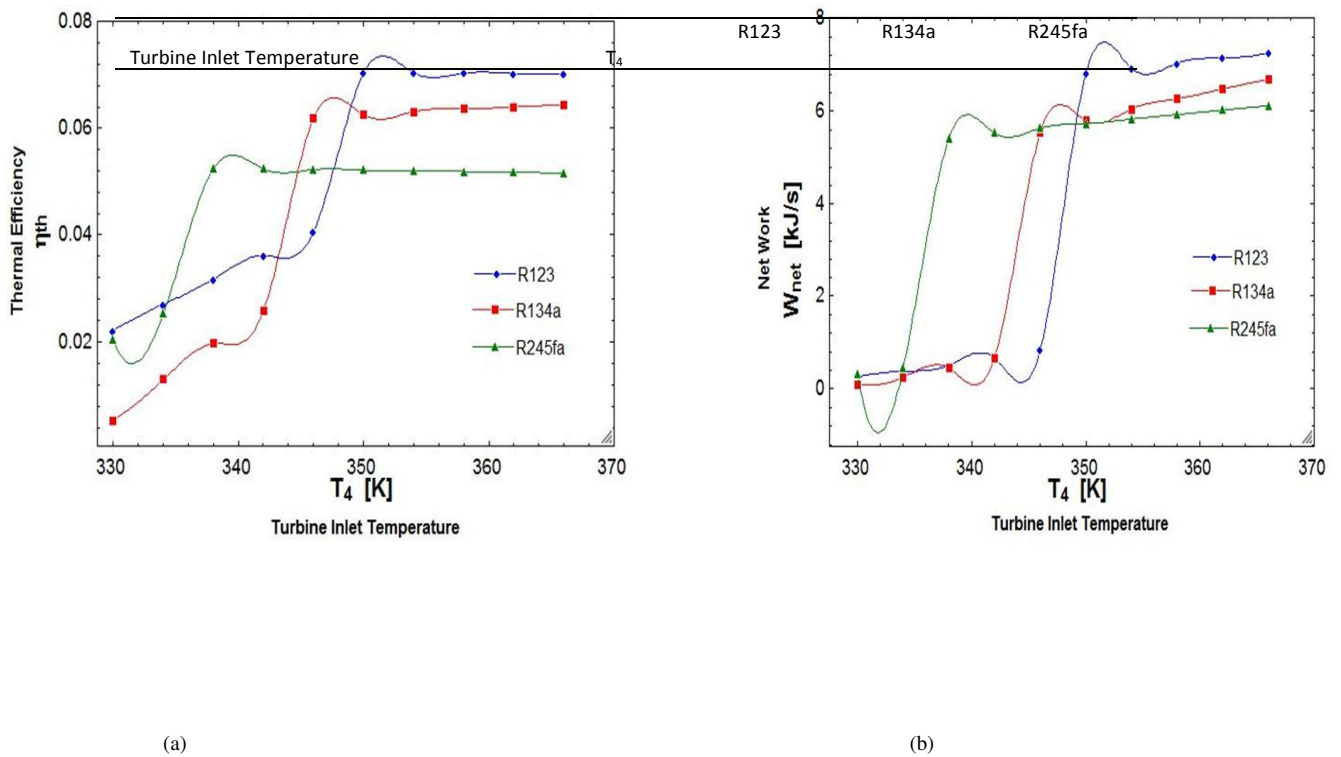


Fig. 7 Turbine inlet Temperature versus Thermal Efficiency(a) and Net work(b)

Table	Condensation Temperature	T_1	R123	R134a	R245fa	7.Optimum Temperature
Turbine inlet			298 K	298 K	298 K	

	358	366	346
	K	K	K

By
optimized
optimum
R123, R134a and

Table 8. Optimum
parameters (variable)

Refrigerants	Thermal Efficiency (%)	Net Work (KJ/s)
R123	8.66	9.11
R134a	7.99	8.86
R245fa	6.93	7.92

considering all
parameters,
performance of
R245fa are:

final results for all

By considering all optimized parameters, optimum performance of R123, R134a and R245fa are:

Table 9. Optimum final results for all parameters (constant)

Refrigerants	Thermal Efficiency (%)	Net Work (KJ/s)	Mass Flow Rate (Kg/s)
R123	8.67	0.984	0.055
R134a	7.99	0.915	0.051
R245fa	6.872	0.981	0.057

5. Conclusion

From the analysis it is concluded that,

- R123 shows the best performance for both variable and constant mass flow rate of working fluid.

- R134a shows better performance than R245fa.

But according to safety and environment comparison of these three refrigerants, R134a is optimal refrigerant for low grade heat energy to use in Organic Rankine Cycle.

Acknowledgements

It has been a great honor to work, right from the conceptualization of the topic to completion of the entire work of the research, under the guidance of our honorable and respected professors, Mr. V. D. Dhiman, Associate Professor in Mechanical Engineering Department, GEC, Surat and Mr. F. S. Jariwala, Assistant Professor in Mechanical Engineering Department, SVMIT, Bharuch. I sincerely acknowledge their valuable contribution. They are a constant source of encouragement and momentum that any difficulty becomes simple. They always supported and tolerated me (including my silly mistakes and lethargy). I gained a lot of valuable guidance and prompt suggestions from them during the entire research work.

I am also thankful to all the faculty members of Mechanical Department as they spent their valuable time in guiding me in my research work.

Last, but not the least, I would like to take an opportunity to express my sincere gratitude to my parents who gave me excellent co-operation to build my morale and support at the time of hardships, agony and anguish during the entire literature work.

References

- [1]. V. Maizza et al., 2000. "Unconventional working fluids in organic Rankine-cycles for waste energy recovery systems" Faculty of Engineering, Polytechnic of Bari, 200 Via Re David, 70125 Bari, Italy.
- [2]. J. Radulovic et al., 2014. "Utilisation of fluids with low global warming potential insupercritical organic rankine cycle", School of Engineering, University of Portsmouth, PO1 3DJ, UK.
- [3]. Van Long Le et al., 2012. "Working fluid selection and performance comparison of subcritical and supercritical organic Rankine cycle (ORC) for low temperature waste heat recovery", Theoretical and Applied Energy and Mechanics Laboratory CNRS, LEMTA, UMR 7563 F-54500 Vandoeuvre-lès-Nancy France.
- [4]. Hung pham et al., 2010. "Next generation refrigerants: Standards and climate policy implications of engineering constraints", Emerson Climate Technologies Harvey Sachs, American Council for an Energy-Efficient Economy.
- [5]. James M. Calm, 2008. "The next generation of refrigerants-historical, review, consideration and outlook", engineering consultant, Elsevier Ltd.
- [6]. Kristen N. Taddonio et al., 2009. "Preparing for next-generation air conditioning and refrigeration technology", U.S. Environmental Protection Agency.
- [7]. Lorenzo P. Polvani et al., 2012. "The importance of the Montreal protocol in protecting earth's hydro climate", Department of Applied Physics and Applied Mathematics and Department of Earth and Environmental Sciences, Columbia University, New York.
- [8]. S. Aghahosseini, I. Dincer, 2013. "Comparative performance analysis of low temperature organic rankine cycle (orc) using pure and zeotropic working fluids", Faculty of Engineering and Applied Science, University of Ontario Institute of Technology, 2000 Simcoe Street North, Oshawa, Ontario, Canada L1H 74K.
- [9]. A. Sunita V. Sanghani, B. Dr. Ragesh G. Kapadia 2011. "Comparative assessment of refrigerants and non-refrigerants as working fluids for a low temperature Organic Rankine Cycle", Institute of technology, nirma university, Ahmedabad – 382 481.
- [10]. Alexander Anderson et al., 2014, "Working fluid selection of low grade heat geothermal Organic Rankine Cycle (ORC)", School of Mechanical and Systems Engineering, Newcastle University, UK, Newcastle Upon Tyne.
- [11]. F. S. Jariwala et al., 2013. "Parametric Analysis Of Solar Organic Rankine Cycle", Gujarat Technological University, Department of Mechanical Engineering Shri S'ad Vidya Mandal Institute of Technology, Bharuch – 392001, 3rd Volume of International Journal of Mechanical Engineering and Research, IIT, Delhi, 2013. ISSN 2249-0019.
- [12]. Bala V. DATLA et al., 2012. "Organic Rankine Cycle System Analysis for Low GWP Working Fluids", Syracuse Turbo Machinery LLC Syracuse, NY 13244.
- [13]. Bahaa Saleh et al., 2005. "Working fluids for low-temperature organic Rankine cycles", Institute für Verfahrens- und Energietechnik, Universität für Bodenkultur, Muthgasse 107, A-1190 Wien, Austria.
- [14]. Yiping Dai et al., 2009. "Parametric optimization and comparative study of organic Rankine cycle for low grade waste heat recovery", Institute of Turbo machinery, Xi'an Jiao Tong University, No. 28 Xianning West Road, Xi'an 710049, PR China.
- [15]. Lars J. Brasz et al., 2004. "Ranking of working fluids for organic rankine cycle applications", International Refrigeration and Air Conditioning Conference at Purdue.

- [16]. Z.Q. Wang et al., 2012. “Fluid selection and parametric optimization of organic rankine cycle using low temperature waste heat”, Institute of Mechanical Engineering, Xiang Tan University, No.13 North Xiangtan University Road, Xiangtan 411105, PR China.
- [17]. P J Mago et al., 2007. “Performance analysis of different working fluids for use in organic Rankine cycles”, Department of Mechanical Engineering, Mississippi State University, Mississippi, USA.
- [18]. S.A. Klein, Engineering Equation Solver (EES), Academic Professional Version, 2007.
- [19]. ASHRAE STANDARDS COMMITTEE 2007–2008. Designation and Safety Classification of Refrigerants.

Report

Report of the Refrigeration, air conditioning and heat pumps. Technical options committee (2010), Montreal protocol on substances that deplete the ozone layer.

Thesis

Fankam TChanche, 2010. “Low grade heat conversion into Power using small scale Organic Rankine Cycles”, Department of Natural Resources and Agricultural Engineering, Agricultural University of Athens, AUA.

A Survey of Performance metrics for Vertical Handover between Wi-Fi and WiMAX

Prof. Madhuri R. Chopade.

Gandinagar Institute of Technology, Gnadhinar, India

Abstract

Mobile communication technology evolved rapidly over the last few years due to increasing demands such as accessing Internet services on mobile phones with a better quality of the offered services. The most important issues in this technology are to provide seamless handover when a mobile node (MN) moves between different access networks. The present communication reveals a survey of Vertical Handover Performance metrics within WiMAX and WiFi and describes two techniques Wi-Fi (Wireless Fidelity) & WiMAX (Worldwide Interoperability for Microwave Access) used in wireless communication along with their comparison. The aim of this paper is to study these two techniques and describe the basic Performance metric used for doing vertical handover procedure

Keywords:

IEEE 802.11, IEEE 802.16, Vertical Handover, Wi-Fi, WiMAX

1. Introduction

In the recent years, there has been huge development in wireless access technologies, to fulfil the need of people to be “Always Best Connected”. There are numerous technologies, networks, systems, applications and devices. These varieties of technology bring a well-known issue to the field of wireless access networks: seamless handover services. Among several candidate technologies for the numerous wireless broadband networks, Worldwide Interoperability for Microwave Access (WiMAX, IEEE 802.16 [1] [2]) shows promising potentials, where Wireless Local Area Network (WLAN, IEEE 802.11 [3]) is one of the most used wireless. The IEEE 802.11 WiFi have been deployed widely and 802.11 access point can cover area of few hundred meters, making them suitable for enterprise networks and public hotspot networks. Recently 802.16 standards (WiMAX) can provide high data rate and wide area of coverage. Integration of these two technologies raises several challenges

When MN changes its current point of access technology handoff occurs. There can be two different types of handoff: horizontal handoff and vertical handoff. Horizontal handoff refers to switching between point of attachment or base station that belongs to same network. Vertical handoff refers to switching between stations that belong to different networks. Process of vertical handoff can be divided into three steps, namely system discovery, handoff decision and handoff execution. During system discovery phase MN search networks and what are the available services in each network. During handoff decision phase MN determines which network it should connect to. Handoff decision may depend on various parameters such as bandwidth, delay, access cost, and transmission power, current battery status of mobile node and user preferences. During handoff execution phase connections are transferred from existing network to new network in seamless manner. This involves authentication, authorization as well as transfer of user’s context information.

Among several candidate technologies for the numerous wireless broadband networks, IEEE 802.16-operated WiMAX shows promising potentials. IEEE 802.16 Fixed WiMAX has been developed by the IEEE 802.16 standard activities. Because it cannot support the mobility of terminals, IEEE 802.16 Fixed WiMAX is not suitable for mobile computing environments. Thus, to support mobility on terminal stations, IEEE 802.16e Mobile WiMAX standard is proposed [4][5]. This paper describe the basic Performance metric used for doing vertical handover procedure and addresses basic vertical handover algorithm for interworking between IEEE 802.11 WiFi and IEEE 802.16e Mobile WiMAX.

2. Wi-MAX TECHNOLOGY

The fiber optic transport services providing the high bandwidth and data rates is replaced by WiMAX wireless technology all across the world. WiMAX is emerging technology to fulfil the high data rate and QoS requirements of the customers, also it is the cheap deployment of voice services with no need of line of sight wireless channel.

WiMAX signals have the property to adopt the atmospheric conditions everywhere. WiMAX electromagnetic waves also offer the support of adoptive coding and different operation modes, so voice and data services can easily be transported by WIMAX network platform.

More familiar terms for these standards are Fixed WiMAX (802.16-2004 [1]) and Mobile WiMAX (802.16e [2]). By definition, Fixed WiMAX does not support mobility and is therefore not useful for this research. That is why in this paper, the term WiMAX used, is for Mobile WiMAX (802.16e). It provides mobility support at frequency bands between 2 and 6 GHz. Mobile WiMAX introduces OFDMA and supports several key features necessary for delivering mobile broad band services at vehicular speeds greater than 120 km/hr[6].

2.1. Architecture

The WiMAX Network Architecture defines a framework consisting of several functional entities and interconnections. Figure1 shows this framework in simplified manner, followed by a description of each entity [7].

- **NAP:** Network Access Provider A business entity that provides WiMAX radio infrastructure.
- **NSP:** Network Service Provider Just like the NAP, the NSP is a business entity. It provides IP connectivity and WiMAX services. The level of services is legally binded through contractual agreements with one or more NAPs.

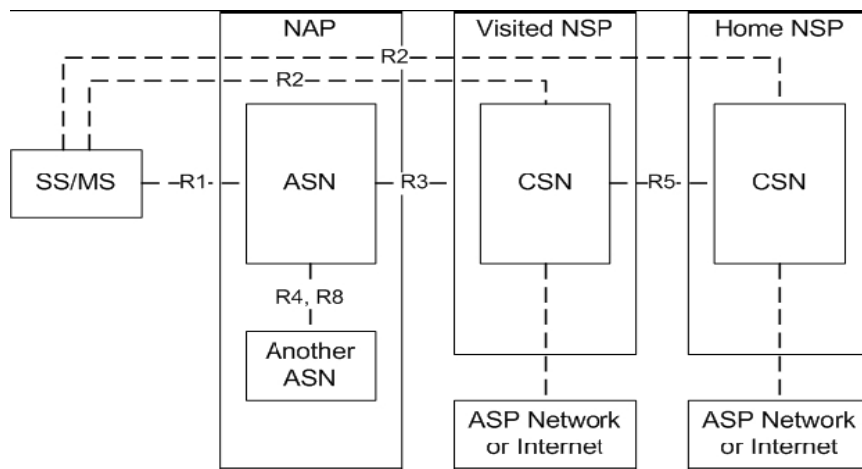


Figure 1. WiMAX Network Architecture

- **SS/MS:** Subscriber Station/Mobile Station Entity which wants to make a connection to the network.
- **ASN:** Access Service Network This is the point of entry for the SS/MS into the WiMAX network. This entity must support a complete set of functions required to connect a client to the network: authorization, authentication, session management, network discovery, IP-address allocation, QoS etc.
- **CSN:** Connectivity Service Network The CSN is the part of the network which provides IP connectivity services. It consists typically of routers, servers, proxies, and gateways etc. providing functions like Internet access and peer-topper services.

Besides these entities the architecture also contains a number of interconnections or reference points. The most important and relevant ones are summarized here.

- **R1:** Protocols between SS/MS and ASN including PHY and MAC layers as specified by the 802.16 standard.
- **R2:** Protocols/procedures between SS/MS and CSN concerning authentication, authorization and IPconfiguration management.
- **R3:** Control procedures between ASN and CSN. Provides tunnelling of user data between the two entities.
- **R4:** Control procedures between ANSs like MS mobility between different ANSs.
- **R5:** Control procedures for supporting roaming from a home NSP to a visited NSP.
- **R8:** When switching between different BSs within the same ASN or between different ANSs (which most likely will also involve a switch between BSs) this is an optional reference point to ensure fast and seamless handover through direct transfer of MAC context and data.

Together, the technology and network architecture give a summarized and simplified view of WiMAX networks.

3. Wi-Fi Technology

Wireless Fidelity (Wi-Fi) is a wireless technology which provides internet connectivity or connectivity among the users. In 1997 IEEE provide a set of specification and standards for Wi-Fi which is under the title 802.11 that explains the structure of the comparatively short range radio signal for Wi-Fi service. After that several specifications came and most commonly used specifications today are 802.11b, 802.11g and 802.11a [8]. Out of these three, 802.11a can provide higher speeds within the various radio frequencies. IEEE is now working for a new standard 802.11n which is more reliable, secure and faster than the other standard .Originally Wi-Fi was created for wireless extension for the wired LAN. That’s why the distance between the Wi-Fi access point and user equipment is limited to around 100 feet indoor and up to 300 feet outdoors [9]. So if a user moves its computer to a new location, he/she should find a new access point for continuing the communication.

Due to the cheap availability of the equipment and its maintenance and servicing cost, Wi-Fi is widely accepted throughout the world and it is widely used in a restaurants, hotels, airports and school campuses. It is also work well in the auditoriums, meeting rooms and small businesses. Internet service providers also use it for individual home connectivity and connectivity to the commercial complexes. All wireless devices that join a Wi-Fi network, whether mobile, portable or fixed, are called wireless stations (STAs). A wireless station might be a PC, a laptop, a PDA or a phone. When two or more STAs are wirelessly connected, they form a basic service set (BSS). This is the basic building block of a Wi-Fi network. The BSS is an example of the simplest Wi-Fi network possible: two wireless stations. A common distribution system (DS) and two or more BSSs create what is called an extended service set (ESS). An ESS is a Wi-Fi network of arbitrary size and complexity. Fig 2 is a representation of an ESS comprised of BSS 1, 2 and 3. The distribution system is not part of the ESS. The distribution system enables mobility in a Wi-Fi network by a method of tracking the physical

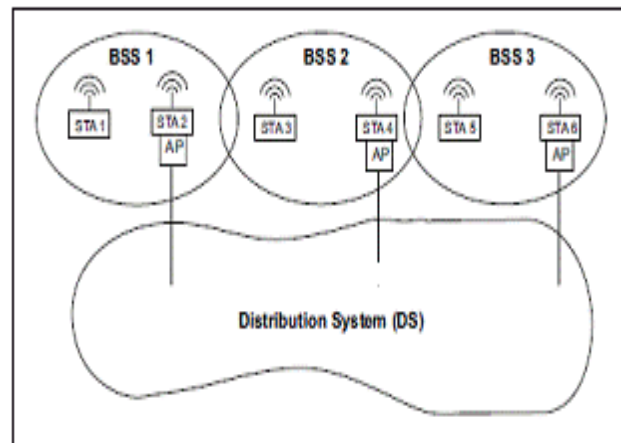


Fig 2. ESS (Extended Service Set)[11]

location of STAs, thus ensuring that frames are delivered to the AP associated with the destination STA. Mobility means a wireless client can move anywhere within the coverage area of the ESS and keep an uninterrupted connection.

These two wireless technologies have common components in their operations with a major difference in the communication range. The following table below gives the detailed comparative analysis of the two broadband wireless access networks (Wi-Fi and WiMAX):

Table 1. Comparison between WiMAX and Wi-Fi [10]

Feature	WiMAX(IEEE 802.16a)	Wi-Fi(IEEE 802.11b)	Wi-Fi(IEEE 802.11a/g)
Primary Application	Broadband Wireless Access	Wireless LAN	Wireless LAN

Frequency Band	Licensed/Unlicensed 2GHz to 11GHz	2.4 GHz ISM	2.4 GHz ISM(g) 5 GHz U-NII(a)
Bandwidth Efficiency	<=5 bps/Hz	<=0.44 bps/Hz	<=2.7 bps/Hz
Modulation FEC	BPSK,QPSK,16,64 ,256-QAM Convolution Code Reed-Solomon	QPSK None	BPSK,QPSK Convolution Code
Encryption	Mandatory-3DES	Optional-RC4	Optional- RC4
Mobility	Mobile WiMAX(802.16e)	in development	In development
Mesh	Yes	Vendor Proprietary	Vendor Proprietary
Access Protocol	Request Grant	CSMA/CA	CSMA/CA

4. Vertical Handover

- Diverse processes are required in order to perform a Vertical Handover (VHO).VHO process into three phases: i) Handover information gathering, ii) Handover decision, and iii) Handover execution [12][13]. The information gathering phase is in charge of collecting relevant information from diverse context sources such as network capabilities, access points, user equipments, and user preferences. The most critical process in a VHO process is the decision phase since, depending on the

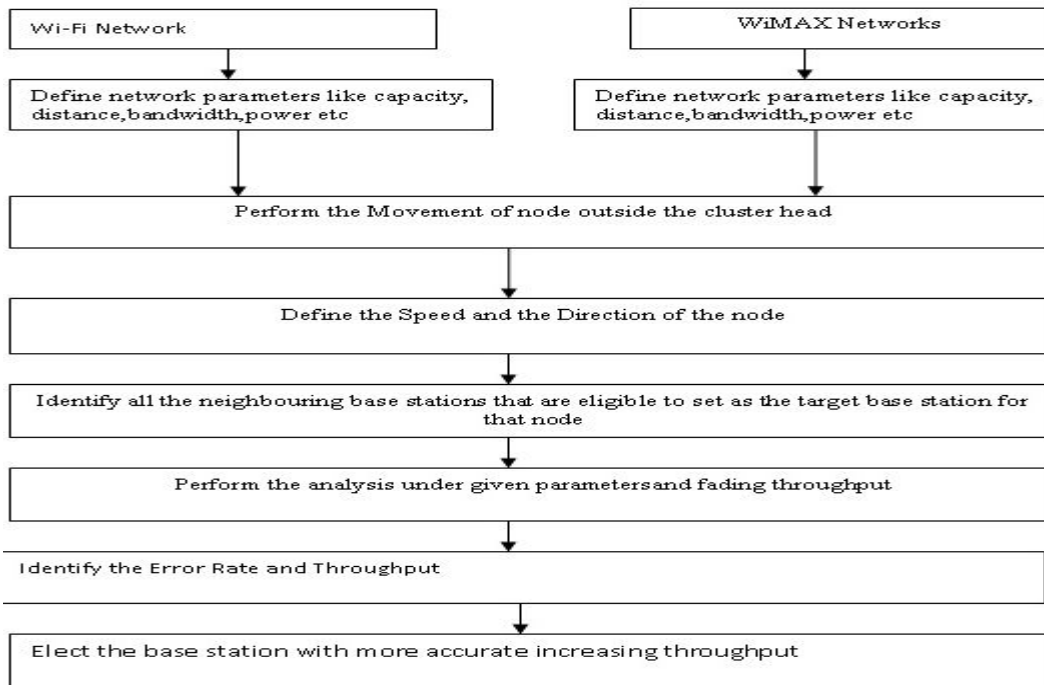


Fig 3. Flow Chart of Vertical Handover

- network candidate chosen, the performance of the system could improve or decrease. This decision should consider several parameters in order to choose the best candidate network to handover to [9]. The execution phase is in charge of committing the VHO itself. In this process the UE (User Equipment) leaves the current network and gets attached to a new network in a seamless manner, experiencing low latencies and minimal packet loss.
- This flow chart [Fig. 3] is about the selection of the next target cell as a node move outside its coverage area. As it moves outside, number of possible base stations that are having the coverage to that node will poll to get the access. The coverage will be decided under the distance coverage. The presented flow chart is about to select this target base station. In flow chart we have defined multiple parameters. In this flow chart to compare the Wi-Fi and WI-Max network and first of all define the network parameters such as capacity, distance, bandwidth and diameters of the network after that to check the movement of the nodes i.e. either randomly or behalf of the cluster head. Cluster head define the speeds and the direction of movement in the network area and cluster head also identifying all the base station that are lies in these network area or to the target of particular node. Base station perform the analysis of the nodes or the cluster head and to

find the throughput of the nodes i.e. the number of the cycle to complete the execution. Identify the error rate according to time frame schedule these are depends on time division multiplexing. Elect the base station with accurate data to increasing throughput and calculate the speeds, diameters and to the target of the node.

5. Performance Matrices for Handoff Mechanism

5.1 Bandwidth

Bandwidth is a measure of the width of a range of frequencies. It is the difference between the upper and lower frequencies in a contiguous set of frequencies. In order to provide seamless handoff for Quality of service (QoS) in wireless environment, there is a need to manage bandwidth requirement of mobile node during movement. Bandwidth is generally known as the link capacity in a network. Higher offered bandwidth ensures lower call dropping and call blocking probabilities; hence higher throughput [14]. Bandwidth handling should be an integral part of any of the handoff technique.

5.2 Handoff Latency

Handover of calls between two BS is encountered frequently and the delay can occur during the process of handoffs. This delay is known as handoff latency. A good handoff decision model should consider Handoff latency factor and the handoff latency should be minimized. Many proposed handoff decision models have tried to minimize the handoff latency by incorporating this factor in their handoff decision models. Handoff Latencies affect the service quality of many applications of mobile users. It is essential to consider handoff latency while designing any handoff technique.

5.3 Power Consumption

In 4G networks, we need to find ways to improve energy efficiency. Power is not only consumed by user terminal but also attributed to base station equipments. Power is also consumed during mobile switching or handoffs. During handoff, frequent interface activation can cause considerable battery drainage. The issue of power saving also arises in network discovery because unnecessary interface activation can increase power consumption. It is also important to incorporate power consumption factor during handoff decision.

5.4 Network Cost

A multi criteria algorithm for handoff should also consider the network cost factor. The cost is to be minimized during VHO in wireless networks. The new call arrival rates and handoff call arrival rates can be analyzed using cost function. Next Generation heterogeneous networks can combine their respective advantages on coverage and data rates, offering a high Quality of Service (QoS) to mobile users. In such environment, multi-interface terminals should seamlessly switch from one network to another in order to obtain improved performance or at least to maintain a continuous wireless connection. Therefore, network selection cost is important in handoff decisions.

5.5 User Preferences

When handover happens, the users have more options for heterogeneous networks according to their preferences and network performance parameters. The user preferences could be preferred networks, user application requirements (real time, non-real time), service types (Voice, data, video), Quality of service (It is a set of technologies for managing network traffic in a cost effective manner to enhance user experiences for wireless environments) etc. User Preferences can also be considered for VHO in 4G wireless networks.

5.6 Throughput:

Throughput or network throughput is the average rate of successful message delivery over a communication channel. These data may be delivered over a physical or logical link, or pass through a certain network node. Throughput is usually measured in bits per second (bit/s or bps), and sometimes in data packets per second or data packets per time slot.

Throughput = $[(\text{Total Bytes Sent} * 8) / (\text{Time Last Packet Sent} - \text{Time First Packet Sent})]$ where 'time' is in seconds.[15]

5.7 End-to-End Delay:

End-to-end delay indicates the length of time taken for a packet to travel from the CBR (Constant Bit Rate) source to the destination. It represents the average data delay an application or a user experiences when transmitting data. The delay is usually measured in seconds.

Average end-to-end delay = (Total of Transmission Delays of All Received Packets)/ (Number of Packets Received)[15]

Where,

Transmission Delay of a Packet = (Time Pkt. Rxvd. at Server – Time Pkt Txd. at Client)

Where ‘time’ is in seconds.

5.8SNR-- Signal to Noise Ratio[15]:

Signal-to-noise ratio is defined as the power ratio between a signal (meaningful information) and the background noise (unwanted signal):

SNR= $[P_{\text{signal}}/P_{\text{Noise}}]$

Where P is average power. Both signal and noise power must be measured at the same and equivalent points in a system, and within the same system bandwidth. If the signal and the noise are measured across the same impedance, then the SNR can be obtained by calculating the square of the amplitude ratio:

SNR= $[P_{\text{signal}}/P_{\text{Noise}}] = (A_{\text{signal}}/ A_{\text{Noise}})^2$

where A is root mean square (RMS) amplitude (for example, RMS voltage). Because many signals have a very wide dynamic range, SNRs are often expressed using the logarithmic decibel scale. In decibels, the SNR is defined as

SNR_{dB} = $10 \log_{10} (P_{\text{signal}}/P_{\text{Noise}}) = 20 \log_{10} (A_{\text{signal}}/ A_{\text{Noise}})$

6. Conclusion

When connections need to migrate between heterogeneous networks for performance and high-availability reasons, seamless vertical handoff is necessary. Handoff occurs when mobile node changes its point of access technology. This paper describe two of the most prominent developing wireless access networks and detailed comparative analysis between the 802.11 (Wi-Fi) and 802.16 (WiMAX) wireless networks. As we have studied above one of the major problems of the mobile networks is the degradation of the throughput during the handover mechanism. The presented work provides different performance metrics that need to consider during handover and the basic operation of a seamless vertical handover process that can takes place under hybrid networks in order to reduce the error rate, improve throughput over the wireless communication.

References

- [1] *IEEE 802.16-2004*, IEEE Standard for Local and metropolitan area networks Part 16: Air Interface for Fixed Broadband Wireless Access systems.
- [2] *IEEE 802.16e-2005*, IEEE Standard for Local and metropolitan area networks Part 16: Air Interface for Fixed and Mobile Broadband Wireless Access Systems Amendment for Physical and Medium Access Control Layers for Combined Fixed and Mobile Operation in Licensed Bands.
- [3] *IEEE 802.11*, IEEE Standards for Information Technology Telecommunications and Information Exchange between Systems, Local and Metropolitan Area Network, Specific Requirements, Part 11: Wireless LAN Medium Access Control (MAC) and Physical Layer (PHY) Specifications.
- [5] IEEE LAN/MAN Standards Committee, “IEEE Standard for Local and metropolitan area networks, Part 16: Air Interface for Fixed Broadband wireless Access Systems,” IEEE Std 802.16-2001, 2001.
- [4] Wonjun Lee, “Movement-Aware Vertical Handoff of WLAN and Mobile WiMAX for Seamless Ubiquitous Access”, IEEE Transactions on Consumer Electronics 0098 3063/07 © 2007 IEEE
- [6] *Mobile WiMAX: A Performance and Comparative Summary*, Doug Gray September 2006, WiMAX Forum
- [7] All-IP network architecture for mobile WiMAX, P. Iyer, N. Natarajan, M. Venkatachalam, A. Bedekar, E. Gonen, K. Etemad and P. Taaghoh, IEEE Mobile WiMAX Symposium, March 2007, pp. 54 – 59.
- [8] Theodore S.Reppeport, *Wireless Communications Principles and Practice*, IEEE Press,Prentice Hall.
- [9] Deep Kaur, Vishal Arora, “Research Agenda for Vertical Handover between WiMAX and Wi-Fi Networks” International Journal of Emerging Research in Management &Technology ISSN: 2278-9359 January 2013
- [10] Sourangsu Banerji, “Wi-Fi & WiMAX: A Comparative Study”
- [11] “A Review: Vertical Handover between Wi-Fi and WiMAX”, Ankur Saini Preeti Bhalla

- [12] Bushra Naeem, "Seamless Vertical Handover in Wi-Fi and WiMAX Networks using RSS and Motion Detection: An Investigation" The Pacific Journal of Science and Technology Volume 12, Number 1, May 2011 (spring)
- [13] Deep Kaur, Vishal Arora, "Research Agenda for Vertical Handover between WiMAX and Wi-Fi Networks" International Journal of Emerging Research in Management & Technology ISSN: 2278-9359 January 2013
- [14] Pramod Goyal & S. K. Saxena, (2008) "A Dynamic Decision Model for Vertical Handoffs across Heterogeneous Wireless Networks", 677 ? 2008 WASET.ORG, World Academy of Science, Engineering and Technology, Issue 41, pp 676-682.
- [15] Rajender Kumar, Brahmjit Singh, "COMPARISON OF VERTICAL HANDOVER MECHANISMS USING GENERIC QOS TRIGGER FOR NEXT GENERATION NETWORK" International Journal of Next-Generation Networks (IJNGN) Vol.2, No.3, September 2010

Clustering in Data Mining: A Brief Survey

Prof. Sweta R. Garasia^a, Prof. Brinda Y. Pandit^a

^a*Gandinagar Institute of Technology, Gnadhinagar, India*

Abstract

Retrieval of information from the databases is now a day's significant issues. The thrust of information for decision making is challenging one. To overcome this problem, different techniques have been developed for this purpose. One of techniques is data clustering. Some applications of data clustering like data mining using data clustering and similarity searching in medial image databases are also discussed. Clustering is the unsupervised classification of patterns (data item, feature vectors, or observations) into groups (clusters). Clustering in data mining is very useful to discover distribution patterns in the underlying data. Clustering algorithms usually employ a distance metric-based similarity measure in order to partition the database such that data points in the same partition are more similar than points in different partitions. Clustering is a division of data into groups of similar objects. The scope of applying clustering algorithms is to discover useful but unknown classes of items. The clustering methods are presented, divided in to: hierarchical, partitioning, density-based, model-based and grid-based methods. In this study, data clustering methods are discussed along with its traditional approaches and their algorithms.

Keywords: Clustering, Data Mining, Unsupervised learning

10. Introduction

Now days we are living in a world full of data. People need to store or represent it as data, for further analysis and management. Cluster analysis is unsupervised learning methods used for the exploration of inter- relationships among a collection of patterns, by organizing them into homogeneous clusters. Clustering aims to organize a collection of data items into clusters, such that items within a cluster are more "similar" to each other than they are to items in the other clusters. Clustering algorithms partition data into a certain number of clusters (groups, subsets, or categories). Detailed surveys of this domain can be found in [1], [2] or [3]. This surveys emphasis is on clustering in data mining. Such clustering is characterized by large datasets with many attributes of different types. Some of the applications of clustering are like Marketing in which clustering is used for discovering of distinct customer groups in a purchase database. Another application is Land use which identifying of areas of similar land use in an earth observation database. Next is Insurance in which clustering is used to identifying groups of motor insurance policy holders with a high average claim cost. One more application is City-planning identifying groups of houses according to their house type, value, and geographical location.

The rest of this paper is organized as follows: - The section 2, discusses measures of Similarity and Dissimilarity feature. In section 3, different clustering methods of data mining are described. The conclusion of survey is described in section 4.

11. Measures of similarity and dissimilarity

Since clustering is the grouping of similar instances/objects, some sort of measure that can determine whether two objects are similar or dissimilar is required. There are two main type of measures used to estimate this relation: distance measures and similarity measures. Similarity function is an alternative concept to that of the distance is the similarity function $s(p_k, p_q)$ that compares the two vectors p_k and p_q [4]. The definition of similarity or dissimilarity between objects depends on the type of the data considered and what kind of similarity we are looking for. It is useful to denote the distance between two instances p_k and q_k as: $\text{dist}(p_k, q_k)$. Table 1 shows some of the similarity and dissimilarity measure.

* Corresponding author. Tel.: 9904405914; 8347010841.

• *E-mail address:* sweta.garasia@git.org.in, brinda.pandit@git.org.in

Table 1. Measures of similarity and dissimilarity

Measures	Forms
----------	-------

Minkowski Distance	$dist = \left(\sum_{k=1}^n p_k - q_k ^r \right)^{\frac{1}{r}}$
Euclidian Distance	$dist = \sqrt{\sum_{k=1}^n (p_k - q_k)^2}$
Cosine Similarity	$s(p_k, p_q) = \frac{p_k^t p_q}{\ p_k\ \ p_q\ }$
Extended Jaccard Measure	$s(p_k, p_q) = \frac{p_k^t p_q}{\ p_k\ ^2 + \ p_q\ ^2 - p_k^t p_q}$
Dice Coefficient Measure	$s(p_k, p_q) = \frac{2 p_k^t p_q}{\ p_k\ ^2 + \ p_q\ ^2}$

12. Classification of Clustering Algorithm

3.1 Hierarchical Methods

In data mining, hierarchical clustering is a method of cluster analysis which seeks to build a hierarchy of clusters. Hierarchical clustering has the distinct advantage that any valid measure of distance can be used. Strategies for hierarchical clustering generally fall into two types build a tree-based hierarchical taxonomy (dendrogram) from a set of documents.

Generally, clustering algorithms can be categorized into partitioning methods, hierarchical methods, density-based methods, grid-based methods, and model-based methods. For reader’s convenience here it is provided with a classification closely followed by this survey. Corresponding terms are explained below.

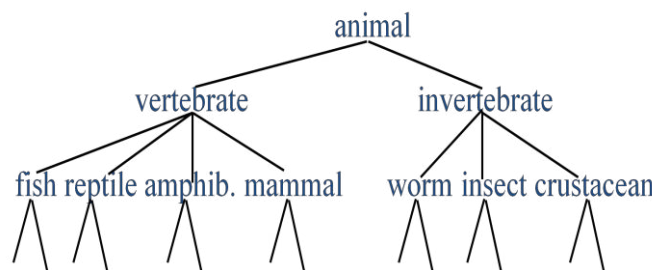


Fig.1 Hierarchical Clustering

Agglomerative algorithms clustering starts with one-point clusters and recursively merges two or more most appropriate clusters. And second is Divisive algorithm starts with one cluster of all data points and recursively splits the most appropriate cluster. A top-down clustering method and is less commonly used.

Some of the hierarchical clustering algorithms are: Balanced Iterative Reducing and Clustering using Hierarchies – BIRCH [5], Clustering Using REpresentatives – CURE [6] and CHAMELEON [7].

3.2 Partitioning Methods

In partitioning methods instances move from one cluster to another, starting from an initial partitioning. In this type of clustering methods numbers of clusters are pre-defined by the user. There are various types of partitioning methods are available but here only brief two approaches are described: K-means [2] and k-medoids [3].

K-means

K-means algorithm is a simple yet popular method for clustering analysis. Its performance is determined by initialization and appropriate distance measure. Choosing the proper initial centroids is the key step of the basic K-means

procedure. The algorithm is composed of the following steps:

1. Select K points as the initial centroids.
2. Assign all points to the closest centroid.
3. Re compute the centroid of each cluster.
4. Repeat steps 2 and 3 until the centroids don't change.

Although it is efficient algorithm it has some disadvantage like, first we have to define mean. Next, we need to specify k, the number of clusters, in advance. It is not able to handle noisy data and outliers. It is not suitable to discover clusters with non-convex shapes.

K-medoid

The objective of K-medoid clustering [3] is to find a non-overlapping set of clusters such that each cluster has a most representative point. These representative points are called medoids. Once again, the algorithm is conceptually simple.

Basic K-medoid Algorithm for finding K clusters.

1. Select K initial points.
2. Consider the effect of replacing one of the selected objects (medioids) with one of the non-selected objects.
3. Select the configuration with the lowest cost.
4. Otherwise, associate each non-selected point with its closest selected point (medoid) and stop.

PAM (Partitioning Around Medoids) [3] is a “K-medoid” based clustering algorithm. CLARA (Clustering LARge Applications) [9] is an adaptation of PAM for handling larger data sets.

3.3. Density Based Clustering

Density-based clustering algorithms based on density (local cluster criterion), such as density-connected points. It is basically depend on two parameters:

Eps: Maximum radius of neighborhood

MinPts: Minimum number of points in an Eps-neighborhood of a point.

One of the most well known density-based clustering algorithms is the DBSCAN [8]. DBSCAN separate data points into three classes CLIQUE and MAFIA are specifically designed for handling clusters in high-dimensional data. Another density-based algorithm is the DENCLUE [9]. It is good for data sets with large amounts of noise. It allows a compact mathematical description of arbitrarily shaped clusters in high-dimensional data sets. Significantly faster than other algorithms, but needs a large number of parameters.

3.4. Grid-Based Methods

These types of clustering algorithm are popular for mining clusters in large multidimensional space where in clusters are regarded as denser region than their surroundings. The computational complexity of most clustering algorithms is at least linearly proportional to the size of the data set. The great advantage of grid-based clustering is its significant reduction of the computational complexity, especially for clustering very large data sets.

The grid-based clustering approach differs from the conventional clustering algorithms in that it is concerned not with the data points but with the value space that surrounds the data points. In general, a typical grid-based clustering algorithm consists of the following five basic steps [10].

1. Creating the grid structure, i.e., partitioning the data space into a finite number of cells.
2. Calculating the cell density for each cell.
3. Sorting of the cells according to their densities.
4. Identifying cluster centers.
5. Traversal of neighbor cells.

Some grid based methods are CLIQUE (CLustering In QUEst) [11], STING (STatistical INformation Grid) [12], MAFIA (Merging of Adaptive Intervals Approach to Spatial Data Mining) [13].

3.5. Model based Methods

MLE (maximum likelihood estimation) is used in model-based clustering method to find the parameter inside the probability model. Since the probability function is a mixture summation of a couple of probability function, it makes the traditional method infeasible to find the maximum value. One model based method is the SOM net [14]. The SOM net can be thought of as two layers neural network. Each neuron is represented by n-dimensional weight vector, $m = (m_1, \dots, m_n)$, where n is equal to the dimension of the input vectors. The neurons of the SOM are themselves cluster centers; but to accommodate interpretation the map units can be combined to form bigger clusters.

13. Conclusion

The aim was to describe different clustering technique available in Data mining. In general, partitioning algorithms typically represent clusters by a prototype. Density-based approaches apply a local cluster criterion and are very popular for the purpose of data set mining. Grid-based clustering algorithms first separate the clustering space into a finite number of cells and then perform the required operations on the quantized space.

References

- [1] Anil K. Jain and Richard C. Dubes.1988, Algorithms for clustering data, Prentice-Hall, Inc.
- [2] Anil K. Jain, M. N. Murty, and P. J. Flynn.,1999.Data clustering: a review. ACM Computing Surveys, 31(3), p.264–323.
- [3] L. Kaufman and P. J. Rousseeuw, 1990. Finding groups in data: an introduction to cluster analysis.,John Wiley & Sons.
- [4] Duda, P. E. Hart and D. G. Stork, 2001.Pattern Classification. Wiley, New York.
- [5] Zhang, T., Ramakrishnan, R., and Linvy, M. ,1997. BIRCH: An efficient data clustering method for very large data sets, Data Mining and Knowledge Discovery, p.141–182.
- [6] Guha, S., Rastogi, R., Shim K,1998. “CURE: An Efficient Clustering Algorithm for Large Data sets”, Published in the Proceedings of the ACM SIGMOD Conference.
- [7] Karypis G., Han E. H. and Kumar V. ,1999.CHAMELEON: A hierarchical clustering algorithm using dynamic modeling, Computer 32(8): pp68-75,.
- [8] Ester, M., Kriegel, H.-P., Sander, J., Wimmer M. and Xu X,1998.“Incremental Clustering for Mining in a Data Warehousing Environment, “Proceedings of the 24th VLDB Conference New York, USA.
- [9] Hinneburg A. and Keim D..1998 “ An efficient approach to clustering in large multimedia data sets with noise,” In Proceedings of the 4th International Conference on Knowledge Discovery and Data Mining, pages 58-65.
- [10] Peter Grabusts, Arkady Borisov,2002. Using Grid-Clustering Methods in Data Classification. p.425.
- [11] Rakesh Agrawal, Johannes Gehrke, Dimirios Gunopulos, Prabhakar Raghavan,2005. Automatic Subspace Clustering of High Dimensional Data”. Data Mining and knowledge discovery, 11, p.5-33..
- [12] J Wei Wang, Jiong Yang, and Richard Muntz. STING : A Statistical Grid Approach to Spatial Data Mining ,Department of Computer Science, University of California, Los Angels .
- [13] Sanjay Goil, Harsha Nagesh and Alok Choudhary, MAFIA: Efficient and Scalable Clustering for very large data sets. editors, Advances in Knowledge Discovery and Data Mining, pages 153-180, 1996
- [14] Kohonen T. ,1997.Self-Organizing Maps, Second Extended Edition, Springer Series in Information Sciences, Vol. 30, Springer, Berlin, Heidelberg, New York.

Multicast Ad-hoc On-Demand Distance Vector Routing Protocol with Low Control Overhead

Kinjal U Adhvaryu^a, Pariza Kamboj^b

R K University, Rajkot, Gujarat, India.

^bSarvajani College of Engineering, Surat, Gujarat, India

Abstract

• Mobile Ad-hoc Network (MANET) is a multi-hop, dynamic and autonomous network composed of number of wireless mobile nodes. Based on the one commonly known shared tree-based multicast routing protocol, Multicast Ad-hoc On-Demand Distance Vector Protocol (MAODV), this paper suggest a way to improve the performance of protocol in terms of the throughput and reduction in the total number of mobile nodes participating in multicast routing. To improve the performance expanding ring search method is modified and because of that it will significantly reduce the overall routing control overhead and also increase the lifetime of the network.

•
Keywords: Control Overhead, Mobile Ad hoc Network, shared tree

1. Introduction

•
• An ad hoc network consists of a collection of autonomous mobile nodes formed by means of multi-hop wireless communication without the use of any existing network infrastructure. Ad hoc networks have become increasingly relevant in recent years due to their potential applications in battlefield, emergency disaster relief and etc. In an ad hoc network, each mobile node can serve as a router. A mobile ad-hoc network (MANET) is characterized by mobile nodes without any infrastructure. Mobile nodes self-organize to form a network over radio links [20]. Group communication are important in MANET. Many ad hoc Network applications which require close association of the member nodes depends on group communication. Disaster relief, conferences, action directions given to the soldiers in a battlefield and communications required during a rescue operation are some examples of these applications. In addition, many routing protocols for MANET need a broadcast/multicast as a communication primitive to update their states and maintain the routes between nodes [1],[15].

•
• Multicast protocols can be categorized in tree based and mesh based protocols. In wired as well as in wireless networks, maintaining group membership information and building an optimal multicast distribution structure (typically in the form of a routing tree) is challenging. A detailed survey of the work done in that area and a discussion of various design tradeoffs can be found in [2]. Group management is one of challenging task for MANET. Nodes are free to move arbitrarily. Bandwidth scarcity, limited power resource and above all dynamicity of topology in a mobile ad hoc network make the multicast protocol design predominantly challenging than that for wired network [15].

•
The primary goal of an ad hoc routing protocol is to establish a correct and efficient route between any pair of nodes with minimum overhead. Routing overhead is a very important metric. If the control overhead of a proposed method is very high, then that method cannot work well in MANET. It would be a difficult and challenging task to offer optimal, reliable, energy efficient with low control overhead multicast routing in MANETs. In recent years, various multicast routing protocols have been proposed to reduce various overheads during routing. These protocols have unique attributes and utilize different recovery mechanisms on overhead reduction. Multicast Ad-hoc on Demand Distance Vector Protocol (MAODV) is the best example of on-demand multicast routing protocol. MAODV is the multicast extension version of Ad-hoc on Demand Distance Vector Protocol (AODV). In MAODV, node discover the route only if it needs send data to the destination nodes and maintain only active routes. So that overhead is reduced .Because of this reason MAODV is widely used in MANET. But, there are two limitations of this protocol: (1) many control messages are transmitted by flooding (2) Tree will not be repaired until link breakage will happens during communication. So that in this paper, based on the expanding ring search method is modified and initial route establishment and repairing the network partitions related procedure is improved which will reduce the total number of control messages during the whole communication process.

The remainder of this paper is organized as follows. In section-2, we explain the working of MAODV. Section-3 explains

the new idea based on which expanding ring search approach is modified to surmount the limitations of original MAODV. Section-4 shows the comparative results for modified and original MAODV. At last section-5 concludes the results.

2. Related Work

A number of multicast protocols have been proposed to provide multicasting in MANET like challenging environments [1-13]. During multicasting, a multicast group is formed by various senders and receivers. For connecting senders and receivers, each protocol constructs either a tree or a mesh as the routing structure. There are some nodes called forwarding nodes in the routing structure that are not interested in multicast packets but act as routers to forward them to receivers. Group members (senders and receivers) and forwarding nodes are also called tree or mesh nodes depending on the routing structure. In the routing structure, a node is an upstream/downstream node of another node if it is closer to / farther away the root of the tree. If the two nodes belong to the same link, the upstream/downstream node is also called the parent/child of the other node. Generally, a sender initially floods a join message to all nodes in the network. Interested nodes reply to the sender via the reverse path. After all reply messages arrive at the sender, a multicast tree rooted at the sender is formed. This kind of tree construction is called a sender-tree-based one. A multicast group usually has several senders and thus it costs high for each sender to build its own tree. Instead of that, Some protocols select a single sender to build a multicast tree that is shared with other senders. This kind of tree construction is called a shared-tree-based one and the selected sender is called the group leader / core node. Other senders first transmit data packets to the group leader and the group leader then relays the packets downward the shared tree to all receivers. The kind of initialization of tree construction by one or more senders is called a sender-initiated scheme. The receiver-initiated scheme requires receivers to initiate the tree construction, and it is often used for the shared-tree structure. Sender-tree-based protocols incur higher control overhead than shared-tree-based ones because each sender builds its own tree. Shared-tree-based protocols have two main drawbacks: single point of failure of the group leader and sub-optimal multicast paths. Moreover, the group leader may locate in a bad position which further decreases multicast efficiency and increases packet latency. The mesh structure is robust against topology changes, but multicast efficiency is reduced [23]. Because of all these reasons, routing and route discovery in MANETs are among the most actively researched issues in the area of wireless communication.

Tree Based Multicast Routing Protocol

Tree based multicast routing protocol maintains either a shared tree or multiple source based multicast routing tree in which one for each group source, to deliver data packets from source/s to receivers of a group. Tree based protocols are generally more efficient in terms of data transmissions but they are not robust against topology changes as there are no alternative paths/links between the source/s and destinations. There are number of tree based multicast routing protocols are designed like MAODV, AMRIS, AMROUTE, MOLSR, ADMR.

Multicast Ad-hoc on Demand Distance Vector Protocol (MAODV)

Multicast Ad-hoc on Demand Distance Vector Protocol is the multicast extension version of unicast routing protocol Ad-hoc on Demand Distance Vector Protocol (AODV). MAODV is enough capable to handle unicasting, multicasting and broadcasting the message/s. MAODV is the best example of on-demand multicast routing protocol i.e. node discover the route only if it needs send data to the destination nodes and maintain only active routes. It establishes routes on demand using the route discovery mechanism with smaller delay [21].

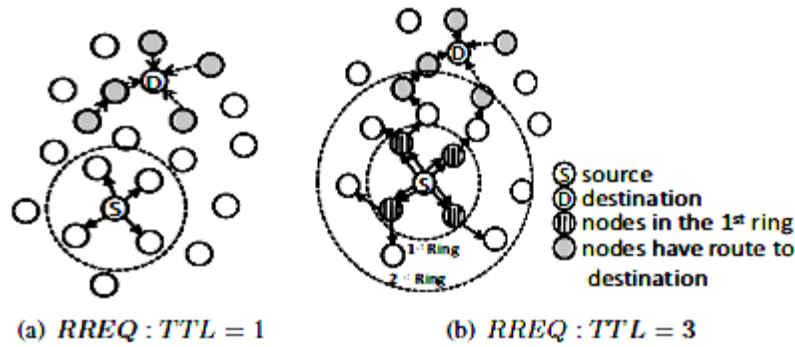


Fig. 1. An example of an expanding ring search.

Route discovery process includes broadcast route request based on Expanding Ring Search (ERS) as shown in figure 1 and unicast route reply discovery cycle. MAODV uses the multicast distribution mechanism of bi-directional shared tree approach, consisting of members of the multicast group and several routers, which are not group member but exist in the tree to connect the group members. In MAODV each multicast group has a unique address, which is known as multicast group address, and one group leader, which is known as core node. The group member who initiates the tree construction is known as group leader. Each broadcast packet has one a broadcast ID which is known as sequence number of that packet. The network address and sequence number collectively identify the packet uniquely. Because of this, multiple times broadcasting of packets can be prevented. Core node/ group leader is responsible to maintain the group sequence number which is periodically broadcasted within the network in the form of Group Hello (GRPH) messages [22].

MAODV describe route discovery to multicast tree and maintenance of the multicast tree. If any node wants to join a multicast group, or wants to send any data to multicast group which does not know about the route to the multicast tree, it will broadcast Route Request (RREQ) message. This message includes RREQ_J and RREQ_NOFLAG, which are used to represent route request to join the group and transmit data to a multicast group respectively. With the RREQ's broadcasting along the whole network, all intermediate nodes prepare the reverse route to the sender nodes and continue to broadcast the messages to their neighbours. When RREQ_J will be received by a member node of the tree or RREQ_NOFLAG will be received by any node which has new route to the multicast group, the node will respond the message and unicast Route Reply back along the reverse route details towards the source node of the tree. The source node chooses one RREP which has greatest sequence number and minimum number of hops the nearest member of the multicast tree. Then it will reply with unicast Multicast Activation (MACT) message along route of this selected route reply message.

During communication, Multicast group links may break due to node's movement or expired route timers. When a link breakage is detected during communication, the downstream node of break (i.e., the node that is further from core node) is responsible to repair the broken link. The downstream node initiates the repair by broadcasting a route request message with Dest_Addr set to the IP address of the core node and with the J_flag set. The Multicast Group Hop Count (Mgroup_Hop) extension is set to the distance of the node from core node. The only nodes which may reply to a RREQ with the Mgroup_Hop extension are nodes that are at least as close to the core node, or the core node itself.

According to the principle of MAODV, it is analyzed that there are some drawbacks in the protocol as below:

- (1) Many control messages in MAODV are transmitted by flooding. The method of blind flooding create the RREQ and GRPH be forwarded to whole network, which will utilize the valuable network resources, and may create network congestion, then increases packet's collision probability and packet's loss.
- (2) Tree will not be repaired until link breakage will happens during communication. And when a node detects link breakage, it sends RRER to the source node and then handle. With the increase of network size and node's movement/speed, this problem will be infinitely zoomed, and will result in degradation of network performance.

3. The Proposed Multicast Routing Protocol with Low Control Overhead

Route discovery in MANET often relies on some form of network flooding where each node in the network forwards a route request message to all of its neighbours. This process is inefficient because it results in control messages visiting the network nodes even if the path to destination is located in a different portion of the network. To improve network utilization

of the flooding-based route discovery protocols, MAODV uses expanding ring search (ERS) technique for controlling dissemination of Route Request Messages. In ERS, the source node will be the center of the search ring. ERS successively searches a larger area till the node having needed information being searched is not found. Using the conventional method of flooding algorithm and expanding ring search method following equation is derived for calculating the total number of transmissions for a farthest destination assuming nodes in the radio range of each mobile node n [21].

$$(n - 2)^{d+1} - d(n - 2) + (d - 3), \text{ where } d \text{ is the network diameter.}$$

As per the expanding ring search algorithm, a node initiates a route request with initial value of Time To Live (TTL) equal to 1. If the originating node will not receive a RREP message within a certain period of time limit then it rebroadcasts the RREQ message with TTL value incrementing by 1. The node continues to broadcast messages with increasing TTL value up to predefined network diameter value until it receives a route reply. One important parameter of ERS is the initial value of TTL. It is a parameter that must be selected carefully to get the best possible result. A good initial TTL value can reduce the number of re-transmitted request messages in the whole route discovery process, which means it can reduce the network overhead. So that instead of choosing the TTL value randomly, in proposed technique, initial value of TTL will be set to 1. After starting the route discovery process with TTL=1, based on the odd and even numbered generated ring for searching the nodes, broadcasting and unicasting is applied respectively. To support that, expanding ring search implementation is modified. Instead of each and every time broadcasting the RREQ to neighbours, if RREQ propagation method will be changed then it will effectively reduce overhead transmissions. If overhead transmissions will be effectively reduced, then utilization of energy of intermediate node for receiving and forwarding the request will be minimized and so that lifetime of network can be prolonged.

4. Simulations

The purpose behind the simulation is to measure the routing overhead for original MAODV and modified MAODV i.e. First is based on original expanding ring search and second is - with the modified expanding ring search for MAODV. It will help us understand how effectively the suggested approach reduces the routing overhead in MAODV. The goal behind the simulation is to determine the effect of changing the value of TTL_INCREMENT and TTL_THRESHOLD with original ERS and modified ERS based MAODV protocol. To evaluate results Throughput, Packet Delivery Fraction (PDF) and Average End-to-End Delay metrics are used. A Simulation model based on NS-2.26 is used for evaluation. Throughput gives the ratio of the total size of received data packets to the duration of time when it receives. Packet Delivery Fraction specifies the ratio of the number of data packets expected to be received to the number of data packets delivered to the destinations and End-to-End Delay indicates the average time a packet takes for delivery to its destination after it was transmitted. It tells how a protocol adapts or arranges for an immediate delivery of packets to its desired destination. Average delay is all possible delays like route discovery latency, queuing at the interface queue, retransmission delays at the MAC etc [9]. As a simulation parameters- Network Size is 500*500, Number of Nodes are 7, IEEE 802.11 for MAC Layer protocol and 200ms as simulation duration are considered. Considering the TTL_START =1, TTL_THRESHOLD and TTL_Increment values are modified to evaluate the performance of original and modified approach.

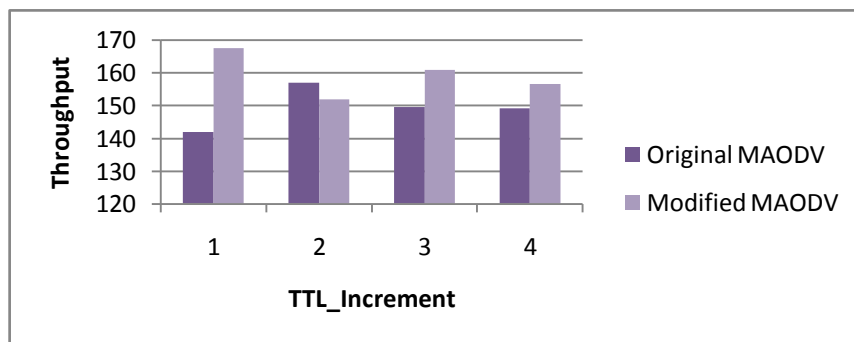


Figure 1. Throughput

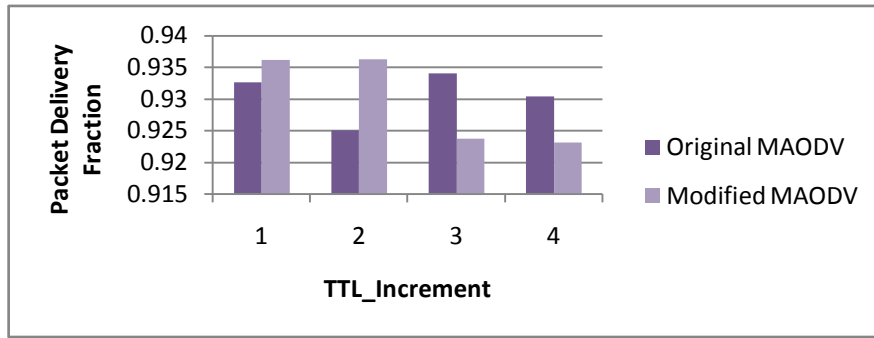


Figure 2. Packet Delivery Fraction

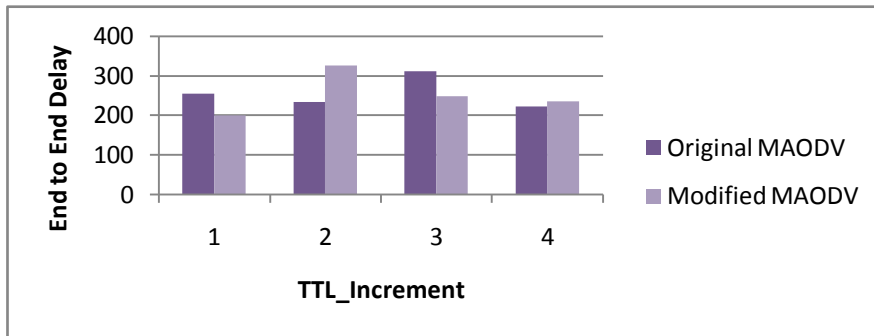


Figure 3. End to End Delay

Above figures show the comparison between MAODV based on original ERS concept and MAODV based on proposed ERS concept. From figure 1 we can observe that overall throughput is increased with proposed modified ERS. Performance improvement done by modified MAODV is also supported by figure 2 and figure 3. Every time, instead of broadcasting the control packets to each node during route discovery process, based on the generated ring, if unicasting or broadcasting will be done then it will directly affect the required total number of retransmissions. Throughput and Packet Delivery Fractions support this fact also. As number of retransmissions will be reduced, transmission overhead will be reduced and if overall overhead will be reduce , it will directly affect the lifetime of individual node as well as whole network also.

5. Conclusions

In this paper, expanding ring search approach which is used by MAODV during the route discovery process is analyzed and based on that new concept is suggested. Using various performance metrics, original and modified MAODV protocols are compared and from results of same it is concluded that suggested idea increase the throughput and also reduces the end to end delay. From the various results it is also observed that at some point for specific TTL_Increment value, modified MAODV does not give the better performance. Several other parameters such as mobility of nodes, radio range of nodes, traffic patterns may affect the routing performance. So this work can be further explored to find out the solution for same.

References

Song Guo, Member, IEEE, and Oliver Yang, Senior Member, IEEE, “Maximizing Multicast Communication Lifetime in Wireless Mobile Ad Hoc Networks”, IEEE Transactions on Vehicular Technology, vol. 57, no. 4, July 2008

V. Li and Z. Zhang, Internet Multicast Routing and Transport Control Protocols, in Proc. of the IEEE, pp. 360-391, Vol. 90, No. 3, March 2002.

S.-J. Lee et al., “A Performance Comparison Study of Ad hoc Wireless Multicast Protocols”, Proc. INFOCOM 2000, Mar. 2000, pp 564-574.

Carlos de Morais et al, “Multicast over wireless mobile ad hoc networks: present and future directions”, IEEE Network, Jan/Feb,2003 pp 52-59.

Aniruddha Rangnekar, Ying Zhang, Ali A. Selcuk, Ali Bicak, Vijay Devarapalli, Deepinder Sidhu, “A Zone-Based Shared-Tree Multicast Protocol for Mobile Ad Hoc Networks”, In Vehicular Technology Conference, 2003

M. Gerla, C.-C. Chiang, and L. Zhang, “Tree Multicast Strategies in Mobile, Multihop Wireless Networks,” Baltzer/ACM Journal of Mobile Networks and Applications (MONET), Vol. 3, No. 3, pp. 193-207, 1999.

X. Xiang, Member, IEEE, X. Wang, Member, IEEE, and Y. Yang, Fellow, IEEE, “Supporting Efficient and Scalable Multicasting over Mobile AdHoc Networks “,IEEE TRANSACTIONS ON MOBILE COMPUTING, VOL. 10, NO. 5, APRIL 2011

- M. Gerla, C.-C. Chiang, and L. Zhang, "Tree Multicast Strategies in Mobile, Multihop Wireless Networks," *Baltzer/ACM Journal of Mobile Networks and Applications (MONET)*, Vol. 3, No. 3, pp. 193- 207, 1999
- Miguel A. Wister, Dante Arias Torres, "LIFT: An Efficient Cross-layer Service Discovery Protocol in MANET", 2009 International Conference on Advanced Information Networking and Applications Workshops
- Aniruddha Rangnekar, Ying Zhang, Ali A. Selcuk, Ali Bicak, Vijay Devarapalli, Deepinder Sidhu, "A Zone-Based Shared-Tree Multicast Protocol for Mobile Ad Hoc Networks", In *Vehicular Technology Conference*, 2003.
- Mohammed S. Al-kahtani, Hussein T. Mouftah, "SERC/LC3R: A New Paradigm for Cluster-based Routing in MANETs", 0-7803-9277-9/05/\$20.00/©2005 IEEE
- Sangman Moh, Chansu Yu, Ben Lee, and Hee Yong Youn, "Energy Efficient and Robust Multicast Protocol for Mobile Ad Hoc Networks", *Proceedings of the 2002 Pacific Rim international Symposium on Dependable Computing (December 16 - 18, 2002)*. *Proceedings of IEEE Computer Society*, Washington, DC, 145.
- Al-Sakib Khan Pathan, Md. Mahub Alam et al. "An Efficient Routing Protocol For Mobile Ad Hoc Networks With Neighbor Awareness And Multicasting", 0-7803-8655-8/04 IEEE
- Lucile Canourgues, Jerome Lephay et al. , "STAMP: Shared-Tree Ad Hoc Multicast Protocol"
- Pariza Kamboj, Ashok. K. Sharma, Scalable And Robust Location Aware Multicast Algorithm (SRLAMA) For Manet, *International Journal of Distributed and Parallel Systems (IJDPS)* Vol.1, No.2, November 2010
- Yi Wang, Hairong Chen, Xinyu Yang and Deyun Zhang, "Cluster Based Location-Aware Routing Protocol for Large Scale Heterogeneous MANET", *Second International Multisymposium on Computer and Computational Sciences*, 0-7695-3039-7/07 IEEE
- M. Transier, H. Fubler, J. Widmer, M. Mauve, and W. Effelsberg, "A Hierarchical Approach to Position-Based Multicast for Mobile Ad-Hoc Networks," *Wireless Networks*, vol. 13, no. 4, pp. 447-460, Aug. 2007.
- Natarajan Meghanathan, "A location prediction based routing protocol and its extensions for multicast and multi-path routing in mobile ad hoc networks", 1570-8705/11 Elsevier B.V.
- Gowrishankar.S , T.G.Basavaraju , Manjaiah D.H , M.Singh, Subir Kumar Sarkar, "Theoretical Analysis and Overhead Control Mechanisms in MANET: A Survey", *Proceedings of the World Congress on Engineering 2008 Vol I WCE 2008*, July 2 - 4, 2008, London, U.K.
- John Sucec and Ivan Marsic, "Clustering Overhead for Hierarchical Routing in Mobile Ad hoc Networks"
- Pariza Kamboj and A.K.Sharma, "An Improved Expanding Ring Search Technique for Mobile Ad Hoc Network (IERST)", communicated to 16thIEEE International Conference on Networks ICON 2008.
- Yufang Zhu and Thomas Kunz "MAODV Implementation for NS – 2.26".
- Chen-Che Huang, Shou-Chih Lo, " A Comprehensive Survey of Multicast Routing Protocols for Mobile Ad Hoc Networks".

Handwritten Character Recognition

Prof. Archana Singh

GGandinagar Institute of Technology, Gnadhinagar, India

Abstract

In handwritten character recognition, the characters are assumed to be written legibly allowing smaller variation in the shape of a character. There is a need to recognize unconstrained or free handwritten characters. Because of different writing styles, recognition of this type of characters is a complex problem. Considering the complexity of the problem, an attempt is made to develop recognition strategies for isolated English characters. The character recognition is important for document verification in Banks, in OCRing, postal sorting and for recognition of handwritten roll number from examination form. Recognition of letters or numbers is also used in sensitive areas like finance and administration. So the system should be accurate and fast. Due to this reason character recognition is essential for their proper working [9]. This research describes LVQ neural network architecture along with novel approach of feature extraction technique is used for off-line handwritten character recognition.

1. Introduction

The constant development of computer tools leads to a requirement of easier interfaces between the man and the computer. Handwritten Character Recognition may for instance be applied to Zip-Code recognition, automatic printed form acquisition, or checks reading. The importance of these applications has led to intense research for several years in the field of Off-Line handwritten character recognition. The recognition system has three steps. The first step is the segmentation one, which consist in analyzing the digitalized image provided by a scanning device, so as to localize the limits of each character, and to isolate them one from each others. Despite the constrains of writing that does often exist on the original printed form, thesegmentation process is not so easy in practice. Indeed, these constrains are not always respected, and, moreover, they do not encourage people to use automatic character recognition systems. The aim of the second step of the recognition structure is to extract discriminant information from an image of a character, as well as to reduce its dimension of representation. This reduction is required in order to make easier the conception of the classification system, when discriminant feature extraction allows presenting competently a character to the classifier. Once discriminant features have been extracted, they are submitted to a logic decision system whose task is to identify the character that they represent and to assign them the corresponding ASCII code. Classification is done last

The technique used for classification is Artificial Neural Networks. Artificial Neural Networks are based on the neural structure of the brain. The brain basically learns from experience. It is natural proof that some problems that are beyond the scope of current computers are indeed solvable by small energy efficient packages. This brain modelling also promises a less technical way to develop machine solutions. This new approach to computing also provides a more graceful degradation during system overload than its more traditional counterparts.

2. Problem Definition

2.1. Problems with features

General feature extraction techniques have problem with features. As these extraction techniques are not complete (two different characters have to be clearly differentiated solely based on the features describing them) and not steady (For example, if a character shape is insignificantly distorted by some noise, the features describing the character should also just change negligibly).

* Archana Singh. Tel.: 9978433988

E-mail address: archana.singh@git.org.in

2.2. Problems with recognition techniques

Artificial Neural Networks have shown good capabilities in performing classification tasks. This is due to the non-linearities that are included in these connections. Systems, and to the discriminant training phase that they are submitted to. However, their performance is strongly affected by the quality of the representation of the characters. This may require a large number of parameters to represent the character, which then results in difficulty in establishing the rules for recognition. In other words the MLPs become difficult to train. Moreover, the greater the size of the network, the greater is the computation time. This can greatly restrict their practical use. So, it is necessary to perform efficient features extraction on the one hand, and to optimize the lay-out of the artificial neural network on the other hand. Recognition of printed and handwritten documents is still one of the most challenging areas in pattern recognition. Although many different methods have been reported and some have shown very high performance, none has been able to achieve the accuracy and speed of human readers, which is the ultimate target. So there is ample scope for improvement in this well-researched problem.

2.3 Proposed Solution

The proposed system is based on neural network classifier. The feature extraction of a character is done by using novel approach of feature extraction technique [4] (direction based technique) extracts important features (features are steady and complete). For recognition of a character Kohonen's LVQ neural network is used [5], which trains the system rapidly and recognizes the characters rapidly. LVQ combines the competitive layer with supervision. For the LVQ network, the winning neuron indicates the subclass, rather than a class. There may be several different neurons (subclasses) that make up each class. Hence LVQ overcomes the limitation of Competitive learning, and it creates the complex class boundaries.

2.4 Objectives

1. The first is design and implementation of A to Z character recognition system.
2. Secondly, the system is tested for handwritten digit as well as character database.
3. Finally, the experiments with various parameters of a LVQ neural network have done for finding out the best parameters for the system.

3. System Implementation

This section contains two algorithms. The feature extraction algorithm, which extracts the features from a preprocessed image. The Kohonen's LVQ algorithm for recognition of a character [2]. An artificial neural network is an information-processing system that has certain performance characteristics in common with biological neural networks Learning Vector Quantization neural network is used for classification purpose [2].

3.1. Feature Extraction

It describes the feature extraction algorithm and its implementation in detail.

Feature Extraction Algorithm

1. Read a valid normalized character image of size $[30 \times 30]$.

Do

- a) Find Starting point and intersection point: The first black pixel in the Upper left hand side of the image is the starting point. Intersection points are determined as being those foreground pixels that have more than two foreground pixel neighbors.

- b) Distinguish individual line segments: The line segments in each character image were categorized into four types:

- i. Vertical lines
- ii. Horizontal lines
- iii. Right Diagonal
- iv. Left Diagonal

Four types of line segments were to be distinguished as compromising each character pattern. Neighbouring pixels along

the thinned pattern/character boundary were followed from the starting point to known intersection points. Upon arrival at each subsequent intersection, the algorithm conducted a search in a clockwise direction to determine the beginning and end of individual line segments.

Hence, the commencement of a new line segment was located. If:

- The previous direction was upper right or down left and next direction is upper left or downright.
 - The previous direction was upper left or down right and next direction is upper right or down left.
 - Direction of line segment-changed more than three types of direction.
 - The length of previous direction type is greater than three pixels.
- c) Labeling line segment information: Once an individual line segment is located, the black pixels along the length of this segment are coded with a direction number as follows: Vertical line segment - 2, Right diagonal line - 3, Horizontal line segment - 4 and Left diagonal line - 5.
- d) Line Type normalization: As line segments were marked by following either the character boundary or thinned image pattern on a pixel by pixel basis, some spurious direction values may have been marked in any particular line segment due to the presence of anomalous pixels introduced through the thinning or boundary extraction process. Hence to “normalize” a particular line segment (discarding spurious direction values), the number of values belonging to each direction type was tallied in a particular line. The direction value most frequently represented in a particular line segment was used to replace spurious direction values.

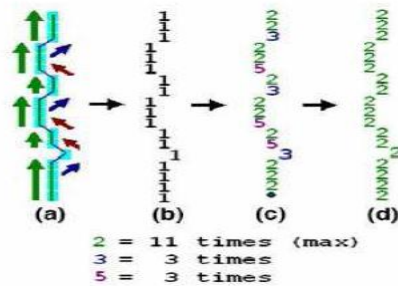


Figure 1: (a) Original line, (b) Line in binary file, (c) after distinguishing directions, (d) after direction Normalization.

e) Feature extraction through Zoning: In the first step, the character pattern marked with direction information was zoned into windows of equal size. The algorithm for extracting and storing line segment information first locates the starting point and any intersections in a particular window. It then proceeds to extract the number and lengths of line segments resulting in an input vector containing nine floating-point values. These nine floating point values are:

- The number of horizontal lines,
- The total length of horizontal lines,
- The number of right diagonal lines,
- The total length of right diagonal lines,
- The number of vertical lines,
- The total length of vertical lines,
- The number of left diagonal lines,
- The total length of left diagonal lines and
- The number of intersection points

Values that tallied the number of line types in a particular window were calculated as follows:

$$\text{Value} = 1 - ((\text{No. of lines } 10) \times 2)$$

If a window has a horizontal line, the input will increase by the length of the line divided by the maximum window length or window height, (depending on which one is the largest) multiplied by two. The reason this formula is used, is because it is assumed that the maximum length of one single line type is two times the largest window size.

$$Value = 1 - ((No. \text{ of pixels (in a particular direction)} / (\text{window height or width}) \times 2)$$

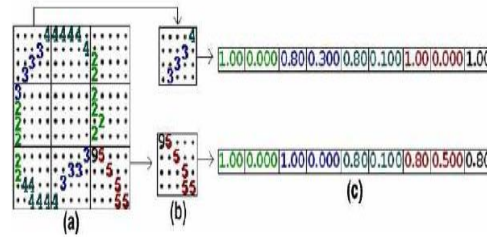


Figure 2: (a) processed image, (b) Zoned windows, (c) Input vector components

End.

2. Create a feature vector with all 10×10 zoned windows; hence there are 9×9 features for a single isolated character of size $[30 \times 30]$, total 81 features from for a single image.

End

The zoning method was used to compute the percentage of black pixels in each zone. The character pattern marked with direction information was zoned into windows of equal size. It then proceeds to extract the number and lengths of line segments resulting in an input vector containing nine floating-point values.

3.2. Implementation of feature extraction algorithm

The labeled image of character “R” and its zoning is shown in figure1. After applying above feature extraction algorithm on preprocessed image, the features obtained are in the range of -1 to 1.

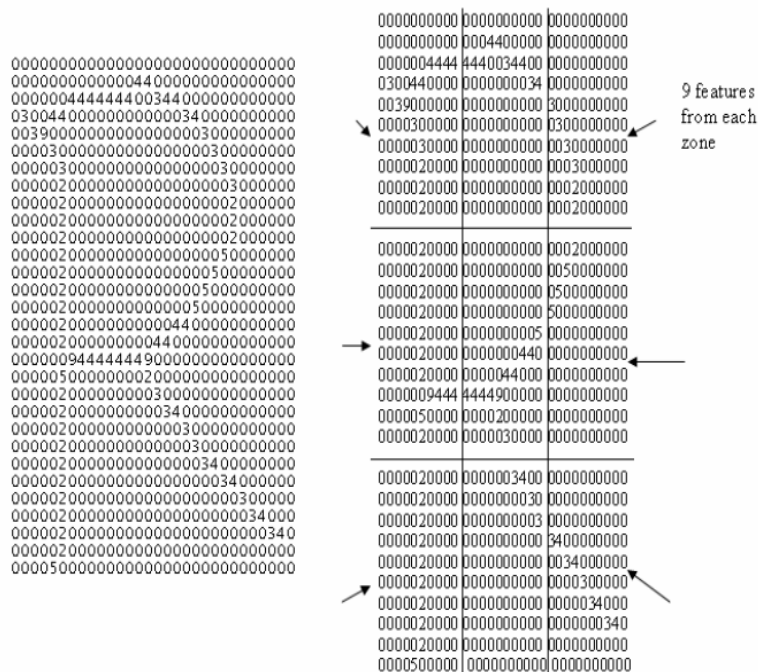


Figure 3: (a) Labeled image of character R, (b) Labeled image is zoned into 9 equal zones

After labeling and zoning 9 features extracted from each zone as described in above algorithm. Total 81 features extracted from these zones are:

-0.2000	0.3000	0.2000	0.2000	0.4000	0.1500	1.0000	0.0000	0.8000
-0.6000	0.4000	0.6000	0.1000	1.0000	0	1.0000	0	1.0000
1.0000	0	0.2000	0.2000	0.6000	0.1000	1.0000	0	1.0000
0.4000	0.1500	1.0000	0	-0.6000	0.4000	0.8000	0.0500	0.8000
-0.6000	0.4000	0.8000	0.0500	0.8000	0.0500	0.8000	0.0500	0.8000
1.0000	0	1.0000	0	0.8000	0.0500	0.4000	0.1500	1.0000
1.0000	0	1.0000	0	-0.8000	0.4500	0.8000	0.0500	1.0000
0.8000	0.0500	0.4000	0.1500	1.0000	0	1.0000	0	1.0000
0.2000	0.2000	0	0.2500	1.0000	0	1.0000	0	1.0000

Figure 4: These features are fed to the neural network for recognition purpose.

3.3. Recognition of Character

Character Recognition is done by using Kohonen’s LVQ Neural Network. Learning Vector Quantization is a pattern classification method in which, there are 81 input nodes representing the features from a single character (81 features). Each output unit represents a particular class or category. In case of Characters there will be total 26 output Nodes.

LVQ Algorithm

Terms used in the algorithm are listed and described here:

- X Training vectors
- T Correct class for the training vector
- w_j weight vector for j^{th} output unit
- $\|x-w_j\|$ Euclidean distance between input vector and (weight vector for) j^{th} output unit.

The LVQ Algorithm:

1. Start
2. Initialize reference vector, Initialize learning rate, $a(0)$.
3. While stopping condition is false, do step 4-8.
4. For each training vector x do steps 5-6.
5. Find J so that $\|x-w_j\|$ is minimum.
6. Update w_j as follows
 - If $T=C_j$, then
 - $W_j(\text{new}) = w_j(\text{old}) - \|x-w_j(\text{old})\|$
 - Else
 - $W_j(\text{new}) = w_j(\text{old}) + \|x-w_j(\text{old})\|$
7. Reduce learning rate.
8. Stop test condition.
9. End.

Implementation of LVQ

The system is trained by using LVQ algorithm, For testing, character features are taken which are not in training data set.

Initialization of weight matrix

The weight matrix of size $[81 \times 78]$ is initialized with some random values for characters. 81 are the number of features of input data. 78 are the number of hidden layer neurons. The weight matrix of hidden layer is of size $[26 \times 78]$. 26 are the number of classes and 78 are the number of hidden layer neuron. The weight vector of the hidden layer neurons are the prototypes, the number of which usually fixed before training begins. The selection of this hidden neuron parameter is made 78 by doing experiments.

Parameters set for Digit Data

Learning rate, $a(0) = 0.5$
 The Number of hidden neurons = 10

No of iterations (epochs) =100

Parameters set for Character Data

Learning rate, α =0.1

The Number of hidden neurons=78

No of iterations (epochs) =100

The training algorithm is stopped after reaching a pre-specified error limit or after reaching a specified number of iterations. The weight matrix obtained from the training algorithm is used for testing purpose. During test phase, the distance of input vector to each processing element of the hidden layer (Stabilized weight matrix) is computed and again the nearest element is declared as the winner, this outputs a particular class or category.

4. Experiments and Results.

In order to investigate the effect of various parameters settings on the Classification and Recognition rate experiments have done varying one parameter at a time.

1. The dimensions of feature vector.
2. The number of iterations of the training algorithm.
3. The learning rate.
4. The number of hidden neurons.

All these experiments were concluded with tests using best parameters.

4.1. Experimentson various for Digits (10 class)

Experiment 1(Dimension of features vectors)

The purpose of these experiments is to investigate the effect of the dimension of feature vector on the recognition rate. The number of iterations (epochs), learning rate and the number of hidden neurons are set to 100, 0.5 and 10 respectively.

Table 1: Alpha 0.5; Epochs 100; Hidden Neurons 10

Training Samples	Dimensions of features	Classification (%)
300	36	87.00
300	54	97.00
300	81	100

Experiment 2 (Number of Iterations of Training Algorithm)

The purpose of this experiment is to investigate the effect of iterations on the Classification rate. The number of features dimension, learning rate and the Hidden Neurons are set to 81, 0.5 and 10 respectively.

Table 2: Alpha 0.5; Epochs 100; Hidden Neurons 10

Training Samples	Number of iterations	Classification (%)
300	2	94.33
300	4	100
300	6	100
300	8	100
300	10	100
300	12	100

Experiment 3 (The Learning rate)

The purpose of this experiment is to investigate the effect of Learning Rate on the Classification rate. The number of features dimension, hidden neurons and the Epochs are set to 81, 10 and 100 respectively.

Table 3: Alpha 0.5; Epochs 100; Hidden Neurons 10

Training Samples	Learning Rate	Classification (%)
300	0.9	79.33
300	0.8	89.66
300	0.7	100
300	0.6	100
300	0.5	100
300	0.4	100
300	0.3	100
300	0.2	100
300	0.1	100

Experiment 4 (The Number of Hidden Neurons)

Table 5.4: Alpha 0.5; Epochs 100; Hidden Neurons 10

Training Samples	Hidden Neurons	Classification (%)
300	5	10
300	10	100
300	20	100

The Table 5 shows the overall result of the above system when tested for a large data set of digits (0-9)

Table 5: Alpha 0.5; Epochs 100; Hidden Neurons 10

Experiment Neuron for (26 Classes)	Training Samples	Testing Samples	Recognition	Time to Recognize	on Hidden parameter Characters
	300 (30 sample each)	200 (20 sample each)	99.5	1.25sec	

The purpose of this experiment is to investigate the effect of the hidden neurons on the Classification Rate. The number of iterations (epochs), learning rate and the number of Dimension are set to 100, 0.1 and 81 respectively.

The Table 6 shows the overall result of the above system when tested for a large data set of alphabets (characters A-Z)

Table 6: Alpha 0.1; Epochs 100; Hidden Neurons 78

Training Samples	Testing Samples	Recognition	Time to Recognize
13000 (500 sample each)	2600 (100 samples each)	96.84	19.54sec

5. Conclusion

Recognition rate is depends upon the parameters which we have tested in experiments and it is concluded that the parameters dimension of feature vector, No. of iterations, Learning rate and hidden neuron affects the recognition rate.

Hidden neuron is important parameter which needs to be set carefully. These parameters vary according to complexity of input-output relationship. Using this feature extraction technique with LVQ, there is no need to normalize data before passing the data to the LVQ neural network, since all the features are in a range of -1 to 1. By using novel approach of feature extraction technique with LVQ gives good recognition rate, and recognizes characters very rapidly.

References

- [1] Rafael C. Gonzalez, Richard E. Woods, "Digital Image Processing", Pearson Education.
- [2] Martin T. Hagan, Oklahoma State University, Howard B. Demuth, University of Idaho, Mark Beale, MHB, Inc. "Neural Network Design", Thomson Learning.
- [3] B. Yegnanarayana, "Artificial Neural Network", PHI publications
- [4] By-Laurene Fausett, "Fundamentals of Neural Networks"
- [5] M. Blumenstein, B. Verma and H. Basli, School of Information Technology, Griffith University-Gold Coast Campus, Australia, "A Novel Feature Extraction Technique for the Recognition of Segmented Handwritten Characters", 0-7695-1960-1/03, 2003 IEEE.
- [6] Gulzar A. Khuwaja, "Fingerprint identification with LVQ", Proceedings of the 9th International Conference on Neural Information Processing.
- [7] Neila Mezghani, Amar Mitiche, "On-line recognition of handwritten Arabic characters using A Kohonen neural network", Proceedings of the Eight International Workshop on Frontiers in Handwriting Recognition, 0-7695-1692-0/02, 2002-IEEE Network.
- [8] Akhtar Jameel and Cris Koutsougeras, "Experiments with Kohonen's Learning Vector Quantization in Handwritten Character Recognition Systems", Computer Science Department Xavier University New Orleans, Louisiana 70125, 1995 IEEE. 64
- [9] Brazilian Bank Check Handwritten Legal Amount Recognition CINTHIA OBLADEN DE ALMENDRA FREITAS, ABDENAIM EL YACOUBI, FLVIO BORTOLOZZI, ROBERT SABOURIN. PUCPR - Pontifícia Universidade Católica do Paraná, R: Imaculada Conceição, 1155, Prado Velho, 80215-901 Curitiba, PR, Brasil.
- [10] <http://www.mathworks.com>
- [11] <https://www.dacs.dtic.mil/techs/neural/neural7.php>

Li-Fi based Optical Attocells using OFDM & SM-MIMO Techniques for 5G VLC Wireless Communication Network

Vineeta Nishad^a, Megha Bhatt^a, Jigisha Sureja^b

^aGandinagar Institute of Technology, Gnadinagar, India

^bMarwadi Education Foundation's Group of Institutions, Rajkot-360003

Abstract

Demands on wireless data links, whether for high-speed internet access or high-quality audio/video streaming, has been growing exponentially and leading to radio frequency (RF) spectrum crisis. Moreover, RF equipments are prohibited in stringent environments like aircraft or hospitals. Ongoing research activities are focusing on alternative means and Optical Wireless Communication (OWC) has the potential to become a viable complement to RF signal transmission and a remedy for the shortage of the RF spectrum with the additional benefits of low energy consumption and high speed transmission. Significant improvements in solid state technology such as advent of high luminance white LED and micro-LED has further increased the interests in Visible Light Communications (VLC). This paper presents an overview of Light Fidelity (Li-Fi) technology and summarizes recent advancements in the OWC including a discussion of applications; physical layer implementation using OFDM and SM-MIMO techniques for enhanced data rates and key design challenges for VLC networks. This paper aims at demonstrating that Optical attocells are the next step in the progression towards ever smaller cells, a progression which is known to be the most significant contributor to the improvements in network spectral efficiencies in RF wireless networks and suggests that Li-Fi would be an integral element of 5G cellular standards.

Keywords: VLC, Li-Fi, OWC, white LED, micro LED, PD, optical attocell, OFDM, SM-MIMO

Nomenclature

ASE	Area spectral efficiency
DD	Direct detection
FOV	Field of view
IM	Intensity modulation
Li-Fi	Light Fidelity
OWC	Optical Wireless Communication
SM	Spacial Modulation
VLC	Visible Light Communications
η	Spectral efficiency
Rx	Rate of x technique in bits per channel use (bpcu)

Introduction

- With the advent of smart phones and rapid increase in wireless services and applications, the limited radio frequency (RF) spectrum is unable to cope with future data rate demands. Over 72 hours of video are uploaded to YouTube every minute and 25% of global YouTube views come from mobile devices [5]. The global Internet video traffic is growing at 48% compound annual growth rate (CAGR) [1]. As a consequence, the limited available RF spectrum is subject to an aggressive spatial reuse and co-channel interference has become a major capacity limiting factor. Despite of huge technological advancements and improvements in the standards in the last 10 years, the spectral efficiency of RF wireless networks has become saturated and the US Federal Communications Commission has therefore warned of a potential spectrum crisis. It is estimated that by 2017, more than 11 exabytes of data traffic will have to be transferred through mobile networks every month [2]. Most recently, VLC has been identified as a potential solution for mitigating the looming RF spectrum crisis.

- Li-Fi, is the future solution to the present spectrum crisis which aims to utilize a vast amount of unused visible light spectrum and provides the high-speed, bidirectional communication and networking variant of VLC (see Fig 1)[5,6]. OWC has gained significant attention as a result of technological breakthroughs in solid state lighting technology [7]. The momentous advantage of OWC is that it offers a very large bandwidth for each transmitting LED. Li-Fi works as a signal transmitter with the off-the-shelf white LEDs typically used for solid-state lighting and as a signal receiver with a PIN photodiode or avalanche photodiode. This means that Li-Fi systems can illuminate a room and at the same time provide wireless data connectivity.

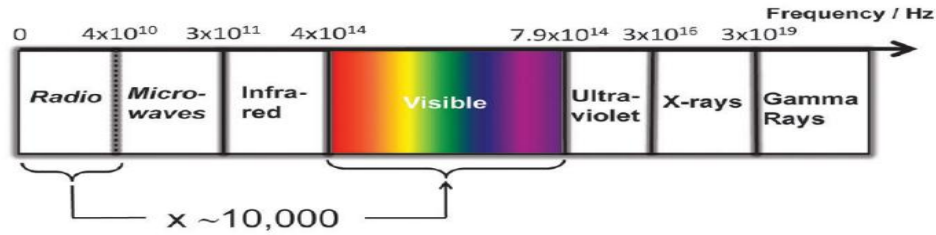


Fig 1. The electromagnetic spectrum and the vast potential of unused, unregulated, safe green spectrum in the visible light part. The visible light spectrum is 10,000 times larger than the entire radio frequency spectrum [3].

- Li-Fi Consortium has already begun promoting this technology with peculiar advantages of an optical wireless system as 1) vast amount of unused bandwidth, 2) no licensing fees, 3) low-cost front end devices, 4) no interference with sensitive electronic systems, 5) use of widely available existing lighting infrastructure, 6) light cannot pass through walls so possibility of eavesdropping is removed.

- The use of the visible light spectrum for high speed data communication is enabled by the emergence of the light emitting diode (LED) which at the same time is at the heart of the next wave of energy-efficient illumination. Due to the physical properties of these components, information can only be encoded in the intensity of the emitted light, while the actual phase and amplitude of the light wave cannot be modulated. This significantly differentiates VLC from RF communications. The Li-Fi concept combines the functions of illumination and communication, therefore offers the potential for tremendous cost savings and carbon footprint reductions. First, the deployment of VLC access points (APs) becomes straightforward as the existing lighting infrastructure can be reused, and there exist off-the-shelf technologies such as power-line communication (PLC) and power-over-Ethernet (PoE) as viable backhaul solutions for retrofit installations, and new installations respectively [8]. Second, because lighting is on most of the time in indoor environments even during day time, the energy used for communication would practically be zero as a result of the piggy-backing of data on illumination. However, if illumination is not required energy efficient intensity modulation (IM) techniques exist that would allow data communication even if the lights are visually off [9].

- The high peak-to-average ratio of the signal in orthogonal frequency division multiplexing (OFDM), typically a disadvantage in RF communications, can be turned into an advantage for Li-Fi [10]. The applicability of multi-carrier modulation techniques such as OFDM has now been proven widely on the link level, which is a single point-to-point transmission from one transmitter to one receiver, and data rates beyond 500Mbps have been reported from a single white LED using offline processing. [11] Indeed, real-time video streaming from a white LED has been demonstrated at data rates up to 130Mbps. [5] Communication networks typically have multiple links that can be point-to-multipoint as well as multipoint-to-point.

- Future networks are moving towards more heterogeneous architectures where multiple APs (e.g., macro-, pico-, femto-cells, relays and/or remote radio heads) are available in each cell [12]. This will lead to an even denser spatial reuse of resources. These heterogeneous networks (HetNets) provide enhanced coverage in standard cellular networks, and improve the capacity of the system.

- Section 2 introduces potential application areas of VLC technology. Optical attocells are the next step in the progression towards ever smaller cells, a progression which is known to be the most significant contributor to the improvements in network spectral efficiencies in RF wireless networks are described in section 3. Advancements of optical transmitter and receiver are discussed in section 4. The practical implementation of OWC system is presented in section 5. It explains the developments in optical transmitters and receivers including feasible modulation techniques, OFDM, MIMO and potential multiple access techniques for optical communications. Section 6 describes challenges and areas for future research. Conclusion is provided in section 7.

Applications

- The future evolution of mobile communications is expected in the Wireless Heterogeneous Networks where smaller cells called attocells can be used to offload and localize traffic. Indeed, the simple concept of cell-size reduction has increased the system spectral efficiency by a factor of 2700 over the last 50 years [13]. To this extent, even smaller VLC attocells are just a logical progression to provide the next 1000 times system capacity increase. VLC communication is best suited for high data rates and a secure interface between a base station (BS) and a mobile station (MS). Such a connection is not needed constantly. A lot of the time, a mobile device is simply dormant, waiting for an incoming data transmission or for the user to request one. For these tasks to be negotiated successfully, a constant connection is

required. Such a connection can be provided by the existing, well-established, RF connectivity. The heavy load of the high-speed data transfer can then be allocated to the VLC network. If a VLC connection is not possible, the MS may be served with RF until an appropriate optical AP is nearby [14]. Principally, Li-Fi requires adapting only the front-ends and physical layers of typical femto- or pico-cells, while the above-lying protocols, authentication, channels, etc., can remain (fundamentally) unchanged. Moreover, a huge amount of unregulated bandwidth is available at infra-red and visible light frequencies. Likewise, optical wireless signals can be confined within a room which inherently addresses concerns over the eavesdropping of data. VLC could also enable indoor as well as improve city canyon navigation where Global Positioning System (GPS) signal is weak/non-existent. Due to the simplicity of its front-end hardware, it can play a significant role in enabling the Internet of things and machine-to-machine communication in general. Car-to-car communication [16] could be one of the first implementation scenarios as manufacturers are beginning to make a move towards solid-state lighting solutions. Other possible areas that stand to benefit from the practical implementation of VLC include museums, hospitals, and underwater communications [17, 18]. Museums could exploit the already present light fixtures to not only illuminate their exposition pieces, but also to continuously transmit information about them. This could redefine the way automated tours are executed. Aircrafts and hospitals could achieve ubiquitous networking without any detriment to equipment that is sensitive to RF radiation. This should improve hospital care and reduce staff workload. Underwater communications stand likely to benefit most where RF and sound communication are unable to provide fast wireless connectivity under water.

Optical Attocells

If we equip a room with multiple light fixtures that each function as a very small radio base station, the result is a network of very small cells that we call ‘optical attocells.’ They are analogous to femtocells in RF communications. Small cells have been the major contributors to the improvements of three orders of magnitude reported in spectral efficiency gains in wireless communications during the past 50 years. LiFi systems are the glue between future energy efficient illumination and cellular communications; harness unregulated, unused and vast amount of electromagnetic spectrum and enable ever smaller cells without the need for new infrastructure (see Fig 2).

The most common link configurations are classified according to the existence of a line of sight (LOS) between the transmitter and the receiver as well as the degree of directionality, that is, source beam-angle and detector FOV (Fig 3). Along with the FOV, the appropriate placing of the transmitters inside the room decides the illumination and required SNR for the data transmission (Fig 4,5)

The key to a high performing system is not merely to increase the link-level spectral efficiency. In fact, the most relevant aspect to a mobile vendor is the area spectral efficiency (ASE), i.e., what mobile data rates can be offered for each user. In this context, Li-Fi is shown to provide at least an order of magnitude improvement in the ASE. The authors in [20] compared the attained ASE with that of a network of optical attocells where the light fixtures served two purposes: optical access points and illumination units ensuring a minimum of 400lx (as required for reading). The indoor cells were surrounded by a macro cellular network that assumed use of the long-term evolution (LTE) standard also common in mobile phones. The femtocells used the same RF frequency spectrum as the macrocell base station, and so the femtocell network suffered from macrocell interference (see Fig 2).

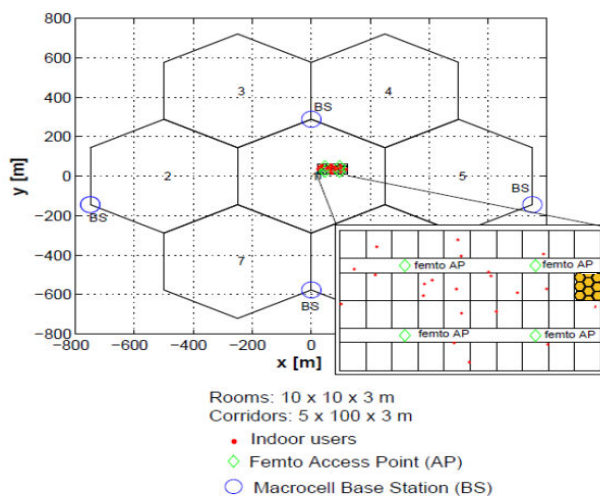


Fig 2 Combined Cell structure of RF and VLC

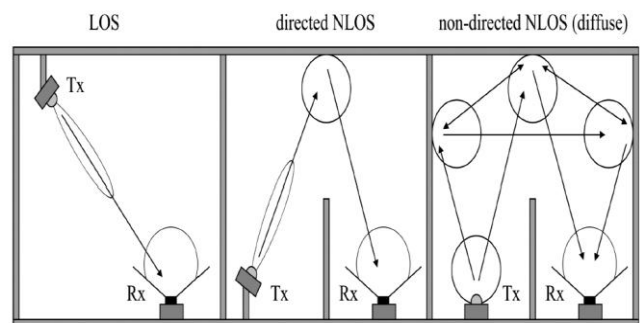


Fig 3 The most common link configurations

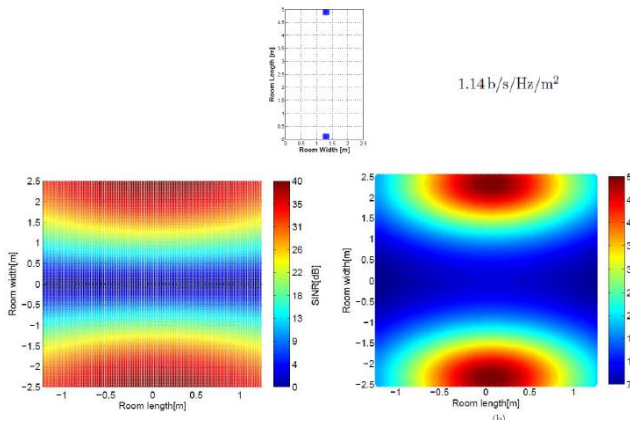


Fig 4 SNR and Illumination diagrams(FOV 85° without light intensity constraints)

As suggested by [3] the ASE gain of the attocell network is higher for smaller rooms. This is because the femtocell network suffers from additional wall losses, whereas the attocell network benefits from complete interference protection by walls, which do not allow light to propagate through them. The gains diminish as the number of femtocells per floor increases, but the gain is still about 12 (i.e., the area spectral efficiency of the optical attocells network is 12 times that of the RF femtocell network) for the largest room and 20 femtocells per floor (Fig 6). The maximum gain in ASE is about 920 for 4 femtocells per floor, which suggests that using optical attocells could achieve another three orders of magnitude improvement in spectral efficiency.

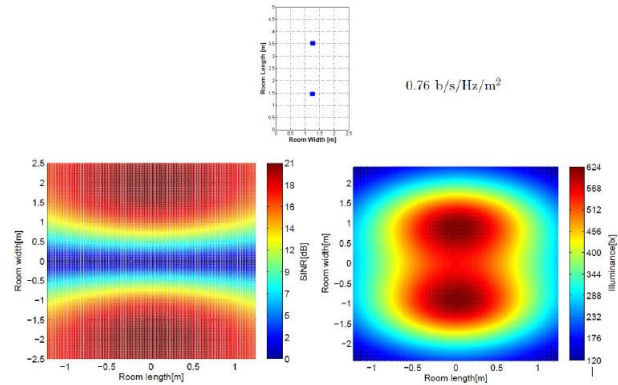


Fig 5 SNR and Illumination diagrams(FOV 85° with light intensity constraints of 400lx for 50% room area and 100lx for rest of the room)

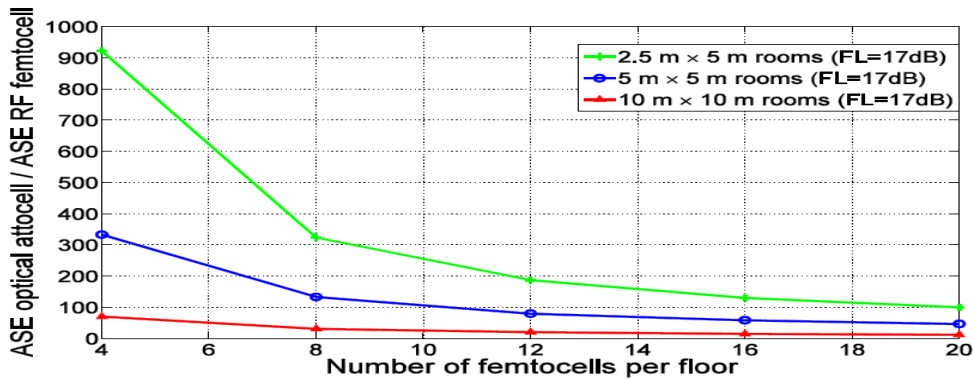


Fig 6 ASE optical attocell/ ASE RF femtocell [3]

Optical Transmitter and Receiver

With the developments in white LED (WLED) technology for solid state lighting and onset of high luminance light-emitting diodes (LEDs), low cost efficient-illumination devices are available which will eventually replace existing light bulbs and fluorescent lamps. LEDs, being electronic devices, can be switched much faster. Therefore, LEDs can not only be used for illumination, but also for high-speed wireless data communications. For instance, the ceiling lights in an office can be used to transmit data to a receiver placed on a desk within a room. Typical light fixtures achieve more than 400 lux to provide sufficient indoor illumination. Those illumination levels are enough to transmit data at high SNRs. At the receiver side, information is decoded by a photo-detector (PD) which converts the optical signals into electrical signals. This direct detection enables the implementation of simple low-cost transceiver devices without the need for complex high-frequency circuit designs. Even if LEDs that radiate in the visible light spectrum are used, the fluctuations in optical power are imperceptible to human eye but can be easily detected by a PD. As such, the LEDs can be used simultaneously for both lighting and data transmission. The information can only be received and decoded by a PD which is within the emitted light beam. The light signals do not penetrate opaque boundaries like walls, the propagation can be restricted to specific spots or areas (rooms). This scheme prevents interception and creates less interference compared to RF devices whose signals propagate through walls. Moreover, the LOS characteristic between transmitter and receiver can provide high SNRs of more than 60 dB at the receiver [22]. Generally, WLEDs used are classified into two types, trichromatic and blue-chip LEDs. Trichromatic LEDs are investigated and simulation results for data rates up to 400 Mb/s are reported [22]. The maximum measured data rate for a VLC system using bluechip LEDs is reported in [22], where a modified version of the classical orthogonal frequency division multiplexing (OFDM) modulation technique is considered to achieve data rates higher than

500 Mb/s.

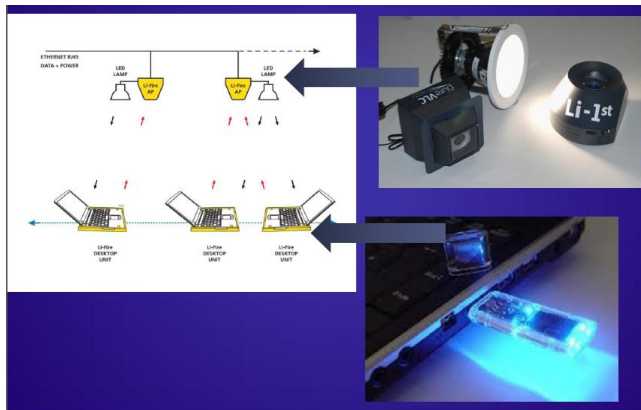


Fig 7 Prototypes of Optical transmitter and receiver [21]

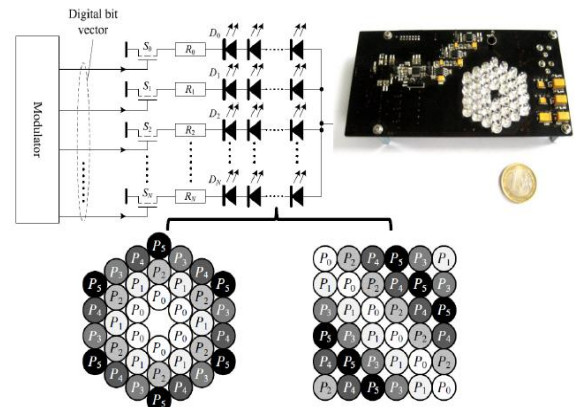


Fig 8 New transmitter concept exploiting LED Array Structures.

Recent researches show two new LEDs- the resonant-cavity light emitting diodes and μ LEDs. Micro-LED or micron-sized LEDs are merely $1\mu\text{m}^2$ (square micrometers) in size. This means that 1,000 more lights could be fit into the same space as a typical LED. Moreover, micro-LEDs can flicker 1,000 times faster than commercial LED. Thus, in theory, a bank of 1,000 micro-LEDs flashing 1,000 times faster could transmit data a million times faster than that of an average LED. Devices, having resonant-cavity LEDs and micro-LEDs have been manufactured that are capable of supporting communication links of up to 3 Gb/s and 512 Mb/s, respectively[22]. Recently, data rates in excess of 1 Gbps has been reported using off-the-shelf phosphor-coated white LEDs [23], and 3.4 Gbps has been demonstrated with an off-the-shelf red-green-blue (RGB) LED [24]. Apart from the visible light spectrum, the near-IR band between about 780 nm and 950 nm is also a potential transmission medium for indoor communications [22]. Although the overall bandwidth in the visible or infrared spectrum is in the terahertz (THz) range, the bandwidth of the signal that can be utilized by an optical IM/DD system using LEDs is inherently limited by the bandwidths of transmitter and receiver frontends. In order to serve multiple users and have ubiquitous system coverage, it becomes necessary to reuse the available bandwidth. In addition, LEDs are highly non-linear due to their optical-power-versus-current characteristic. This non-linearity largely restricts the dynamic range and the transmission power of common optical transmitters as well as the overall system performance. Moreover, the non-linearity of LEDs requires complex pre-distortion and intricate equalization techniques [25-30]. A novel transmitter is proposed which employs discrete power level stepping. The transmitter consists of several on-off-switchable emitter groups. These groups are individually controlled and emit fixed specific optical intensities in parallel. As optical intensities constructively add up, the total emitted intensity is generated by the sum of the emitted intensities of all activated emitter groups. Therefore, the proposed transmitter solution can generate several discrete optical intensity levels which can be used for optical wireless signal transmission. The transmitter design allows the utilization of the full dynamic range of LEDs or laser diodes by avoiding non-linearity issues. Moreover, costs and complexity of the optical front-end are significantly reduced as neither a digital-to-analog converter (DAC) nor high-speed current controllers are required.

Implementation Techniques of OWCSystems

A basic OW system consists of a light source, free space as the propagation medium, and a light detector(fig 9). Information, in the form of digital or analog signals, is input to electronic circuitry that modulates the light source. The source output passes through an optical system (to control the emitted radiation, e.g., to ensure that the transmitter is eye safe) into the free space. The received signal comes through an optical system (e.g., an optical filter that rejects optical noise, a lens system or concentrator that focuses light on the detector), passes along the detector, and the resulting photocurrent is amplified before the signal processing electronics. For most indoor applications, LEDs are the favoured light sources due to the relaxed safety regulations, low cost, and high reliability compared to LDs. PIN PDs are commonly used due to their lower cost, tolerance to wide temperature fluctuations, and operation with an inexpensive low-bias voltage compared to avalanche photodiodes (APDs). Simple and low-cost optical carrier modulation and demodulation are usually achieved through intensity modulation with direct detection (IM/DD). The desired waveform is modulated onto the instantaneous power of the optical carrier, and the detector generates a current proportional to the received instantaneous power; that is, only the intensity of the optical wave is detected, and there is no frequency or phase information. The diagram of an OWC system is presented in Fig. 10. The incoming bits are divided into data chunks and mapped to symbols using quadrature amplitude modulation (M-QAM) or M-PAM. The MQAM/M-PAM symbols are modulated onto different frequency subcarriers according to one of the following schemes: DCO-OFDM, ACO-OFDM, PAM-DMT, U-OFDM.

Then, the resulting time domain signal is subjected to a number

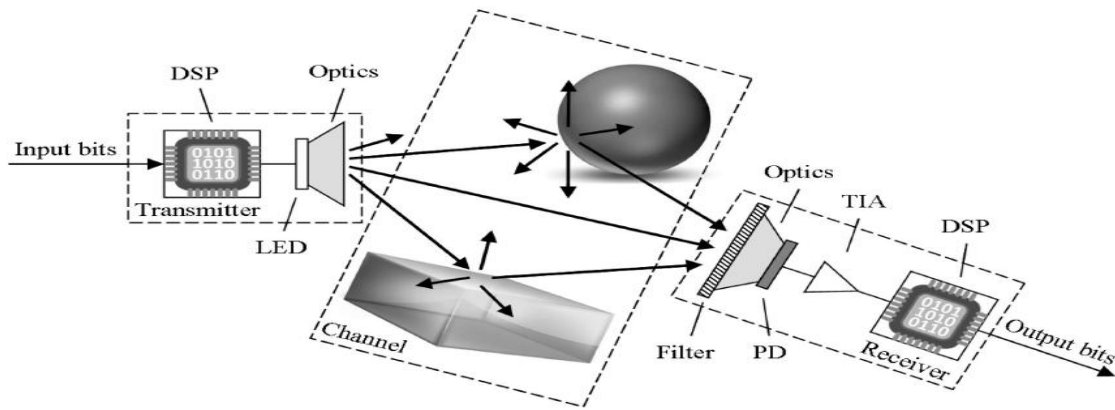


Fig 9 Link level communication system

of pre-distortion techniques, which makes it suitable for transmission. This block includes oversampling, pulse shaping as well as clipping any values below the allowed minimum or above the allowed maximum. Clipping is performed because a digital-to-analog converter (DAC), an amplifier, and an LED can only operate in a limited range, specified by their electrical properties. The conditioned signal is fed to a DAC which outputs an analog signal. This stage of the system consists of a zero-order-hold element or other type of interpolator followed by a low pass filter. The output signal from the zero-order hold is continuous in time. However, because the signal has discrete amplitude levels, corresponding to the samples of the oversampled pulse-shaped and clipped signal $s'[t]$, it is analyzed in terms of the discrete time-domain signal $s'[t]$. The analog output of the DAC is encoded into a current signal by a voltage-to-current transducer with appropriate bias and supplied to the LED. OFDM-based OWC with incoherent off-the-shelf illumination devices can only be realized as a baseband communication technique. Therefore, frequency up-conversion is not required. Light intensity at the LED varies with the current. At the receiver side, a PD transforms the variations in the intensity of the received light into variations of a current signal, which is turned into a voltage signal by a trans-impedance-amplifier (TIA). The resulting signal is discretized at an ADC and passed on to the processing circuitry, which includes a matched filter, an OFDM demodulator with an equalizer, as well as a bit demodulator.

OFDM is a bandwidth efficient transmission technique which can cope with frequency-selective Fading. In contrast to pulsed modulation techniques, OFDM provides high data rates even in severe multipath scenarios. In order to mitigate multipath effects and to avoid ISI, OFDM uses a guard interval, the so-called cyclic prefix, which is placed between the transmitted OFDM symbols. Moreover, the actual OFDM symbol duration is typically much longer than the delay spread caused by multipath propagation. OFDM conveys digital data on multiple orthogonal sub-carrier frequencies. Hence, a wideband channel is subdivided into several narrowband sub-channels. These orthogonal sub-carrier channels are used to transmit independent data streams in parallel in the frequency domain. The frequency division multiplexed channels are summed up and transformed into the time domain by using an inverse fast Fourier transformation (IFFT). The utilization of narrowband sub-channels enables a low-complex channel equalization: each sub-channel can be regarded as a non-frequency-selective channel which is individually equalized in the frequency domain using a single-tap zero forcing (ZF) equalizer. These properties make OFDM an ideal candidate for diffuse and scattered OWC transmission scenarios.

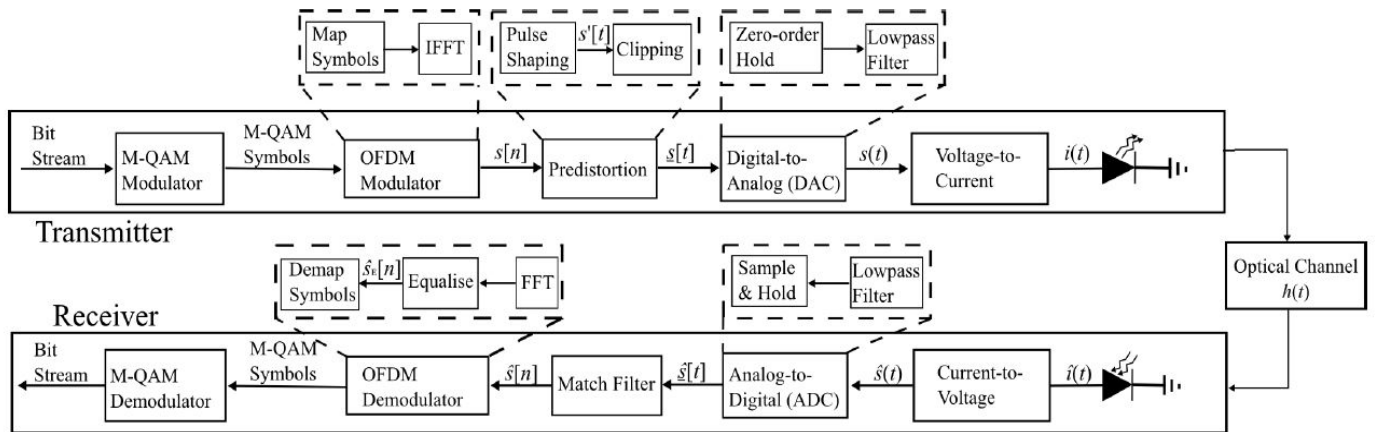


Fig 10 The complete block diagram of OWC System

Moreover, due to the use of fast Fourier transformation (FFT) and IFFT, OFDM enables simple and efficient signal processing implementations. For instance, compared to -PAM, OFDM requires approximately three times less computational complexity [31]. The optical wireless channel is a linear time-invariant channel, where the channel output can be obtained by a linear convolution of the impulse response of the channel and the transmitted signal. In general, in OWC systems, the ambient light produces high-intensity shot noise at the receiver. In addition, thermal noise arises due to the electronic pre-amplifier in the receiver front-end. Both of these noise sources can be accurately modelled as additive white Gaussian noise (AWGN) which is independent from the transmitted signal [32].

5.1 Modulation Techniques

Practical candidates for data modulation are the single-carrier pulse modulation schemes such as multilevel pulse position modulation (M-PPM) and multilevel pulse amplitude modulation (M-PAM). However, the time dispersion of the optical wireless channel is a major data rate limiting factor for these modulation schemes because of the severe inter-symbol interference (ISI). Multicarrier modulation has inherent robustness to ISI, because the symbol duration is significantly longer than the root-mean-square (RMS) delay spread of the optical wireless channel. As a result, Optical-OFDM(O-OFDM) with multilevel quadrature amplitude modulation (M-QAM) promises to deliver very high data rates. In O-OFDM, the time domain signal envelope is utilized to modulate the intensity of the LED. For this purpose, the signal needs to be real and non-negative. A real-valued signal is obtained when Hermitian symmetry is imposed on the OFDM subcarriers by cancellation of the imaginary components of the IFFT output. This real-valued signal can be sent by incoherent light sources. However, the time domain signal is still bipolar. In order to provide unipolar signals which can modulate the intensity of the optical carrier, further processing is required. To this end, the multi-carrier techniques direct-current-biased optical OFDM (DCO-OFDM), asymmetrically clipped optical OFDM (ACO-OFDM), pulse-amplitude-modulated discrete multitone modulation (PAM-DMT) and unipolar orthogonal frequency division multiplexing (U-OFDM) have been presented [AF].

- DCO-OFDM adds a DC offset to the waveform to be sent in order to provide non-negative time domain signals. The DC offset can be added by adjusting the bias point of the transmitter LED. The DC bias has to be chosen appropriately to provide non-negativity of the time domain signals, while keeping upper and lower clipping effects to a minimum. The spectral efficiency of the scheme is:

$$\eta_{DCO} = \frac{\log_2(M)(N_{FFT} - 2)}{2(N_{FFT} + N_{CP})} \text{ bits/s/Hz} \quad (1)$$

- In ACO-OFDM transmission, only the odd-numbered sub-carriers are modulated, whereas the even-numbered sub-carriers are set to zero by applying hard-clipping to the entire negative signal amplitudes without affecting the data conveyed in the OFDM signal. The spectral efficiency of scheme is:

$$\eta_{ACO} = \frac{\log_2(M)N_{FFT}}{4(N_{FFT} + N_{CP})} \text{ bits/s/Hz} \quad (2)$$

- In contrast to DCO-OFDM and ACO-OFDM which employ complex-valued QAM symbols, PAM-DMT uses real-valued PAM symbols to modulate the sub-carriers. The spectral efficiency of the scheme is:

$$\eta_{PAM-DMT} = \frac{\log_2(M)(N_{FFT}-2)}{2(N_{FFT}+N_{CP})} \text{bits/s/Hz} \quad (3)$$

- In U-OFDM, all possible subcarriers in the frequency domain are modulated as in DCO-OFDM. After the time-domain signal is obtained, it is divided into two blocks: a positive and a negative one. The positive block is a copy of the original signal frame, where all negative samples are set to zero. The negative block is a copy of the original signal frame, where all samples are multiplied by -1 to switch signs. After this operation, the negative samples are set to zero. The spectral efficiency of the scheme is:

$$\eta_U = \frac{\log_2(M)(N_{FFT}-2)}{4(N_{FFT}+N_{CP})} \text{bits/s/Hz} \quad (4)$$

The findings [33] suggest that as only the odd-numbered sub-carriers convey data symbols, ACO-OFDM provides half the spectral efficiency of DCO-OFDM. The latter three schemes are equally valid approaches with respect to spectrum efficiency and energy efficiency. A brief analysis demonstrates that the optimal choice of a modulation scheme depends on the operating conditions and can change with variations in the system parameters. Multiple access techniques allow several users to get access simultaneously to the available network services. Single cell topology using a single optical access point (OAP) per-user; or per-room; and a cellular topology with spatial reuse using multiple OAPs are three probable topologies for indoor coverage.

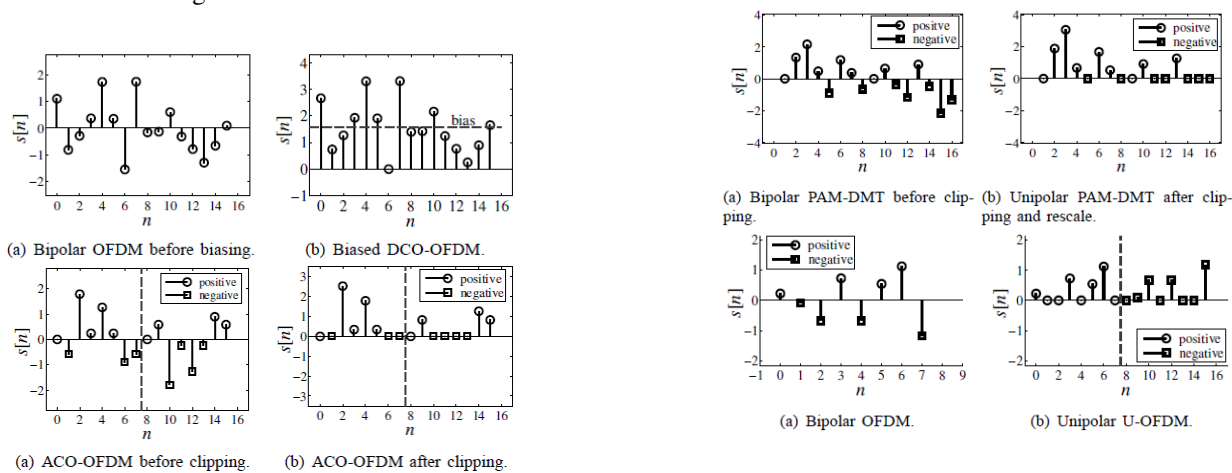


Fig 11 Generation of DCO-OFDM, ACO-OFDM, PAM-DMT and U-OFDM

There are two possible strategies to realize multiple access schemes in a single cell per room or cellular topology namely electrical multiplexing and optical multiplexing. Electrical multiplexing techniques include time-division multiple access (TDMA), frequency-division multiple access (FDMA), or code-division multiple access (CDMA). Optical multiplexing techniques include wavelength-division multiple access (WDMA) and space-division multiple access (SDMA). TDMA is a synchronous technique where users are allocated non overlapping time slots to different users based on the requested data rates and QoS, so users cannot communicate independently and simultaneously. TDMA provides high power efficiency, which is the most important metric for OW systems, while reducing the transmission capacity per user [34]. FDMA transmission allows multiple users to transmit simultaneously using different frequencies within a single cell per room topology. In a cellular system, the bandwidth is divided into non overlapping frequency bands, and each OAP is allocated a different band. In orthogonal frequency-division multiple access (OFDMA), users are allocated time/frequency slots (chunks) spanning several OFDM symbols and subcarriers. In general, power efficiency is the main drawback of FDMA and worsens as the number of subcarriers increases. For optical CDMA systems, the commonly used techniques rely on direct sequence spreading where users can access the same channel using optical orthogonal codes (OOCs). This means flexibility of adding users and asynchronous access capability. Users are able to transmit at overlapping times and wavelengths; therefore, it is also possible to implement hybrid optical systems such as WDMA/CDMA or TDMA/CDMA. In WDMA, for example, a number of users transmit simultaneously using different wavelengths. Each user has an independent wavelength together with an optical tunable reception filter. In general, such a complex structure is expensive and not desirable. The short wavelength of the optical signal makes it possible to achieve high angular resolution; therefore, SDMA uses angle-diversity receivers (ADRs) to discriminate signals and reduce co-channel interference (CCI) between channels in the same cell [35]. The potential disadvantage of this technique is increased complexity. The ability to serve multiple users is crucial for any communication system. Both time division multiple access (TDMA) and code division multiple access (CDMA) are viable alternatives in addressing the multiple access limitation of Li-Fi. Indeed, TDMA was utilized within the OMEGA project for

the optical wireless medium access control (MAC) [36]. To this extent, the underlying modulation scheme is irrelevant for enabling multiple access in an optical wireless system. However, since OFDM is widely considered as the most viable modulation technique for VLC, orthogonal frequency division multiple access (OFDMA) is the natural extension to provide multiple access. OFDMA can be employed in VLC in a similar manner to RF communications, where each user is allocated a portion of the total available subcarriers in each time slot. Furthermore, subcarrier allocations may be varied over time, such that users’ potentially varying traffic requirements and channel conditions can be accommodated [7].

5.2 Optical MIMO

In order to provide sufficient illumination, light installations are typically equipped with multiple LEDs. This property can readily be exploited to create optical MIMO communication systems. MIMO techniques are well-established and widely implemented in many RF systems as they offer high data rates by increasing the spectral efficiency. Both the WiMAX and LTE-A physical-layer standards heavily rely on MIMO technology for realizing their achievable throughput. In paper [37] N_t and N_r are denoted as the number of transmit antennas (TAs) and receive antennas (RAs), respectively. The cardinality of the signal constellation diagram is denoted by M . Either PSK or QAM are considered. In general, N_t , N_r , and M can be chosen independently of each other. In Fig. 12, the SM–MIMO concept is illustrated for $N_t = M = 2$, and it is compared to the conventional SMX scheme and the OSTBC scheme (Alamouti) designed for transmit diversity.

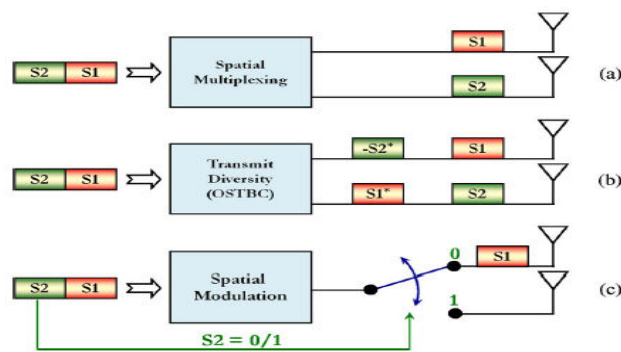


Fig. 12. Illustration of three MIMO concepts: (a) spatial multiplexing; (b) transmit diversity; and (c) SM.

In SMX–MIMO, two PSK/QAM symbols (S_1 and S_2) are simultaneously transmitted from a pair TAs in a single channel use. For arbitrary N_t and M , the rate of SMX in bits per channel use (bpcu) i.e. $R_{SMX} = N_t \log_2 M$ bpcu. In OSTBC–MIMO, two PSK/QAM symbols (S_1 and S_2) are first encoded and then simultaneously transmitted from a pair of TAs in two channel uses. For arbitrary N_t and M , the rate of OSTBC is $R_{OSTBC} = R_c \log_2 M$ bpcu where $R_c = N_M/N_{cu} \leq 1$ is the rate of the space-time block code and N_M is the number of information symbols transmitted in N_{cu} channel uses the Alamouti code is chosen, then we have $R_c = 1$. In SM–MIMO, only one (S_1) out of the two symbols is explicitly transmitted, while the other symbol (S_2) is implicitly transmitted by determining the index of the active TA in each channel use. In other words, in SM–MIMO, the information symbols are modulated onto two information-carrying units: a) one PSK/QAM symbol; and b) a single active TA via an information-driven antenna-switching mechanism. For arbitrary N_t and M , the rate of SM is $R_{SM} = \log_2(M) + \log_2(N_t)$ bpcu. In Figs. 13 and 14, the encoding mechanism of SM–MIMO is illustrated for $N_t = M = 4$ by considering two generic channel uses, where the concept of “SM or spatial constellation diagram” is also introduced. The rate of this MIMO setup is: $R_{SM} = \log_2(M) + \log_2(N_t)$ bpcu = 4 bpcu hence the encoder processes the information bits in blocks of four bits each. In the first channel use shown in Fig. 15, the block of bits to be encoded is “1100.” The first $\log_2(N_t) = 2$ bits, “11,” determine the single active TA (TX_3), while the second $\log_2(M) = 2$ bits, “00,” determine the transmitted PSK/QAM symbol. Likewise, in the second channel use shown in Fig. 16, the block of bits to be encoded is “0001.” The first $\log_2(N_t) = 2$ bits, “00,” determine the single active TA (TX_0), while the second $\log_2(M) = 2$ bits, “01,” determine the transmitted PSK/QAM symbol. The activated TA may change every channel use according to the input information bits. Thus, TA switching is an effective way of mapping the information bits to TA indices and of increasing the transmission rate. The information bits are modulated onto a 3-D constellation diagram, which generalizes the known 2-D (complex) signal-constellation diagram of PSK/QAM modulation schemes. The third dimension is provided by the antenna array, where some of the bits are mapped to the TAs. In SM–MIMO research, this third dimension is termed the “spatial-constellation diagram” [37]. Major advantages of SM-MIMO are higher throughput, simpler transmitter/receiver design, lower transmit power supply, better efficiency of power amplifiers, fast antenna switching, spectral efficiency suboptimality, time-limited pulse shaping and directional beamforming.

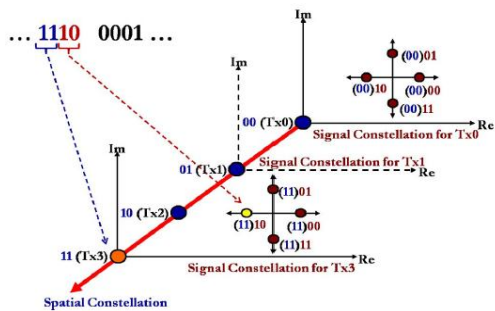


Fig. 13. Illustration of the 3-D encoding of SM (first channel use).

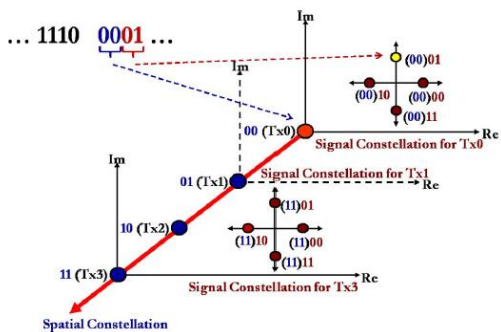


Fig. 14. Illustration of the 3-D encoding of SM (second channel use).

Challenges

Currently, the question of combating non-linearity in OWC systems is one of the biggest challenges for VLC systems. The key design challenges affecting high-speed OW transmission indoors stem from the free space loss (FSL), ambient light noise, and/or interference, and multipath dispersion causing intersymbol interference (ISI). The induced signal degradation is greatly influenced by the link configuration. There are two important aspects to consider with small cells, the first being coordination with the macro-network and to enable seamless interoperation between optical attocells and RF femtocells/macrocells to ensure maximum spectrum relief for the RF systems., while the second aspect is the integration of Wi-Fi capabilities with 3rd Generation Partnership Project (3GPP) technologies for smart phone utilities. If VLC is to become widespread, a number of challenges pertaining to its commercialization must be addressed. In particular, the drive toward an industry standard, possible market penetration and applications must be considered. However, these applications must offer a sufficient incentive for potential companies and the standard must look ahead of the current technology. Some consideration has already been given to VLC standardization. Most notably, the IEEE 802.15.7 standard has been established in 2009 for short range optical wireless communications using visible light where the physical (PHY), MAC and logical link control (LLC) layers are specified with very high associated LED bandwidths. Visible Light Communication Consortium (VLCC), Infrared Communication Systems Association (ICSA) and Infrared Data Association (IrDA) are contributing significantly towards development and standardization of VLC.

Conclusion

In this paper, VLC has been introduced as a unique and viable alternative to RF indoor communication strategies, and furthermore presented a plethora of application scenarios for future systems. The significant improvements of indoor data coverage can be expected from an optical attocell network which can perfectly complement RF systems as there is no interference between the systems. OWC technology and researches have been explored and the design challenges that still need to be overcome before being able to realize an entire OW system that can be commercially deployed are studied. Visible light communication (VLC) has been identified as well equipped to provide additional bandwidth and system capacity, without aggregating the interference in the mobile network. Furthermore, energy efficient indoor lighting and the large amount of indoor traffic can be inherently combined. MIMO communications constitute promising techniques for the design of future wireless communications systems, including the 5G cellular networks.

References

- Cisco, Cisco visual networking index: Global mobile data traffic forecast update, 2010–2015, Feb. 1, 2011. [Online]. Available:
http://newsroom.cisco.com/ekits/Cisco_VNI_Global_Mobile_Data_Traffic_Forecast_2010_2015.pdf.
- Cisco, Cisco visual networking index: Global mobile data traffic forecast update, 2012–2017, Feb. 6, 2013. [Online]. Available: http://www.cisco.com/en/US/solutions/collateral/ns341/ns525/ns537/ns705/ns827/white_paper_c11-520862.pdf.
- Haas, H., "High-speed wireless networking using visible light." Retrieved from <https://spie.org/x93593.xml> (2013).
http://www.youtube.com/t/press_statistics
- TED Talk online by Harald Haas on wireless data from every light bulb. <http://bit.ly/tedvlc>
- T. Komine and M. Nakagawa, "Fundamental analysis for visible-light communication system using LED lights", IEEE Trans. Consumer Electron. 50 (1), pp. 100–107, February 2004.
- H. Elgala, R. Mesleh, and H. Haas, "Indoor Optical Wireless Communication: Potential and State-of-the-Art," IEEE Commun. Mag., vol. 49, no. 9, pp. 56–62, Sep. 2011, ISSN: 0163-6804.
- J "Light Fidelity (Li-Fi): Towards All-Optical Networking", D. Tsonev, S. Videv and H. Haas; Institute for Digital Communications, Li-Fi R&D Centre, The University of Edinburgh, EH9 3JL, Edinburgh, UK.
- Tsonev, D., Sinanović, S., and Haas, H., "Novel Unipolar Orthogonal Frequency Division Multiplexing (U-OFDM) for Optical Wireless," in [Proc. of the Vehicular Technology Conference (VTC Spring)], IEEE, IEEE, Yokohama, Japan (May 6–9 2012).
- M. Afgani, H. Haas, H. Elgala, and D. Knipp, Visible light communication using OFDM, Proc. 2nd Int'l Conf. Testbeds Res. Infrastruct. Dev. Networks Communities, pp. 129–134, Barcelona, Spain, March 2006.
- J. Vucic, C. Kottke, S. Nerreter, K. D. Langer, and J. W. Walewski, 513 Mbit/s visible light communications link based on DMT modulation of a white LED, J. Lightwave Technol. 28 (24), pp. 3512–3518, December 2010.
- D. Lopez-Perez, I. Guvenc, G. de la Roche, M. Kountouris, T. Quek, and J. Zhang, "Enhanced intercell interference coordination challenges in heterogeneous networks," IEEE Wireless Communications, vol. 18, no. 3, pp. 22 –30, Jun. 2011.
- W. Webb, Wireless Communications: The Future. John Wiley & Sons, 2007.

- Harald Burchardt, Nikola Serafimovski, Dobroslav Tsonev, Stefan Videv, and Harald Haas, VLC: Beyond Point-to-Point Communication, draft Nov, 2013
- 3GPP, "X2 General Aspects and Principles (Release 8)," 3GPP TS 36.420 V8.0.0 (2007-12), Dec. 2007. Retrieved Sep. 1, 2009 from www.3gpp.org/ftp/Specs/
- N. Kumar, D. Terra, N. Lourenco, L. Alves, and R. L. Aguiar, "Visible light communication for intelligent transportation in road safety applications," in Wireless Communications and Mobile Computing Conference (IWCMC), 2011 7th International, 2011, pp. 1513–1518.
- "Visible Light Communication (VLC) - A Potential Solution to the Global Wireless Spectrum Shortage," GBI Research, Tech. Rep., 2011. [Online]. Available: <http://www.gbiresearch.com/>
- Markets and Markets, "Visible Light Communication (VLC)/Li-Fi Technology & Free Space Optics (FSO) Market (2013–2018)," Markets and Markets, Tech. Rep., Jan. 2013
- Harald Haas, My Li-Fi Revolution Tam Dalyell Prize Lecture
- I. Stefan, H. Burchardt, and H. Haas, "Area Spectral Efficiency Performance Comparison between VLC and RF Femtocell Networks," in Proc. of International Conference on Communications (ICC), Budapest, Hungary, Jun. 2013, pp. 1–5.
- pureVLC, "pureVLC Li-1st." video. <http://purevlc.co.uk/li-fire/purevlc-li-1st/>.
- Fath, T.; Haas, H., "Performance Comparison of MIMO Techniques for Optical Wireless Communications in Indoor Environments," IEEE Transactions on Communications, vol.61, no.2, pp.733,742, February 2013, doi: 10.1109/TCOMM.2012.120512.110578 (among the top 10 downloads in April 2013)
- Khalid, A. M., Cossu, G., Corsini, R., Choudhury, P., and Ciaramella, E., "1-Gb/s Transmission Over a Phosphorescent White LED by Using Rate-Adaptive Discrete Multitone Modulation," IEEE Photonics Journal 4, 1465–1473 (Oct. 2012).
- Cossu, G., Khalid, A. M., Choudhury, P., Corsini, R., and Ciaramella, E., "3.4 Gbit/s Visible Optical Wireless Transmission Based on RGB LED," Optics Express 20, B501–B506 (2012).
- B. Inan, S.C. J. Lee, S. Randel, I. Neokosmidis, A.M. J. Koonen, and J. W. Walewski, "Impact of LED nonlinearity on discrete multitone modulation," IEEE/OSA J. Opt. Commun. Netw., vol. 1, no. 5, pp. 439–451,
- I. Neokosmidis, T. Kamalakis, J. W. Walewski, B. Inan, and T. Spicopoulos, "Impact of nonlinear LED transfer function on discrete multitone modulation: Analytical approach," J. Lightw. Technol., vol. 27, no. 22, pp. 4970–4978, Nov. 2009.
- H. Elgala, R. Mesleh, and H. Haas, "A study of LED nonlinearity effects on optical wireless transmission using OFDM," in Proc. WOCN, Cairo, Egypt, Apr. 28–30, 2009.
- I. Stefan, H. Elgala, R. Mesleh, D. O'Brien, and H. Haas, "Optical wireless OFDM system on FPGA: Study of LED nonlinearity effects," in Proc. IEEE VTC, Budapest, Hungary, May 15–18, 2011, pp. 1–5.
- H. Elgala, R. Mesleh, and H. Haas, "Non-linearity effects and predistortion in optical OFDM wireless transmission using LEDs," Intersci. Int. J. Ultra Wideband Commun. Syst. (IJUWBCS), vol. 1, no. 2, pp. 143–150, 2009.
- A. Behravan and T. Eriksson, "PAPR and other measures for OFDM systems with nonlinearity," in Proc 5th Int. Symp. Wireless Personal Multimedia Commun., Honolulu, HI, USA, Oct. 27–30, 2002, vol. 1, pp. 149–153.
- Thilo Fath, Christoph Heller, and Harald Haas, "Optical Wireless Transmitter Employing Discrete Power Level Stepping Member" 1734 Journal of Lightwave Technology, VOL. 31, NO. 11, JUNE 1, 2013, pp 1734.
- J.M. Kahn and J. R. Barry, "Wireless infrared communications," Proc. IEEE, vol. 85, no. 2, pp. 265–298, Feb. 1997.
- Tsonev, D., Sinanovic, S., and Haas, H., "Complete modeling of nonlinear distortion in ofdm-based optical wireless communication," Journal of Lightwave Technology 31(18), 3064–3076 (2013).
- J.M. Kahn and J. R. Barry, "Wireless infrared communications," Proc. IEEE, vol. 85, no. 2, pp. 265–298, Feb. 1997.
- J. B. Carruther and J. M. Kahn, "Angle Diversity for Nondirected Wireless Infrared Communication," IEEE Trans. Commun., vol. 48, no. 6, June 2000, pp. 960–99.
- Porcon Pascal, "ICT-213311 OMEGA: Deliverable D4.3 Optical Wireless MAC Specification," Retrieved: Oct., 2013, from <http://www.ict-omega.eu/publications/deliverables.html>, Nov. 2009.
- Marco Di Renzo, Harald Haas, Ali Ghayeb, Shinya Sugiura and Lajos Hanzo, "Spatial Modulation for Generalized MIMO: Challenges, Opportunities, and Implementation", Proceedings of the IEEE | Vol. 102, No. 1, January 2014, pp 56.

Quantitative and Qualitative analysis of Single Electron Transistor

Shweta Khakhkar^{a*}

^aGandinagar Institute of Technology, Gnadhinar, India

Abstract

Single Electron Transistor is a key element in research of nanoscale devices. It is based on one by one electron tunneling by utilizing coulomb blockade effect. Power consumption is roughly proportional to the electron number transferred from voltage source to the ground. The single- electron transistor is generally utilized as an ULSI element to reduce the power consumption. Thus, the Single electron transistor can offer low power consumption and the controlled tunneling of a single electron makes its high operating speed.

Keywords: Coulomb blockade, Conducting Island, single electron tunneling

Nomenclature

E_C	electrostatic energy
e	charge of electron
C	capacitance
K_B	Boltzmann's constant
T	Temperature in Kelvin

14. Introduction

The MOSFET is the common element in both digital and analog circuits. The channel of MOSFET is composed of n-type or p-type of the semiconductor material, and respectively called an nMOSFET or a pMOSFET. The growth of digital technologies has provided the inspiration to advance MOSFET technology. The digital CMOS logic gives the success to MOSFET technology. The reduction in the feature size in integrated circuits helped to produce products with high density at lower cost. The smaller transistors operate faster than larger ones. The cost of a chip decreases with area rather than with the number of transistors. The MOSFET is scaled down, particular in the channel length, results in increase the standby power of the chip, placing the limit on the integration level as well as on the switching speed. The main factors are power, threshold voltage, leakage current and short-channel effect. The standby power and the active power of a chip will increase below the 45nm technology. The performance of MOSFET device is no longer sufficient by creating smaller MOSFET, and thus substitute like SETs are being pursued.

Single electron transistors have come to be considered candidates as elements for future low power, high density integrated circuits because of their potential for ultra-low power operation involving only a few electrons. Single electron devices have a simple operation even when device size is reduced. These properties are beneficial for large scale integration.

A single electron transistor may be considered as a field effect transistor whose channel consist of a small, low capacitance, conducting Island [Quantum Dot] which is coupled to the source and drain leads by two tunnel junctions and capacitive coupled to one or more gate which is used to control the transfer of single electron from source to drain. Here, the tunnel junction is a thin insulating barrier between two conducting electrodes. The SET is operated in a single electronics regime in which only one electron can transfer from source to drain via island under the application of constant gate voltage on the island. Single electron device is based on an intrinsically quantum phenomenon known as the Tunnel effect. This single electron tunneling technology presents the ability to control the transfer of individual electrons.

For the practical application, it is absolutely necessary for the SET to be operated at room temperature. For this purpose, the size of the island of SET must be as small as possible. Generally, the size of island is considered as 10 nm for practical applications to reduce the total capacitance of SET and to overcome the problems of the thermal fluctuation.

15. Single Electronics

The concept behind the single electronics shows that the more accurate measurement of the strength of the tunneling effect is charging energy or electrostatic energy, which is given by [6]:

$$E_c = e^2/2C \quad (1)$$

From the above given equation, it is clear that if capacitance is very small, the charging energy may be dominating. The current flows through a conductor in a continuous manner because the number of free electrons is available in it.

If a tunnel junction is placed in an ordinary conductor, the flow of electrons penetrating this thin insulating barrier will be restricted by it. Thus, the current through a conductor may be quantized in this situation. Now, if discrete electrons can tunnel through the junction, the charge will be accumulated at the tunnel junction. When a high bias voltage is applied across this junction, one electron gets transferred. If the tunnel junction is biased with constant source, single electron tunneling oscillation will be appeared.

The charging and discharging of tunnel junction and thermal fluctuations are related to each other. Therefore, coulomb energy must be greater than the thermal fluctuations. Thus, the required condition is [6]:

$$E_c = e^2/2C > K_B T \quad (2)$$

Where K_B is Boltzmann's constant and T is temperature in Kelvin.

There are two fundamental conditions to observe the charging effect at room temperature. First condition is that the capacitance C must be smaller. The second condition is that the quantum fluctuations of number of electrons must be negligible. This required condition can be maintained if tunnel resistance R_t is larger than the quantum resistance, $R_t > h/e^2 = 25.813 \text{ K}\Omega$ Where h is plank's constant and e is electronic charge.

16. Orthodox Theory

The orthodox theory of single electron tunneling describes an important charging effect such as coulomb blockade and coulomb oscillation. It also describes an electron transport in an arbitrary single electron circuit consisting of tunnel junctions, capacitors and voltage sources, as a sequence of jumps of single electrons. The orthodox theory makes the following approximations [2]:

1. The electron energy quantization inside the conductors is ignored, i.e. the electron energy spectrum is treated as continuous.
2. The time T_t of electron tunneling through the barrier is assumed to be negligibly small in comparison with other time. This assumption is valid for tunnel barriers used in single electron devices of practical interest, where $T_t = 10^{-15} \text{ s}$.
3. The quantum process consisting of several simultaneous tunneling events are ignored. This assumption is valid if the resistance of the tunnel barriers of the system is much higher than the quantum unit of resistance.

4. Coulomb Blockade

As shown in fig 1, a tunnel junction is considered as a thin insulating barrier between two conducting electrodes. No current can flow through an insulating barrier. But according to the quantum mechanics approach, there is some probability (i.e. greater than zero) for an electron located at one side of the barrier (tunnel junction) to reach the other side, thus the transfer of electrons through the barrier charging quantum dot. Now, this would result in an

increase of the electrostatic energy which is given by $E_C = e^2/2C$, where C is an effective capacitance of the island. Later on, this electrostatic energy became known as Coulomb charging energy or coulomb blockade energy. This coulomb blockade energy is the repelling energy of previous electron present in the island to the next electron coming towards the island. The capacitance C of the island is very small. The coulomb charging or blockade energy (E_C) will be very high and due to this reason, electrons are unable to move simultaneously, but pass one-by-one. This phenomenon is known as “Coulomb blockade.”

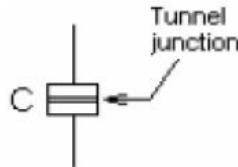


Fig. 1. Tunnel Junction [6]

The suppression of electron transfer can be removed by one of these two possible cases:

1. When the coulomb charging energy is overcome by thermal excitations at a temperature T , i.e. $T = E_C/K_B$
2. When the coulomb charging energy is overcome by an externally applied voltage V , i.e. $V = E_C/e = e/2C$

Where, V_t is known as “Threshold voltage” which is defined as an applied voltage that is just sufficient to increase the energy of electron above the coulomb blockade of tunneling so that the current can start to flow through the tunnel junction (Barrier).

Thus, if the voltage V is less than the threshold voltage, the system is in Coulomb blockade state. In case, when the voltage V exceeds, an electron tunnels through the tunnel junction into the quantum dot.

Now, tunneling current is proportional to the applied bias voltage. In other words, we can say that a tunnel junction behaves like a resistor of a constant value which depends on the barrier thickness. Since, the tunnel junction is composed of two conductors and an insulating layer in between these two conductors. Therefore, tunnel junction is described by the tunnel resistance R and tunnel capacitance C . In this case, tunnel junction acts as a capacitor and the insulating layer works as a dielectric medium for tunnel capacitor C .

The current flowing through a tunnel junction is a series of events in which only one electron passes through the tunnel junction because of discrete nature of charge. As electron tunnels the junction, tunnel capacitance is charged with an elementary charge building up a voltage which is represented by $V = e/C$. If the capacitance of the tunnel junction is very small, the voltage developed in the tunnel junction may be sufficient to prevent another electron to tunnel. Now, in this situation, the electric current is suppressed if the bias voltage is lower than the voltage developed in the tunnel junction. Thus the increment of the tunnel junction resistance around zero bias is considered as the coulomb blockade.

To achieve the Coulomb blockade, three criteria have to be met [10]:

1. The bias voltage must be lower than the charge divided by the self-capacitance of the island $V_{bias} < e/C$
2. The thermal energy in the source contact plus the thermal energy in the island, i.e. $K_B T$ must be below the charging energy: $E = e^2/C > K_B T$
3. The tunneling resistance, should be greater than h/e^2

5. SET schematic and its working

Single-electron transistor is a three terminal switching device in which the effect of coulomb blockade can be observed. This tunnel effect may be observed when two metallic electrodes are separated by an insulating barrier known as tunnel junction. This device can transfer electrons from source to drain one by one.

- As shown in fig 2, Single electron transistor circuits are made of small tunnel junctions, capacitances, and voltage sources. A gate voltage V_g is used to control one-by-one electron transfer. The tunnel junctions are located in between electrode and island, which are described by tunnel capacitance and tunnel resistance.

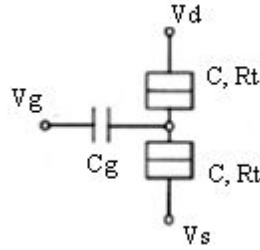


Fig. 2 Equivalent Circuit of SET [7]

- SET is composed of two tunnel junctions along with one island which are capacitive coupled to gate electrode. The island is located in between two tunnel junctions with capacities C1 and C2. SET can electro-statically controlled by the gate capacitance Cg. Thus the total capacitance of the island is given by $C = C_1 + C_2 + C_g$.

6. SET Macro Model

The macro model for simulation of single electron transistor is shown in Fig 3. It consists to resistor R_G with a large resistance of $100G\Omega$ connected gate and source. Symmetric $I_{ds}-V_{ds}$ characteristic obtained with two branches consisting of resistors, diodes, and voltage sources are identical. The directions of D_2 and V_2 are opposite to those of D_3 and V_3 to have the flow of current in both positive and negative drain-source bias. R_1 is the primary resistor in coulomb blockade region. R_2 and R_3 are resistors of SET in non-coulomb blockade region when its V_{ds} is larger than a certain value in positive and negative direction, respectively.

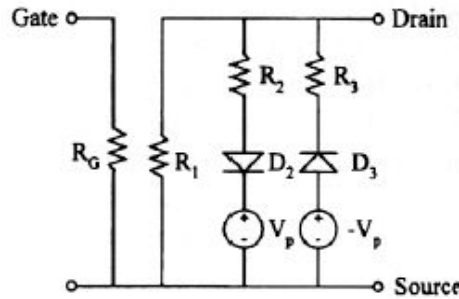


Fig. 3 SET Macro Model [7]

The charging energy periodically changing as a function of the gate bias is included in R_1 , R_2 and R_3 as the cosine of the gate bias. They are expressed as follows [7];

$$R_1(V_G) = CR_1 + CR_2 \cdot \cos(CF_1 \cdot V_G)$$

$$R_2(V_G) = R_3(V_G) = \frac{CV_p}{CI_2 - \frac{2CV_p}{R_1(V_G)}} \tag{3}$$

Where, CF_1 , CV_p , CI_2 , CR_1 and CR_2 are used as the fitting parameters for the current-voltage characteristics at different gate biases. The SET has the gate capacitance $C_g = 3.2aF$, the junction capacitance $C = 1.6aF$, the tunnel resistance $R_t = 100 M\Omega$, and the temperature $T = 30 K$. The macro model parameters are determined by fitting the Monte-Carlo result with piecewise linear approximation. The macro model parameters are the functions of T .

The parameter values,

- $CF_1 = 60$
- $CV_p = 0.02$
- $CI_2 = 0.2 * 10^{-9}$
- $CR_1 = 300 * 10^6$
- $CR_2 = 100 * 10^6$

• 7. Simulation Results

• Fig. 4 shows the I_{ds} - V_{ds} characteristics obtained for both the Coulomb blockade and the non-Coulomb blockade regions. Fig. 5 shows the I_{ds} - V_{ds} characteristics obtained for the Coulomb blockade region in positive direction only. The presence of the Coulomb blockade in the I_{ds} - V_{ds} characteristics of the SET is a region of zero current for a range of small drain-source voltage biases. The drain-source current I_{ds} is a linear function of V_{ds} .

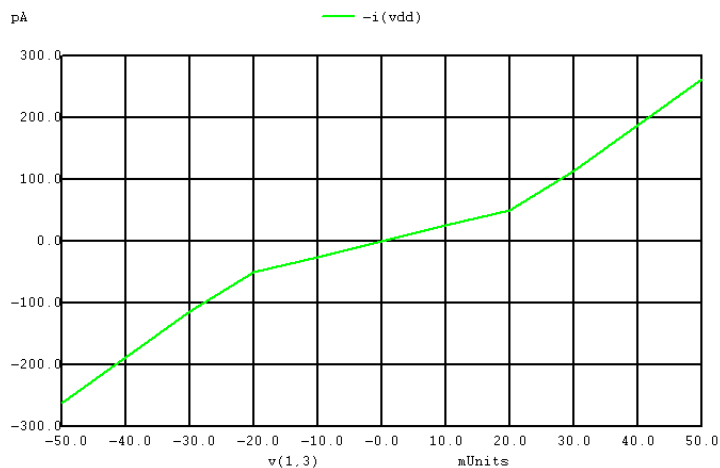


Fig. 4 I_{ds} - V_{ds} characteristic

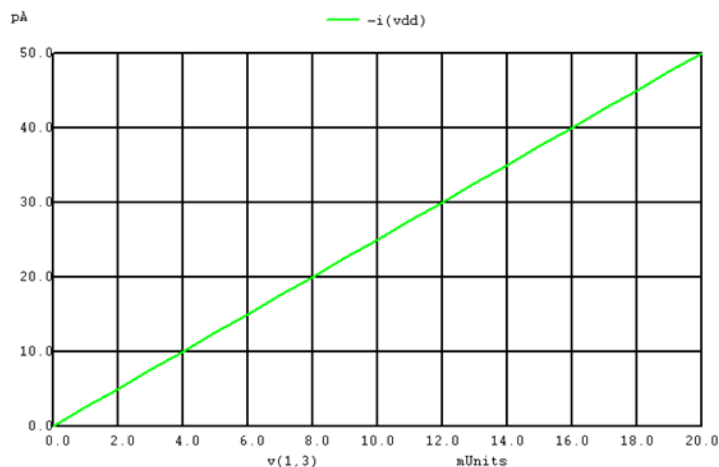


Fig. 5 I_{ds} - V_{ds} characteristic in coulomb blockade region

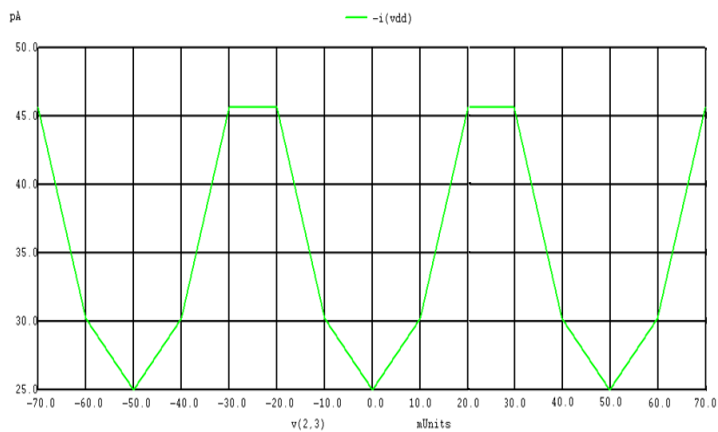


Fig. 6 I_{ds} - V_{gs} characteristic

• The current flowing from the source to the drain in a SET depends on the tunneling probability through both the drain-tunneling junction and the source tunneling junction. Fig 6 shows the I_{ds} - V_{gs} characteristic in which

coulomb oscillations of I_{ds} as a function of V_{gs} are observed due to capacitive coupled tunnel junction and Coulomb Island. The current flowing between gate and source was added to I_{ds} . In an ideal SET, the isolation between the gate and Coulomb Island makes the current flowing from gate to source negligibly small.

-
- Table 1: Comparison of simulated data with measured data
-

• Model	• Parameter	• Simulated Data	• Measured Data
• Macro model-I	• Id (in non-coulomb blockade at Vdd=0.03V)	• 110pA	• 130pA
	• Id (in coulomb blockade at Vdd=0.02V)	• 50pA	• 50pA
	• PVCR	• 1.83	• 2

- -
- Conclusion**

A SET allows transferring the electrons one by one using coulomb blockade effect. In the age of nanotechnology, it provides low power consumption and high operating speed in the field of ULSI design for the fabrication of various electronic devices. Macro model gives linear function of I_{ds} w.r.t V_{ds} . Coulomb oscillations of I_{ds} as a function of V_{gs} is also observed.

References

[1] Konstantin K. Likharev, “Single Electron Devices and Their Application”, IEEE Vol. 87, April 1999.
 [2] Amiza Rasmi, Uda Hashim, “Single Electron Transistors (SET): Literature Review”. 2005
 [3] Om kumar and Manjit kaur, “Single electron transistor: Applications & problems”, International journal of VLSI design and communication system (VLSICS) Vol. 1, No. 4, Dec. 2010
 [4] Andreas Scholze, “Simulation of single-electron devices,” Ph.D. dissertation, Univ. of Jena, Germany, 2000
 [5] Vinay Pratap Singh, Arun Agrawal, and Shyam Babu Singh, “Analytical discussion of single electron transistor”, International Journal of Soft Computing and Engineering (IJSCE), Vol. 2, July 2012
 [6] Khadijeh Feizi and Saeed Haji Nasiri, “DC Characteristic Analysis of Single-Electron Transistor Based on MIB Model”, International Conference on Nanotechnology and Biosensors, IPCBEE Vol. 2, 2011
 [7] Y. S. Yu, H. S. Lee, and S. W. Hwang, “SPICE Macro-Modeling for the Compact Simulation of Single Electron Circuits”, Journal of the Korean Physical Society, Vol. 33, Nov 1998
 [8] You-Lin Wu, Shi-Tin Lin, “An Improved Single Electron Transistor Model for SPICE Application”, Nov 2003
 [9] Yongshun Sun, Rusli, and Navab Singh, “Room-Temperature Operation of Silicon Single-Electron Transistor Fabricated Using Optical Lithography”, IEEE Transactions on Nanotechnology, Vol. 10, Jan 2011
 [10] Amiza Rasmi, Mohammad Nuzaihan Md Nor, and Uda Hashim, “SOI Single Electron Transistors (SET) Design and Process Development”, 2005

Harmonics Mitigation Using Shunt Active Filter

Pankaj.C.Patel^a, Prof.D.R.Vyas^a

^aLCIT Bhandu

Abstract

Voltage, current and frequency are physical characteristic that define the power quality of the system. If any disturbance in physical characteristics of that results in damage, upset or failures of end use equipment. These are higher switching frequency and the non linearity in the properties of the power electronics being mostly responsible for the power quality problem. So the development of active filter to solve this problem to improve power quality among this which shunt active power filter used to compensate the harmonics and reactive power. A shunt active power filter with instantaneous active and reactive power theory (P-Q theory) has been proposed for its performance and ability to compensate the harmonics and reactive power. It has been investigated through simulation that under three phase, three wire system with balanced and unbalance sinusoidal source voltage. Shunt active filter is able to mitigate the total THD specified by power quality standard. Matlab/simulink is used as a simulation tool for analyzing.

17. *Keywords:* Shunt active filter, pq theory, THD

Nomenclature

THD _v	total harmonics distortion in voltage
THD _i	total harmonics distortion in current
IGBT	insulated gate bipolar transistor

Introduction

Harmonics current produced by non linear loads like use of power electronics in system can interact adversely with a wide range of power system equipment, mainly transformer, capacitors and motors, causing additional losses, overheating and overloading[2]. These harmonics current is also cause interference with telecommunication lines and errors in protective relays and power metering. In the past tuned passive filter are used to solve the problem of harmonic distortion but this filter offered some disadvantage like: They filter the frequency only tuned for it, their operation cannot be limited to a certain load, resonance can occur because of the interaction between the passive filter and load with severe effects[2]. To compensate this drawback use of active power filter line conditioners or simply active power filter. The performance of active power filter mainly depends on the reference current generation strategy, control technique and topology of filter inverter. There are basically two types of Active filters one is shunt active filter and other is series active filter[1]. They reduce harmonics specified by power quality standard[3].

1.2 Shunt Active Filters

Shunt active filter mostly have two mains blocks:

1. The PWM converter (power processing)
2. The active filter controller (signal processing)

The PWM converter is responsible for power processing in synthesizing the compensating current that could be drawn from the power system. The active controller is responsible for signal processing in determine in real time the instantaneous compensating current reference, which is continuously passed to the PWM converter[1].

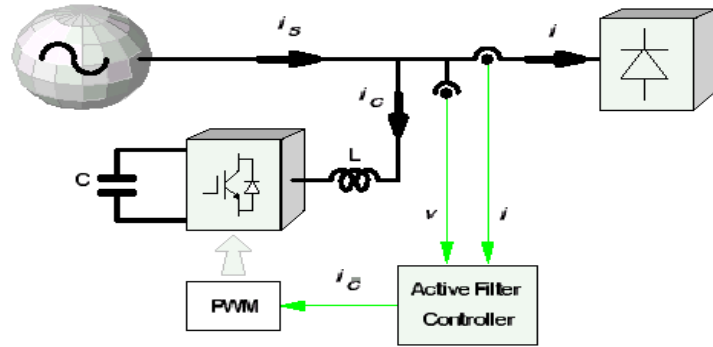


Fig: 1 Block Diagram of Shunt Active Filter

Fig.1 shows the basic block diagram of a shunt active filter[1] for harmonic current compensation of a specific load. It consists of a voltage source converter with a PWM current controller and an active filter controller that realizes an instantaneous control algorithm[4]. The shunt active filter controller works in a closed loop system. The controller senses continuously the load current i_c and calculates current reference i_c^* for the PWM converter[5]. When compensating current i_c is equal to i_c^* reference current, the PWM converter may work as a linear power amplifier. The dc capacitor and the IGBT (insulated gate bipolar transistor) with antiparallel diode are used to indicate a shunt active filter that is built up from a voltage source converter. Both voltage source converter and current source converter can be used in shunt active filter[6].

2. Controller Design in Shunt Active Filter.

2.1 Mathematical Modelling of Instantaneous P-Q Theory

The Instantaneous active and reactive power theory or simply the $p-q$ theory is based on a set of instantaneous values of active and reactive powers defined in the time domain[7]. There are no restrictions on the voltage or current waveforms, and it can be applied to three-phase systems with or without a neutral wire for three-phase generic voltage and current waveforms.

Thus, it is valid not only in the steady state, but also in the transient state[13]. This theory is very efficient and flexible in designing controllers for power conditioners based on power electronics devices. Other traditional concepts of power are characterized by treating a three-phase system as three single-phase circuits[8]. The $p-q$ Theory first uses Clarke transformation to transform voltages and currents from the abc to $\alpha\beta 0$ coordinates, and then defines instantaneous power on these coordinates. Hence, this theory always considers the three-phase system as a unit, not a superposition or sum of three single-phase circuits[15].

2.1.1 The Instantaneous Powers of the P-Q Theory

The $p-q$ Theory can be defined in three-phase systems with or without a neutral conductor. Three instantaneous powers: the instantaneous zero-sequence power p_0 , the instantaneous real power p , and the instantaneous imaginary power q are defined from the instantaneous phase voltages and line currents on the $\alpha\beta 0$ axes are given in equation (2.1)[10].

$$\begin{bmatrix} p_0 \\ p \\ q \end{bmatrix} = \begin{bmatrix} V_0 & 0 & 0 \\ 0 & V_\alpha & -V_\beta \\ 0 & V_\beta & V_\alpha \end{bmatrix} \begin{bmatrix} i_0 \\ i_\alpha \\ i_\beta \end{bmatrix} \quad (2.1)$$

Since there are no zero-sequence current components in three-phase, three-wire systems, that is, $i_0 = 0$. In this case, only the instantaneous powers defined on the $\alpha\beta$ axes exist, because the product $v_0 i_0$ in (2.1) is always zero. Hence, in three-phase, three-wire systems, the instantaneous real power p represents the total energy flow per time unity in terms of $\alpha\beta$ components. In this case, $p_3\phi = p$ [9].

2.1.2 The Instantaneous P-Q Theory in Three-Phase Three Wire Systems

Let us consider a three phase system with voltages $v_a, v_b,$ and v_c are the instantaneous phase voltages and $i_a, i_b,$ and i_c the instantaneous line currents. Since zero sequence power in three-phase three wire system is always zero, the equation (2.1) becomes:

$$\begin{bmatrix} p \\ q \end{bmatrix} = \begin{bmatrix} V\alpha & V\beta \\ -V\beta & V\alpha \end{bmatrix} \begin{bmatrix} i\alpha \\ i\beta \end{bmatrix} \quad (2.2)$$

In the proceeding discussion, the $\alpha\beta$ currents will be set as functions of voltages and the real and imaginary powers p and q to explain the physical meaning of the powers defined in the p - q Theory[11]. From (2.2), it is possible to write

$$\begin{bmatrix} i\alpha \\ i\beta \end{bmatrix} = \frac{1}{v\alpha^2+v\beta^2} \begin{bmatrix} V\alpha & -V\beta \\ V\beta & V\alpha \end{bmatrix} \begin{bmatrix} p \\ q \end{bmatrix} \quad (2.3)$$

If current and voltages from $\alpha\beta$ variables are replaced to their equivalent abc variables in equation (2.2), the instantaneous imaginary power will be:

$$\begin{aligned} q &= V_\alpha i_\beta - i_\alpha V_\beta = \frac{1}{\sqrt{3}} [(Va - Vb)i_c + (Vb - Vc)i_a + (Vc - Va)i_b] \\ &= \frac{1}{\sqrt{3}} [(Vab)i_c + (Vbc)i_a + (Vca)i_b] \quad (2.4) \end{aligned}$$

This expression is similar to that implemented in some instruments for measuring the three-phase reactive power. The difference is that voltage and current phasors are used in those instruments. Here, instantaneous values of voltage and current are used instead. According to p-q theory real and reactive powers can be written as:

$$p = \check{p} + \bar{p}, \quad q = \check{q} + \bar{q}, \quad p_0 = V_0 i_0 \quad (2.5)$$

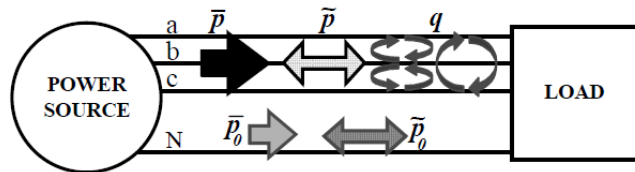


Fig.2. Power components of the p-q theory in a-b-c coordinate.

3. Pulse Width Modulation Controller

PWM controller is used to produce switching signals for the voltage source inverter of shunt active filter. In VSI IGBT is used for the switch of the shunt active filter[12].

4. Simulation Model

Simulation is very important and powerful tool to reduce development time and study the dynamic of the systems. In this work matlab/simulink is used as a simulation tool to implement the proposed active filter and study the operation of the active power filter under different operating conditions. In this model close loop control is used[14].The model so in fig:3.

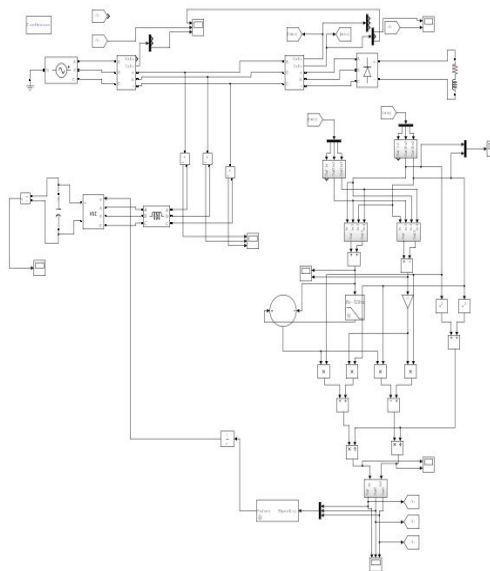


Fig:3 Simulation model of shunt active filter

5.Simulation Results and Discussions

The analysis of the three-phase system has been done in simulink/matlab environment. The system parameters values are shown in table 1.

Table.1 System Parameters

Name	symbols	value
AC Voltage Source	Vs	400v
Fundamental frequency	F	50Hz
Load	RL	50ohms/100mH
DC bus capacitor	Cdc	440F
Filter inductor	Lf	0.7H

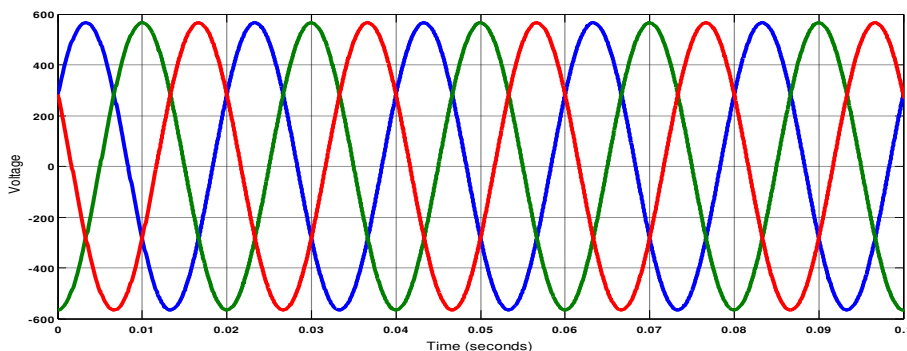


Fig:4 Three phase supply voltage at balance condition

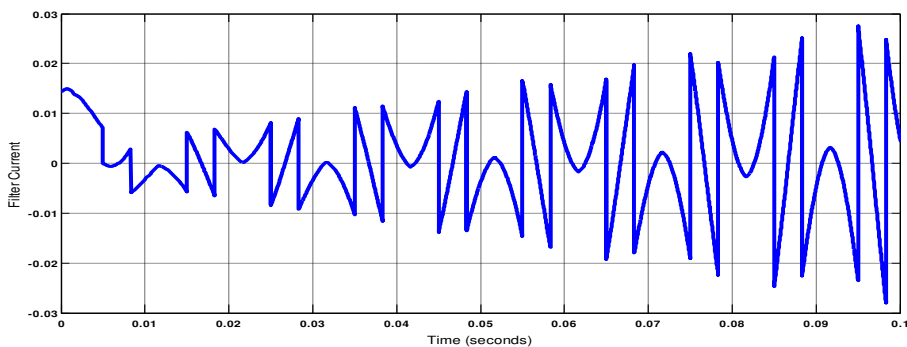


Fig:5 Filter current at balance supply voltage

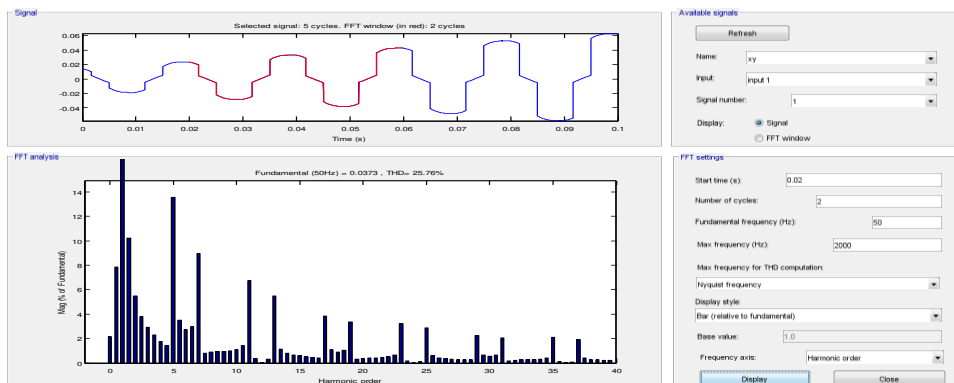


Fig:6 THDi at without filter in balance supply

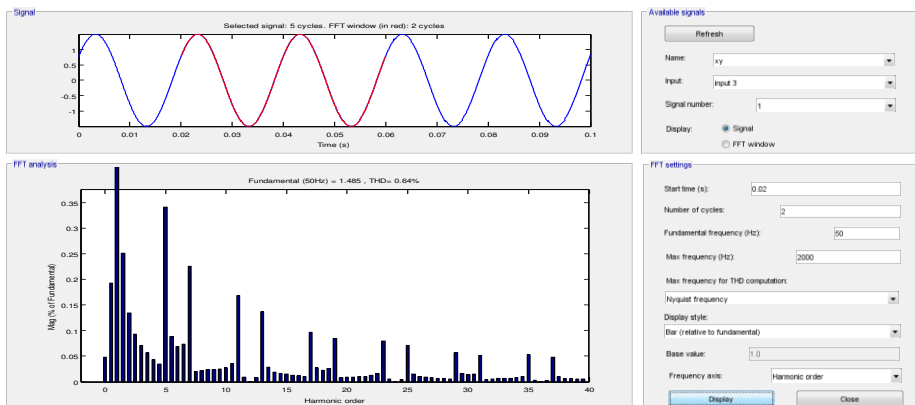


Fig:7 THDi at with filter in balance supply

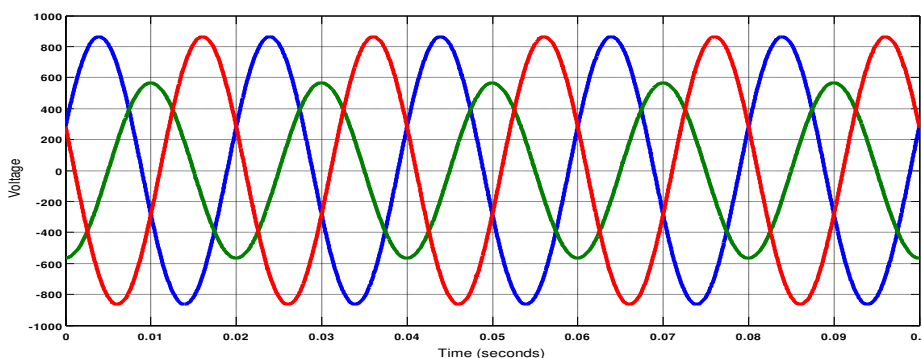


Fig:8 Three phase supply voltage at unbalance condition

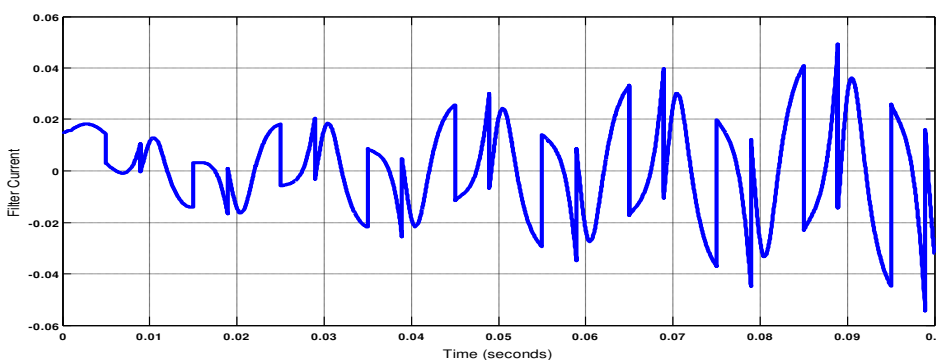


Fig:9 Filter current at unbalance supply voltage

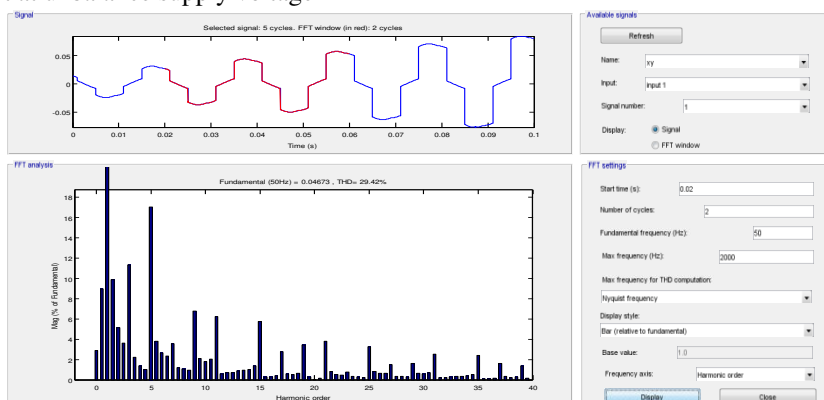


Fig:10 THDi at without filter in unbalance supply

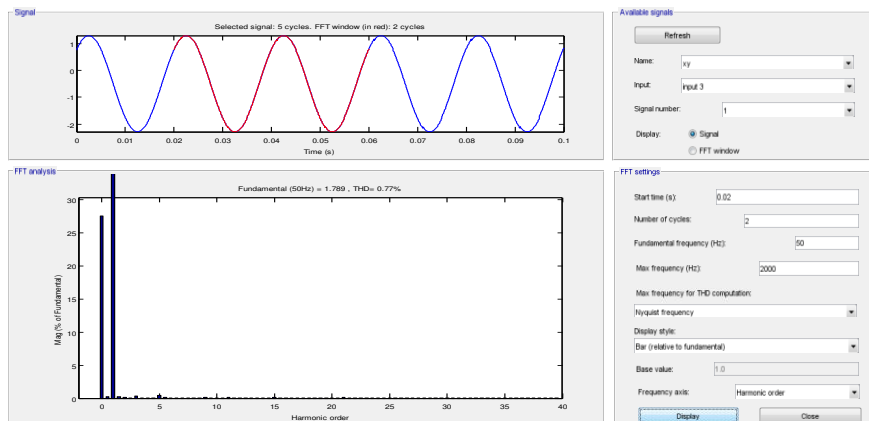


Fig:11 THDi at with filter in balance supply

The total harmonics current distortion in balance supply condition is 25.67% without filter then using shunt filter THDi reduced to 0.64%. The total harmonics current distortion in unbalance supply condition is 29.42% without filter then using shunt filter THDi reduced to 0.77%. They are so in above figure 6,7 and 10,11. In figure 5 and 9 so the filter wave form during balance and unbalance condition.

5. Conclusion

The three phase three wire shunt active filter with controller based on instantaneous active and reactive power (p-q) theory is simulated in matlab/simulink to compensate the problems of the harmonics and reactive power which are encountered from power electronic non linear load. The performance of shunt active power filter is investigated under different scenarios. It is investigated that the p-q theory based active filter manages to compensate the harmonics and reactive power of the three phase three wire network even under balance and unbalance supply voltage. The shunt active filter is able to reduce the THD in source current at a 25.67% to 0.64% in balance condition and 29.42% to 0.77% in unbalance condition that level well below the defined standards specified by power quality standards. so shunt active power filter is best topology for harmonics mitigation than passive filter.

ACKNOWLEDGEMENT

“Obstacles are what we see when we take our eyes off the goals”

Adversity is often one of the best teachers. Even the people that somehow gripped our meanest imagination, violated us in some way, even those people are due their honor for what they have taught us. We wish to acknowledge all for their role in our life.

We are also grateful to our beloved principle, which is dynamic and single-handed efforts have inspired us to do something in the time to come.

There are special mentors that we must acknowledge due to their importance in our work. We would therefore like to thank our guide Prof.D.R.Vyas for his valuable guidance for this project.

We also thank our teaching & Non-teaching staff for their kind help in bringing out this project within stipulated time. Finally we thank our Parents and Friends for their unconditional support throughout the project.

References

- [1] H. Akagi, E.H. Watanabe, and M. Aredes, "Instantaneous power theory and applications to power conditioning", Electrical Engineering, 2007. Page No.111 to 120.
- [2] Roger C.Dugan, Mark F.McGranaghan, Surya Santoso and H.Wayne Beaty, Electrical Power System Quality, Tata McGraw-Hill, New Delhi 2008. Page No.220 to 225.

- [3] Jos Arrillaga and Neville R.Waston "Power System Harmonics" Second Edition John Wiley & Sons, Ltd.page no.11
- [4] R.Belaidi,A.Haddouche,H.Guendouz "*Fuzzy logic controller based three-phase shunt active power filter for compensating harmonics and reactive power under unbalanced mains voltages*" published by Elsevier Ltd.(2012).
- [5] M.S Priya,Uthaya Suresh Balu "*Simulation results of a shunt active power filter using p-q theory power components calculations*" International journal of Advance Research in Computer Science and Management Studies. volume 2.issue 2,february (2014).
- [6] Suresh Mikkili,A.K. Panda "*Real time implementation of PI and Fuzzy logic controllers based shunt active filter control strategy for power quality improvement*" Elsevier Ltd (2012).
- [7] Sakshi Bangia , P.R.Sharma, Maneesha Garg "*Comparison of Artificial Intelligence Techniques for The Enhancement of Power Quality*" IEEE(2013)
- [8] Madhukar waware , Pramod Agarwal, "*Use of Multilevel Inverter for Elimination of Harmonics in High Voltage Systems*" IEEE (2010)
- [9] Naimish Zaveri,Ajitsinh Chudasama "*Control strategies for harmonic mitigation and power factor correction using shunt active filter under various source voltage conditions*"Elsevier Ltd (2012).
- [10] Sushree Sangita Patnaik,Anup Kumar Panda "*Real time performance analysis and comprisation of various control schemes for particle swarm optimization based shunt active power filters*" Elsevier Ltd (2013).
- [11] Gayadhar Panda,Pravat Kumar Ray,Pratap S. Puhan,Santanu K. Dash "*Novel schemes used for estimation of power system harmonics and their elimination in a three-phase distribution system*" Elsevier Ltd (2013).
- [12] Wei Lu, Chunwen Li,Changbo Xu "*Sliding mode control of a shunt hybrid active power filter based on the inverse system method*" Elsevier Ltd.(2014).
- [13] M. Bouzidi, A. Benaissa, S. Barkat "*Hybrid direct power/current control using feedback linearization of three-level four-leg voltage source shunt active power filter*" Elsevier Ltd (2014).
- [14] Fatiha Mekri, Mohamed Machmoum, Nadia Ait-Ahmed, Benyouness Mazari "*A comparative study of voltage controllers for series active power filter*" Elsevier Ltd (2010).
- [15] Nadhir Mesbahi, Ahmed Ouari, Djaffar Ould Abdeslam, Tounsia Djamah, Amar Omeiri "*Direct power control of shunt active filter using high selectivity filte (HSF) under distorted or unbalanced conditions*" Elsevier Ltd (2014).

PD Electromagnetic Pulse Analysis in Transformer by FDTD Simulation Technique

Hitesh Manani

Gandinagar Institute of Technology, Gnadhinagar, India

Abstract

The Partial Discharge (PD) is one of the main causes for eventual equipment failure and it occurs where the electric field across the insulation exceeds the local dielectric strength. The importance of detecting or analyzing accurately the partial discharge in high voltage power industry becomes obvious as the infrastructure ages. In this work electromagnetic sensing for detecting the electromagnetic radiation, associated with partial discharge in an insulated medium of transformer is used. The Finite Difference Time Domain (FDTD) technique, which is a widely used electromagnetic computational method, has been used to model propagation of PD discharges generated in the form of a Gaussian pulse. The wave propagation in free space, oil and with a cylindrical metallic obstruction representing core/winding, in the two dimensions is realized and presented in this work. Here, Absorbing Boundary Conditions (ABC) like Perfectly Matched Layer (PML) has also been incorporated in the simulation. Further work is carried out for localization of PD source by UHF detection method.

Keywords: Electrical Insulation, Partial Discharge, Electromagnetic Wave, FDTD, UHF, PML

Nomenclature

E	Electrical Field
H	Magnetic Field
<i>Greek symbols</i>	
η	Intrinsic impedance
ϵ	Permittivity
μ	Permeability
<i>Subscripts</i>	
x, y, z	Direction coordinator

Introduction

Partial discharge is a High Voltage (HV) Phenomenon [1]. According to IEC 60270, “Partial Discharge is a localized electrical discharge that only partially bridges the insulation between conductors and which may or may not occur adjacent to a conductor”. PD is caused due to existence of void or cavity in insulation and insulating materials gradually degrades due to cumulative effect of electrical, chemical and thermal stress [2, 6]. These continuous PD activities may result in breakdown of insulating materials which lead the whole equipment towards failure.

Defects in transformer insulation cause partial discharges (PD), which can progressively result in electrical breakdown. Therefore, early detection of partial discharges is important [1]. PD measurements can also provide information about the ageing condition of transformers and thus enable conclusions about their lifetime. The so called UHF PD measuring method bases on the fact that PD under oil are very fast electrical processes and radiate Electro Magnetic (EM) waves with frequencies up to the ultrahigh range (UHF: 300 – 3000 MHz). PD phenomenon can be detected accurately by Electro- magnetic radiation detection technique. These methods employ Electro Magnetic sensors to detect the radiation emitted from PD activity and it has been shown to provide valuable information on the condition of insulators [2]. To analyze electromagnetic wave FDTD technique is used which allows an accurate investigation of EM fields in dielectric medium [3]. The Gaussian pulse model for PD has been used for simulating EM radiation that propagates in insulating medium.

In this work, FDTD is used to study the EM radiation emitted from a PD source. The PD event was approximated by a Gaussian pulse [3]. The radiation spectrum of the Gaussian source located within an insulating material is investigated. The impact of the dielectric material and the cavity parameters on the radiation pattern and the power density is presented. The propagation of EM waves from cavities within insulating materials is assessed. The aim of this work is to improve the assessment of remaining service life of HV insulators based on their fault level reflected in the radiation pattern.

FDTD Formulation

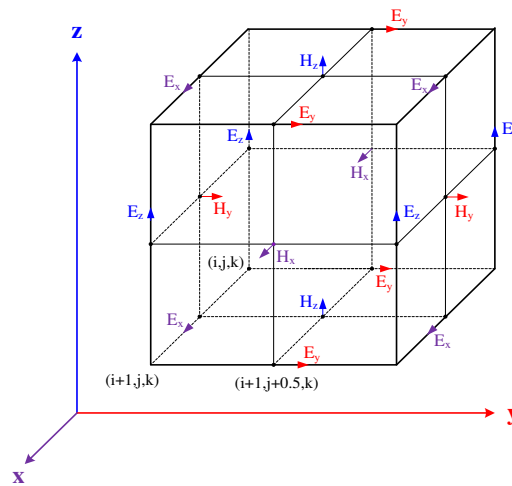
Finite Difference Time Domain

In 1966 Yee proposed a technique to solve Maxwell’s curl equations using FDTD technique [4]. The FDTD formulation is a convenient method for solving electromagnetic field problems. This method is widely applied to the field of electromagnetic computation, can be used to simulate the electric and magnetic fields within defined simulation space and specified boundary condition.

The equations are solved in a leapfrog manner means the electric field is computed for a given instant in time and the magnetic field is obtained for the next instant in time, and the process is repeated over and over again [5]. The FDTD technique is based on approximations which permit replacing differential equations by finite difference equations through which one can analyze pattern of electromagnetic PD pulse.

Yee’s Cell Technique

There are number of finite-difference schemes for Maxwell’s equations, but the Yee scheme persists as is very robust and versatile. In Yee’s scheme, the model is first divided into many small cubes. For simplicity the cubes are assumed to be of same size. The region being modeled is represented by two interleaved grids of discrete points [4]. One grid contains the point at which the magnetic field is evaluated. The basic element of the FDTD space lattice is shown in Figure 1. Yee positions the components of ‘E’ and ‘H’ fields about a unit cell of the lattice. ‘E’ and ‘H’ fields are evaluated at alternate half time steps, such that all field components get calculated in each time step Δt and both electrical and magnetic field surrounding each other.



• Fig. 1 Perfectly Matched Layer (PML)

Absorbing boundary conditions are needed to keep outgoing electric field ‘E’ and magnetic field ‘H’ from being reflected back into the problem space. The basic requirement of FDTD technique is that while calculating ‘E’ field, one need to know the surrounding ‘H’ field. As the wave propagates outward, it will finally come to the edge of the problem space [4]. The use of a Perfectly Matched Layer (PML) as absorbing boundary condition helps to avoid the problem of reflections from the boundary in this work.

When wave is propagated in one medium strikes the boundary of another medium, reflection is generated. The reflection coefficient depends on the intrinsic impedance of the media and is given by the following equation.

$$\Gamma = \frac{\eta_A - \eta_B}{\eta_A + \eta_B}$$

Where η_A = intrinsic impedance of medium A

η_B = intrinsic impedance of medium B

$$\eta = \sqrt{\frac{\mu}{\epsilon}}$$

A medium that is lossy so the pulse will die out before it hits the boundary. This is accomplished by making both μ and ϵ equation complex.

Simulation in 1D and 2D

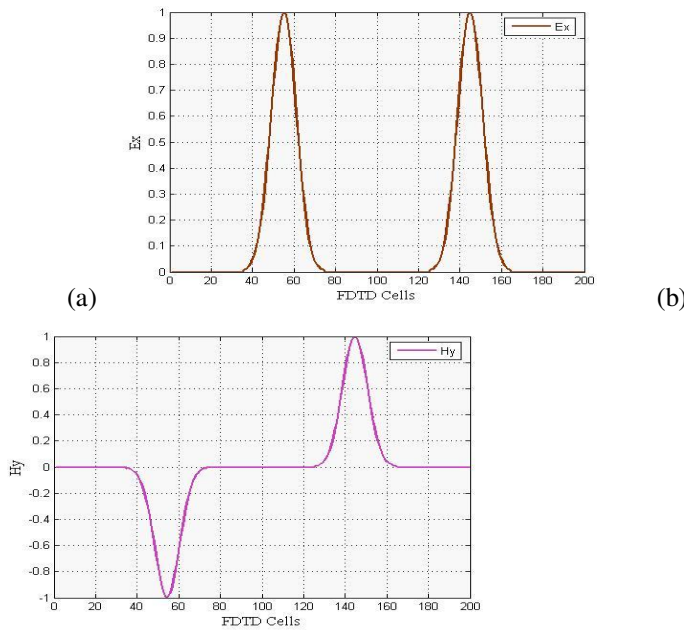
Simulation in One Dimension

Based on Maxwell curl’s equation for an isentropic medium in one dimension space, electromagnetic wave is made up of E_x and H_y through time dependent Maxwell curl equation becomes scalar equation as follow:

$$\frac{\partial E_x}{\partial t} = -\frac{1}{\epsilon_0} \frac{\partial H_y}{\partial z} \quad \frac{\partial H_y}{\partial t} = -\frac{1}{\mu_0} \frac{\partial E_x}{\partial z}$$

Here electric field is oriented in x direction and magnetic field is oriented in y direction and both travelling in z direction. Taking central difference approximation for time and space for the implementation in MATLAB with initial condition:

- Problem space dimension: 200 cells
- Source: Gaussian pulse
- Time step: 130



• Fig. 2 (a) E_x field in One Dimension (b) H_y Field in One Dimension

Simulation in Two Dimension

In two-dimensional simulations, we choose Transverse Magnetic (TM) mode which is composed of E_z , H_x , and H_y [9]. Same as in 1D simulation central difference approximation for time and space is taken and then modified equation which are discretized and implanted in MATLAB program with initial condition.

$$\frac{\partial D_z}{\partial t} = \frac{1}{\sqrt{\epsilon_0 \mu_0}} \left[\frac{\partial H_y}{\partial x} - \frac{\partial H_x}{\partial y} \right]$$

$$\frac{\partial H_x}{\partial t} = -\frac{1}{\sqrt{\epsilon_0 \mu_0}} \frac{\partial E_z}{\partial y} \quad \frac{\partial H_y}{\partial t} = -\frac{1}{\sqrt{\epsilon_0 \mu_0}} \frac{\partial E_z}{\partial x}$$

- Problem space dimension: 100 × 100 cells
- Cell size: 0.01 meter

- Source: Gaussian pulse
- Time step: 1.66×10^{-11} sec

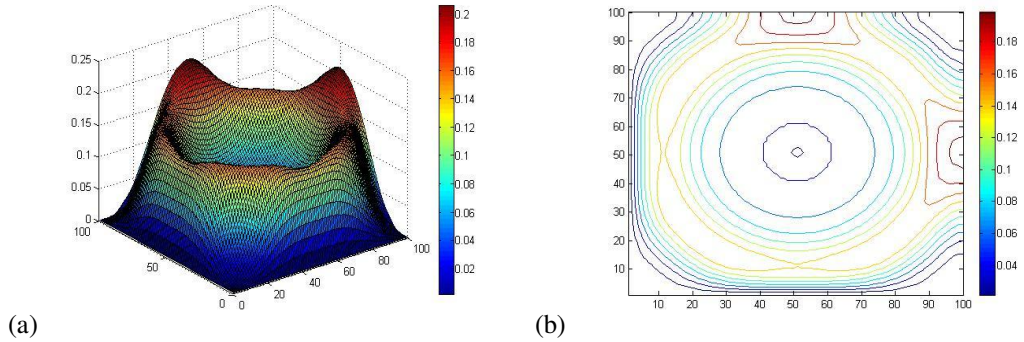


Fig.3 E_z Field Plot after 130 time steps without PML in 2D

It is also implemented with PML which is one kind of absorbing boundary condition implemented in MATLAB program to avoid reflection problem space as shown in Figure 4.

- No. of PML layers to avoid reflection: 5 Layer

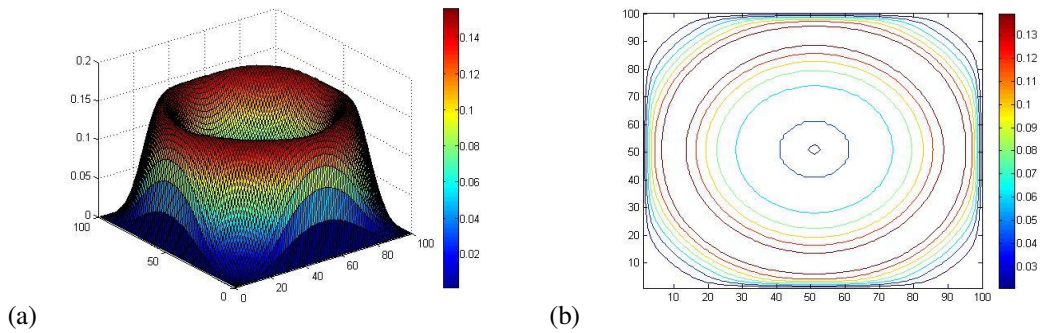


Fig.4 E_z Field Plot after 130 time steps with PML in 2D

3.2 Simulation result in oil with obstruction

A real transformer will contain oil as the insulating medium and also obstructions for the radiated wave, like the winding and core. Here such obstructions are simulated by two representative and scaled down hexagon objects with centered at (30, 30) and (70, 70). This simple geometry is assumed for verification of the algorithm. An oil medium with relative permeability $\mu_r = 1$, relative permittivity $\epsilon_r = 2.2$ and conductivity $\sigma = 0$, and two circular obstructions with relative permeability $\mu_r = 1$, relative permittivity $\epsilon_r = 1$ and conductivity $\sigma = 5.8 \times 10^7$ (S/m) representing simplified copper winding structure are considered. In Figure 5 ' E_z ' field propagation contour, with pulse originated at (30, 30), after 130 time steps is shown. The wave takes a path along the surface of the obstruction which may be the shortest route for the wave travel.

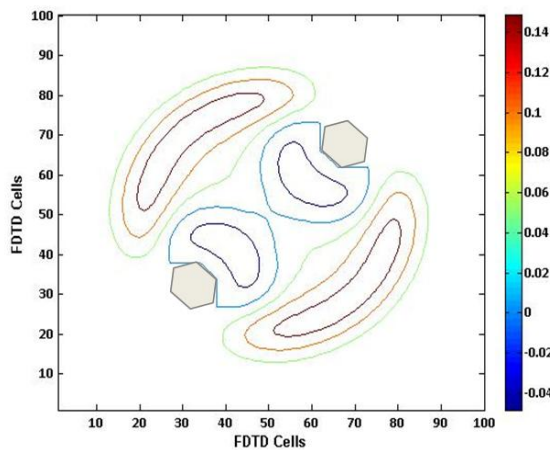


Fig.5 PD pulse propagation through two hexagonal obstacles

In the literature, Gaussian pulse has been used to describe the current due to PD [8]. Hence the propagation due to a Gaussian current pulse has been studied here. Consequently, there is no single frequency propagation. Instead, the disturbance generated due to all the frequencies present in the spectrum of this impulse is relayed along the mathematical grid in the simulation. Since the current used for simulation has a nature similar to that of the PD pulse, the signals received at the hypothetical sensors will help to understand the signals that may be expected in reality. However, from FDTD perspective, cell size has to be lesser than $(1/10)^{th}$ of wavelength for the highest frequency. Hence, the shortest wavelength that will be suitably captured is 0.1 m, which is equivalent to a frequency of 3 GHz in air, and very close to 2 GHz for oil. Thus, these FDTD simulations can help understand PD UHF wave propagation. Eventually, such an analysis tool is expected to help in detecting the PD source location using UHF signals.

4. Partial Discharge Detection with UHF Sensor

- As discuss in the introduction, Ultra High Frequency (UHF) method was initially applied for PD diagnostics, detection and its localization. The practical detection circuit of PD consists of a few UHF sensors along with recording and interpreting instruments. Once the sensor detects a PD, the next important task for operator is to identify the location of PD occurrence [8]. For simulation a 100 x 100 problem space with a cell size of 0.01 m has been again considered. For the simplicity problem space is first specified as free space. A general case illustration of placement of sensors, source location and Line-of-Sight (LoS) distance is as shown in Figure 6. The position of sensors $S_1 (X_1, Y_1)$ and $S_2 (X_2, Y_2)$ corresponds to $S_1 (40, 40)$ and $S_2 (85, 20)$ respectively in the problem space. The minimum distance for the signal to travel through the LoS and in FDTD code Gaussian pulse is located at $(60, 60)$. From given Figure, we can analyze that the Gaussian pulse will hit the sensor which is nearer to its location. For a sample source location $(60, 60)$, the plots of E_z vs Time steps are shown in Figure 6.

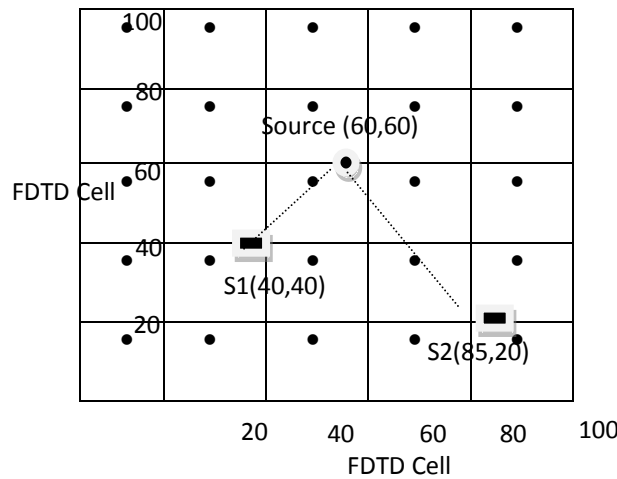


Fig.6 Dimension view of Problem Space with Sensor location

Table 1 LoS distance and FDTD grid distance of sensors from signal location

Source Location	Finite Grid Distance (cm)		Line of Sight Distance (cm)	
	$S_1(40, 40)$	$S_2(85, 20)$	$S_1(40, 40)$	$S_2(85, 20)$
(60, 60)	0	65	28.28	47.16

The signal reaches the nearest sensor first and subsequently to the other sensors depending on their placement. Thus there are two time differences starting from the first hit reference sensor. This time difference can be effectively criticized by Time Difference of Arrival (TDOA) to find out location as well as amplitude of PD propagation pulse [8].

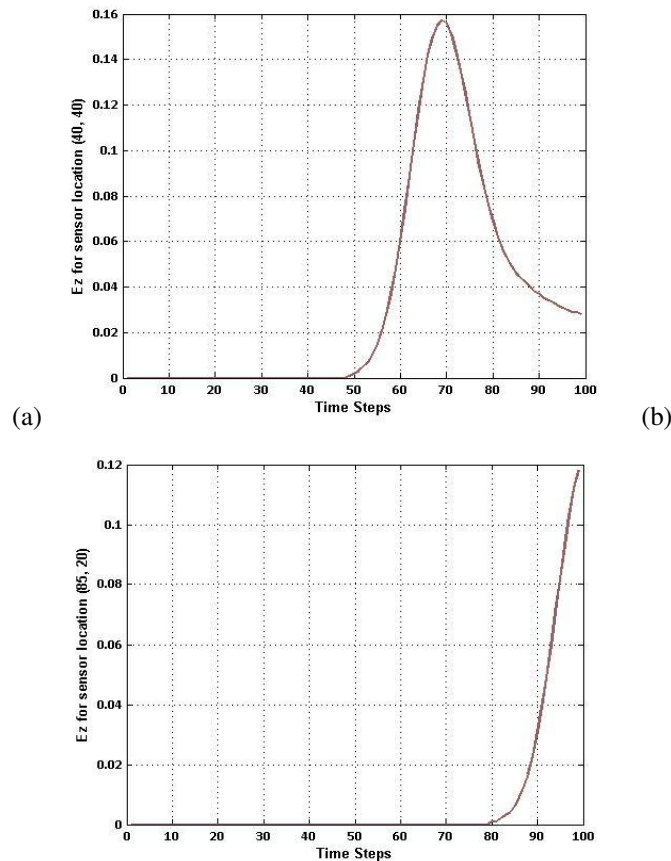


Fig 7 Plot of E_z vs Time steps for sensor (a) S_1 (40, 40) (b) S_2 (85, 20)

5. Conclusion

This paper deals with the analysis of PD pulse propagation in the UHF range. The implementation of the FDTD has also been carried out by MATLAB environment. The FDTD technique is used to simulate propagation of PD signals model as Gaussian pulse in MATLAB. Simulation analysis of FDTD for 1D, 2D is utilized to study wave propagation characteristic in free space. To resolve the reflection problem in 2D, perfectly matched layer condition has been implemented to observe reflection of wave.

Moreover, the obstacle is added in problem space and then analyzes the characteristic of PD propagating wave in 2D. Representations of the E_z field allowed evaluation of the factors that contribute to different radiation patterns through which UHF sensors can be effectively works to detect the impurities in insulating materials used in power apparatus.

6. Future Enhancement

As a future enhancement, the methodology used in simulation can be extended for three dimensions along with absorbing boundary conditions and actual dimensions of various power apparatus may be incorporated for the effective analysis of PD pulse. Analysis of signal captured by multiple sensors in simulation space is also carried out with change in location of sensors by consider PD source at fixed location and Effect of change in PD source location by locating sensor location fixed. An experimental validation effort of the simulated results for detection and localization of impurities in problem space is also proposed.

References

- [1] R. J. Van Brunt, October 1994, "Physics And Chemistry of Partial Discharges And Corona", IEEE Transaction On Dielectric And Electrical Insulation, Vol. 1, No. 5, pp. 761-784.
- [2] R. Bartnikas, 2002, "Partial Discharge: Their Mechanism, Detection And Measurement", IEEE Transaction on Electrical Insulation, Vol. 9, pp. 763-808.

- [3] T. S. Ramu, H. N. Nagamani, 2010, “Partial Discharge based Condition Monitoring of High Voltage Equipment”, New Age International Publishers, Delhi.
- [4] C. Abraham, S. V. Kulkarni, January 2009, “FDTD Simulated Propagation of Electromagnetic Pulses due to PD for Transformer Diagnostics”, IEEE Transaction on Dielectric and Electrical Insulation.
- [5] W. Li, S. Su and L. Zhou, “The Deduction of Partial Discharge Pulse Current from Its Radiating UHF Signal”, IEEE Power Engineering Conference, pp. 193-198, January 2005.
- [6] Guide for Electrical Partial Discharge Measurements in compliance to IEC 60270, No. 241, December 2008, Electra 61.
- [7] F. H. Kreuger, “Partial Discharge Detection in High-Voltage Equipment”, London, United Kingdom: Butterworth & Co Ltd.
- [8] A. Taflove and S. Hagness, “Computational Electrodynamics: The Finite Difference Time Domain Method”, Artech House.
- [9] M. Sullivan, “Electromagnetic Simulation using FDTD Method”, New York: IEEE Press.

A STUDY ON PRODUCT RELATED FACTORS INFLUENCING DECISION OF CUSTOMERS PURCHASING LIFE INSURANCE PRODUCT IN GUJARAT

Prof. Jaideepsingh H Jetawat^a, Dr. Snehalkumar H. Mistry^b

Gandinagar Institute of Technology, Gnadhinagar, India

^bC.K. Pithawalla Institute of Management, Surat, Gujarat, India

Abstract

The aim of this study was to identify the factors influencing the purchase decision of customers while selecting life insurance products. Thus an attempt has been made to study the customer buying behaviour with a focus on product related factors affecting the customers' preferences while selecting life Insurance product. Many life insurance products related variables were identified from previous studies and respondents of Gujarat state were queried about the product variables which strongly influence their purchase decision. Founded Variables were reduced through factor analysis to find out most influential variables and its importance on purchase decision. Findings reveal that return, customer needs, sum assured, customer awareness about products and Liquidity options are some of the products related factors that drastically influence the choice of any life insurance product.

Keywords: Consumer Behaviour, Consumer preference, Life insurance, Purchase decision.

1. INTRODUCTION

Insurance industry helps societies by two ways, on one side it helps sufferer of losses by overcoming their economical perils and on other side it provide fuel to economical development of nations through long term investment of funds collected in form of premium from customers. Life Insurance contract is a contract where by the insurer inconsideration of premium paid either in lump sum or in periodical instalments undertakes to pay annuity or a certain sum of money either on the death of insured or on expiry of a certain numbers of years. Thus goal of life insurance is to provide a measure of financial security for the family after the person who passed away. So, before purchasing a life insurance policy, one should consider financial situation and the standard of living he or she wants to maintain for his dependents or survivors.

The principles which are applicable to life insurance are as follows:

- Principles of Utmost Good faith
- Insurable interest

1.1 History of life insurance in India

In India, insurance has a deep-rooted history. It finds mention in the writings of Manu (Manusmriti), Yagnavalkya (Dharmasastra) and Kautilya (Arthasastra). The writings talk in terms of pooling of resources that could be re-distributed in times of calamities such as fire, floods, epidemics and famine.

1818 saw the advent of life insurance business in India with the establishment of the Oriental Life Insurance Company in Calcutta. This Company however failed in 1834. In 1829, the Madras Equitable had begun transacting life insurance business in the Madras Presidency. 1870 saw the enactment of the British Insurance Act and in the last three decades of the nineteenth century, the Bombay Mutual (1871), Oriental (1874) and Empire of India (1897) were started in the Bombay Residency. This era, however, was dominated by foreign insurance offices which did good business in India, namely Albert Life Assurance, Royal Insurance, Liverpool and London Globe Insurance and the Indian offices were up for hard competition from the foreign companies.

In 1914, the Government of India started publishing returns of Insurance Companies in India. The Indian Life Assurance Companies Act, 1912 was the first statutory measure to regulate life Insurance business. In 1928, the Indian Insurance Companies Act was enacted to enable the Government to collect statistical information about both life and non-life business transacted in India by Indian and foreign insurers including provident insurance societies. In 1938, with a view to protecting the interest of the public, the earlier legislation was consolidated and amended by the Insurance Act, 1938 with comprehensive provisions for effective control over the activities of insurers. The Insurance Amendment Act of 1950 abolished principal agencies. However, there were a large number of insurance companies and the level of competition was high. There were also allegations of unfair trade

practices. The Government of India, therefore, decided to nationalize insurance business.

An Ordinance was issued on 19th January, 1956 nationalizing the Life Insurance sector and Life Insurance Corporation came into existence in the same year. The LIC absorbed 154 Indian, 16 non-Indian insurers as also 75 provident societies—245 Indian and foreign insurers in all. The LIC had monopoly till the late 90s when the Insurance sector was reopened to the private sector.

The IRDA opened up the market in August 2000 with the invitation for application for registrations. Foreign companies were allowed ownership of up to 26% which may be increased to 49% probably in future. The Authority has the power to frame regulations under Section 114A of the Insurance Act, 1938 and has from 2000 onwards framed various regulations ranging from registration of companies for carrying on insurance business to protection of policyholders’ interests.

Today there are 24 life insurance companies operating in India as on 16th January 2015 as per IRDA Updated list.

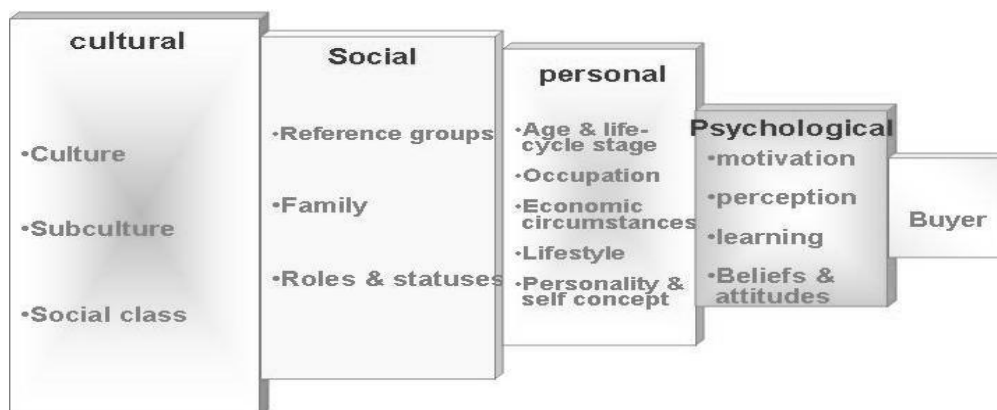
The insurance sector is a colossal one and is growing at a speedy rate of 15-20%. Together with banking services, insurance services add about 7% to the country’s GDP. A well-developed and evolved insurance sector is a boon for economic development as it provides long- term funds for infrastructure development at the same time strengthening the risk taking ability of the country.

1.2 Consumer behavior:

Belch and Belch, (2001) defined consumer behavior as the process and the activities people engage in when searching for, selecting, purchasing, using, evaluating and disposing of products and services so as to satisfy their needs and desires. They found that for many products and services, purchase decision is the result of a long, detailed process while sometime it is more incidental and may result from little more than seeing a product prominently displayed at a discount price in a store.

Schiffmand and Kanuk, (2000) defined consumer behavior as the behavior displayed by consumers in the search for purchasing, evaluating and disposing of products, and services. Consumer behavior is concerned not only with what consumers buy, but how they buy, and how often they buy it.

In simple words Consumer behavior is defined as “all psychological, social & physical behavior of potential customers as they become aware of, evaluate, purchase, consume, & tell others about product & services”.



(a)

Fig.1 (a) Major factors influencing buyer behavior

1.3 Models of consumer behaviour: We have already seen that there are many factors which influence the decision-making of consumers. There are various consumers’ models which help in the understanding of consumer behaviour. These are listed below.

1. Economic Model
2. Psychological Model
3. Pavlovian Model

4. Input, Process Output Model-Gandhi: Philip Kotler
5. Sociological Model
6. HowarthSheth Model
7. Engel-Blackwell-Kollat Model
8. Model of Family Decision-making
9. Nicosia Model
10. A Model of Industrial Buying Behaviour.
11. The Psychoanalytical Model

1.4 Model of consumer decisions making process

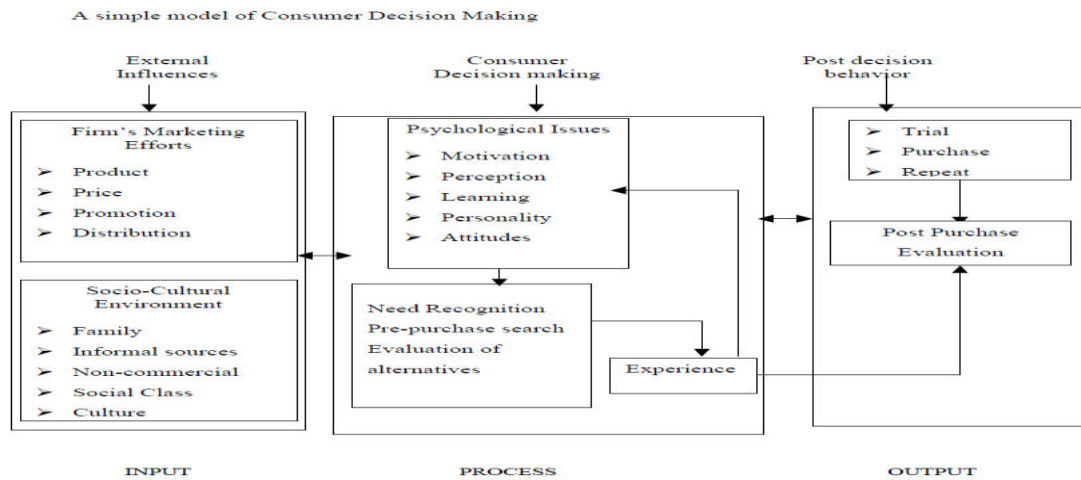


Fig. 2 (a) A simple model of consumer decision making process.(Sources: E-Journal of Business and Economic Issues, Fall 2009, Volume IV Issue III

<http://www.business.subr.edu>)

2. REVIEW OF LITERATURE

J. Stávková, L. Stejskal, Z. Toufarová (2007) analyzed following 14 factors and its impact on consumer behavior : tradition and habit, necessity of need, former experience, recommendation of friends and relatives, recommendation of specialists, products' characteristics and parameters, product or services quality, brand, price, discount action, inspiration by an advertisement, endeavor to try out novelties, fashion trends, and design of product for different product when they purchase Food and non-alcoholic drinks, Alcoholic drinks and tobacco, Clothing and footwear, Health, pharmaceuticals and vitamins, Transport, Post and telecommunications, Recreation and culture need, Education, Boarding and accommodation, Other goods and services, and Housing equipment. Percentages of expenses on different commodity factor are as follow: Housing equipment-6.6% of the expenses per one household's member. Transport- forms 13.5% of the households' expenses. Postage and telecommunication-constitutes 2.8% of the expenses, Boarding and accommodation-9.0% of the consumers 'expenses., Other goods and services-9.9%, Health, pharmaceuticals, vitamins: constitute 3.5% of the expenses per one households member ,Recreation and culture :9.4% of the general expenses and Education presents only 1% from the general households' expenses thus we can see that transportation is major reason for expenses. From above factor major five factors influencing during buying decision are quality, price, former experience, need and product characteristics.

Oriah Akir and Md. Nor Othman (2008) study integrates several dimensions affecting consumer decision making like attributes importance, demographic variables, and interpersonal influence and repurchase intention as well as the possible relationship among variables is developed. The findings revealed that purchasing high involvement products was regarded as a very important decision in comparison to purchasing low involvement products. Second, quality, price, brand name and product information had significant direct relationship on repurchase intention for high involvement products. While for low involvement products, price and brand name significantly predict consumers' repurchase intention.

Huihui Wang (2010) stated that increased levels of income, higher education levels, and demographics (such as family structure and the number of dependent children) were important factors in determining life insurance

demand in China. Consumers with a broader knowledge of life insurance have a higher probability of owning life insurance. Moreover male Chinese consumers are having higher probability to own life insurance than a female.

Soumya Saha and Munmun Dey (2011) found that savings objective of majority of individual investors is 'to provide for purchase of assets' followed by the objectives 'to meet contingencies' and 'tax reduction' for which bank deposits are the most popular savings instrument among individual investors of Kolkata, as they are unique financial products which enable an average salaried person to get a balanced proportion of reasonable returns, along with safety of capital and liquidity. The liquidity provided will help investors meet the contingencies, which is one of their primary objectives of saving. This is followed by life insurance which again ensures safety of the capital along with reasonable returns and also provides tax savings. UTI MF occupies the third position highlighting its growing popularity among retail investors. The other saving instruments are not so popular due to the lack of awareness among investors. In the turbulent market conditions, MFs have been rated as the 'Most Favoured Instrument' followed by bonds and shares. The investors are interested in earning higher return rather than regular safe returns. Investors' need for safety is foremost, followed by good return, liquidity, flexibility, tax benefit, capital appreciation, diversification benefits and professional management. Most influencing sources that investors attach high priority to reference groups, closely followed by published information, thereby preferring newspapers (general and business), and financial magazines prior to their purchase decision. Awareness about MF among respondents is dependent on age and income while independent of gender.

Dharmendra Singh (2011) reveals that product features, accessibility, low premium amount, advertising, proper redressal of complaints and better claim settlement are some of the factors that drastically influence the choice of a company. Most people admitted that their purchase decision was affected by the agents/brokers suggestions and advices of friends. While buying an insurance policy, most important criterion is whether a company is public or private. Older people consider life coverage as the most important reason while youngsters consider tax rebate as most prominent factors. Peoples regard word of mouth as very relevant factors for selecting a company.

Jordan Kjosevski (2012) researched results show that higher GDP per capita, inflation, health expenditure, level of education and rules of law are the most robust predictors of the use of life insurance. Real interest rates, ratio of quasi-money, young dependency ratio, old dependency ratio control of corruption and government effectiveness do not appear to be robustly associated with life insurance demand. Protection and enforcement of property rights will facilitate the demand of life insurance policies.

3. OBJECTIVES OF THE STUDY

- To identify product related factors affecting purchasing decision of customer when purchasing any life insurance product.
- To measure the influence of various product factors on purchase decision of customer and thereby to identify major influencing product factors.

4. RESEARCH METHODOLOGY

The study is Quantitative & descriptive in nature. The researcher adopted this research design to gather information from the respondents to identify major product related factors affecting the preferences and purchase decision of consumers when buying life insurance. The study was conducted with 127 samples from Gujarat state. The sampling method adopted for the study was non-probability convenience where the researcher can select the sample elements based on the ease of researcher. Structured questionnaire was prepared to survey the respondents. The primary data has been collected through a structured questionnaire from the respondents. The secondary data has been collected from the books, journals, magazines, online databases and websites.

With the help of literature reviews of previous studies researcher found out 15 various products related variables which affect the purchase decision of customers when purchasing life insurance products. Factor analysis is done on it to reduce it to manageable number and to identify the most influential variables.

5. RESULTS ANALYSIS & INTERPRETATIONS

Around 85 % that is 108 numbers of the respondents were male and remaining 15 % that is 19 respondents were female and 40% (51 Nos.) were single and 60 % i.e. 76 respondents were married. In this study researchers had focused on income level (per month in INR) of respondents. Respondents having income less than 10000 were 13%, 10001-20,000 were 19% of respondents, 20001-40000 were 42%, 40001-80000 were 19% & above 80000 were 7 % respectively. Education Level of respondent was: 66% of respondents were post graduate, 31% were graduates and only 3% had done higher secondary schooling. Majority of respondent fall in the age group of 21-30 years of age that is 67% and 26% belongs to 31 to 40 years of age. Most of sample was from working class that is 51% were private service peoples, 17% government services and 9% were Business owners.

Table 1. Responses given by respondents

Sr. No	Variables'	Strongly Disagree	Strongly Dis-agree(%)	Disagree	Disagree(%)	Neutral	Neutral(%)	Agree	Agree(%)	Strongly Agree	Strongly Agree(%)
1	Risk coverage	1	0.78740157	3	2.362205	22	17.3228	41	32.28	60	47.24409
2	Return	12	9.4488189	26	20.47244	39	30.7087	27	21.26	23	18.11024
3	Family Safety	0	0	3	2.362205	16	12.5984	35	27.56	73	57.48031
4	Low but gaurranted return	3	2.36220472	14	11.02362	24	18.8976	51	40.16	35	27.55906
5	High but uncertain return	37	29.1338583	48	37.79528	23	18.1102	10	7.874	9	7.086614
6	Customize product(flexi bility)	5	3.93700787	8	6.299213	37	29.1339	51	40.16	26	20.47244
7	Liquidity option	6	4.72440945	10	7.874016	37	29.1339	44	34.65	30	23.62205
8	Product term(duration -short)	25	19.6850394	23	18.11024	27	21.2598	33	25.98	19	14.96063
9	Avalability of loan	21	16.5354331	28	22.04724	29	22.8346	23	18.11	26	20.47244
10	Ownership of firm	7	5.51181102	17	13.38583	29	22.8346	46	36.22	28	22.04724
11	Tax rebate	6	4.72440945	10	7.874016	16	12.5984	45	35.43	50	39.37008
12	Product popularity	17	13.3858268	19	14.96063	23	18.1102	44	34.65	24	18.89764
13	Bonus rate	4	3.1496063	18	14.17323	29	22.8346	42	33.07	34	26.77165
14	Special award by reputed credit agencies	18	14.1732283	26	20.47244	35	27.5591	35	27.56	13	10.23622
15	Future Liabilities	4	3.1496063	7	5.511811	18	14.1732	56	44.09	42	33.07087

5.1 Checking the Reliability of Scale: Cronbach's Alpha Test

		N	%
Cases	Valid	121	88.3
	Excluded ^a	16	11.7
	Total	137	100.0

a. Listwise deletion based on all variables in the procedure.

5.2 Reliability

Cronbach's Alpha	N of Items
.756	15

Here Cronbach's Alfa value is 0.756 which is greater than 0.7 i.e. scale reliability is proved.

6. FACTOR ANALYSIS

6.1 Bartlett's test of sphericity.

Bartlett's test of sphericity is a test statistic used to examine the hypothesis that the variables are uncorrelated in the population. In other words, the population correlation matrix is an identity matrix; each variable correlates perfectly with itself ($r = 1$) but has no correlation with the other variables ($r = 0$).

	Kaiser-Meyer-Olkin Measure of Sampling Adequacy.	.610
Bartlett's Test of Sphericity	Approx. Chi-Square	270.602
	df	105
	Sig.	.000

- Approx. chi-square 270.602, df 105, significance = 0.000
- Kaiser-Meyer-Olkin measure of sampling adequacy = 0.610
- The value of KMO statistic (0.610) is also large (> 0.5).
- So reject null hypothesis and accept alternative hypothesis so here the correlation matrix is not an identity matrix

Hence factor analysis may be considered for analyzing the correlation matrix

Table 5. Correlation Matrix

Variables	Risk coverage	Return	Family safety	low but guaranteed	uncertain but higher return	Customize product	Liquidity options	Short term	Loan availability	Ownership of firm	Tax rebate	Popularity of product	Bonus rate	Special award given by reputed credit agencies	Future liabilities
Risk coverage	1.000	-.096	.273	.246	-.048	.116	.140	-.031	.045	.108	-.128	.044	.078	.012	.132
Return is more important than risk covered	-.096	1.000	-.153	.106	.162	.148	-.072	.190	-.169	-.016	.112	-.026	.303	.126	.017
Family safety is important than return	.273	-.153	1.000	.253	-.067	.185	.142	.038	.122	.165	-.081	-.107	-.029	.027	.127
Low but guaranteed return	.246	.106	.253	1.000	-.214	.315	.171	.248	.035	.144	.158	.094	.307	.101	.258
Uncertain but higher return	-.048	.162	-.067	-.214	1.000	.107	.074	.083	.255	-.024	.036	.141	.058	.254	.047
Customize product	.116	.148	.185	.315	.107	1.000	.063	.091	.085	.070	.081	.123	.332	.141	.173
Liquidity options	.140	-.072	.142	.171	.074	.063	1.000	.042	.218	-.005	.271	.110	.101	.288	.057
Short term	-.031	.190	.038	.248	.083	.091	.042	1.000	.130	.048	.287	.170	.114	.202	-.045
Loan availability	.045	-.169	.122	.035	.255	.085	.218	.130	1.000	.117	.170	.328	.194	.099	.006
Ownership of firm	.108	-.016	.165	.144	-.024	.070	-.005	.048	.117	1.000	.075	.191	.267	.131	.217
Tax rebate	-.128	.112	-.081	.158	.036	.081	.271	.287	.170	.075	1.000	.252	.170	.198	-.008
Popularity of product	.044	-.026	-.107	.094	.141	.123	.110	.170	.328	.191	.252	1.000	.292	.158	-.035
Bonus rate	.078	.303	-.029	.307	.058	.332	.101	.114	.194	.267	.170	.292	1.000	.380	.252
Special award given by reputed credit agencies	.012	.126	.027	.101	.254	.141	.288	.202	.099	.131	.198	.158	.380	1.000	.083
Future liabilities	.132	.017	.127	.258	.047	.173	.057	-.045	.006	.217	-.008	-.035	.252	.083	1.000

- We can't see any very strong relationship between various variables because if the correlation is more than .5 then we can say that there is some strong correlation ship with each other. So from the above matrix we can't judge about the correlation ship of the various factors.

Table 6. Communalities		
	Initial	Extraction
Risk coverage	1.000	.421

Return is more important than risk covered	1.000	.660
Family safety important than return	1.000	.551
Low but guaranteed return	1.000	.700
Uncertain but higher return	1.000	.726
Customize product	1.000	.394
Liquidity options of money	1.000	.577
Short term duration	1.000	.463
Loan availability	1.000	.599
Ownership of firm	1.000	.548
Tax rebate	1.000	.585
Popularity of product	1.000	.617
Bonus rate	1.000	.659
Special award given by reputed credit agencies to that product	1.000	.486
Future liabilities	1.000	.427
Extraction Method: Principal Component Analysis.		

The communalities above measure the percent of variance in a given variable explained by all the factors. That is, the communality is the squared multiple correlation for the variable using the factors as predictors. Communality for a variable is the sum of squared factor loadings for that variable (row), and thus is the percent of variance in a given variable explained by all the factors. For full orthogonal PCA, the communality will be 1.0 and all of the variance in the variables will be explained by all of the factors, which will be as many as there are variables.

In the above communality table we can find that the factors which score more than 0.5 indicates that more than 50% of the variance in that variable are explained by all factors. The variables are as below:

Table : 7 variance found in following variables

Return	Family safety	Low guaranteed return	Uncertain but higher return	For liquidity options of my money
Loan available	Ownership of firm	Tax rebate	Popularity of product	Bonus Rates

6.2 Determine the Number of Factors: Here we determine number of factor on the bases of Eigen value .As per this approach only factors with Eigen values greater than 1.0 are retained. An Eigenvalue represents the amount of variance associated with the factor. Hence, only factors with a variance greater than 1.0 are included. Factors with variance less than 1.0 are no better than a single variable, since, due to standardization, each variable has a variance of 1.0.

The "Total Variance Explained" table below shows the Eigen values, which are the proportion of total variance in all the variables which is accounted for by that factor. A factor's eigenvalue may be computed as the sum of its squared factor loadings for all the variables. A factor's eigenvalue divided by the number of variables (which equals the sum of variances because the variance of a standardized variable equals 1) is the percent of variance in

all the variables which it explains. The ratio of Eigen values is the ratio of explanatory importance of the factors with respect to the variables. If a factor has a low eigenvalue, then it is contributing little to the explanation of variances in the variables and may be ignored as redundant with more important factors. The table shows **15 factors**, one for each variable. However, only the **first five** are extracted for analysis because, under the Extraction options, SPSS was told to extract only factors with Eigen values of 1.0 or higher.

The "Initial Eigen values" and "Extraction Sums of Squared Loadings" columns are the same, except the latter only lists factors which have actually been extracted in the solution. The "Rotation Sums of Squared Loadings" give the Eigen values that shows that for the first factor the eigenvalue decreased while for other factor Eigen values increase it means that the variability explain by other four variables are increased while for the first variable it is decreased. (Researcher used Varimax rotation, which minimizes the number of variables which have high loadings on each given factor). Note that the total percent of variance explained is the same (**see the cumulative value for factor 5 – 56.070%**) but rotation changes the Eigen values for each of the extracted factors. That is, after rotation each extracted factor counts for a different percentage of variance explained, even though the total variance explained is the same.

Component	Initial Eigenvalues			Extraction Sums of Squared Loadings		
	Total	% of Variance	Cumulative %	Total	% of Variance	Cumulative %
1	2.755	18.370	18.370	2.755	18.370	18.370
2	1.805	12.033	30.403	1.805	12.033	30.403
3	1.486	9.906	40.309	1.486	9.906	40.309
4	1.235	8.232	48.541	1.235	8.232	48.541
5	1.129	7.529	56.070	1.129	7.529	56.070
6	.996	6.639	62.709			
7	.901	6.004	68.713			
8	.847	5.646	74.359			
9	.758	5.054	79.413			
10	.675	4.498	83.910			
11	.639	4.261	88.172			
12	.519	3.460	91.632			
13	.492	3.277	94.909			
14	.433	2.888	97.797			
15	.330	2.203	100.000			

Extraction Method: Principal Component Analysis.

Here from the above chart we can say that the first five components have Eigen value of more than 1 and cumulatively they explain the variance of 56.070%

Every consumer have different perception and every individual have different need an expectation so here we can say that this five variable explain more than 57% of the variability which is quite good when talking about the practical scenario and in this type of product.

Now to find out various factors and to find out which are the variables can be combined in one factor we need rotated component metrics.

Table 9. Rotated Component Matrix^a

	Component				
	1	2	3	4	5
Bonus rate	.715				
Future liabilities	.563				
Customize product	.557				
Return is more important than risk	.512		-.423	-.372	
Low but guaranteed return	.489	.430	.417		-.319
Tax rebate		.724			
Short term duration		.669			
Family safety than return			.733		
Risk coverage			.605		
Liquidity options		.414	.494		.384
Popularity of product				.711	
Loan availability				.628	.362
Ownership of firm	.407			.569	
Product which provide Uncertain but higher return					.825
Special award given by reputed credit agencies to that product	.319				.536

Extraction Method: Principal Component Analysis.

Rotation Method: Varimax with Kaiser Normalization.

a. Rotation converged in 11 iterations.

Table 10: Factorization of variables

Factor 1	Factor 2	Factor 3	Factor 4	Factor 5
Guaranteed return	Short term maturity	Risk coverage		Uncertain but high return
Customize product	Tax rebate	Family safety	Ownership of firm	Liquidity option of money
Bonus rates			Popularity of product	Availability of loan on product
Future liability of purchaser				Special award given by rating agency
Low but Fixed return				
Return	Customer needs	Sum Assured	Customer awareness	Liquidity options

Above are the five major factors which identified by factor analysis and on the basis of which fifteen variables can be reduced to 5 major factors.

7. CONCLUSION

The study helped in understanding the consumer buying decision process, thereby answering the questions ‘why’ and ‘how’ a customer buys life insurance product and following conclusions can be drawn:

It was found that the most important reason, why a customer buys an insurance product is their own need, return they get, sum assured they receives, customer awareness about the products and Liquidity options of their money. Other product features like tax rebate, duration of maturity, and their future liability can be strongly considered as determining factors for selection of particular life insurance product.

8. LIMITATIONS

This study was carried out in Gujarat; therefore, the results obtained may not be pertinent to the country as a whole. However study can be extended to other states of India. Secondly, the present study has been conducted by taking a sample of 127 respondents hence cannot lead to the generalizability of the findings and the results may not be implied conclusively to the whole country. Additional studies are recommended to fill this gap. Thirdly, in the current study, exploratory factor analysis using principal component method with varimax rotation has been used. Moreover, the results of this study may further be validated by employing confirmatory factor analysis technique. The respondents responses are assumed to be true and without any biasness.

REFERENCES

- Journal articles:

- [1] J. Stávková, L. Stejskal, Z. Toufarová (2007),” Factors influencing consumer behaviour”. <http://www.agriculturejournals.cz/publicFiles/01585.pdf>
- [2] Kanwal Garg and Dr. Pankaj Garg paper Published on topic “Factors Influencing for Investment Decision in Life Insurance Sector through PCA- a Statistical Data Mining Technique”. *Assst. Professor, MMICT & BM, M.M. University, Mullana (Ambala), E-mail id: gargkanwal@yahoo.com, gargpankaj107@gmail.com

- [3] Mohd Nor A. and Muhamad A. (2005),” Individual Factors that Predict Customer-Orientation Behaviour of Malaysian Life Insurance Agents”, *Jurnal Pengurusan* 24, pp 125-149.
- [4] Penetration, *Geneva Papers on Risk and Insurance*, 25(3): 396-406.
- [5] Raj Kumari, M. (2007), "A Study on Customers Preference Towards Insurance Services and Bancassurance", *The ICFAI Journal of Risk and Insurance* Vol. IV, No. 2, pp. 49-59.
- [6] Saha S. and Dey M. (2011),” Analysis of Factors Affecting Investors’ Perception of Mutual Fund Investment”, *The IUP Journal of Management Research*, Vol. X, No. 2, pp.23-44
- [7] Soo, Hak Hong (1996), *Life Insurance and Economic Growth: Theoretical and Empirical Investigation* University of Nebraska: Dissertation
- [8] Singh D., (2011),” Factors Affecting Customers’ Preferences for Life Insurers: An Empirical Study”, *The IUP Journal of Risk & Insurance*, Vol. VIII, No. 2.

- Websites:

- [1] http://en.wikipedia.org/wiki/Life_insurance
- [2] www.licindia.in/
- [3] www.irda.gov.in/ADMINCMS/cms/NormalData_Layout.aspx?page=PageNo129&mid=3.1.9_ accessed on 16/01/2015
- [3] www.oppapers.com/essays/Insurance-In-2020/294984
- [4] www.an-insurance-agents-career.com/Discussing-the-life-insurance-Sales-Process.html
- [5] <http://shodhganga.inflibnet.ac.in/visual/index.htm#India>
- [6] http://www.bimabazaar.com/index.php?option=com_content&view=section&id=19&Itemid=70
- [7] <http://gnionline.org/download/pdfresearchprojects/study%20of%20consumer%e2%80%99s%20perception%20on%20life%20insurance%20policies.pdf>
- [8] <http://www.business.subr.edu>

Personality and Career Success

Asst. Prof. Nirupama Patel

Gandinagar Institute of Technology, Gnadhinagar, India

Abstract

The relationship between personality and career success has provoked a great deal of speculation. It has often been asserted that achievement (especially in capitalist economies) can be explained largely by factors such as individual initiative, effort, and merit. Personality is probably a significant determinant of how people will do in their careers. At the same time, luck and institutional factors—such as privilege or inheritance—may influence career success in a way that would attenuate the relationship with personality significantly. Empirical research identified several categories of explanations for career success and found that research has generally favored institutional explanations over individual explanations. Whereas the most commonly investigated influences were demographic (age, sex, marital status, number of children) and human capital (training, work experience, education), researchers have increasingly investigated the possible role of personality in explaining career success. Below, we discuss the dispositional factors that have been related to career success in past research. Before doing so, however, it is important to discuss what we mean by career success and to discuss an organizing framework for our discussion of trait influences on career success.

Keywords: Personality; career; research.

1. DEFINITION OF CAREER SUCCESS

Career success can be defined as the real or perceived achievements individuals have accumulated as a result of their work experiences. Most research has divided career success into extrinsic and intrinsic components. Extrinsic success is relatively objective and observable and typically consists of highly tangible outcomes such as pay and ascendancy [1]. Conversely, intrinsic success is defined as individuals' subjective appraisal of their success and is most commonly expressed in terms of job, career, or life satisfaction. Research confirms the idea that extrinsic and intrinsic career success can be assessed as relatively independent outcomes, as they are only moderately correlated [2]. The three criteria most commonly used to index extrinsic career success are (a) salary or income, (b) ascendancy or number of promotions, and (c) occupational status. The last factor is perhaps the most intriguing. Occupational status can be viewed as a reflection of societal perceptions of the power and authority afforded by the job. Occupational status has long been studied in sociology as a measure of occupational stratification. Sociologists have gone so far as to conclude that occupational status measures "reflect the classical sociological hypothesis that occupational status constitutes the single most important dimension in social interaction" [3] and to term occupational status as sociology's "great empirical invariant" [4]. The required educational skills, the potential extrinsic rewards offered by the occupation, and the ability to contribute to society through work performance are the most important contributors to occupational status. As a result, sociologists often view occupational status as the most important sign of success in contemporary society. Viewed from this perspective, occupational status indicates extrinsic success because of its prestige and because it conveys increased job-related responsibilities and rewards. Intrinsic career success is measured in several distinct ways. The most common marker for intrinsic career success is a subjective rating of one's satisfaction with one's career. Items that fit under the career satisfaction umbrella ask respondents to directly indicate how they feel about their careers in general, whether they believe that they have accomplished the things that they want to in their careers or if they believe that their future prospects in their careers are good. Job satisfaction is often closely related to career satisfaction, but there are some important differences. Particularly, job satisfaction usually is directed around one's immediate emotional reactions to one's current job, whereas career satisfaction is a broader reflection of one's satisfaction with both past and future work history taken as a whole.

2. WHY DOES PERSONALITY AFFECT CAREER SUCCESS?

Starting from the premise that personality can be related to numerous work-relevant outcomes, it is worth considering how personality traits might have an effect on careers. We first propose that personality leads individuals to possess certain jobs both through the process of attraction to the jobs of interest as well as by leading organizations to select certain individuals. Personality also influences individual performance on the job in a way that will lead to higher compensation, new job responsibilities, and promotions into higher organizational ranks. Finally, personality influences the ways in which individuals engage in social interactions at work. Social

interactions can lead to any number of outcomes, ranging from improved knowledge of the job and role to more visibility in the organization. These factors combine, in turn, to predict the job features individuals encounter on the job, including both extrinsic and intrinsic features known to predict job satisfaction. The static nature of this model is a simplification, because it is likely that there would be multiple non recursive links (e.g., over time, job features affect social behavior, career success affects job features), but we present this simplified model because there is not sufficient research to discuss these reciprocal relationships at the present time and our model is based on extant empirical results. To demonstrate the relevance of this model, it is first necessary to determine if there is in fact a relationship between personality and career success to explain in the first place.

3. FIVE-FACTOR MODEL

Consensus is emerging that an FFM of personality can be used to describe the most salient aspects of personality. The first researchers to replicate the five factor structure were Norman and Tupes and Christal (1961), both of whom are generally credited with founding the FFM. The five-factor structure has been recaptured through analyses of trait adjectives in various languages, factor analytic studies of existing personality inventories, and decisions regarding the dimensionality of existing measures made by expert judges [5]. The cross-cultural generalizability of the five-factor structure has been established through research in many countries. Evidence indicates that the Big Five are substantially heritable and stable over time. The dimensions comprising the FFM are emotional stability, extroversion, openness to experience, agreeableness, and conscientiousness. Emotional stability represents the tendency to exhibit positive emotional adjustment and seldom experience negative effects such as anxiety, insecurity, and hostility. Extroversion represents the tendency to be sociable, assertive, and active and to experience positive effects such as energy and zeal. Openness to experience is the disposition to be imaginative, nonconforming, unconventional, and autonomous. Agreeableness is the tendency to be trusting, compliant, caring, and gentle. Conscientiousness comprises two related facets, achievement and dependability. The Big Five traits have been found to be relevant to many aspects of life, such as interpersonal relations and even longevity. As we will see, these traits are also relevant to several aspects of career success. We will also discuss other personality traits that might be relevant for career success where relevant research exists.

Below, is the review of the literature on the relationship of the Big Five to aggregate career success, with the review organized according to each of the Big Five traits. Within each trait, we first discuss the link between the trait and intrinsic success, followed by a discussion of the link between the trait and extrinsic success.

3.1 *Conscientiousness*

In general, conscientiousness is positively correlated with measures of intrinsic career success, though the multivariate evidence is far less consistent. Meta-analytic evidence indicates that conscientiousness is positively associated with job and life satisfaction[6]. Conscientiousness strongly predicted intrinsic success, even when personality was measured during childhood and the latter variables were measured in mid adulthood. On the other hand, several studies have found limited incremental validity of conscientiousness in predicting career success with a multivariate design. Though evidence suggests that the vicariate relationship between conscientiousness and indices of intrinsic career success is positive. This relationship tends to deteriorate and becomes less consistent when the influence of the other Big Five traits is taken into account. Conscientiousness is theoretically linked to extrinsic career success most strongly through the achievement orientation of conscientious persons. Conscientiousness also seems to enable persons to obtain promotions into more complex and prestigious jobs. A consistent finding from the assessment center literature is that ratings of achievement orientation effectively predict promotions. In sum, it appears that the multivariate results on the relationship between conscientiousness and intrinsic and extrinsic success are far from consistent. There is a trend for the relationship to be positive in both cases, but in general, the results vary from moderately strong and positive to quite weak.

3.2 *Emotional Stability*

Evidence generally indicates that emotional stability is positively associated with intrinsic career success or, equivalently, that neuroticism is negatively associated with intrinsic career success. Meta-analytic evidence reliably indicates that those who score high on emotional stability are more satisfied with their jobs and lives. It is found that emotionally stable individuals were more satisfied with their careers. Emotional stability positively predicted career satisfaction. It has been found that emotional stability failed to predict subjective career success. Here again, the results are somewhat inconsistent, but in general, emotional stability appears to be negatively related to intrinsic career success. Although not quite as consistent, evidence also indicates a positive relationship between emotional stability and extrinsic career success. In sum, evidence indicates that emotional stability is positively related to intrinsic and extrinsic career success. The former results are more consistent than the latter, though both sets of results show inconsistency when the influence of the other Big Five traits is taken into account.

3.3 *Extroversion*

In general, extroversion is positively associated with intrinsic career success. Extroversion is closely linked to positive emotionality, which in turn expresses itself in positive moods, greater social activity, and more rewarding interpersonal experiences. Meta-analytic evidence indicates that extroverts report higher levels of job and life. Extroversion failed to predict subjective career success. Thus, in general, it appears that extroversion is positively related to intrinsic career success, though the results are not fully consistent. Extroversion and its facets appear to be positively related to extrinsic career success. The measures of dominance and sociability differentiated successful and unsuccessful executives when pay and job title were considered as indices of success. Extroversion was also predictive of salary and job level in two recent studies conducted in the United Kingdom. Well-controlled longitudinal studies also have supported a link between extroversion and extrinsic success. Thus, extroversion tends to be positively related to intrinsic as well as extrinsic career success. The results are not totally consistent, as one would expect based on data from multiple samples. However, the majority of the evidence suggests that extroverts are more extrinsically successful in their careers and more satisfied with them as well.

3.4 *Openness to Experience*

Openness displays an inconsistent relationship with career success. Judging from the meta-analytic evidence, the association of openness with job satisfaction is weak and variable. Big Five traits and intelligence were taken into account. Openness failed to predict subjective career success. Thus, it appears that openness bears little consistent relationship with intrinsic or extrinsic career success.

3.5 *Agreeableness*

Evidence tends to indicate a relatively modest but positive relationship between agreeableness and job satisfaction. However, the relationship appears to disappear once adjusted for the influence of the other Big Five traits. Agreeableness was unrelated to any measure of intrinsic career success. Agreeableness negatively predicted career satisfaction, though the effect size was rather small. What is more intriguing is that agreeableness appears to be negatively related to extrinsic career success. Thus, it appears that agreeableness is unrelated to intrinsic career success but negatively related to extrinsic career success.

3.6 *Proactive Personality*

Proactive personality is positively associated with employee creativity and employee creativity is positively associated with career satisfaction and perceived insider status. In addition, employee creativity fully mediated the relationships between proactive personality and career satisfaction and perceived insider status.

3.7 *Core Self-Evaluations*

Core self-evaluations (CSEs) are a relatively recent addition to the personality literature. CSEs are a set of closely linked traits that include emotional stability, an internal locus of control, self-esteem, and self-efficacy. Those higher in CSEs tend to appraise situations more positively, have higher levels of motivation, and have greater confidence in their ability to positively influence the world around them. We are aware of no research that has explicitly linked CSEs to career success. However, beyond the emotional stability evidence reviewed above, evidence has linked the other core traits to career success. Because CSEs may be somewhat more malleable than most traits [7], it is possible that career success causes one to have a positive self-concept.

4. MEDIATORS OF THE PERSONALITY/CAREER-SUCCESS RELATIONSHIP

Given the evidence that personality is at least sometimes related to career success, it is worth considering why personality traits might lead to superior career outcomes. It will become clear in this section that these relationships are necessarily tenuous because of the conceptual distance from personality as an internal trait to final measures of career success. The stages of the mediating model considered next are as follows: (a) personality leads individuals to possess certain jobs, (b) personality also influences individual performance on the job, and (c) personality influences the ways in which individuals engage in social interactions at work. These factors are proposed to combine to predict the extrinsic and intrinsic features known to predict job and career satisfaction.

4.1 *Personality and Jobs Held*

One mechanism that might lead to a relationship between personality and career success is the effect of personality on the types of jobs that individuals might acquire. These relationships can be broadly divided into the effects of personality on job preferences and the ways in which personality can lead an individual to be considered desirable by employers. In other words, personality can influence what you want as well as what you can get. The

dominant paradigm in the literature on personality and job preferences comes from the long-established program of research on the realistic-investigative-artistic-social-enterprising conventional circumplex. The basic proposition is that there are stable individual differences in preferences for job characteristics and that individuals who are in jobs that match their preferences will be more satisfied. Openness to experience correlates fairly strongly with the artistic type and the investigative type, and extroversion correlates fairly strongly with the enterprising type and the social type. The relationship between personality traits and success in the selection process has been explored in several studies. As will be shown later, personality has been related to job performance, so it makes sense that employers might well prefer certain “types” of individuals based on their impressions of who will do best on the job. In a study examining interviewers’ perceptions of applicants’ “fit” with their organization, the two most predictive variables after general employability was factored out were interpersonal behaviors such as listening and warmth and goal orientation characteristics, such as having goals and plan. Interviewers also perceive that conscientiousness is a significant predictor of hirability across multiple job types and that counterproductive behavior can be predicted by emotional stability, conscientiousness, and agreeableness. Not all interview types are equally affected by personality traits. Some research has suggested that success in situational interviews is less related to extroversion than success in behavioral interviews. Another reason why personality might influence interview success is because of the behaviors associated with different personality traits. An increasing number of studies have suggested that impression management is an important component of interview success. Given the meta-analytic evidence suggesting that impression management is, at best, weakly related to job performance, it appears that the tendency for interviewers to favor the extroverted and, in particular, the immodest extroverted is an error in judgment. The results to date suggest that conscientiousness and extroversion are the dimensions of personality that are most related to success in the screening process. This is interesting in light of the generally positive relationships between these personality traits and career success. Research also suggests that interviewers deliberately try to select conscientious individuals in the hope of obtaining better performance on the job, whereas extroverts are able to improve their success through social influence. As we will see, the linkage of extroversion with social behavior and conscientiousness with performance appears in other areas as well.

4.2 Personality and Job Performance

The relationship between personality and job performance has received a huge amount of attention. Seminal meta-analyses demonstrated that there were consistent relationships between the trait of conscientiousness and job performance across a number of jobs, while other personality traits were not associated with performance. Subsequent studies have generally confirmed this result when more specific measures of the FFM are used [9]; when specific occupations such as sales are examined; when data are collected exclusively among the European community or when specific dimensions of performance, such as citizenship performance, or counter productivity are the focus. More recent research has shown that the trait of CSEs is also related to job performance and, moreover, that this trait shows incremental validity in predicting job performance beyond the FFM of personality. A study of 91 sales representatives demonstrated that conscientiousness leads employees to set goals to be more committed to these goals. Goal setting was related to sales volume and performance ratings, and goal commitment was related to sales volume and performance ratings. An alternative, but conceptually related, model of personality and performance was examined in a study of 164 sales agents [10]. In this study, conscientiousness was related to accomplishment striving and extroversion was related to status striving; accomplishment striving was related to status striving, which was related to job performance.

4.3 Personality and Social Ties

The established paradigms proposing that career success is largely a matter of individual initiative, choice, and effort on the job have been supplemented more recently by research demonstrating that careers are made by social ties as well. Individuals with superior positions in social networks are able to achieve superior work outcomes, including access to information, access to resources, and career sponsorship which showed that career success was greater among individuals who fill a “structural hole,” meaning that they were a crucial intermediary between groups of individuals who otherwise have little contact. The core variables that are studied in the social domain of personality at work include measures of relationship building, knowledge of the political domain of the organization, and efforts to actively understand which behaviors are rewarded. A longitudinal study of the FFM of personality and proactive adjustment among organizational newcomers found that extroversion was significantly related to seeking feedback and building relationships with colleagues, while openness to experience was related to feedback seeking. Relationship building was related, in turn, to social integration, role clarity, and job satisfaction and negatively related to intention to turnover, while feedback seeking was positively related to job satisfaction and negatively related to turnover. Proactive personality has also been investigated in this domain. One study involving 180 employees found that proactive personality was significantly related to political knowledge and career initiative on the job, both of which were positively related to subsequent salary progression and subjective perceptions of career satisfaction. A longitudinal examination involving organizational newcomers found that proactivity was associated with greater role clarity, work group integration, and political knowledge.

Commitment was found to be higher among those with greater role clarity and work group integration, but political knowledge was not significantly related to any markers of newcomer adjustment. The relationship between lower-level employees and more experienced, powerful members of an organization has been of significant interest in the careers literature. Some research suggests that protégés have an important role in initiating relationships. Initiation of relationships was positively related to internal locus of control, self-monitoring, and emotional stability; initiation was positively related to having mentoring relationships, and these mentoring relationships were positively related to career attainment and perceived career success. Research in a similar strain involving 184 early-career-stage Hong Kong Chinese has shown that extroversion leads to protégé-initiated mentoring relationships.. Unfortunately, because of the co relational nature of these studies, it is difficult to assess causality in any meaningful way. Some studies have suggested, using essentially the same methodology, that having a mentor can increase self-esteem, need for achievement, and need for dominance. In sum, the research suggests that individuals who are extroverted are likely to have positive social relationships, which may again serve as a potential mediator of extroversion and career success. Proclivity's effect on career success may also be explained by social relationships. Given the close relationship between extroversion and proclivity, future research should attempt to examine whether one of these variables is the more immediate explanation for career success through social connections.

5. PERSONALITY AND JOB FEATURES

Researchers have long proposed that there is an important relationship between personality and job features.. One of the most controversial areas for research in the study of personality at work is the role of negative affectivity or neuroticism in perceptions of job characteristics. Personality shapes the subjective perception of job characteristics, which in turn leads to lower career satisfaction. Research has also shown that employee perceptions of appropriate emotional displays at work are predicted based on employee extroversion and neuroticism, with extroversion being related to perceptions that jobs demand more positive emotional displays and neuroticism being related to perceptions that jobs demand more suppression of negative emotional displays. Perceptions of demands for positive emotional displays were associated with higher job satisfaction, while perceptions of demands for suppression of negative emotional displays were associated with lower job satisfaction. There is evidence beyond simple negative affectivity related to job characteristics. This relationship is at least partially due to the influence of emotional stability described earlier, but it also incorporates the more motivationally loaded traits of self-esteem, self-efficacy, and locus of control. This study also further supports the idea that personality can have a direct effect on objective job characteristics. To determine if personality characteristics act as a cause or effect of employee reactions, researchers must find ways to move beyond simple co relational designs. One way to approach this problem comes from a two-wave panel study of bank employees and teachers, in which growth needs, strength and upward striving were measured at multiple points in time. In sum, the research on personality and job characteristics suggests that there is a complex relationship that involves personality shaping selection into certain jobs and certain jobs leading to changes in personality. The evidence generally suggests that neuroticism is likely to result in lower levels of actual and perceived job characteristics, which can explain at least Personality and Career Success

6. CONCLUSION

The literature on personality and career success has received increased attention over the years. It may be a surprise to many readers that the effect sizes are relatively modest and the results relatively inconsistent. This does not mean, of course, that the effect sizes are zero. Indeed, four of the Big Five traits appear to bear some relation to either extrinsic or intrinsic career success, with conscientiousness and extraversion being associated with slightly higher levels of extrinsic and intrinsic career success and neuroticism and agreeableness being associated with slightly lower levels of career success. Beyond providing an appraisal of the effects of personality and career success, we sought to review evidence on why personality is related to career success. We reviewed evidence on various mediators of the relationship between personality and career success. We also discussed the linkage between personality and job features, as well as dispositional and situational factors that moderate the personality/career-success relationship. Although research on personality and career success has come a long way in the past 20 years, there is considerable room for further development. Below, we outline a few areas that especially require further study.

6.1 *Need for Careful Research Design*

Researchers have tended to rely frequently on the use of data gathered at a single point in time to measure the influence of personality on career success. While such designs have shown a considerable correlation between personality traits and career outcomes, several of the studies we reviewed here suggest that conclusions from such

studies could be potentially spurious. Moreover, the debate regarding negative affectivity and career outcomes clearly suggests that researchers can be most informative when they make an effort to eliminate alternative explanations for observed correlations.

6.2 Inclusion of Work-Family Balance as an Outcome

Because men and women are increasingly occupying the dual roles of breadwinner and homemaker, the issue of work-family conflict has become more prominent. The issue of work-family balance is conspicuously absent from the literature on personality and career success, however. Do certain personalities emphasize work over family, or the converse? Are some personalities able to better balance work and family demands than others? Is the fit between work and family contingent on personality? Does the balance between work and family demands evolve over time based on personality?

6.4 Moderators

Although we reviewed various moderators of the personality/career-success relationship, other moderators need to be investigated. Some areas for future analysis include family status and industry characteristics. In the personality/jobperformance literature, more systematic progress has been made on the moderator front, including investigations of the situational and dispositional moderators. Some of these moderators should be investigated in the context of career success, and others are undoubtedly worthy of consideration as well.

6.5 Other Traits

Although traits beyond the FFM have been investigated, we have only scratched the surface of traits that might prove useful. Examination of the lower-order facets of the FFM might prove especially fruitful. In sum, although considerable advances have been made in our understanding of the dispositional basis of career success, further development is needed. In particular, there is a need to investigate factors that explain the relatively modest and apparently inconsistent results. Process models that investigate mediation will contribute to our understanding of the specific mechanisms by which personality leads to career success; examples of mediators in the current literature include task motivation, social interactions, and goal setting. Studies should also make a greater effort to investigate some of the ways in which personality interacts with the environment to produce career success by studying the ways in which traits moderate the effect of situations and situations moderate the effects of traits.

References

- [1] Jaskolka, G., Beyer, J. M., & Trice, H. M. (1985). Measuring and predicting managerial success. *Journal of Vocational Behavior*, 26, pp.189–205.
- [2] Judge, T. A., & Bretz, R. D. (1994). Political influence behavior and career success. *Journal of Management*, 20, pp. 43–65.
- [3] Ganzeboom, H. B. G., & Treiman, D. J. (1996). Internationally comparable measures of occupational status for the 1988 International Standard Classification of Occupations. *Social Science Research*, 25, pp. 201–239.
- [4] Featherman, D. L., Jones, F. L., & Hauser, R. M. (1975). Assumptions of social mobility research in the U.S.: The case of occupational status. *Social Science Research*, 4, pp.329–360.
- [5] McCrae, R. R., & John, O. P. (1992). An introduction to the five-factor model and its applications. *Journal of Personality*, 2, pp.175–215.
- [6] Judge, T. A., Heller, D., & Mount, M. K. (2002). Five-factor model of personality and job satisfaction: A meta-analysis. *Journal of Applied Psychology*, 87, pp.530–541.
- [7] Bono, J. E., & Judge, T. A. (2003). Core selfevaluations: A review of the trait and its role in job satisfaction and job performance. *European Journal of Personality*, 17, pp. S5–S18.
- [8] Hunter, J. E., & Schmidt, F. L. (1990). *Methods of meta-analysis: Correcting error and bias in research findings*. Newbury Park, CA: Sage.
- [9] Hertz, G. M., & Donovan, J. J. (2000). Personality and job performance: The Big Five revisited. *Journal of Applied Psychology*, 85, pp. 869–879.
- [10] Barrick, M. R., Stewart, G. L., & Piotrowski, M. (2002). Personality and job performance: Test of the mediating effects of motivation among sales representatives. *Journal of Applied Psychology*, 87, pp. 43–51.

Study of Pressure Dependence of The Superconducting State Parameters of Ga, Cd and Sn Using Parameter Free Pseudopotential

Priyank Kumar^a, N. K. Bhatt^b, P. R. Vyas^c

^aGovernment Polytechnic, Gandhinagar-382024, Gujarat, India

^bS. P. University, Vallabh Vidyanagar-388120, Gujarat, India

^cGujarat University, Ahmedabad-380009, Gujarat, India

Abstract

Theoretical investigation of superconducting state parameters (SSP), viz. electron-phonon coupling strength (λ), Coulomb pseudopotential (μ^*), superconducting transition temperature (T_c), effective interaction strength (N_0V) and isotopic effect parameter (α) and their pressure dependence for gallium (Ga), cadmium (Cd), and tin (Sn) have been carried out in the BCS-Eliashberg-McMillan framework by using parameter free form of Ashcroft's empty core (AEC) pseudo potential. The variation of Debye temperature has been considered by using Gruneisen model. Critical volumes for Ga, Cd and Sn at which $\lambda = \mu^*$, where T_c and N_0V becomes zero have been predicted. Computed results of SSP and critical volumes are in good agreement with other reported values.

Keywords: Superconductors, superconducting state parameters, pressure dependence, critical volume, pseudopotential.

Introduction

There are two main aspects to understand phenomenon of superconductivity, firstly to understand the material properties like, electron-phonon coupling strength (λ), the coulomb pseudopotential (μ^*), and average phonon frequency and secondly to calculate superconducting transition temperature (T_c) as a function of λ , μ^* and average phonon frequency. The well established BCS-Eliashberg McMillan formalism has been used to compute SSP of metals [1-11], alloys [12-13] and metallic glasses [14-16] by many researchers in recent years and past. But study of pressure dependence of SSP are scattered. Few such theoretical [17-21] and experimental [22-24] study regarding pressure dependence of T_c are reported by different researchers. Many researchers have adjusted pseudopotential parameter with some observed physical properties to study SSP which is not be extended for the comprehensive and unified study of physical properties of metals, alloys and glasses .

Superconductivity at high pressure has attracted considerable interest in the identification of new materials and in the understanding of mechanism of high pressure superconductivity. Main problem associated with effect of compression is that whether pressure and hence compression reduces T_c of superconductors to zero i.e. superconductivity quenches without changing crystal structure i.e. whether superconductivity can be destroyed in that range of pressure where there are no first – order phase transition [25].

Validity of any theoretical model can be tested with its capability to predict the changes in the lattice parameter in the normal state and superconducting state. In the present communication, SSP and their pressure dependence have been studied by using parameter free form of well known Ashcroft's empty core (AEC) pseudopotential.

Theory

The electron phonon coupling strength (λ) is given by [9]

$$\lambda = \frac{12m^* Z \hbar^2}{16M K_B \Theta_D^2} \int_0^{\frac{q}{k_f}} x^3 |V(x)|^2 dx \quad (1)$$

Where m^* is specific heat mass, Z is valency, M is ionic mass, K_B is Boltzmaan constant, Θ_D is Debye temperature at 0^0K and $x = q/k_f$, k_f is Fermi momentum.

Where

$$V(q) = \frac{V_{ion}(q)}{\epsilon(q)} \tag{2}$$

Where $V_{ion}(q)$ is the Ashcroft’s empty core (AEC) pseudopotential [26] and $\epsilon(q)$ is dielectric function with Taylor’s exchange and correlation function [27]. The pseudopotential contains single parameter r_c (core radius) which is determined using relation given in reference [28].

The Coulomb pseudopotential (μ^*) is given by [1]

$$\mu^* = \frac{\mu}{1 + \mu \ln \left(\frac{E_f}{K_B \theta_D} \right)} \tag{3}$$

Where E_f is Fermi energy and μ is given by [9]

$$\mu = \frac{m_b}{\pi k_f} \int_0^2 \frac{dx}{x \epsilon(x)}$$

Where $\epsilon(x)$ is screening dielectric function. m_b is band structure density of mass at Fermi surface. We have computed m_b using following equation [6].

$$m^* = m_b (1 + \lambda) \tag{4}$$

The superconducting transition temperature, T_c is given by [9]

$$T_c = \frac{\theta_D}{1.4} \exp \left[- \left\{ \frac{1.04(1 + \lambda)}{\lambda - \mu^*(1 + 0.62\lambda)} \right\} \right] \tag{5}$$

The effective interaction strength (N_0V) is given by [9]

$$N_0V = \frac{\lambda - \mu^*}{1 + \frac{10}{11} \lambda} \tag{6}$$

The isotopic effect parameter (α) is given by [9]

$$\alpha = \frac{1}{2} \left[1 - \left(\mu^* \ln \frac{\theta_D}{1.45 T_c} \right)^2 \frac{1 + 0.62\lambda}{1.04(1 + \lambda)} \right] \tag{7}$$

Result and Discussion

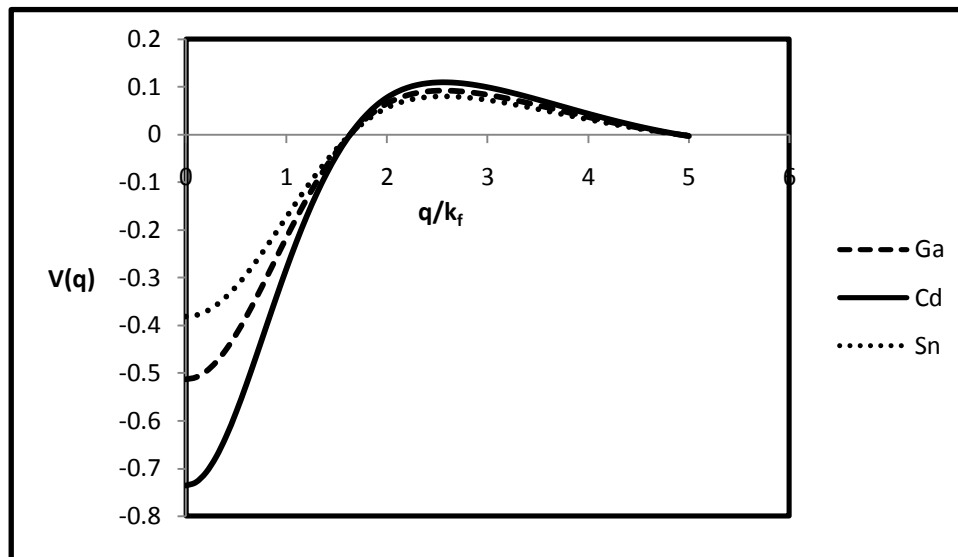


Fig. 1. Form factors of Ga, Cd and Sn.

Table 1 Superconducting state parameters for Ga, Cd and Sn.

SSP	Present	Others (Theoretical)	Exp.
$\lambda(\text{Ga})$	0.105	0.24[1], 0.3330[5], 0.4645[5], 0.4780[5], 0.4859[5], 0.3965[5], 0.25[6], 0.29[6], 0.22[6], 0.23[6], 0.23[6], 0.42[7]	
$\lambda(\text{Cd})$	0.440	0.21[1], 0.3006[5], 0.4312[5], 0.4450[5], 0.4532[5], 0.3632[5], 0.10[6], 0.40[6], 0.22[7]	
$\lambda(\text{Sn})$	0.295	0.40[2], 0.4230[5], 0.6379[5], 0.6691[5], 0.6825[5], 0.5151[5], 0.78[6], 0.99[6], 1.07[7]	
$\mu^*(\text{Ga})$	0.088	0.0998[1], 0.1327[5], 0.1439[5], 0.1454[5], 0.1457[5], 0.1393[5], 0.15[7]	
$\mu^*(\text{Cd})$	0.070	0.10[1], 0.1288[5], 0.1395[5], 0.1409[5], 0.1412[5], 0.1352[5], 0.12[7]	
$\mu^*(\text{Sn})$	0.119	0.13[2], 0.1252[5], 0.1352[5], 0.1366[5], 0.1368[5], 0.1311[5], 0.12[7]	
$T_c(\text{Ga})$	1.058×10^{-40}	0.90[1], 0.0728[5], 0.9422[5], 1.0905[5], 1.1979[5], 0.3274[5], 0.006[6], 0.05[6], 0.0003[6], 0.0009[6], 0.390[7]	1.091[5]
$T_c(\text{Cd})$	2.101	0.30[1], 0.0154[5], 0.4149[5], 0.4985[5], 0.5608[5], 0.1101[5], 5.95×10^{-9} [7]	0.56[5]
$T_c(\text{Sn})$	2.357×10^{-2}	0.30[2], 1.19×10^{-8} [3], 9.98×10^{-14} [4], 0.5044[5], 3.0330[5], 3.5043[5], 3.7224[5], 1.3426[5], 6.2[6], 10.2[6]	3.722[5]
$N_0V(\text{Ga})$	0.016	0.1538[5], 0.2254[5], 0.2318[5], 0.2359[5], 0.1891[5], 0.364[7]	
$N_0V(\text{Cd})$	0.265	0.1350[5], 0.2096[5], 0.2165[5], 0.2210[5], 0.1714[5], 0.086[7]	
$N_0V(\text{Sn})$	0.139	0.160[2], 0.2151[5], 0.3182[5], 0.3311[5], 0.3368[5], 0.2615[5], 0.482[7]	0.263[5]
$\alpha(\text{Ga})$	-33.482	0.0077[5], 0.2393[5], 0.2485[5], 0.2568[5], 0.1470[5], 0.228[7]	
$\alpha(\text{Cd})$	0.463	-0.1083[5], 0.2165[5], 0.2292[5], 0.2399[5], 0.0930[5], 0.301[7]	0.50[7]
$\alpha(\text{Sn})$	0.032	0.45[2], 0.2914[5], 0.3923[5], 0.3989[5], 0.4021[5], 0.3472[5], 0.42[7]	0.47[5]

Pseudopotential form factors are plotted in figure 1 for Ga, Cd and Sn respectively. These are well behaved with having first zero of the pseudopotential form factors very close to conventional values [29] for Ga and Sn. This confirms that method adopted to determine pseudopotential can be justified.

Further, we have computed SSP of Ga, Cd and Sn which are given in table 1 along with available experimental as well as other theoretical results. Our computed values of λ , μ^* , N_0V and α are in good agreement with other reported values. Values of T_c are not in good agreement. But reported values of T_c are also abnormal and scattered [2, 4, 7, 5]. Recently, Vora has used presently used pseudopotential whose parameters are determined to

reproduce experimental T_c [5, 30]. We have not made any kind of adjustment of pseudopotential parameter. In this sense, present model is considered to be free from any kind of adjustment of parameter. It depends only on observed lattice constants at 0^0K .

Further, the present model is tested by carry out study of pressure dependence of SSP and critical volume is computed at which $\lambda = \mu^*$ where T_c and N_0V become zero. The well known Debye-Gruneisen theory has been used for the volume dependence of Debye temperature [19].

$$\theta_D = \theta_{D0} \left(\frac{\Omega}{\Omega_0} \right)^{-\gamma} \quad (7)$$

Pressure dependence of λ and μ^* for Ga, Cd and Sn are shown in figures 2, 3, and 4 respectively.

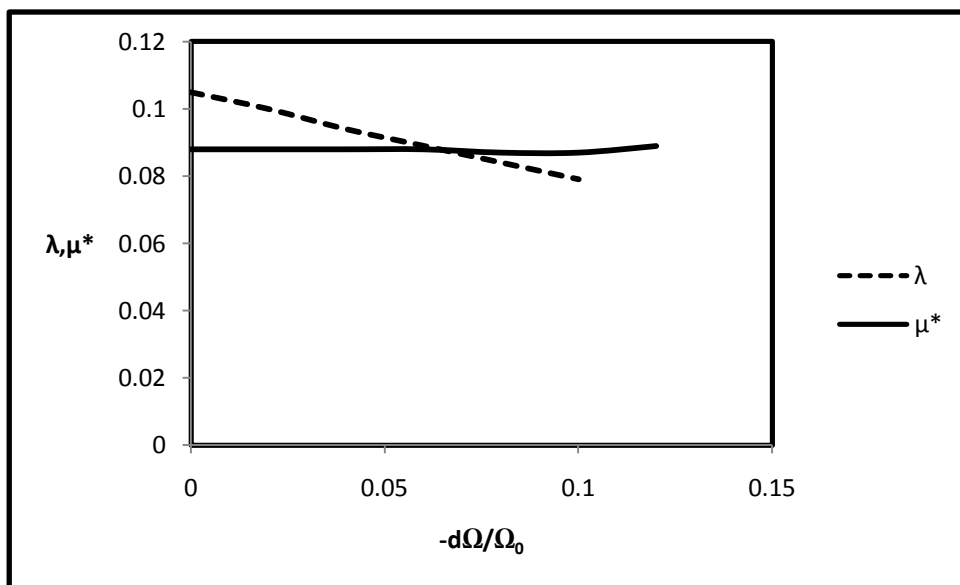


Fig. 2. Volume variation of electron phonon coupling strength (λ) and Coulomb pseudopotential (μ^*) for Ga.

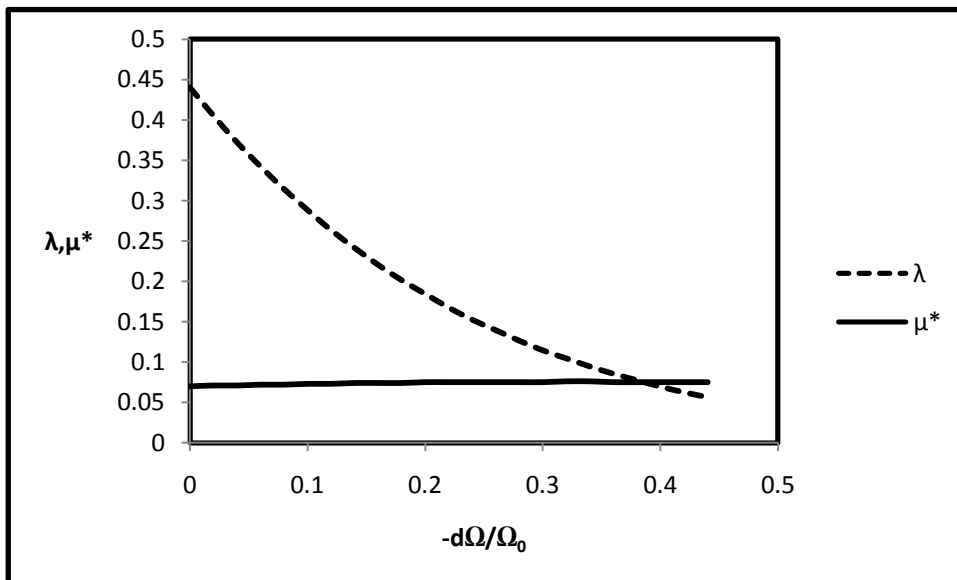


Fig. 3. Volume variation of electron phonon coupling strength (λ) and Coulomb pseudopotential (μ^*) for Cd.

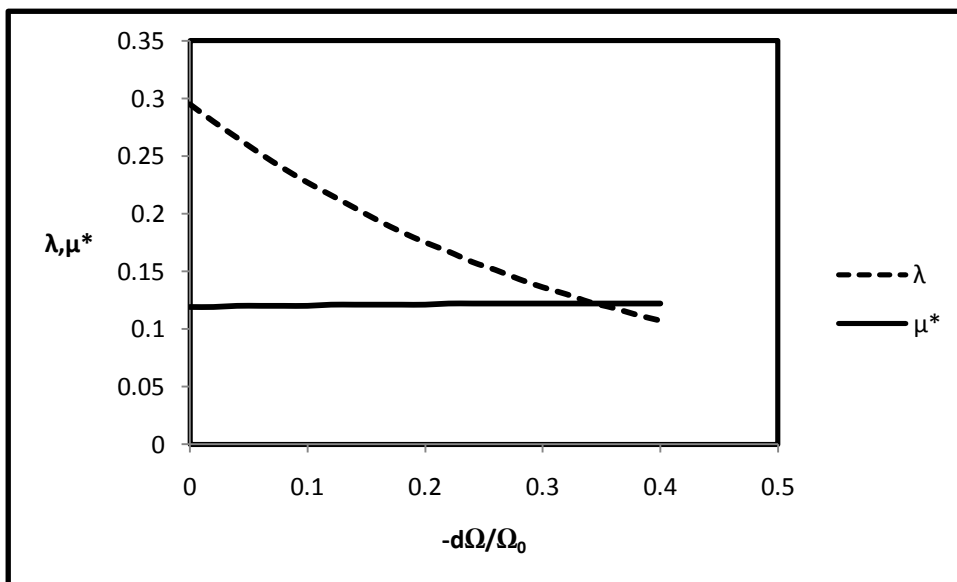


Fig. 4. Volume variation of electron phonon coupling strength (λ) and Coulomb pseudopotential (μ^*) for Sn.

Volume variation of reduced superconducting transition temperature, $T_c(\Omega)/T_c(\Omega_0)$ for Ga, Cd and Sn are shown in figure 5 which gives volume, known as critical volume at which T_c becomes zero. Where $T_c(\Omega)$ is superconducting transition temperature at compressed volume and $T_c(\Omega_0)$ is superconducting transition temperature at normal volume.

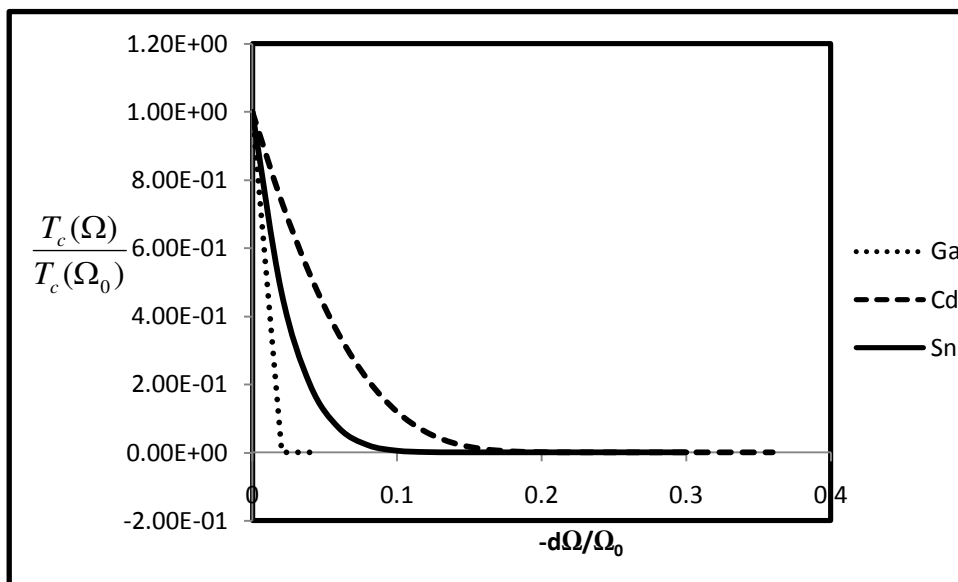


Fig. 5. Volume variation of reduced transition temperature of Ga, Cd and Sn.

Volume variation of effective interaction strength (N_0V) is shown in figure 6 for Ga, Cd and Sn which gives critical volume at which N_0V becomes zero.

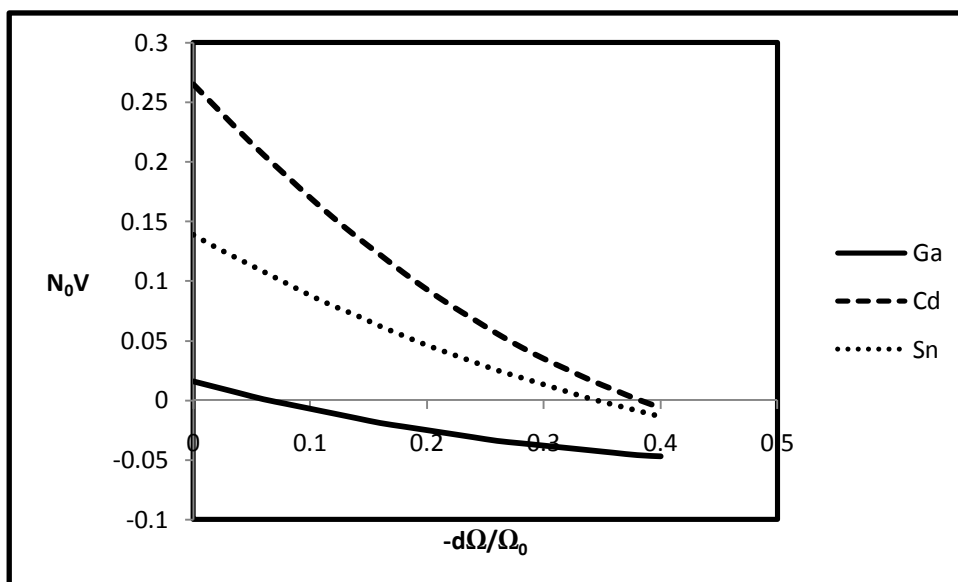


Fig. 6. Volume variation of N_0V for Ga, Cd and Sn.

Intersections of λ and μ^* curves give critical volume (figures 2, 3 and 4) at which superconductivity quenches and T_c becomes zero (figure 5). At this volume (critical volume) interaction strength becomes zero (figure 7) and coulomb repulsion equals the attractive electron phonon interaction so that the net interaction becomes to be attractive.

Our computed values of compressions ($-d\Omega/\Omega_0$) which give critical volumes for Ga, Cd and Sn by the three approaches discussed above are in good agreement with each other and are also comparable with other reported

results which are displayed in table 2.

Table 2. Critical values for Ga, Cd and Sn.

Metal	Compression ($-d\Omega/\Omega_0$)			
	At which $\lambda = \mu^*$	At which $T_c=0$	At which $N_0V=0$	Others
Ga	0.06	0.04	0.06	-
Cd	0.38	0.36	0.38	0.317[19], 0.063[20], 0.139[20]
Sn	0.34	0.30	0.34	0.540[19], 0.484[19], 0.148[20]

From figures 2, 3 and 4 it is quite clear that critical volumes correspond to 6%, 38% and 34% compressions of volume for Ga, Cd and Sn respectively at which $\lambda = \mu^*$. Same compressions (6%, 38% and 34% for Ga, Cd and Sn respectively) are obtained from figure 6 at critical volume where effective interaction strength (N_0V) becomes zero. It is also observed that T_c becomes zero (figure 5) which gives critical volume at 4%, 36% and 30% compressions of volume respectively for Ga, Cd and Sn. The critical volumes computed theoretically by all the three approaches are in excellent agreement (table 2).

Siden[19] has used point ion pseudopotential for core repulsion and experimental Debye temperature with Jellium phonon spectrum. He has used an undetermined parameter σ which is evaluated by fitting theory to the measured zero pressure T_c to obtain proper zero-pressure result. He has also used Gruneisen parameter (γ) as an adjustable parameter. Our model is better in the sense that we have not used such type of adjustment. We have computed Gruneisen parameter (γ) using relation given in reference [17].

Conclusion

We would like to conclude present work with following remarks:

1. Validity of presently proposed very simple parameter free model is confirmed by satisfactory reproduction of SSP and critical volumes of Ga, Cd and Sn respectively.
2. Looking to the success, simplicity, physical transparency and transferability it can be extended for the remaining metals, their alloy and metallic glasses. Such study is in progress, results are encouraging which will be published elsewhere.
3. We would like to highlight one of the limitations of the present computation, in our opinion, is that Debye temperature (Θ_D) and Gruneisen parameter (γ) should be computed using same theoretical model instead of the observed values in absence of reliable experimental values.

Acknowledgements

Authors are highly grateful to Dr. V. B. Gohel, Department of Physics, Gujarat University, Ahmedabad for his continuous encouragement, guidance and valuable suggestions throughout the period of work.

Authors are also thankful for computational facilities developed using financial assistance provided by Department of Sciences and Technology (DST), New Delhi through the DST-FIST (Level 1) project (SR/FST/PST-001/2006).

Reference

- Jayprakash Yadav, S. M. Rafique and Shanti Kumari, 2009, Impact of Eigenvalues on the Pseudopotential Calculation of Superconducting Parameters of Metals Ga, Cd and In, Indian J. Phys. Vol. 83, no 10, p.1487.
- S.C. Jain and C. M. Kachhava, 1981, Pseudopotential Calculation of the superconducting State Parameters, Transition Temperature And Isotopic Effect in Non-Transition Metals, Indian J. Phys. Vol. 55A, p. 89.
- J. S. Rajput and A. K. Gupta, 1969, Superconductivity in Nontransition Metals, Phys. Rev. Vol.181, p. 743.
- J. S. Rajput, 1971, Phys. Status Solidi (b), Vol.45, p. 287.
- A. M. Vora, 2007, Superconducting State Parameters of Amorphous Metals, Physica C, Vol. 458, p. 21. And references there in.
- P. B. Allen and M. L. Cohen, 1969, Pseudopotential Calculation of the Mass Enhancement and Superconducting Transition Temperature of Simple Metals, Phys.Rev. Vol. 187 No. 2, p. 525.
- R. Sharma, K. S. Sharma and L. Daas, 1986, Linearised Screened Pseudopotential and Superconducting State Parameters of a Number of Metals, Phys. Stat. Sol. (b), Vol. 133, p.701.
- W. L. McMillan, 1968, Transition Temperature of Strong-Coupled Superconductors, Phys. Rev., Vol. 167, No. 2 p. 331.
- P. N. Gajjar, A. M. Vora and A. R. Jani, 2004, Superconducting State Parameters of Metals, Indian J. Phys. Vol. 78(8), p. 775.
- Vibha Vansola, Hiral Patel, N. K. Bhatt, P. R. Vyas and V. B. Gohel, 2014, Superconducting State Parameters for Alkaline Earth Metals Using First Principle Pseudopotential, Int. J. Chemical and Physical Sciences, Vol. 3, p. 179.

- Vibha Vansola, Gunjan Shah, N. K. Bhatt, P. R. Vyas and V. B. Gohel, 2013, The Comparative Study of Superconducting State Parameters for Noble Metals Using Non Local Pseudopotential, *Int. J. Advancement in Electronics and Computer Engineering*, Vol. 2, Issue 9, p. 257.
- A. M. Vora, Minal H. Patel, P. N. Gajjar and A. R. Jani, 2002, Superconducting State Parameters of Indium Based Binary Alloys, *Pramana J. Phys.*, Vol. 58, Nos. 5 & 6, p. 849.
- A. M. Vora, Minal H. Patel, P. N. Gajjar and A. R. Jani, 2003, The Study of Superconducting State Parameters of In-Based Binary Alloys by Pseudopotential, *International J. Modern Phys. B*, Vol. 17, Nos. 31 & 32, p. 6001.
- Ritu Sharma and K. S. Sharma, 1996, A Pseudopotential Approach to the Superconducting State Properties of Metallic Glass $\text{Ca}_{70}\text{Mg}_{30}$, *Supercond. Sci. Technol.* Vol. 10, p. 557
- P. N. Gajjar, A. M. Vora and A. R. Jani, 2004, Pseudopotential in the Study of Superconducting State Parameters of Metallic Glasses, *Modern Phys. Lett. B*, Vol. 18, No. 12 & 13, p. 573.
- Manish Gupata, K. S. Sharma and Lachhman Dass, 1997, Superconducting State Parameters of Metallic Glass $\text{Mg}_{70}\text{Zn}_{30}$ Using Linearized Screened Pseudopotential, *Pramana J. Phys.*, Vol. 4, No. 4, p.923.
- Manish Gupta, K. S. Sharma and Lachhman Dass, 1999, Pressure Dependence of the Superconducting State Parameters of Metallic Glass Superconductor $\text{Mg}_{70}\text{Zn}_{30}$, *Pramana J. Phys.* Vol. 3, No. 4, p. 765.
- Aditya M. Vora, 2010, Pressure Effects on $\text{Ca}_{60}\text{Al}_{40}$ Metallic Glass Superconductors, *Iranian J. Phys. Research*, vol. 10, No. 1, p.15.
- P. E. siden, 1969, Pressure Dependence of Superconducting Transition Temperature, *Phys. Rev.* Vol. 179, No. 2, 458.
- T. F. Smith and C. W. Chu, 1967, Will Pressure Destroy Superconductivity ?, *Phys. Rev.*, Vol. 159, No. 2. P. 353. and references their in.
- J. S. Rajput, 1971, Volume Dependence of Transition Temperature and Effective Interaction Strength in Tin, *J. physical Society of Japan*, Vol. 31, No. 4, p. 1053.
- M. Levy and J. L. Olsen, 1964, Can Pressure Destroy Superconductivity in Aluminium?, *Sol. Stat. Comm.*, Vol. 2, p. 137.
- L. D. Jennings and C. A. Swenson, 1958, Effects of Pressure on Superconducting Transition Temperature of Sn, In, Ta, Tl, and Hg, *Phys. Rev.*, Vol. 112, No. 1, p. 31.
- M. Garfinkel and D. E. Mapother, 1961, Pressure Effects on Superconducting Lead, *Phys. Rev.*, Vol. 122, No. 2, p. 459.
- N. B. Brandt and N. I. Ginzburg, 1966, Pressure Dependence of the Superconducting Transition Temperature in Zinc, *Soviet Physics JEPT*, Vol. 23, No. 5, p.838.
- N. W. Aschroft, 1966, Electron-Ion Pseudopotentials in Metals, *Phys. Lett.* vol. 23, p. 48.
- R. Taylor, 1978, *J. Phys.* F8, p. 1699.
- V. Heine and D. Weaire, 1970, *Solid State Physics* 24, Eds. Ehrenreich H., Seitz F. and turnbull D. (Academic Press, New York), p.250.
- C. Fiolhais, John P. Perdew, Sean Q. Armster and James M. MacLaren, Marta Brajczewska, 1994, Dominant Density Parameters and Local Pseudopotential for Simple Metals, *Phys. Rev. B*, Vol. 51, No. 20, p. 14001.
- A. M. vora, 2012, Study of Superconducting Properties of Bulk Metallic Superconductors by Pseudopotential Theory, *Bulg. J. Phys.*, Vol. 39, p. 215.

Electron Scattering with 1 Pentene and Cyclopentane Molecules by SCOP Method – Total Ionization Cross sections

Umang R Patel^{a,b,*}, K N Joshipura^b

^aGandinagar Institute of Technology, Gnadhinagar, India

^bSardar Patel University, Vallabh Vidyanagar-388120, Gujarat, India

Abstract

In this paper we report theoretical total ionization cross sections for C₅H₁₀ (1 Pentene and Cyclopentane) molecules by electron impact from threshold to 2000 eV. Theoretical formalism employed presently, viz., *Complex Scattering Potential- ionization contribution* method has already been used successfully for a variety of polyatomic molecules. The present calculations are very important since results available for the studied targets are either scarce or none. In this work, new data are reported for the title target isomers.

1. Introduction

In this paper we have focused attention on hydrocarbons which play an important role in plasma diagnostics, as impurities in the Tokamak fusion divertor, as seed gases for production of radicals and ions in low temperature plasma processing, and many other technological fields [1]. Carbon based material is one of the most widely used materials for a divertor plate and wall of the magnetically confined fusion devices. In a next step device, such as ITER, for steady state operation, it is very important to estimate lifetime of carbon plasma facing components. Chemical sputtering reduces their lifetime and increases fuel retention via redeposition [2]. Szmytkowski *et. al.* [3] have calculated ionization cross sections for C₅H₁₀ i.e. 1 Pentene, whose data are scarce. In spite of continuous interest in the electron driven processes for media containing hydrocarbons, the data for somewhat more complex compounds still remain fragmentary. So it is worth to calculate Q_{ion} for C₅H₁₀ isomers too. We have employed here the Complex Scattering Potential - ionization contribution (CSP-*ic*) method developed and applied successfully by us, over a wide range of molecular targets in the recent years [4-7].

We have carried out theoretical studies on a few C₅ hydrocarbons whose TCS data are available in literature but electron impact ionization cross sections (Q_{ion}) data are scarce. Szmytkowski *et. al.* [8] have calculated ionization cross sections for C₅H₁₀ i.e. 1 Pentene through BEB method for which software packages are available. In spite of continuous interest in the electron driven processes for media containing hydrocarbons, the data for somewhat more complex compounds still remain fragmentary. So it is worthwhile to calculate Q_{ion} for C₅H₁₀ isomers too. A slight difference in the total ionization cross sections for the different isomers can be caused by the different dissociative pathways of the two molecules. It is well known that the parent ionization of complex hydrocarbons accounts for only a small fraction of the total ionization cross sections while dissociative ionization dominates the ionization process. Here we have employed the Complex Scattering Potential ionization contribution (CSP-*ic*) method to different functional groups of the complex molecule [4].

2. Theoretical methodology

At the incident energies (E_i) from ionization threshold to 2000 eV, it becomes meaningful to represent the electron - molecule system by a complex (spherical) potential, which seeks to club together all admissible inelastic (including ionization) channels in the background of elastic scattering. For an electron interacting with a molecule (or a functional chemical group), the total complex potential $V(r, E_i) = V_R(r, E_i) + iV_I(r, E_i)$, consists of real potential V_R and imaginary potential V_I . The total complex potential $V(r, E_i)$ introduced in the Schrodinger equation, along with its solution obtained numerically, leads to the total (complete) cross section Q_T defined as follows.

$$Q_T(E_i) = Q_{el}(E_i) + Q_{inel}(E_i) \quad (1)$$

Where, Q_{el} is the total elastic cross section while its inelastic counterpart is denoted by Q_{inel} . The total (cumulative)

*Corresponding author: +91 8347010863

umangpatel193@yahoo.ca

inelastic cross section Q_{inel} includes all energetically allowed electronic excitation as well as ionization channels of scattering, so that

$$Q_{inel}(E_i) = \sum Q_{exc}(E_i) + \sum Q_{ion}(E_i) \quad (2)$$

The inelastic cross section Q_{inel} is not a directly measurable quantity in a single experiment, but in view of the equation (2), we have in general,

$$Q_{inel}(E_i) \geq Q_{ion}(E_i) \quad (3)$$

At incident energies above I , the ionization processes begin to play a dominant role due to the availability of infinitely many open channels of scattering. There is no rigorous way of projecting out Q_{ion} from the theoretical quantity Q_{inel} . Hence, we have introduced an approximation by defining a ratio function,

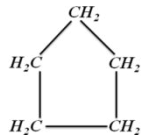
$$R(E_i) = \frac{Q_{ion}(E_i)}{Q_{inel}(E_i)} \quad (4)$$

Obviously $R = 0$ when $E_i \leq I$. For a number of stable atomic – molecular targets like Ne, Ar, O₂, N₂, CH₄, H₂O, etc., for which several experimental ionization cross section data-sets are known accurately [4-7], the ratio is seen to be rising steadily as the energy increases above the threshold, and approaching unity at high energies. We follow the general observation [4-7] that at energies close to peak of Q_{inel} the ionization contribution Q_{ion} is about 70-80% in the total inelastic cross section Q_{inel} and it increases with energy. It has been demonstrated in our publications [4-7] that total ionization cross sections can be reasonably determined from this approximation and the resulting Q_{ion} are within the experimental uncertainties of about 10-15%. Now, for the actual calculation of Q_{ion} from Q_{inel} we need R as a continuous function of energy E_i . Hence, we represent [5] the ratio $R(E_i)$ in the following manner.

$$R(E_i) = 1 - f(U_i) = 1 - C_1 \left[\frac{C_2}{(U_i + a)} + \frac{\ln U_i}{U_i} \right] \quad (5)$$

Where $U_i = E_i/I$, is a dimensionless and target-specific variable corresponding to energy E_i . The reason for adopting a particular functional form of $f(U_i)$ i.e. second term of the right hand side of equation (5) is as follows. As E_i increases above I , the ratio R increases from zero and approaches value 1, since the ionization contribution rises and the discrete excitation-sum in equation (2) decreases. The discrete excitation cross sections, dominated by dipole transitions, fall off as $\ln(U_i)/U_i$ at high energies. Accordingly the decrease of the function $f(U_i)$ must also be proportional to $\ln(U_i)/U_i$ in the high range of energy. However, the two-term representation of $f(U_i)$ given in equation (5) is more appropriate since the 1st term in the square bracket ensures a better energy dependence at low and intermediate E_i . Equation (5) involves dimensionless parameters C_1 , C_2 , and a , characteristic of the target in question. The detail description of the equation (5) and complete theoretical approach is described in [4,7]. Table 1 shows the molecular properties of the title targets.

Table 3 Properties of the targets studied

Target	Geometry	Ionization Potential (eV)	Bond length (Å)
C ₅ H ₁₀	CH ₂ = CH – CH ₂ – CH ₂ – CH ₃	9.49	C=C 1.34 C-H 1.089
C ₅ H ₁₀		10.33	C-H 1.114

3. Results and discussions

In this paper, CSP-ic method followed by group additivity approach has been adopted to determine electron impact total ionization cross sections for C₅ hydrocarbon isomer. The results obtained are plotted below with comparison. Also, the present cross section data are exhibited in table 2.

Table 2 Q_{ion} (\AA^2) for e^- - C_5H_{10} isomers

E_i (eV)	1 Pentene	Cyclopentane
20	9.13	6.80
30	14.25	11.86
40	15.83	13.64
50	16.01	13.97
60	16.03	13.99
70	15.76	13.80
80	15.35	13.50
90	14.89	13.14
100	14.44	12.76
200	11.11	9.67
300	9.08	7.84
400	7.70	6.62
500	6.68	5.74
600	5.91	5.07
700	5.30	4.54
800	4.80	4.12
900	4.39	3.78
1000	4.05	3.49
2000	2.25	1.96

$(e^- - C_5H_{10})$ 1 Pentene and Cyclopentane

The data in the electron driven processes for complex compounds still remain fragmentary. So, here in figure 1 electron impact ionization cross sections are presented for C_5H_{10} isomers. As the data for the present C_5H_{10} isomers are scarce, we have shown Q_{ion} for both 1 Pentene and Cyclopentane in figure 1. The only comparison has been made for 1 Pentene with BEB cross sections calculated by Szmytkowski *et. al.*[8]. Present Q_{ion} are higher in comparison with BEB cross sections of Szmytkowski *et. al.* [8] and running parallel with it at high energy region. The present Q_{ion} for Cyclopentane are smaller than the Q_{ion} for 1 Pentene. It agrees with the observations by Bettega *et. al.* [9] that cross sections for closed chain isomers are always lower than the open chain isomers. Present results for both the C_5H_{10} isomers contracted with the general observation that increment in ionization potential results into reduction of cross section and vice versa.

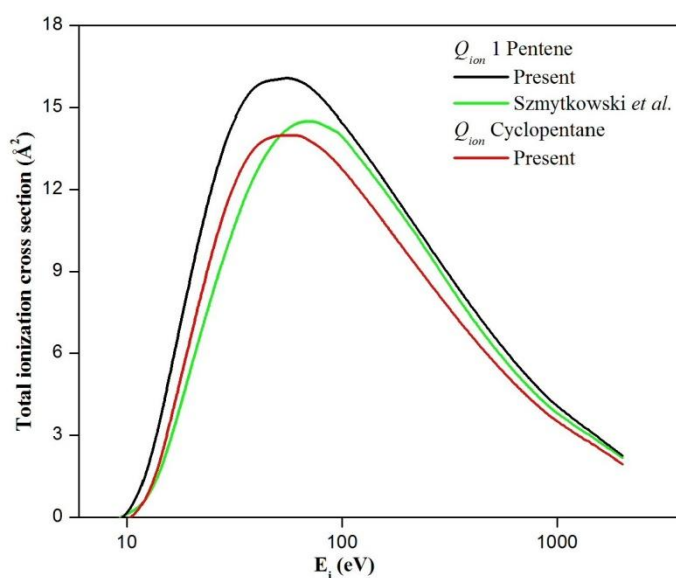


Figure 1: Total ionization cross section for isomers of C_5H_{10} . Black solid line: the present 1 Pentene; green solid line: Q_{ion} by Szmytkowski *et al.* [8] and red solid line: the present Q_{ion} for Cyclopentane

4. Conclusions

We have successfully calculated the electron impact ionization cross sections for C_5H_{10} isomers. Present results are compared with available results from published literature, which are in accord with each other. The results of open chain 1 Pentene are larger than closed chain Cyclopentane, as the general trends depict. The ionization potential can also cause the change in cross sections as observed here for both C_5H_{10} isomers.

Our findings are more meaningful in the absence of experimental data for the studied targets.

References

- [1] Makochekanwa C., Kato H., Hoshino M., Cho H., Kimura M., Sueoka O. and Tanaka H., 2005, Probing the isomer, fluorination and bond effects in C_3H_6 , cyclo- C_3H_6 and C_3F_6 molecules using electron impact, *Eur. Phys. J. D.* **35**, p. 249
- [2] Kawazome H., Ohya K., Inai K., Kawata J., Nishimura K. and Tanabe T., 2010, Calculation of D/XB Values of Hydrocarbon Molecules in Tokamak Edge Plasmas, *Plasma and Fusion Research*; regular article **5** S p. 2073
- [3] Szmytkowski C. and Kwitniewski S., 2002, Total cross sections for electron scattering with some C_3 hydrocarbons *J. Phys. B: At. Mol. Opt. Phys.* **35**, p. 3781
- [4] Patel U., Joshipura K., Kothari H. and Pandya S., 2014, Electron ionization of open/closed chain isocarbonic molecules relevant in plasma processing: theoretical cross sections, *J. Chem. Phys.* **140**, p. 044302
- [5] Joshipura K., Vinodkumar M., Limbachiya C. and Antony B., 2004, Calculated total cross sections of electron-impact ionization and excitations in tetrahedral (XY_4) and SF_6 molecules, *Phys. Rev. A* **69**, p. 022705
- [6] Pandya S., Shelat F., Joshipura K. and Vaishnav B., 2012, Electron ionization of exotic molecular targets CN, C_2N_2 , HCN, HNC and BF— Theoretical cross sections, *Int. J. Mass Spectrom.* **28**, p. 323-324
- [7] Patel U., Joshipura K., 2014, Cross sections for electron scattering with C_6H_6 and C_6F_6 – A Theoretical investigation, *GIT JET* **7**
- [8] Szmytkowski C., Mozejko P., Zawadzki M. and Denga E., 2013, Electron-scattering cross sections for 1-pentene, $H_2C=CH-(CH_2)_2CH_3$, molecules, *J. Phys. B: At. Mol. Opt. Phys.* **46**, p. 065203
- [9] Bettgega M H F, Lopes A., Lima M A P and Ferreira L., 2006, Electron collisions with Cyclobutane, *Braz. J. of Phys.* **36**, 2B

Structural and Lattice Dynamical Properties of Al-Li Intermetallic Alloy

N. Y. Pandya^a, A. D. Mevada^a, P. N. Gajjar^a

University School of Sciences, Gujarat University, Ahmedabad-380 009, Gujarat, India

Abstract

Aluminum-Lithium alloys are best option to fulfill the crying need of light weight alloys for use as structural materials in aerospace applications. Al-Li alloys have been found to have superior mechanical properties e.g. higher specific strength, enhanced resistance to high cycle fatigue and fatigue crack growth as compared to conventional Al alloys. The present paper reports a comprehensive first principles calculation of structural and lattice dynamical properties of B2 structured Al-Li in its ground state and high pressure phases using plane-wave pseudopotential density functional theory as implemented in Quantum ESPRESSO code. Calculated equilibrium lattice constants and isothermal bulk modulus are in good agreement with other theoretical results. Pressure induced structural phase transitions, phonon dispersion curve and phonon density of states for B2 structured Al-Li are also calculated. Further, the electronic band structures along with total and projected density of states are calculated at ground states and high pressures. Our presently calculated results may serve as a reliable set of data of structural and lattice dynamical properties of B2 structured Al-Li alloy.

Keywords: Al-Li; Pseudopotential; Negative pressure; Phonon dispersion curve; Band structure

18. Introduction

Despite the fact that both elements aluminium and lithium are quite normal metals, their alloys manifest rather unusual thermodynamic and electrochemical properties which have lately prompted a number of theoretical studies of the Al-Li system [1]. If the net weight of the structure is reduced considerably, the substantial improvements in structural efficiency, fuel saving and payload in aerospace can result. Aluminium-Lithium alloys are the best light weight alloys for using as structural materials in aerospace application compared to other structural materials. Al-Li alloys exhibit superior mechanical properties as compared to conventional Al alloys [2]. The desire for more efficient aircraft materials has given the force to the research of Al-Li alloy. Further, Al-Li alloys are technologically more attractive as compared to the newer structural materials such as Ti alloys and composites, which are so expensive [2]. In the present work, we describe ground state, electronic and lattice dynamical properties of B2 structured Al-Li alloy using plane wave pseudopotential density functional theory as implemented in Quantum ESPRESSO package [3]. Condensed matter can sustain negative pressures because of attractive interactions between molecules. Under negative pressure (tensile stress), the intermolecular distance r increases, and the medium under the tension is in a metastable state [4]. Such phase transitions, under the influences of negative pressures, are also reported. The paper is presented as follows. The next section describes the theoretical method of calculation used in the present study. The section 3 describes the results and discussion. The section 4 describes the conclusions.

19. Computational Methodology

In the present work, ground state and lattice dynamical properties of B2 (CsCl) structured Al-Li are calculated using plane wave pseudopotential density functional theory as implemented in Quantum ESPRESSO code [3]. The calculation is performed using ultrasoft pseudopotential with non-linear core correction within generalized gradient approximation (GGA) [5]. The Aluminium Lithium (Al-Li) crystallizes into Cesium chloride (B2) structure at ambient condition and remains stable up to very high pressures. The Al and Li atoms occupy positions (0, 0, 0) and (0.50, 0.50, 0.50), respectively, in a SC (Simple Cubic) primitive cell. Total energy calculation of B2 structured Al-Li is performed at various lattice constants in the step of 0.1 a.u. (atomic unit). The convergence test gave an 8x8x8 Monkhorst-Pack (MP) k-point grid [6] for Brillouin-zone (BZ) sampling along with the kinetic energy cutoff as 116 Ry. This ensures the convergence of total energy to 0.1 mRy. Total energy in other two cubic phases namely rock salt (B1) and zinc blende (B3) is also calculated. The calculated total energies were fitted to Murnaghan equation of state [7], in order to estimate equilibrium lattice constant, isothermal bulk modulus and its pressure derivatives. To analyze the electronic properties of B2 structured Al-Li, we present the electronic band structure along with total and partial (projected) density of states (PDOS) using the calculated equilibrium lattice constant. Further, phonon dispersion curves are obtained employing the linear response theory within the density functional perturbation theory (DFPT) [8-9]. Further, full phonon dispersion and p-dos (phonon density of states) of B2 structured Al-Li along major symmetry directions are also calculated at zero pressure. For a given pressure, a stable structure is one for which enthalpy has its lowest value [10-11]. The pressure induced structural phase transitions in Al-Li is studied by calculating enthalpies of three cubic phases B1, B2 and B3 under the influence of positive and negative pressures. The

cohesive energy of all three cubic phases i.e. B1, B2 and B3 are calculated by subtracting energy of an isolated free atom from the total energy of bulk crystal.

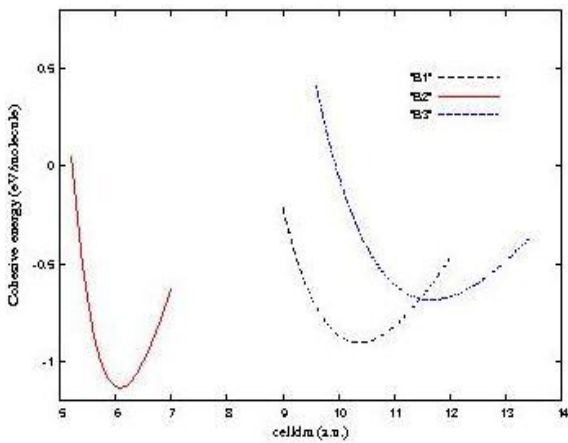


Fig.1 Cohesive energy of Al-Li as a function of cell parameter

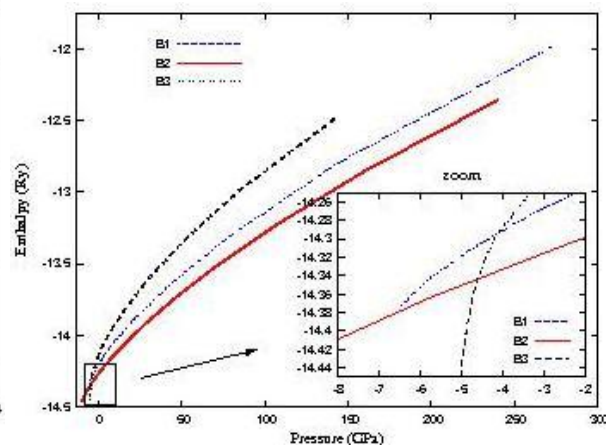


Fig.2 Enthalpy versus pressure curve for B2 Al-Li

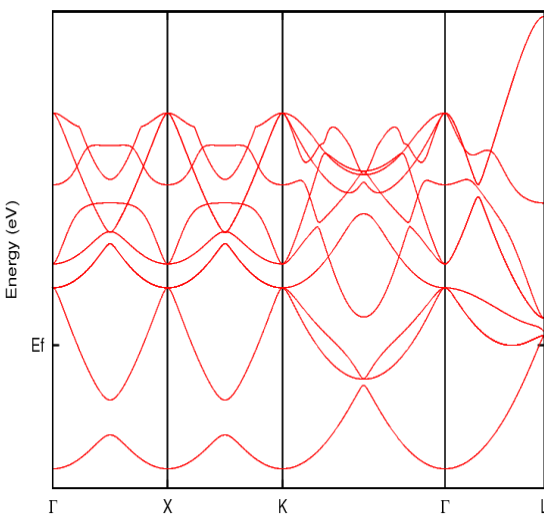


Fig.3 Electronic band structure of B2 structured Al-Li

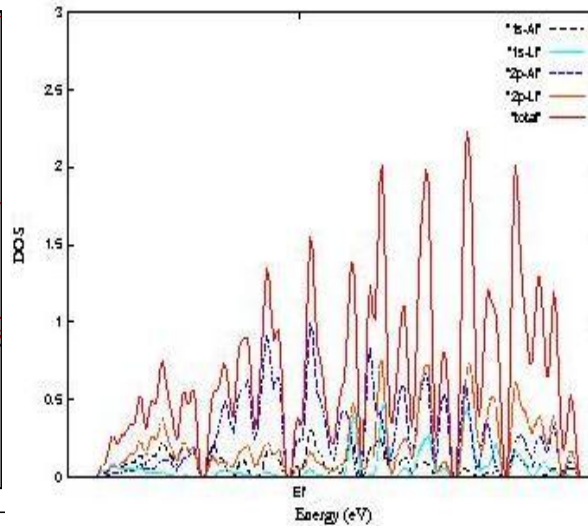


Fig. 4 Total and projected density of states of B2 structured Al-Li

20. Results and Discussion

In the present work, we have calculated various ground state and lattice dynamical properties of only B2 structure of Al-Li because it has the lowest energy at equilibrium. B2 (CsCl) phase of Al-Li has also lowest enthalpy at equilibrium (at zero pressure) (Fig. 2). The ground state properties of B2 structured Al-Li are calculated by minimizing the total energy with respect to the cell volume by means of Murnaghan equation of state [7]. As a result, we obtained the equilibrium lattice constant, isothermal bulk modulus and first order derivative of bulk modulus for B2 structure Al-Li, which is presented in table 1, together with the other available theoretical data [12]. We notice that, there is an excellent agreement of our results with the other theoretical findings [12].

Table 1. Calculated structural properties of B2 structured Al-Li alloy

Structure	Properties	Present	Others [12]	Exp.
CsCl (B2)	a_0 (Å)	3.217	3.175	---
	B_0 (GPa)	37.1	40.7	---

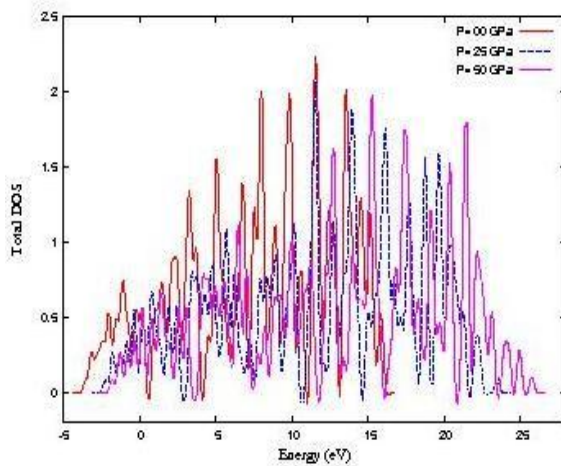


Fig. 5 Total DOS of B2 structured Al-Li at high pressures

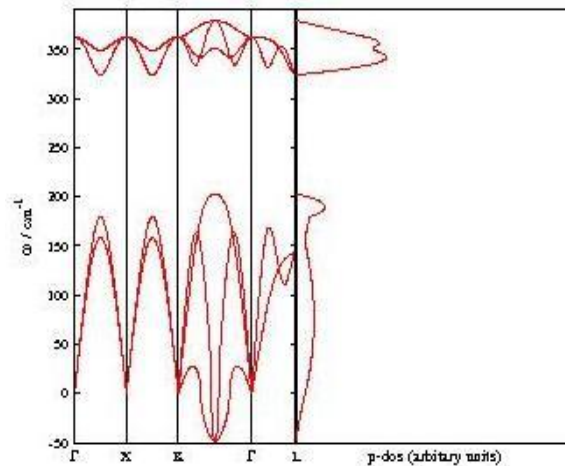


Fig.6 Phonon dispersion curve and phonon density of states of B2 structured Al-Li in ground state

Cohesive energy of all three cubic phases i.e. B1, B2 and B3 of Al-Li are presented in fig.1, which indicates the structural stability of B2 (CsCl) structure of Al-Li alloy at equilibrium. Further, we have calculated enthalpies for three cubic phases i.e., B1, B2 and B3 of Al-Li under the influences of positive and negative pressure values in fig. 2, in order to estimate structural phase transitions in Al-Li. From the graph, it is clear that, no structural phase transition is observed in B2 structured Al-Li up to approximately 250 GPa pressure and B2 phase has stable structure up to this high pressure. The three phase transitions are shown in Fig.2, in which the negative pressure dependence of the cell volume is displayed. Zooming view clearly indicates the structural phase transitions at negative pressures such as (i) from B1 (Rock salt) to B3 (Zincblende) at -4.1 GPa and (ii) from B2 (CsCl) to B3 (Zincblende) at -4.7 GPa. The negative pressure means that, for example at -4.1 GPa pressure, we have to expand the B1 (Rock salt) structure to obtain B3 (Zincblende) structure. These pressures are confirmed by calculating the enthalpy dependence on the pressures (Fig.2). To analyze the electronic properties, we have calculated the electronic band structure of B2 structured Al-Li alloy along the high symmetry directions in first Brillouin zone using calculated equilibrium lattice constant in Fig.3. We observe that the Al-Li in CsCl structure exhibiting a metallic nature with no energy gap at Fermi level. Total and Projected density of states (PDOS) of B2 structure Al-Li is presented in fig.4. From the PDOS in fig.4, we can say that total density of states of B2 structure Al-Li is mainly dominated by 2p-Al and 2p-Li states. Effect of pressures on total density of states (TDOS) of B2 structure Al-Li at ground state and various high pressures ($P = 25$ GPa and $P = 50$ GPa) is presented in fig. 5, which indicates the spreading of total DOS towards higher energy side with the increase in pressure i.e. electrons occupy higher energy states at high pressures. Further, we have calculated full phonon dispersion at theoretically obtained equilibrium lattice constant along major symmetry directions in the Brillouin zone for B2 structure Al-Li using density functional perturbation theory (DFPT) [8-9], which is presented in Fig. 6. The fig. 6, clearly reveal that the phonon dispersion curve contain negative acoustic phonon frequencies along $K \rightarrow \Gamma$ directions in the Brillouin zone, which indicates dynamical instability of Al-Li in B2 structure.

21. Conclusions

In conclusion, we conclude that present work reports various ground states, electronic and lattice dynamical properties of CsCl structured Al-Li. Our calculated equilibrium lattice constant and isothermal bulk modulus agrees well with the other theoretical findings [12] by using same Quantum espresso code. Calculated cohesive energies and enthalpies for three cubic phases clearly reveal the structural stability of B2 structure Al-Li at equilibrium. Pressure induced phase transitions are reported at negative pressures. From the band structure and projected density of states (PDOS), we conclude that the Al-Li shows metallic nature in CsCl phase and 2p-Al and 2p-Li contribute significantly to the total density of states, respectively. Occurrence of negative frequency in phonon dispersion curve indicates the dynamical instability of Al-Li in CsCl (B2) structure. Our present results form a useful set of data of structural, vibrational and electronic properties of B2 structure Al-Li which may be useful for further research in this field.

Acknowledgements

Computer facility developed under DST-FIST Level-I program from Department of Science and Technology, Government of India, New Delhi and financial assistance under DRS-SAP-I from University Grants Commission, New Delhi is highly acknowledged.

References

- [1] Korzhavyi, P. A., Ruban, A. V., Simak, S. I., and Vekilov, Yu.Kh., 1994. Phys. Rev. B 49, p. 14229
- [2] Eswara Prasad, N., Gokhale A. A., and Rama Rao, P., 2003, Mechanical Behaviour of Aluminium-Lithium Alloys, Sadhana 23, pp. 209-246
- [3] www.quantum-espresso.org
- [4] Debenedetti, P. G., 1996. Metastable Liquids, Princeton University Press, Princeton
- [5] Perdew, J. P., Burke, K. and Ernzerhof, M., 1996. Phys. Rev. Lett. 77, p. 3865
- [6] Monkhorst, H. J. and Pack, J. D., 1976. Phys. Rev. B 13, p. 5188
- [7] Murnaghan, F. D., 1944. Proc. Natl. Acad. Sci. USA 30, p. 244
- [8] Hohenberg, P., Kohn, W., 1964. Phys. Rev. B 136, p. 864
- [9] Kohn, W., Sham L.J., 1965. Phys. Rev. 140, p. 1133
- [10] Trinadh, C.U.M., Ph.D. thesis, Anna University, Chennai (India), Page no. 72, (1997)
- [11] Born, M. and Huang, K., 1954. Dynamical Theory of crystal lattices, Clarendon, Oxford
- [12] Khambholja, S. G., Ph.D. thesis, S.P. University, Gujarat (India), Page no. 101, (2012)

Delineation of Potential Groundwater Zones using Remote Sensing and GIS – A Review

Madhu S. Trivedi ^a, G. P. Vadodaria ^b

^a Gujarat Technological University, Ahmedabad, Gujarat, India and ^bL. D. College of Engineering, Ahmedabad, Gujarat, India

Abstract

Water Crisis is a growing concern these days all over the world. Natural Recharge of the groundwater is the worst hit due to urbanization. A proper groundwater management should be adopted to utilize groundwater in a sustainable manner. This requires the identification of the potential ground water zones in the study area which could be suitable for artificial recharge for sustenance. Application of remote sensing (RS) and GIS in finding the potential ground water zones have been done by many researchers across the world and have found good results. This is a review paper to highlight the integrated use of GIS and RS in delineating the ground water potential zones as studied by the various researchers. It is concluded that application of high resolution satellite data combined with information collected through geophysical and ground surveys can be integrated to produce different GIS Layers of ground features. Subsequently expert choice and relational methods can be used in GIS environment to conjunctively analyze all layers to converge evidences and delineate promising and preferable regions of potential aquifer.

Keywords: Delineation , Remote Sensing, GIS, Groundwater potential, recharge.

Nomenclature

DEM Digital Elevation Model
GIS Geographical Information System
RS Remote Sensing
SOI Survey of India
IDW Inverse Distance Weighted
AHP Analytical Hierarchy Process
MCDM Multi-Criteria Decision Making
WIOA Weighted Index Overlay Analysis
GWPI Groundwater potential index
(LISS) III Linear image self-scanning system III
IRS Indian Remote Sensing Satellite

1. Introduction

To sustain the groundwater, it is very much necessary to identify the groundwater potential zones. Geomorphological studies coupled with hydrogeological and structure/lineaments proved to be very effective in locating groundwater potential zones (Bahuguna et al., 2003; Jagadeeswara Rao, Harikrishna & Suryaprakasa Rao 2004). Geospatial technology is a rapid and cost-effective tool in producing valuable data on geology, geomorphology, lineaments slope, etc. that helps in deciphering groundwater potential zone. Satellite remote sensing provides an opportunity for better observation and more systematic analysis of various geomorphic units/landforms/lineaments due to the synoptic and multi-spectral coverage of a terrain. GIS is an effective tool to analyze spatial and non-spatial data on drainage, geology, landforms parameters to understand their interrelationship. Integrated remote sensing and GIS can provide the appropriate platform for convergent analysis of diverse data sets for decision making in groundwater resource mapping and planning (M.Kavitha Mayilvaganan et al. (2011). The concept of integrated Remote sensing and GIS has proved to be an indispensable tool in integrating urban planning and groundwater studies (Nag S. K. et al., 2011)

* Corresponding author. Tel.: +918347010902 ;

E-mail address: trivedimadhu@gmail.com

1.1. Data Collection

- Contour data for the study area in India were procured from the Survey of India (SOI) in the form of topographical map.
- Drainage data for the study area were also procured from the Survey of India in the form of Topographical map.
- Rainfall data for the study area were obtained from the Indian Meteorological Department (IMD) gauge stations.
- Geological map of the study area was required.
- Indian Remote Sensing (IRS- 1C, 1D, LISS-III, IV) data were required to identify different hydrogeomorphological units. These satellite images were geo-referenced and merged using Image Processing Software to topographical map scale obtained from the Survey of India.
- Data pertaining to land use, land cover, slope in the form of remote sensing imagery were required for the study area.

2. Methodology

The various toposheet maps obtained from the Survey of India were digitized in ArcGIS platform. The rainfall map was prepared from the rainfall data collected from the Indian Meteorological Department gauge stations. Interpolation of the spatially missing rainfall data was carried out using Inverse Distance Weighted (IDW) method to obtain the rainfall distribution map in most of the research papers. This interpolation method combines the concepts of proximity to Thiessen polygons with gradual change of the trend surface. The drainage density and lineament density maps were prepared using the line density analysis tool in ArcGIS (N.S. Magesh et. al. (2012).

2.1. Generation of thematic maps

Analysis and interpretation of satellite data was carried out in order to produce thematic maps, such as Land use, Geomorphology, Drainage, Drainage density, Lithology, Lineament density, Surface water body, Slope etc., as shown in Appendix A. All the remotely sensed images were rectified using the SOI Toposheet initially, followed by image digitization and then processing these digital images using the various processing techniques, viz., enhancement, filtering, classification and other GIS processes. Spatial Database was thus built up after bringing all the appropriate data and other collateral data together into a GIS database (Biswas Arkoprovo et. al. (2012).

2.2. Satellite Data Interpretation

Several researchers have used RS and GIS techniques for the delineation of groundwater potential zones (Chi & Lee 1994; Kamaraju et al. 1995) with successful results. The type and number of thematic layers used for assessing groundwater potential by RS and GIS vary considerably from one study to another and also, in a majority of studies, personal judgment has been used for assigning weights to different thematic layers and their features (Machiwal et al. 2011). For quantitative analysis each of them has been assigned some weight which defines its influence on groundwater potential.

Many researchers have found that multi-criteria decision-making (MCDM) provides an effective tool for water management by adding structure, transparency and rigour to decisions (Dunning et al. 2000; Flug et al. 2000; Joubert et al. 2003). Others have classified Weighted Index Overlay Analysis (WIOA) for combining multi class layers based on their relative importance to represent the actual ground situation.

Few other researchers have used Analytical Hierarchy process (AHP) for assigning relative weights to the various thematic maps. The weights were decided based on the local field experience, as well as expert opinions. The weights thus assigned to different thematic maps and their individual features were normalized by using Saaty's AHP. The normalization process reduces the subjectivity associated with the assigned weights of the thematic maps and their features. The normalized weights of the thematic layers and those of their features were examined for consistency as recommended by Saaty (1980). Fig. 1 shows the flow chart of the methodology for delineating the groundwater potential zones for the Palamu district, Jharkhand in India.

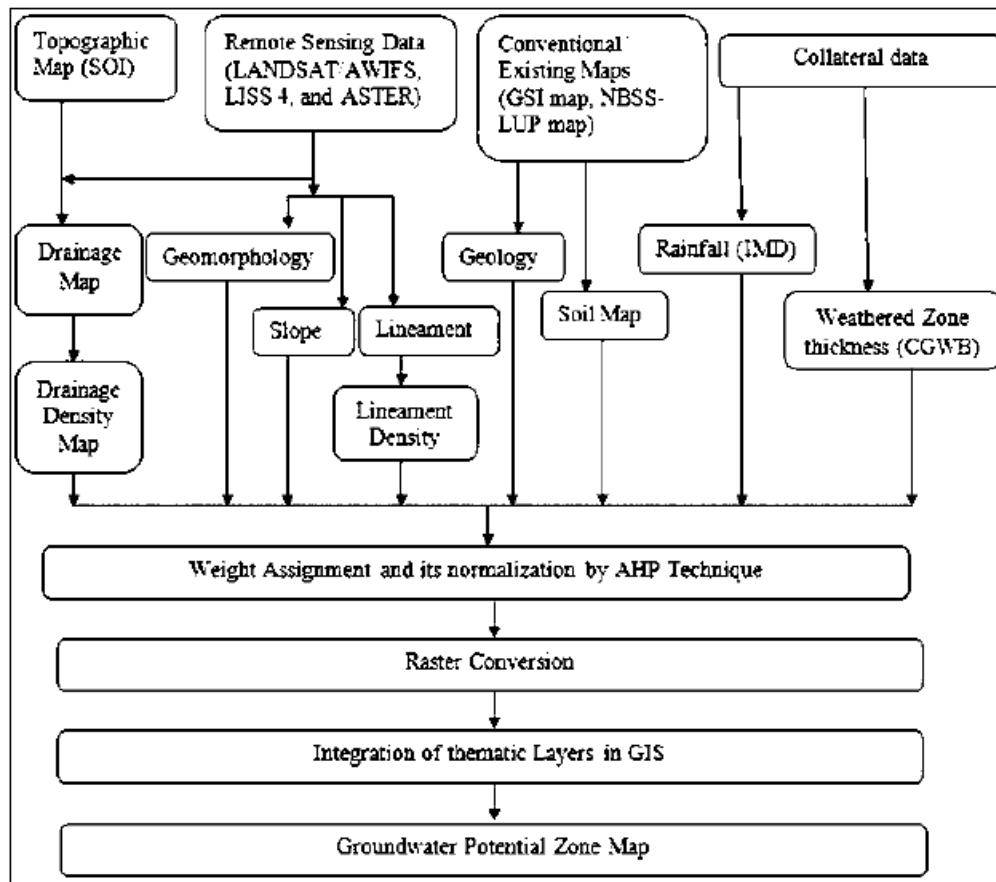


Fig. 1. Flow chart of the methodology for assessing groundwater potential zone (Shashank Shekhar et al., 2014)

2.3. Classification of groundwater potential zones

Using the AHP, MCDM or WIOA theory by various researchers for similar studies, each of the thematic layers were categorized depending on the recharge characteristics, and suitable weightages were assigned to them. Groundwater potential index (GWPI) in the research study was determined by the formula as shown below:

$$GWPI = (G_g^w G_g^r + D_g^w D_g^r + D_d^w D_d^r + L_h^w L_h^r + L_t^w L_t^r + L_d^w L_d^r + W_w^w W_w^r + S_s^w S_s^r) / \text{Total Weight.}$$

Where: Gg: geomorphology, Dg: drainage, Dd: drainage density, Lh: lithology, Lt: lineament, Ld: lineament density, Ww: surface water body, Ss: slope. With “w” representing weight of a theme and “r” the rank of a feature in the theme. The themes/features may vary from place to place.

Suitable weightage was given to each class of a particular thematic layer based on their contribution towards ground water potentiality. The rank of each thematic map was scaled by the weight of that theme as shown in Table 1. All the thematic maps were then registered with one another through ground control points and integrated step by step using normalized aggregation method in GIS for computing groundwater potential Index of each feature. GWPI is a dimensionless quantity that helps in indexing the probable groundwater potential zones for the study area (Biswas Arkoprovo et al., 2012). Then after combining all the thematic maps in the ArcGIS environment, the study area was classified according to their identified groundwater prospects such as excellent, good, moderate, poor etc., (Appendix B), based the Groundwater Potential Index (GWPI) value.

Table 1. Thematic Map Weight and Feature Ranking

Theme	Weight	Features	Rank
Geomorphology (G_g)	5	Younger Coastal Plain	10
		Valley Fill	8
		Shallow Buried Pediplain	7
		Residual Hill	2
Lithology (L_h)	4	Beach Alluvium	9
		Older Alluvium	8
		In situ Laterite	5
		Transported Laterite	4
		Unclassified Crystalline Rocks	2
Drainage density (D_d)	3	0.00 – 0.75 km	10
		0.75 – 1.50 km	8
		1.50 – 2.25 km	6
Lineament density (L_d)	2	>110	8
		50-110	6
		20-50	4
		<20	3
Slope (S_s)	1	Level to nearly level (0–1%)	10
		Very gently sloping (1–3%)	9
		Gently sloping (3–5%)	7
		Moderately sloping (5–10%)	5
		Moderate steeply sloping (10–30%)	3

2.4. Verification of the groundwater potential zone map

Validation of groundwater potential map in few of the research papers were done with reference to the well yield data over the final output map of groundwater prospect zones to check the accuracy of the study.

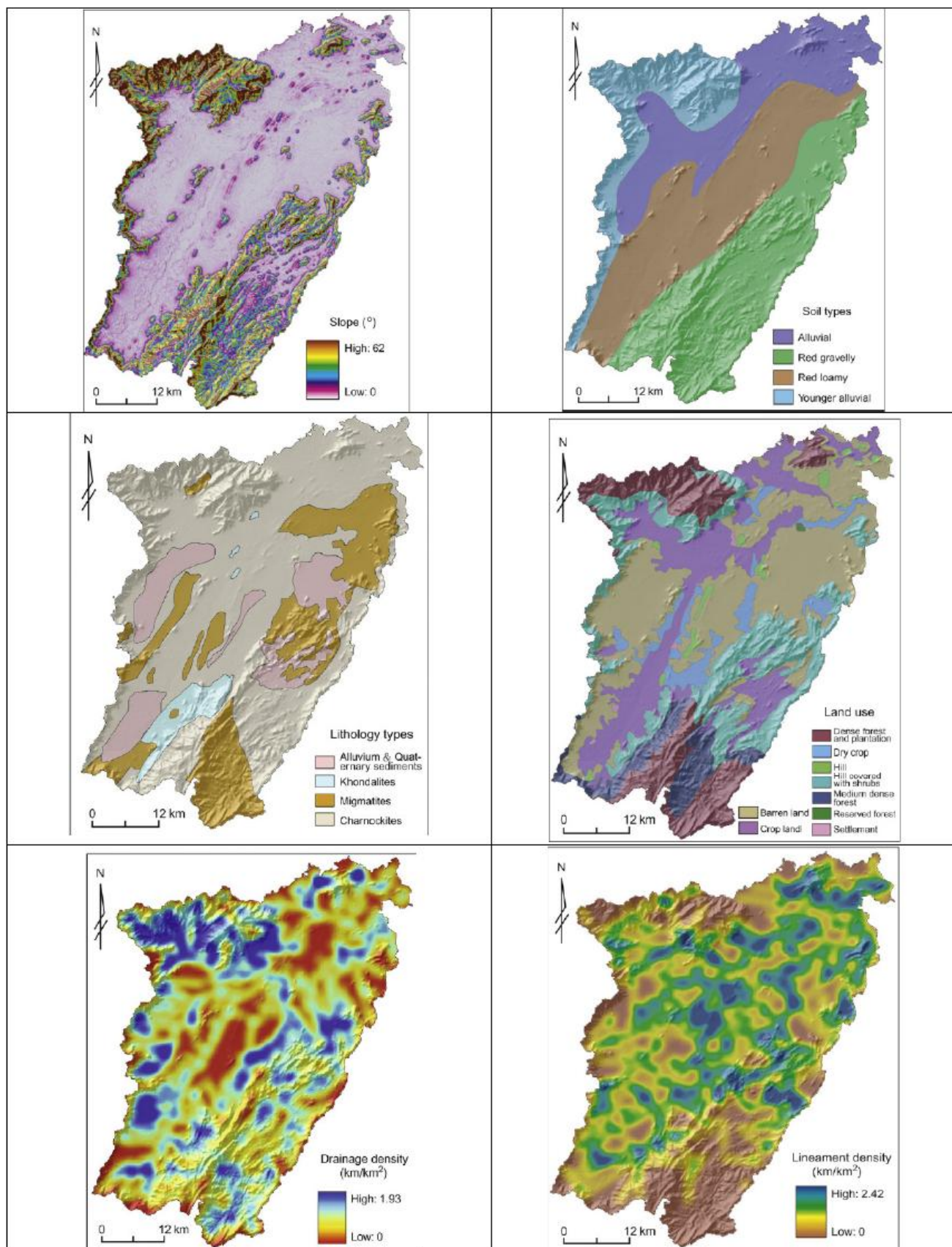
3. Conclusions

Remote sensing enables to view large areas instantly to achieve a prospective view which is not possible through ground surveys. Application of remote sensing techniques with conventional hydrogeological surveys and its integration on the GIS platform helps to decipher ground water potential zones, using the procedure of feature identification. The groundwater potential zones can be helpful in better planning and management of groundwater resources. Identification of the groundwater potential zones on a regional scale can serve as guidelines for planning future artificial recharge projects in the area in order to ensure sustainable groundwater utilization. It can also help to identify the favourable location for the construction of wells to extract water for the agricultural purposes.

References

- [1] Biswas. A., Jana A., Sharma, S., P., 2012, "Delineation of Groundwater Potential Zones using Satellite Remote Sensing and Geographic Information System Techniques: A Case study from Ganjam district, Orissa, India", Research Journal of Recent Sciences Vol. 1(9), pp. 59-66.
- [2] Chahar Bhagu R., 2014. Groundwater Hydrology, McGraw Hill education.
- [3] Hutti, B., Nijagunappa. R., 2011. "Identification of Groundwater Potential Zone using Geoinformatics in Ghataprabha basin, North Karnataka, India", International Journal of Geomatics and Geosciences, Volume 2 Issue 1, pp. 91-109.
- [4] Lillesand T.M. and Kiefer R.W., 2000, Remote Sensing and Image Interpretation, Fifth Edition, John Wiley and Sons, Asia Pvt. Ltd, Singapore, 820.
- [5] Magesh, N., S., Chandrasekar, N., Soundranayagam, J., P., 2012, "Delineation of groundwater potential zones in Theni district, Tamil Nadu, using remote sensing, GIS and MIF techniques", Geoscience Frontiers 3(2) pp.189-196.
- [6] Murugiah, M., Venkatraman, P., 2013, "Role of Remote Sensing and GIS in artificial recharge of the ground water aquifer in Ottapidaram taluk, Tuticorin district, South India", International Journal of Geomatics and Geosciences, Volume 3, No 3, pp. 405-415.
- [7] Saaty, T.L. (1980), the Analytic Hierarchy Process: Planning, Priority Setting, Resource Allocation (New York: McGraw-Hill).
- [8] Saraf A.K. and Choudhury P.R., 1998, "Integrated Remote Sensing and GIS for Groundwater Exploration and Identification of artificial recharge sites", Intl. J. Rem. Sen, 19(10), pp. 1825-1841.
- [9] Shekhara, S., Pandey, A., C., 2014, "Delineation of groundwater potential zone in hard rock terrain of India using remote sensing, geographical information system (GIS) and analytic hierarchy process (AHP) techniques", Taylor & Francis, Geocarto International.

Appendix A. Various Thematic maps created in GIS after image processing (N.S. Magesh et al., 2012)



Appendix B. Groundwater potential zone map of the study area (N.S. Magesh et al., 2012)

